Technical University of Denmark

DTU

REBECa WP IV - Formation and transformation of particles and other pollutants from engines using biofuel
WP IV final report (DTU project no. 50502)

Hansen, Brian Brun; Jensen, Anker Degn; Jensen, Peter Arendt

Link back to DTU Orbit

DTU Library
Technical Information Center of Denmark

REBECa WP IV– Formation and transformation of particles and other pollutants from engines using biofuel
WP IV final report (DTU project no. 50502)

Brian Brun Hansen, Anker Jensen and Peter Arendt Jensen

September 2011

Department of Chemical & Biochemical Engineering
Technical University of Denmark
Building 229
DK-2800 Kgs. Lyngby
Denmark

CHEC NO: R1106

_____

Abstract

   This project expands present knowledge regarding diesel engine emissions and diesel particulate filter (DPF) performance and regeneration during biodiesel usage. This is done through a literature survey, a pilot-scale experimental study of DPF performance and thermo gravimetric studies of PM/catalyst/ash interactions. A pilot-scale experimental study of DPF performance and NO_2 influence indicated a lower engine out particulate concentration while using Rapeseed methyl ester (RME, 26 mg/m^3) compared to ultra low sulphur diesel (ULSD, 58 mg/m^3). Filter regeneration with a 50 % diluted exhaust also showed an improved performance with RME (regeneration at 475 ^{o}C and 120 mbar filter pressure loss) compared to ULSD (500 ^{o}C and 125 mbar filter pressure loss). The improved filter performance was most likely due to the lower particulate concentration when using RME (lower deposition flux to overcome), because no significant differences in particulate reactivity or engine out NO_x concentration were seen. The introduction of 400 ppm NO_2 to the RME exhaust (normal NO_x concentration ~ 250 ppm (can be oxidized to NO_2 by an oxidation catalyst)) caused an improved filter regeneration performance (regeneration at 435 ^{o}C and 80 mbar filter pressure loss), which illustrates the importance of NO_2 for particle oxidation and thereby the importance NO to NO_2 conversion either in a separate oxidation catalyst or as part of the DPF's catalytic performance. Thermo gravimetric (TG) studies of PM/catalyst/ash interactions in N_2 with 10 % O_2 showed that diesel PM conversion (5:1 wt. ratio with commercial catalyst) benefits from the presence of biodiesel salts such as Na_2CO_3, K_2CO_3 or K_3PO_4 – TG peak conversion temperature decreased from 526 ± 19°C to ~ 400-420 ^{o}C, with a limited dependence on salt concentration. Other lube oil derived salts ($CaSO_4$ and $Ca(H_2PO_4)$) or combinations of lube oil and fuel (K_2SO_4) can have a detrimental effect on catalytic PM conversion. However, utilization of high biodiesel fractions over a prolonged period of time will likely be necessary before any of these effects can be seen, because of the stringent fuel specifications (EN 14214: $\leq$ 5 mg Na + K/kg; $\leq$ 5 mg Ca + Mg/kg; $\leq$ 4 mg P/kg).

_____

Preface

   This report describes the work carried out by work package IV of the REBECa project (Renewable Energy in the transport sector using Biofuels as Energy Carriers). The work has been conducted in collaboration with work package III "Emission measurements and vehicle engine inspection test" (The National Environmental Research Institute and The Danish Technological Institute). Within WP IV the following papers, reports and B.Eng/M.Sc projects have been generated:

Papers:

Hansen, B.; Jensen, A.D.; Jensen, P.A. Performance of Diesel Particulate Filter catalysts in the Presence of Biodiesel Ash Species. *To be submitted to Fuel*

Technical reports:

Hansen, B.; Jensen, A.D.; Jensen, P.A. *Emissions from engines using biodiesel – Literature survey*. CHEC report 1002; Department of Chemical and Biochemical Engineering, Technical University of Denmark: Lyngby, Denmark, 2010.

Hansen, B.; Jensen, A.D.; Jensen, P.A. *Diesel engine setup – Design, construction and commissioning*; Department of Chemical and Biochemical Engineering, Technical University of Denmark: Lyngby, Denmark, 2011.

B.Eng/M.Sc projects:

Hubeck-Graudal, H.; Rønde, V.K. *Emissions from Biodiesel Engines with Particulate Filters*, B.Sc. Thesis; Department of Chemical and Biochemical Engineering, Technical University of Denmark: Lyngby, Denmark, 2011.

Nielsen, J.B. *Filtration of diesel exhaust gas*, M.Sc. Thesis; Department of Chemical and Biochemical Engineering, Technical University of Denmark: Lyngby, Denmark, 2011.

Table of Contents

1. Introduction

Recent years have seen a growing concern regarding CO_2 emissions as well as street-level air quality - in particular regarding particulate (PM) emissions from the transport sector. The EU have responded with a aim of a 10 % share of renewable energy in the transport sector by 2020 and a 20 % renewable energy share of the overall energy consumption. The implementation of biofuels (ethanol, biodiesel etc.) into the transport sector is expected to contribute significantly to these goals. The introduction of such new fuels, with their changed fuel properties, may affect engine performance, emissions, ash composition and long-term interactions with cleaning technologies such as the oxidation catalyst (DOC) and the diesel particulate filter (DPF). The flow though DOC is capable of oxidising CO as well as gaseous hydrocarbons, that otherwise could condense and contribute to particle formation. The highly efficient DPF traps 95-99 % PM by forcing the exhaust trough a porous wall, thereby initially capturing PM in the pores followed by cake filtration on top of the channel walls. To avoid excessive backpressures, periodically DPF cleaning/regeneration by conversion of soot/PM into CO_2 (reaction with O_2 or NO_2) is necessary. The regeneration can facilitated by catalytic fuel additives, a catalytic coating on the DPF or by increasing the exhaust temperature through control of fuel injection/engine load. Incombustible residues generated from lubrication oil, fuel/fuel additives and engine/exhaust wear (ash) will accumulate in the DPF eventually constitute a large fraction of the trapped material. The accumulated ash may prevent proper contact between soot and catalyst and it may furthermore react with the catalytic coating, thereby deactivating it, and deteriorating DPF regeneration/performance. A swift, cheap and energy efficient filter regeneration is desired, while maintaining filter integrity (no thermal run away or steep temperature gradients). DPF regeneration will consequently depend on catalytic activity, PM concentration, PM reactivity, NO_2 concentration and ash accumulation and the introduction of new fuels, such as bio-fuels, may change the DPF regeneration performance.

The objectives of the present work were:
- To establish an experimental setup and compare exhaust concentrations (PM, HC, NO, NO_X, CO, CO2 & SO_2) from standard ULSD and biodiesels
- The investigate the influence of particulate concentration, particulate reactivity and NO_2 concentration on DPF regeneration

- To investigate how accumulated ash from biodiesel and lube oil may affect DPF regeneration performance.

The following activities were conducted:
- Literature survey
- Construction and commissioning of a pilot-scale experimental setup with diesel engine and DPF unit
- Pilot scale experimental study of DPF performance and the influence of NO_2
- Thermo gravimetric studies of PM/catalyst/ash interactions

_____

2. Literature survey

In order to survey the present knowledge regarding emissions from biodiesel combustion and potential interactions with exhaust cleaning technologies a literature survey was initially performed (see Appendix I). The following main conclusions could be drawn:

- A growing concern regarding CO_2 emissions and as street-level air quality/emissions from the transport sector has caused an introduction of exhaust cleaning technologies and a gradual increase of the share of renewable energy (10 % by 2020 in the EU)

- Biodiesel possess favourable characteristics in terms of its renewable character and the potential for reduced greenhouse emissions. However, the limited availability of waste fractions of animal fat that can be used for biodiesel production, concerns regarding the use of a considerable fraction of the agricultural land area for energy production and poor biodiesel cold flow properties constitute substantial barriers for a more widespread application.

- Most studies indicate that biodiesel implementation into existing engines can reduce the emissions of gaseous hydrocarbons (~ -50 % HC), carbon monoxide (~ -70 % CO) and particulate matter (~ -25 to 50 % PM) because of the absence of sulphur and soot precursors in the fuel, the advanced combustion process and higher oxygen accessibility in the flame (fuel oxygen). Slightly increased emissions of nitrogen oxides ($\leq$ +10 % NO_x) may however also be generated. The composition of the emitted PM is also changed - lower fractions of soot and sulphuric acid and a higher proportion of condensed hydrocarbons (soluble organic fraction (SOF)). An increased fraction of small particles have furthermore been observed in some studies.

- The use of biodiesel/biodiesel blends has furthermore been reported to benefit the regeneration of diesel particulate filters (i.e. lower regeneration temperatures). 3 different mechanism have been suggested to explain this: an increased particulate reactivity, an increased NO_2 concentration (benefits the oxidation) or a decreased particle concentration (lower deposition flux to overcome). The impact of long-term accumulation of the biodiesel ash species on DPF performance, furthermore, remains unknown.

_____

_____

3. Design and construction of pilot scale setup

A new experimental setup was designed and constructed to make it possible to study the influence of different diesel fuels on the performance of a catalytic diesel particulate filter. The facility includes a diesel generator (max output 6 kW) that can supply exhaust to the diesel particulate filter. The filter temperature can be controlled by an oven and an electrical exhaust preheater. The facility makes it possible to perform experiments with: different fuels, DPF performance/regeneration and filter interaction with engine emissions (particle concentration, particulate properties and NO_2 concentration). Figure 1 illustrates the outline of the experimental setup (further details can be found in the attached design report (Appendix II)). The constructed experimental setup possesses the following properties/possibilities:

- Generation of a representative diesel engine exhaust
  - *O_2, CO, CO_2, gaseous hydrocarbons, NO_x, SO_2*
  - *Particulate concentration, composition and properties*
- Opportunity to preheat exhaust before particulate filer
  - *Decoupling of engine performance and DPF performance*
- Opportunity to dilute exhaust before particulate filer
  - *Simulation of different emission levels/engine optimisations*
- Opportunity to add NO_2 to exhaust before particulate filer
  - *Simulation of upstream oxidation catalyst to increase NO_2 concentration*
- Flexible exhaust flow
  - *Exhaust can for example pass the DPF and be led directly to the stack*
- Sampling and measurement of exhaust composition before and after DPF
  - *Gaseous hydrocarbon (Flame ionizing detector)*
  - *CO, CO_2, O_2, SO_2, NO and NO_x*
  - *Particle size distribution*
  - *Particle concentration (diluted and undiluted exhaust)*
  - *Particle composition (soot vs. condensates) and properties (ignition temperature)*
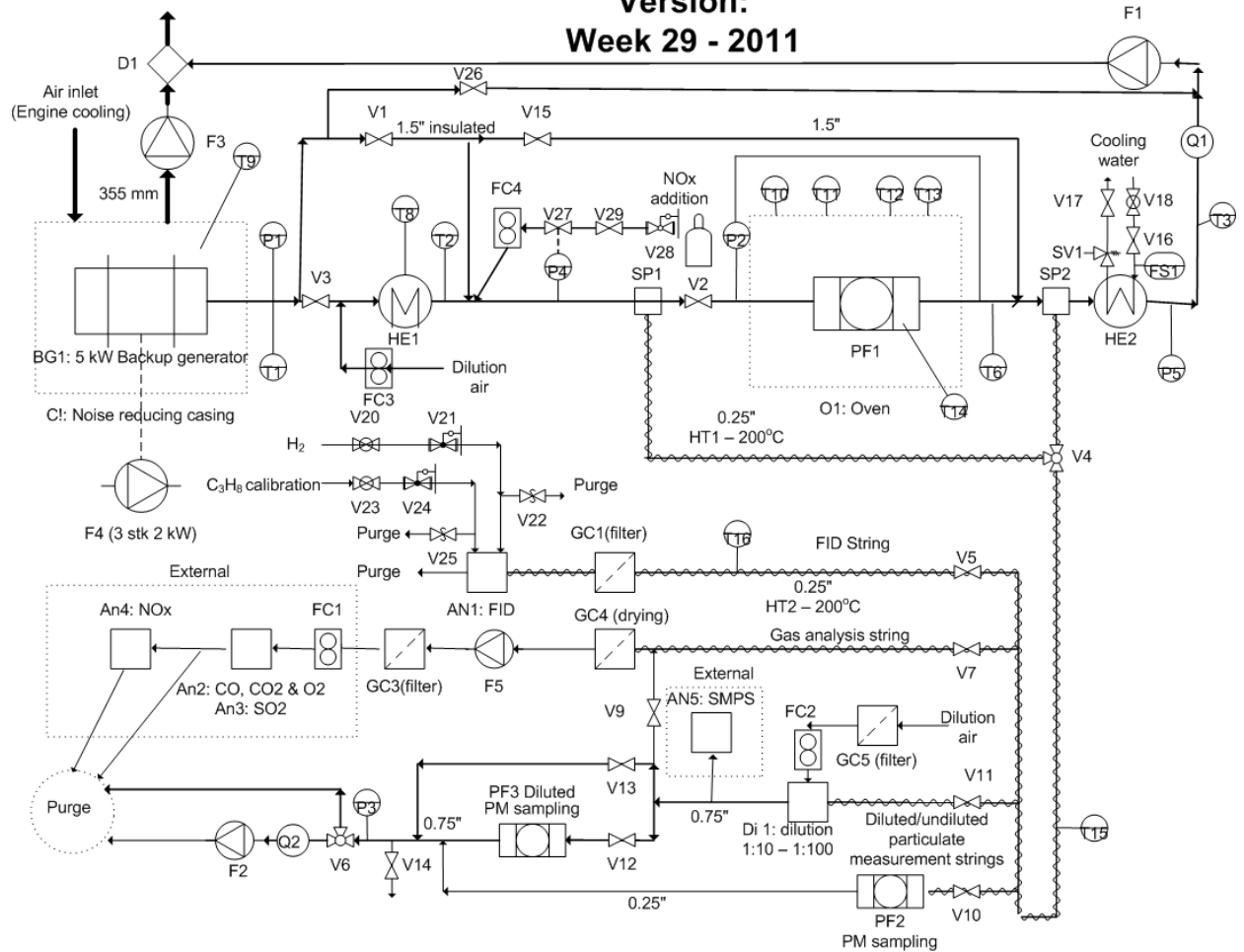
Figure 1: PI diagram for diesel engine experimental setup.

_____

4. Pilot scale experiments of DPF performance and NO$_2$

The exam projects of *Hubeck-Graudal & Rønde, 2011* and *Nielsen, 2011* commissioned the experimental setup described in the previous section and tested the performance of 3 fuel types (Q8 ultra low sulphur diesel (ULSD), Emmelev rapeseed methyl ester (RME) & DAKA tallow methyl ester). The main findings are presented below - Further details can be found in appendix III.

PM emissions of 58 mg/m^3 and 26 mg/m^3 were obtained for the combustion of ULSD and RME respectively (at 80 % engine load). These PM measurements are, however, sensitive to changes to sampling conditions. These PM emissions are approximately 3 times greater than the PM emission from older automotive engines. The DPF was able to capture app. 90 % of the soot and convert ~ 90 % of the CO, while condensation of gaseous hydrocarbons/SOF took place after the filter (see figure 2)
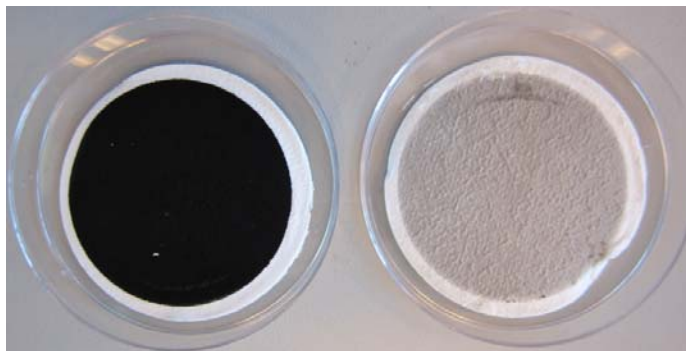
Figure 2: PM samples collected before and after DPF
(DAKA biodiesel at 80 % engine load and T$_{filter}$ ~ 50 ^{o}C).

The minimum temperature required to initiate filter regeneration (decrease in pressure drop) was determined while no exhaust passed the filter – corresponding to the break-even temperature at infinite dilution. Similar values were obtained for the 3 fuels: Petrodiesel ~ 380 ^{o}C (40 % load), Rapeseed methyl ester & tallow methyl ester ~ 360-370 ^{o}C(80 % load), indicating a similar reactivity. Experiments concerning regeneration during engine operation were performed with a pre-heated and 50 % diluted exhaust, to decouple engine performance/emissions and DPF performance (no further dilution could be performed due to bypass valve limitations). Figure 3 shows that both temperature and filter loading influence filter regeneration performance, indicating a contribution from non-catalytic conversion

within the soot layer. An improved performance was seen for RME (regeneration at 475 $^{\circ}$C and 120 mbar filter pressure drop) compared to ULSD (500 $^{\circ}$C and 125 mbar filter pressure drop). This improved performance was most likely due to the lower particulate concentration, because no significant differences in particulate reactivity or engine out NO_x were seen. It has furthermore been demonstrated that the introduction of 400 ppm NO_2 into the RME exhaust (normal NO_x concentration ~ 250 ppm (can be oxidized to NO_2 by an oxidation catalyst)) caused an increased reactivity/regeneration performance (regeneration at 435 $^{\circ}$C and 80 mbar), which illustrates the importance of NO to NO_2 conversion either in a separate oxidation catalyst or as part of the DPF's catalytic performance
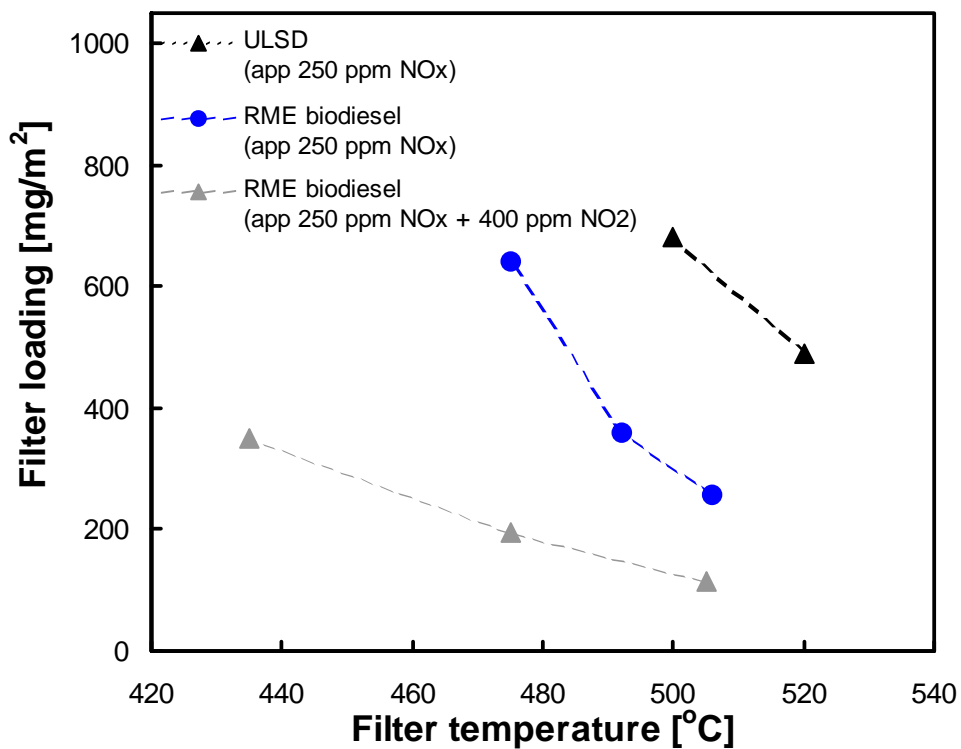

Figure 3: Filter loading and temperature yielding a constant pressure drop (PM deposition equals conversion) for ultra low sulphur diesel, RME biodiesel and RME biodiesel with 400 ppm NO_2 added to the exhaust.

_____

5. Lab-scale study of DPF catalysts and simulated biodiesel ash

The deposition of inorganic species, originating from the fuel and lube oil, may influence DPF performance and in some cases deactivate the catalytic material. Use of different fuels may change the filter ash deposit composition. A series of STA (Netzsch STA 449 F1 Jupiter) experiments were performed to study the influence of different inorganics, that could originate from ordinary diesel, biodiesel and lube oil, on the soot oxidation capacity of the filter catalyst in N_2 with 10 % O_2. Mixtures of soot, catalyst and ash species were brought into tight contact, by dissolution, evaporation and grinding. The STA analysis was used to determine the temperatures at which maximum soot conversion took place. Figure 4 provides an overview of the peak conversion temperature for the different mixtures. The pure automotive PM sample had a peak temperature of 662 ^{o}C, which is shown with a solid line. The addition of a commercial catalyst (Dinex A/S: $\sim$ 2 % Pt, $\sim$ 20 % CeO_2 and $\sim$ 78 % TiO_2) in the absence of salts/simulated ash (5:1 PM to catalyst wt. ratio) in tight contact with the particulate matter caused a $\sim$ 150 ^{o}C decrease in peak conversion temperature (to 526 ^{o}C $\pm$ 19). The experiments with biodiesel salts demonstrated that catalytic diesel PM conversion benefits from the presence of biodiesel salts such as Na_2CO_3, K_2CO_3 or K_3PO_4 - peak conversion temperature decreased from 526 $\pm$ 19°C to $\sim$ 400-420 ^{o}C, with a limited dependence on salt concentration. Other salts which could be formed from lube oil ($CaSO_4$ and $Ca(H_2PO_4)$ or combinations of lube oil and fuel (K_2SO_4) can have a detrimental effect on catalytic PM conversion - i.e. peak conversion temperatures increased to 569 ^{o}C $\pm$ 6; 699 ^{o}C $\pm$ 13 and 581 ^{o}C $\pm$ 16 respectively.

Kinetic parameters (A and E_a) obtained from Arrhenius plots of the STA data, show a lower activation energy in the presence of the commercial catalyst (E_a = 91 $\pm$ 5 kJ/mol) or CeO_2 (E_a = 62 $\pm$ 8 kJ/mol) compared to pure SRM 2975 automotive PM (E_a = 220 $\pm$ 3 kJ/mol) The kinetic data was able to simulate/describe the peak conversion temperature and the associated part of the conversion/mass loss curve, but an initial gradual increase in conversion was not adequately described.
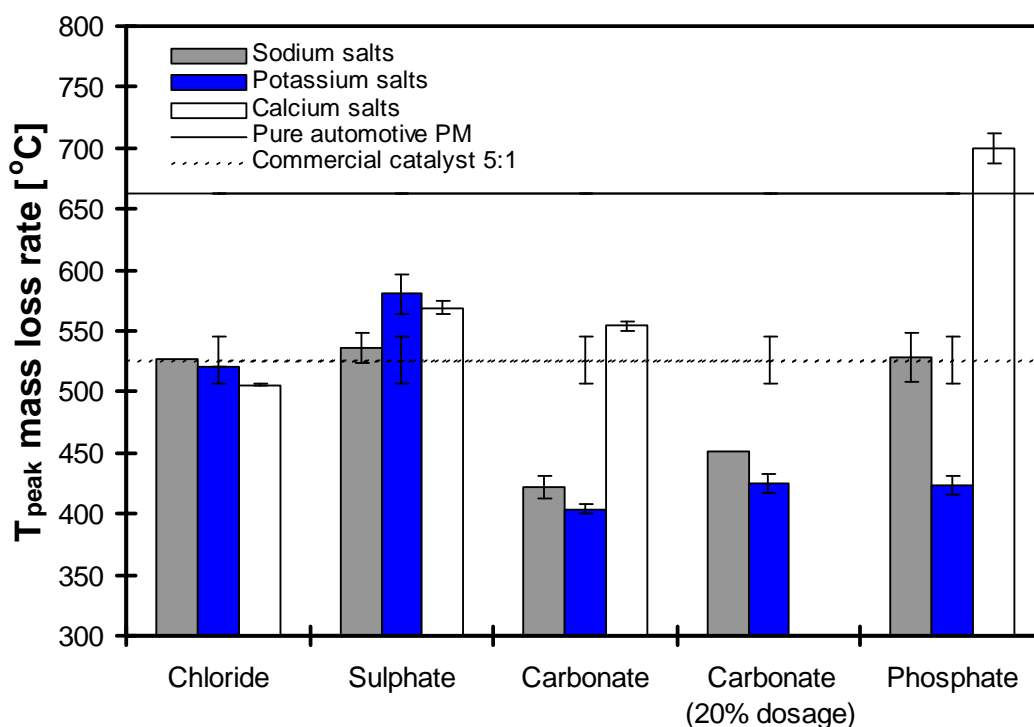
Figure 4: Temperature at which maximal mass loss rate took place for carbon/catalyst/salt mixtures (heating rate 10 K/min at 10 % O_2). Error bars indicate standard deviation. The solid and the dashed line illustrate the temperature at which mass loss rate peaked for standard SRM 2975 automotive PM and a 5:1 mixture with the commercial catalyst respectively.

With respect to operation of DPF's while using biodiesel as fuel, the results obtained imply that the presence of sodium or potassium as carbonates or phosphates benefit the diesel particulate matter conversion and thereby improve DPF regeneration. However, ash accumulating in the filter may decrease the required tight PM/catalyst contact and build-up of excessive level of ash in the filter may furthermore be detrimental to DPF regeneration performance. Limited amounts of sodium, potassium, calcium, magnesium and phosphorous are allowed in the fuel according to EN 14214, so utilization of high biodiesel fractions over a prolonged period of time will likely be necessary to obtain the effects observed in the STA experiments.

Further details can be found in appendix IV.

_____

6. Conclusion

Recent years have seen the implementation of biofuels (ethanol, biodiusel etc.) and diesel particulate filters (DPF) in the transport sector, due to growing concerns regarding CO_2 emissions as well as street-level air quality. This has created a need for a better understanding of the influence of biodiesel utilization on particle emissions. This project has addressed this by studies of DPF performance, DPF regeneration, DPF interaction with engine out NO_2 and long-term DPF/ash interactions by both lab and pilot scale experiments. The following activities have been conducted:

- Literature survey
- Construction of pilot-scale DPF test facility
- Pilot scale experimental study of DPF performance and the influence of NO_2
- Thermo gravimetric studies of PM/catalyst/ash interactions

The literature survey showed that biodiesel possess favourable characteristics in terms of its renewable character, the potential for reduced greenhouse emissions and reduced emissions of gaseous hydrocarbons, carbon monoxide and particulate matter. However, the limited availability of waste fractions of animal fat, concerns regarding the use of a considerable fraction of the agricultural land area for energy production and poor biodiesel cold flow properties constitute barriers for a more widespread application of biodiesel. The use of biodiesel/biodiesel blends has furthermore been reported to benefit the regeneration of diesel particulate filters (i.e. lower regeneration temperatures), but different explanations have been suggested to explain this: an increased particulate reactivity, an increased NO_2 concentration (benefits the oxidation) or a decreased particle concentration (lower deposition flux to overcome). The impact of long-term accumulation of the biodiesel ash species on DPF performance, furthermore, remains unknown.

Pilot scale experiments with a diesel backup generator were performed to study of DPF performance during biodiesel combustion and to test the influence of NO_2 on DPF regeneration. PM emissions of 58 mg/m^3 and 26 mg/m^3 were obtained at 80 % engine load for the combustion of ULSD and RME respectively. These emissions are approximately 3 times greater than the PM emission of older automotive engines and higher break-even temperatures (soot deposition rate equals conversion) and contributions from both catalytic and non-

catalytic soot combustion in the DPF were seen for both ULSD and RME. The minimum temperature required to initiate filter regeneration was determined while no exhaust passed the filter, corresponding to the break-even temperature at infinite exhaust dilution. Similar values were obtained for ULSD (40 % load ~ 380 ^{o}C) and rapeseed methyl ester & tallow methyl ester (80 % load ~ 360-370 ^{o}C). Filter regeneration with a 50 % diluted exhaust also showed an improved performance with RME (regeneration at 475 ^{o}C and 120 mbar filter pressure loss) compared to ULSD (500 ^{o}C and 125 mbar filter pressure loss). The improved performance was most likely due to the lower particulate concentration (lower deposition flux to overcome), because no significant differences in particulate reactivity or engine out NO_x were seen. The introduction of 400 ppm NO_2 into the RME exhaust (normal NO_x concentration ~ 250 ppm (can be oxidized to NO_2 by an oxidation catalyst)) caused an improved regeneration performance (regeneration at 435 ^{o}C and 80 mbar), which illustrates the importance of NO to NO_2 conversion either in a separate oxidation catalyst or as part of the DPF's catalytic formulation

With respect to operation of diesel particulate filters while using biodiesel as fuel, the results obtained imply that the DPF regeneration benefits from biodiesel combustion due to a lower exhaust PM concentration and that higher engine out NO_2 level also can be beneficial. The study strongly indicate that using RME biodiesel to replace fossil diesel in diesel engines with DPF's will lead to decreased PM emissions and improved DPF regeneration performance.

Thermo gravimetric studies of PM/catalyst/ash interactions in 10 % O_2 were performed to test the impact of long-term biodiesel ash accumulation on DPF performance. Catalytic diesel PM conversion (5:1 wt. ratio with commercial catalyst) benefits from the presence of biodiesel salts such as Na_2CO_3, K_2CO_3 or K_3PO_4 - peak conversion temperature decreased from 526 ± 19°C to ~ 400-420 ^{o}C, with a limited dependence on salt concentration. Other salts, which could be formed from lube oil ($CaSO_4$ and $Ca(H_2PO_4)$ or combinations of lube oil and fuel (K_2SO_4) can have a detrimental effect on catalytic PM conversion - i.e. peak conversion temperatures of 569 ^{o}C ± 6; 699 ^{o}C ± 13 and 581 ^{o}C ± 16 respectively. With respect to operation of DPf's while using biodiesel as fuel, the results obtained imply that the presence of sodium or potassium as carbonates or phosphates benefit the diesel particulate matter

conversion and thereby DPF regeneration. However, as diesel particulate matter is converted the ash may accumulate locally in the filter, thereby removing the required tight PM/catalyst/ash contact. Build-up of excessive level of ash in the filter may furthermore still be detrimental to DPF regeneration performance. However, utilization of high biodiesel fractions over a prolonged period of time will likely be necessary before any of these effects could be encountered in real world DPF's, because of the stringent fuel specifications (EN 14214: ≤ 5 mg Na + K/kg; ≤ 5 mg Ca + Mg/kg; ≤ 4 mg P/kg).

Appendices

Appendix I.
Report: Emissions from engines using biodiesel – Literature survey
Brian Brun Hansen, Peter Arendt Jensen, Anker Degn Jensen.

Appendix II.
Report: Diesel engine setup - Design, construction and commissioning
Brian Brun Hansen, Peter Arendt Jensen, Anker Degn Jensen.

Appendix III.
Report: Filtering of diesel Exhaust gas (M.Sc Project)
Joachim Bachmann Nielsen, Brian Brun Hansen, Peter Arendt Jensen, Anker Degn Jensen.

Appendix IV.
Article: Performance of Diesel Particulate Filter catalysts in the Presence of Biodiesel Ash Species
Brian Brun Hansen, Peter Arendt Jensen, Anker Degn Jensen.

Appendix I

REBECA – WP IV
Emissions from engines using biodiesel – Literature survey

Brian Brun Hansen, Peter Arendt Jensen, Anker Degn Jensen

May 2010

Department of Chemical Engineering
Technical University of Denmark
Building 229
DK-2800 Kgs. Lyngby
Denmark

R1002

Abstract

The substitution of fossil oil-derived fuels with liquid biofuels in the transport sector has received considerable political and public attention in recent years, due to concerns regarding energy renewability, political dependability and public health (generated emissions). Biodiesel is one such liquid biofuel, which is produced from vegetable oils or animal fats by conversion of the tri-glyceride fats to mono-esters via transesterfication with alcohols. The properties of the obtained fuel differ from conventional diesels in terms of higher cetane numbers but also lower energy densities, poor cold flow properties and an increased degradation of rubber fittings. The use of biodiesel/petroleum-derived diesel blends has so far been used to overcome these obstacles.

Apart from its renewable character and reduced greenhouse gas emissions, biodiesel furthermore reduce the emissions of gaseous hydrocarbons (HC), carbon monoxide (CO) and particulate matter (PM) but increase the emissions of nitrogen oxides (NO_x). The composition of the emitted PM is also changed - lower fractions of soot and sulphuric acid and a higher proportion of condensed hydrocarbons (soluble organic fraction (SOF)). An increased fraction of small particles have furthermore been observed in some studies.

This report survey the present knowledge concerning the combustion and emissions generated by automotive compression ignition engines when conventional diesel is used and the changes facilitated by biodiesel blends. The present European automotive emission legislation and the measures taken to comply with this will furthermore be outlined.

Contents

List of abbreviations

A/F: Air to fuel ratio

B20:   Blend consisting of 20 % biodiesel and 80 % petroleum-derived diesel

B100:   Pure biodiesel

BDC: Bottom dead centre

COP: Conformity of production

DI: Direct injection

DOC: Diesel oxidation catalyst

ECE: Economic Commission for Europe

EGR: Exhaust gas recirculation

EU: European Union

EUDC: Extra-Urban Driving Cycle

FTIR: Fourier transform infra red absorption spectroscopy

HC: Hydrocarbons

IDI: In-direct injection

LFOR: Lean flame out region

LFR: Lean flame region

LNT: Lean NO_x traps

NEDC: New European Driving Cycle

NMHC: Non-methane hydrocarbons

NO_x: Nitrogen oxides ($NO + NO_2$)

NSCR: Non-selective catalytic reduction

PAH: Poly aromatic hydrocarbons

PM: Particulate matter

PSD: Particle size distribution

RME: Rapeseed methyl ester

RPM: Rounds per minute

SCR: Selective catalytic reduction

SOF: soluble organic fraction of particulate matter

SO_x: Sulphur oxides ($SO_x = SO_2 + SO_3$)

TDC: Top dead centre

TEM: Transmission electron microscopy

TGA: Thermo gravimetric analysis

THC: Total hydrocarbons

ULSD: Ultra low sulphur diesel

XRD: X-ray diffraction

Chapter 1

Literature review

Recent years have featured a growing political attention and public awareness towards energy renewability, security/political dependability and the environmental side effects of the world's energy consumption. The transport sector in particular has received considerable attention triggering initiatives such as the implementation of emission control devices and fuel substitution (liquid biofuels or electricity). The liquid biofuels (methanol, ethanol, biodiesel etc.) possess a considerable reduction potential in terms of gaseous hydrocarbons (HC), particulate matter (PM) and carbon dioxide (CO_2) emissions, but concerns regarding the utilisation of agricultural land, the storage stability and the wear of the engine/fuel system have been raised. The initial approach has been to establish targets of a biofuel share in transport fuels (5.75 % by 2010 in the European Union (EU), *Dieselnet, 2008*). The superior self-ignition properties of biodiesel, compared to methanol and ethanol, make it well suited for diesel substitution.

This report consists of a brief introduction to the diesel engine followed by sections concerning the combustion process, the emissions generated, the emission legislation, control options and the effect of biodiesel utilisation (fuel substitution). Special emphasis will be placed on the legislation within the EU and the emissions of PM.

1.1 Diesel engine fundamentals

The compression-ignited diesel engine was invented in the late 19th century by Dr. Rudolf Diesel. It is the most efficient internal combustion engine and it is associated with a favourable fuel economy and a high durability/reliability. It has, however, traditionally also been associated with emissions of nitrogen oxides (NO_x), PM and odorous/sooty exhausts (*Majewski & Khair, 2006*). The diesel engine is widely used in stationary as well as mobile applications, particulary where high torque at low speeds or high fuel efficiencies are required (*Maricq, 2007*). Charge air boosting, either mechanically by pumps (superchargers) or compressors driven by the exhaust gas (turbochargers), may further increase the power output of the diesel engine.

The combustion process takes place at the high pressures and temperatures generated within the engine cylinders. The cylinder operation consists of four steps: air intake, compression, combustion and exhaust, which may take place separately (four stroke engine) or be combined (two-stroke engine). The combustion process generates an expansion of volume, which acts on a piston that drives the crankshaft thereby providing work. Figure 1 shows the cylinder pressure as a function of the crankshaft angle/piston location for a four-stroke diesel engine. Top dead centre (TDC) corresponds to maximal compression of the engine cylinder and bottom dead centre (BDC) the maximal cylinder expansion. Towards the end of the cycle the intake valve opens (point 1) and charge air flows into the cylinder as the piston moves from TDC to BDC. The air charge is then compressed and fuel injection begins (point I) towards the end of the compression stroke. The amount of injected fuel depends on the load of the engine and a varying air to fuel ratio, $\lambda \in [1.1\text{-}6]$, is consequently obtained (*Neeft et al., 1996*). The injected fuel evaporates and mixes with the charge air during the compression, thereby using energy and decreasing the rise in cylinder temperature and pressure. The self-ignition of the air/fuel mixture is followed by a sharp increase in pressure, as well as temperature (may exceed 1500 K in large marine diesel engines (*Zevenhoven, 2001*)), which drives the expansion stroke. Towards the end of the expansion stroke the exhaust valves open and the cylinder is emptied during the subsequent exhaust stroke.
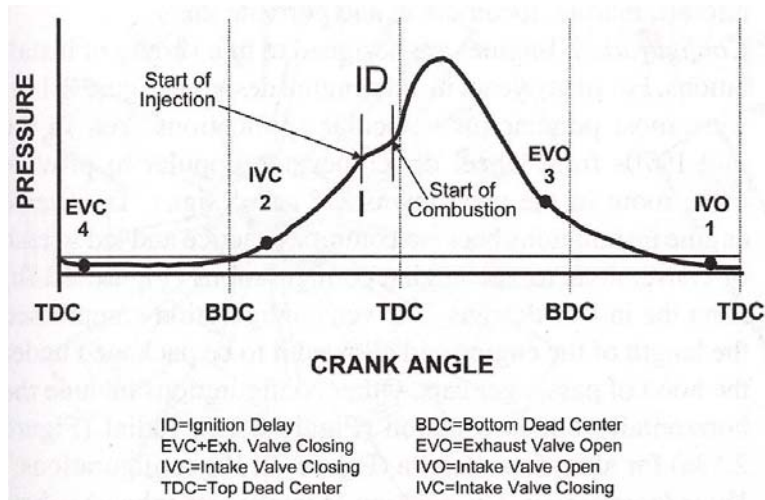
Figure 1: Pressure- crank angle diagram for a four-stroke diesel engine.
(*Majewski & Khair, 2006*)

The fuel injection system controls the timing, quantity and atomisation of the fuel injected into the engine cylinders. High injection pressures (~ 2000 bar) and small nozzles are used to obtain a good fuel atomisation. Traditionally the pump-line nozzle system, featuring a high-pressure pump supplying the mechanical valves in each cylinder through fuel lines of equal length, has been used. However, new initiatives such as the common rail system (high-pressure accumulator from which the fuel is distributed to the electronically controlled injector valves) separates the pressure generation and the injection process and enable higher nozzle pressures and a more flexible control of the injection timing and profile. The fuel may be introduced into a pre-chamber (indirect-injected (IDI) engines) or directly into the engine cylinder (direct-injected (DI) engines). The majority of new engine designs are of the DI type, because of the superior fuel economy and recent improvements concerning noise reductions (*Majewski & Khair, 2006*).

1.2 Diesel fuels - Biodiesel

The classical source of diesel fuels is fractional distillates of petroleum, containing paraffinic, naphthenic and aromatic hydrocarbons with boiling point in the range 150 to 380 $^{\circ}$C (*Majewski & Khair, 2006*). Alternative sources, such as natural gas, synthesis gas or biomass are, however, emerging. Biodiesel is an oxygenated fuel made from vegetable oils (soybean, rape, sunflower, coconut or algae) or animal fats (frying oil) by conversion of the tri-glyceride fats (R denoting the hydrocarbon chains) and methanol/ethanol into esters and glycerol via an alkali hydroxide catalysed transesterfication (*Majewski & Khair, 2006; Mccormick et al., 2001; Neeft et al., 1996*).

$$(CH_2OOCR)(CHOOCR^{'})(CH_2OOCR^{''}) + 3\ CH_3OH \rightarrow \qquad (1)$$
$$(CH_2OH)(CHOH)(CH_2OH) + 3\ RCOOCH_3$$

The produced glycerol is subsequently removed and a fairly homogenous biodiesel ester mixture with a narrow boiling point range is usually obtained, i.e. carbon chain containing 16 to 18 atoms, and an oxygen content ~ 11 wt % (*Majewski & Khair, 2006*). Biodiesel possess favourable characteristics in terms of its renewable character and the potential for reduced greenhouse emissions. However, the limited availability of waste fractions of animal fat and concerns regarding the use of a considerable fraction of the agricultural land area for energy production, constitute substantial barriers for a more widespread application of biodiesel.

The biodiesel and petroleum-derived diesel (petrodiesel) quality, in terms of physical properties and chemical composition, is regulated by international standards (EN 14214, ASTM D6751 and EN 590 respectively). The different properties of biodiesel, as illustrated by table 1 and appendix I, can alter the fuel injection, ignition and combustion processes and thereby the emissions formed.

Table 1: Comparison of selected properties of conventional diesel and biodiesel (*EN590, 2000; EN14214, 2003; Majewski & Khair, 2006*).

Property	Unit	Petrodiesel	Biodiesel
Cetane number[*]		44	55
Lower heating value	MJ dm^{-3}	36.2	32.6
Cloud point	^{o}C	- 19	-2
Density (15 ^{o}C)	kg m^{-3}	820-845	860-900
Viscosity (40 ^{o}C)	mm^2 s^{-1}	2.00-4.50	3.5-5.0
Ash	wt%	≤ 0.01	-
Aromatics	vol %	34	0
Sulphur	mg kg^{-1}	≤ 50	≤ 10
		≤ 10 (2009)	
Alkali metals (Na + K)	mg kg^{-1}	-	≤ 5
Phosphor	mg kg^{-1}	-	≤ 10

*Cetane number: A measurement of a diesel fuels combustion quality (ignition delay) during compression ignition. higher cetane numbers means shorter ignition delays and consequently more time for the combustion process to complete.

The lower energy density of biodiesel induces a higher fuel consumption (fuel penalty), which may exceed 13 % in the case of pure biodiesel used in U.S heavy-duty FTP transient test cycle (*Majewski & Khair, 2006*). The faster propagation of biodiesel towards the atomising nozzles (caused by a lower compressibility) advance the injection and combustion, thereby decreasing the extent of premixed combustion and increasing the pressure and temperature gradients yielding a re-centred combustion (compared to the delayed combustion used today to limit NO$_x$) and an increased thermal efficiency (*Lapuerta et al., 2008*). The poor cold flow properties and higher viscosity of biodiesel necessitates either blending with petrodiesel or the use of fuel heaters to avoid plugging of filters/injectors and incomplete fuel atomisation at cold ambient conditions. The low aromatics and sulphur content in biodiesel reduce particle formation, however conventional "ultra low sulphur diesel (ULSD)" with $10 \leq$ mg Sulphur kg^{-1} has become standard in Europe from 1st of January 2009. Biodiesel are furthermore more susceptible to fuel degradation and water absorption, may cause increased degradation of conventional rubber fittings and failure to meet the specifications concerning the content of alkali metals and phosphorous can have a significant impact on emission control systems (*McCormick, 2008*). In order to control the cost increase associated with biodiesel and to minimise the necessary engine/fuel system modifications, blends of biodiesel and conventional diesel have been introduced in the Western Europe and the United States.

1.3 Combustion and Emissions

1.3.1 The combustion process

   The compression induced combustion process begins shortly after the diesel has been injected as small droplets into the engine cylinder. Initially (ignition delay) the atomized fuel evaporates and mixes with air. The continued compression, performed by the piston, heats the mixture until it reaches its ignition point. The fuel/air mixture is then converted in a premixed flame, while the remaining fuel droplets are consumed by diffusion flames (*Maricq, 2007*). The combustion process in DI diesel engines is an unsteady, heterogeneous three-dimensional process, which depends on engine load/speed, injection timing, engine design and the application of emission control devices (*Majewski & Khair, 2006; Maricq, 2007*). Figure 2 presents a conceptual understanding of the combustion process in diesel engines.
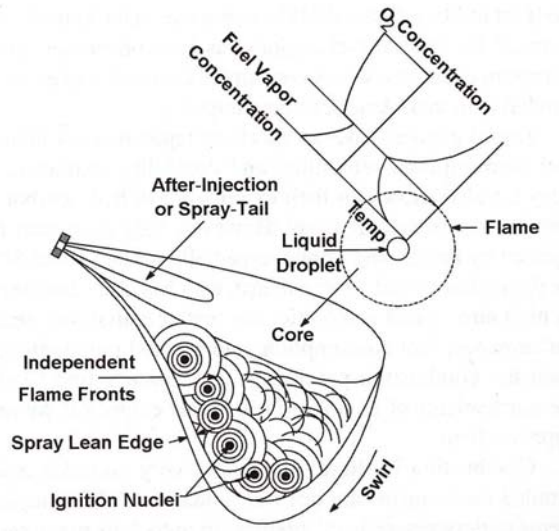
Figure 2: Schematic illustration of fuel/air mixing

and combustion in a diesel engine.

(*Majewski & Khair, 2006*)

The high-pressure fuel injection system transfers diesel into the engine cylinder through orifices/nozzle, thereby atomising it into small droplets. Absorption of heat from the surrounding compressed air allows the fuel droplets to evaporate and mix with the charge air. During the ignition delay the swirl air will mix with the evaporated fuel and carry the smaller fuel droplets downstream of the fuel jet. As the compression continues several ignition nuclei will be formed in this downstream lean flame region (LFR), and flames will propagate from

the nuclei thereby igniting the combustible fuel/air mixture surrounding them (*Majewski & Khair, 2006*). Following the ignition the flames propagate towards the spray core, containing the remaining larger fuel droplets as well as the fuel fraction injected late in the compression stroke. The approaching flame front enhances the evaporation rate and surrounds the remaining fuel droplets, which are combusted by diffusion flames. The combustion of the evaporated fuel in the spray core are mainly affected by the local Air/Fuel (A/F) ratio, which are influenced by the interaction between fuel spray and swirling air (*Majewski & Khair, 2006*).

Towards the end of the fuel injection a decreased injection pressure and an increased cylinder pressure yields a smaller pressure differential, thereby generating larger droplets and a poor spray penetration. The high cylinder temperature at this time will enhance evaporation, but oxygen availability may be scarce (especially at high loads), yielding decomposition or partial oxidation products. At medium to high engine loads a small amount of fuel may erroneously be injected late in the expansion stroke, called after injection/secondary injection, which also yields gaseous hydrocarbons and products of partial decomposition. In the case of high-speed engines the fuel droplets may furthermore be deposited on the cylinder walls where it will burn by a diffusion flame as it evaporates and oxygen arrives. Outside the LFR the fuel/air mixture is too lean to ignite/support stable combustion, but decomposition or partial oxidation may take place. This region is called the lean flame out region (LFOR) and its extent/size depends on cylinder temperature, pressure and air swirl (*Majewski & Khair, 2006*).

The combustion process taking place within DI diesel engine cylinders is consequently a complex series of reactions influenced by fuel properties, the engine design and operational conditions.

- The chemical/physical fuel characteristics:
  - Heating value, viscosity, vapour pressure, lubricity and especially the cetane number. A high cetane numbers correspond to a short ignition delay and consequently more time for the completion of the combustion process at the expense of a lower extent of premixed combustion.
- The atomisation and penetration of the injected fuel:
  - Injection pressure, nozzle size and spray geometry.

- The charge air volume, temperature and flow pattern within the cylinder:
  - Valve design/configuration, compression ratio as well as engine cylinder outline.

1.3.2 Emissions

The exhaust from diesel engines primarily consists of unused charge air and products of complete combustion (70-75 % N_2; 3-17 % O_2; 2-12 % H_2O and 2-12 % CO_2). The lower limits of H_2O and CO_2 represent low engine load or idle operation. The composition may furthermore vary depending on the engine design (*Majewski & Khair, 2006*). However, lower concentrations of products from incomplete combustion and high temperature/pressure reactions involving both fuel and lube oil are also formed (*Majewski & Khair, 2006; Neeft et al., 1996*).

- 0.01-0.1 % Carbon monoxide (CO)
- 0.005-0.05 % HC:
- 0.003-0.06 % NO_x (NO + NO_2).
- 5-30 ppm Sulphur oxides ($SO_x = SO_2 + SO_3$) with 500 ppm fuel.
- 20-200 mg PM m^{-3}.

Figure 3 illustrates the formation of the various pollutants during the combustion process.
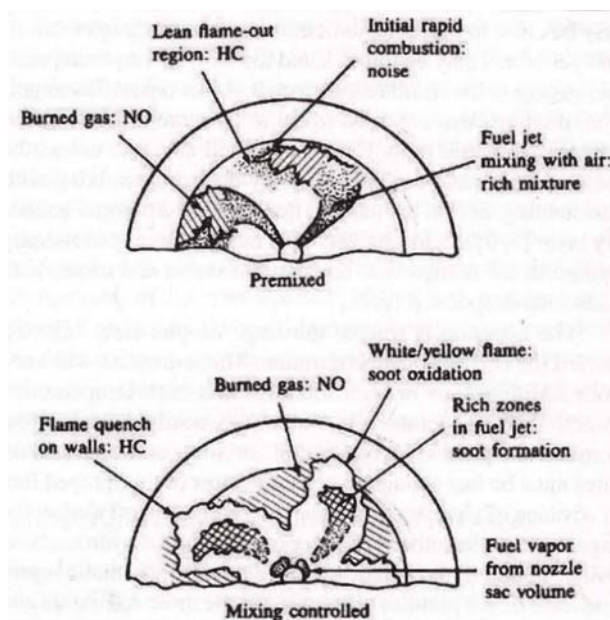

Figure 3: Mechanisms of pollutants formation in DI diesel engine (*Majewski & Khair, 2006*)

Diesel engines are characteristically fuel lean ($\lambda \in$ [1.1-6], *Neeft et al., 1996*) and most of the air charge is compressed and heated but never engages in the combustion process. The generated exhaust will consequently be of an oxidising nature and have the potential of CO and HC conversion during the expansion stroke and in the exhaust system. Traffic has been identified as the main contributor of CO, HC and NO_x in urban areas and compared to the emissions from older spark ignited gasoline vehicles (without a three-way catalyst) the exhaust from diesel vehicles will be significantly lower in HC and CO concentration, comparable in NO_x concentration and considerably higher in emitted PM (*Majewski & Khair, 2006; Neeft et al., 1996*). However the introduction and penetration of the three-way catalyst during the 80es have shifted the emission performance in favour of gasoline vehicles (*Majewski & Khair, 2006*).

Table 2: Emissions from 7.0 L heavy-duty diesel and gasoline engines (*Majewski & Khair, 2006*).

	HC [g/bhp-h][*]	CO [g/bhp-h][*]	NO_x [g/bhp-h][*]	PM [g/bhp-h][*]
Diesel engine out	0.15	1.5	3.40	0.07
Gasoline engine out	0.81	30.22	4.30	-
Gasoline – three-way catalyst	0.07	2.20	0.04	-

[*] *gram per brake horsepower hour – unit used in U.S Federal emission standards*

1.3.2.1 Gaseous emissions

Carbon monoxide (CO) is an odourless, colourless and toxic gas that is formed during incomplete combustion, due to insufficient oxygen concentrations, low temperatures, short residence times or poor mixing. Fuel rich combustion consequently favours CO formation, while the fuel lean diesel combustion process maintains low levels (*Majewski & Khair, 2006*).

Sulphur dioxide (SO_2) is a colourless gas with an irritating odour that is formed by the oxidation of sulphur species present in the fuel and as anti-wear additives in the lube-oil. A minor fraction of the released sulphur (2-4 %) will be in the form of SO_3, a precursor of sulphuric acid (H_2SO_4) and thereby particulate emissions. The lube-oil consumption only constitute 0.1-0.2 % of the fuel consumption, but its high content of sulphur ($\sim$ 5000 ppm) and stringent fuel specifications have increased its influence on the overall SO_2 emissions (*Majewski & Khair, 2006*).

Nitrogen oxides (NO_x) formed in diesel engines primarily originate from the nitrogen in the intake air, which reacts according to the extended Zeldovich mechanism at the high cylinder temperature. The emission level depends on the temperature, the availability of oxygen as well as the residence time in the cylinder. The NO fraction (usually 70-90 %) of NO_x will be oxidised to NO_2 in the atmosphere after emission. NO_2 is a toxic red-brown gas with an unpleasant odour and reactive/oxidising properties. The complete combustion taking place in the premixed lean flame region releases considerable amounts of heat which favours NO_x formation (*Majewski & Khair, 2006*).

Emissions of HC can be divided into either total hydrocarbons (THC) or non-methane hydrocarbons (NMHC) and consist of a wide range of volatile fuel and lube-oil derived compounds (products of decomposition, partial oxidation or recombination). The HC emissions from diesel combustion consists of aliphatic as well as aromatic species with up to approximately 24 carbon atoms (*Majewski & Khair, 2006*). The properties of these compounds may range from an irritating odour to toxic/carcinogenic. At light engine load the hydrocarbon emission will mainly be generated within the lean flame out region, through decomposition and partial oxidation of fuel molecules. At higher loads the extent of this region diminishes, but fuel rich zones such as the spray core, the cylinder walls and the spray tail will instead facilitate decomposition and recombination forming hydrocarbons both lighter and heavier than the original fuel molecules (*Majewski & Khair, 2006*).

1.3.2.2 Particulate emissions

Measurements of the diesel PM emissions and its particle size distribution (PSD) are usually performed in dilution tunnels, which simulate the cooling and dilution taking place in the atmosphere.

The PM emissions are defined as the mass retained by the filtration of a cooled and diluted exhaust stream (52 ^{o}C, *Neeft et al., 1996*). The PSD in the exhaust depends on the prior engine operation, the dilution ratio, the dilution air temperature and humidity and the residence time in the tunnel (*Yokoi et al., 2001*). Low dilution ratios and long residence times favour particle agglomeration while dilution air temperature and humidity affects the extent of condensation and the stickiness of the particles (*Yokoi et al., 2001*). Prior low temperature

operation/idling cause accumulation of soot and hydrocarbons on the walls of the exhaust system, which may subsequently be released during operation at higher temperatures. A preconditioning operation involving high exhaust temperatures and low PM and HC concentrations is therefore of importance (*Yokoi et al., 2001*). The PM collected on the filter will consist of soot and other solid combustion products as well as condensates. Diesel PM is traditionally divided into the following three main fractions: a solid fraction (elemental carbon (soot) and ash), a soluble organic fraction, SOF, extracted by dichloromethane (fuel, lube-oil and products of their partial combustion) and sulphate particulates (from the sulphur fraction in fuel/lube-oil). The origin (fuel or lube oil) of the soluble and insoluble fraction can be determined by gas chromatographic techniques (*Majewski & Khair, 2006*). The particulate emissions from a 1988 Californian heavy-duty engine consisted of a 48 wt. % insoluble fraction (mainly from the fuel ~ 90 %), a 39 wt. % soluble fraction (mainly from the lube oil ~ 75 %) and 13 wt. % H_2O and SO_4 (*Majewski & Khair, 2006*). Figure 4 shows a conceptual drawing of the PM composition leaving the exhaust.
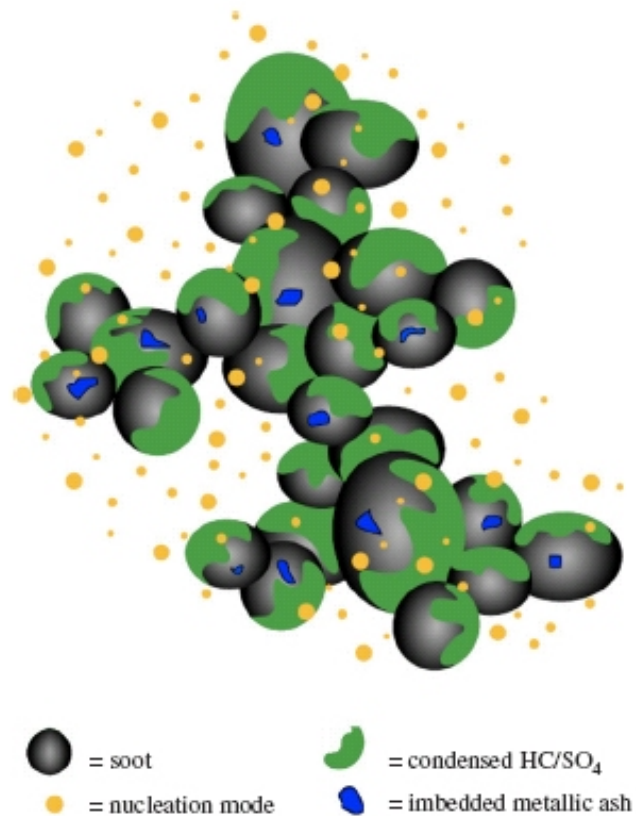

Figure 4: Conceptual drawing of diesel PM (*Maricq, 2007*).

The PM leaving the engine cylinder mainly consists of individual soot particles as well as elongated soot agglomerates and some metallic ash. Soot particles are formed in diffusion flames within local sub-stoichiometric regions of the cylinder (spray core, cylinder walls and spray tail) through fuel molecule pyrolysis, soot nucleation and growth (*Majewski & Khair, 2006; Neeft et al., 1996*). Soot may subsequently be oxidised at the flame boundary in the presence of oxygen and high temperatures as well as outside the engine cylinder. Soot aggregation, yielding a fractal resembling structure, takes place in the exhaust gas (*Neeft et al., 1996*). As the exhaust gas is cooled condensation of some of the heavier hydrocarbons as well as H_2SO_4 and water will take place, by nucleation if an insufficient particle surface area is available. Particle agglomeration as well as thermophoretic deposition may furthermore take place in the exhaust system (*Majewski & Khair, 2006; Kittelson, 1998*).

The PM composition will depend on the engine technology, test conditions (engine load, dilution ratio etc.) and fuel characteristics. Light engine loads enables a good air/fuel mixing thereby limiting soot formation, but a considerable LFOR will be present, generating fuel and lube-oil derived hydrocarbons. Low ambient and exhaust temperatures may furthermore limit SOF oxidation and facilitates condensation/nucleation, yielding a PM containing up to 90 wt. % SOF (*Kittelson, 1998; Ning et al., 2004*). Higher engine loads increase the extent of diffusion limited combustion and more soot will be formed at the somewhat less fuel-lean conditions. The higher exhaust gas temperature will furthermore improve SOF oxidation, thereby limiting the extent of nucleation (*Maricq, 2007; Tsolakis, 2006*). The total PM emissions generally increase as a function of load (especially at high load) as well as the extent of cooling of the exhaust gas (*Ning et al., 2004*).

The particulate emissions from diesel vehicles can be divided into three 3 modes: A nanoparticle mode (< 50 nm), an accumulation mode (50-1000 nm) and a coarse mode (> 100 nm), as illustrated by figure 5. The nanoparticle mode consists of SOF and H_2SO_4 nuclei formed during dilution and consequent cooling of the exhaust gas stream. The Soluble Organic Fraction (SOF) dominates the nanoparticle mode of heavy-duty vehicles, while H_2SO_4 is the main component in the case of light-duty vehicles (*Maricq, 2007*). The nanoparticle mode constitutes the majority of the particle number concentration, but only a limited fraction of the mass. The accumulation mode consists of the soot agglomerates formed

during the combustion process as well as the material subsequently absorbed onto these agglomerates. The majority of the PM mass is located within the accumulation mode. The coarse mode mainly consists of reentrained wall deposits (*Kittelson, 1998; Lapuerta et al., 2008*). New low PM engines generate a considerable lower accumulation mode than older engines, but the nuclei mode are of a similar magnitude (*Majewski & Khair, 2006*).
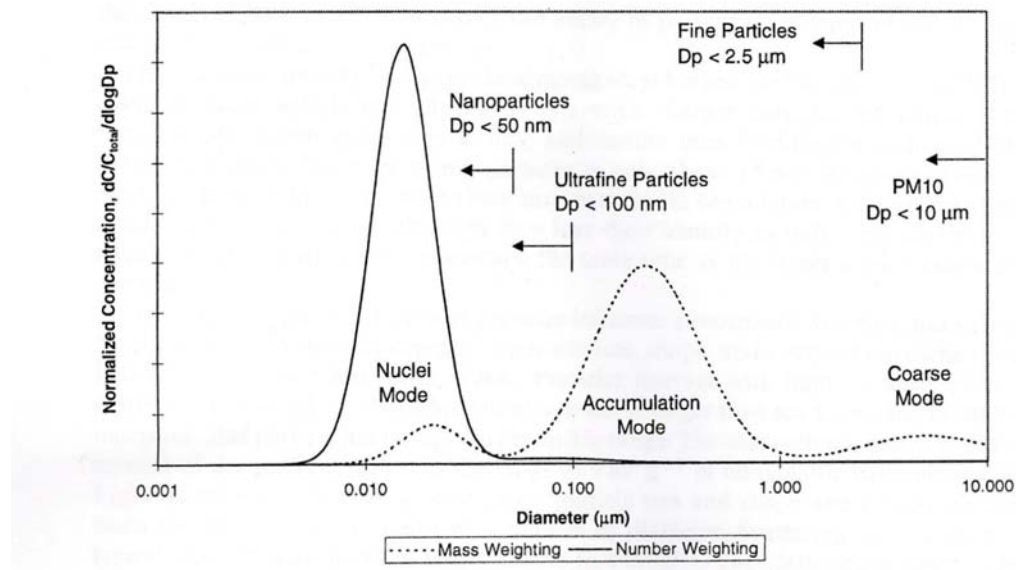
Figure 5: Illustration of the tri-modal Particle size distribution formed by diesel engines (*Kittelson, 1998*).

Other diesel applications, apart from cars/trucks, include the two-stroke engines in ships, locomotives, construction equipment, agricultural machinery, and back-up generators. The operating modes of these two-stroke engines differ in terms of lower speeds and higher power. The PM generated by a 2-stroke marine engine has been reported to be smaller (20 to 40 nm), than the particles generated by 4-stroke automobile engines, and rich in condensed semi-volatile matter (*Maricq, 2007*).

1.4 Legislation

The legislation concerning emission from light-duty vehicles (cars and light commercial vehicles) within the EU is outlined by directive 70/220/EEC with later amendments. The directive concerns the quality of diesel fuels used for road transport in Europe as well as the corresponding emission levels from road vehicles. The fuel quality regulations concern properties such as minimal cetane number, density, content of poly aromatic hydrocarbons (PAH) and sulphur content. A special emphasis has been placed on a reduction in the maximal sulphur content of the fuel (*Dieselnet, 2008; Directive 98/70/EC, 1998*):

- ≤ 350 ppm since 2000
- ≤ 50 ppm since 2005
- ≤ 10 ppm since 2009

Table 3 shows the development in EU emission standards for diesel fuelled passenger cars. The emission testing is performed with a chassis dynamometer following a sequence of changing loads specified in the New European Driving Cycle (NEDC). The driving cycle has been developed to represent typical car usage in Europe. The driving cycle consist of four repeated driving cycles (Economic Commission for Europe - ECE-15) and an Extra-Urban Driving Cycle (EUDC). The ECE cycle represents city driving and is characterised by low speeds, low engine loads and low exhaust temperatures. The EUDC cycle consist of more aggressive high speed driving.

Table 3: EU emission standards for Diesel Passenger cars (Category M_1[a]) [g km^{-1}] (*Dieselnet, 2008*)

Tier	Date	CO	HC + NO$_x$	NO$_x$	PM
Euro 1[b]	1992.07	2.72 (3.16)	0.97 (1.13)	-	0.14 (0.18)
Euro 2, IDI	1996.01	1.0	0.7	-	0.08
Euro 2, DI	1996.01[c]	1.0	0.9	-	0.10
Euro 3	2000.01	0.64	0.56	0.50	0.05
Euro 4	2005.01	0.50	0.30	0.25	0.025
Euro 5	2009.09[d]	0.50	0.23	0.18	0.005[e]
Euro 6	2014.09	0.50	0.17	0.08	0.005[e]

[a] At the Euro 1-4 stages, passenger vehicles > 2,500 kg were type approved as Category N_1 (light commercial vehicles)

[b] Values in brackets are conformity of production (COP) limits

[c] Until 1999.09.30 (after that date DI engines must meet the IDI limits)

[d] 2011.01 for all models

[e] Proposed to be changed to 0.003 g/km using the measurement procedure developed by the United nations/ECE particulate measurement programme.

From the Euro 3 stage vehicles should be equipped with onboard diagnostic systems, that alert the driver in case mandatory emission thresholds were exceeded, indicating a malfunction or deterioration of the emission control systems. The draft EURO 5 and 6 legislation furthermore introduce a particle number emissions limit of $5 \cdot 10^{11}$ solid particles (> 20 nm) km^{-1} (*Dieselnet, 2008*).

1.5 Emission control options

The combustion process taking place within diesel vehicles, and thereby the emissions formed, is influenced by fuel properties and engine layout. Various emission control devices may furthermore be applied to reduce tailpipe emissions. Significant progress concerning engine design, fuel injection strategy and fuel quality has been made during the last decades, but stringent emission limits concerning NO_x and PM will be introduced in the U.S, Europe and Japan the coming years, necessitating further engine optimization and the introduction of emission control devices. Table 4 provides an overview of the commercial status of various emission control technologies.

Table 4: Overview of emission control technologies (*Majewski & Khair, 2006*)

Technology	Affected pollutants	Commercial status
Diesel oxidation catalyst	CO, HC, PM (SOF) & odour	Cars/trucks: Commercial
Urea SCR catalysts:	NO_x	Stationary sources: Commercial
		Marine engines: Some installations
		Cars/trucks: Under development
DeNO$_x$ catalyst (Hydrocarbon SCR)	NO_x, CO, HC, PM (SOF)	Some commercial oxidation catalyst features a minor DeNO$_x$ activity
NO_x adsorber	NO_x, CO, HC	Lean burn gasoline engines: Commercial
		Stationary sources: Commercial
		Cars/trucks: Under development
Particulate filter (catalytic/non-catalytic)	PM	Cars/trucks: Commercial

1.5.1 NO$_x$ control

Initial approaches for controlling NO$_x$ emissions from diesel engines, were aimed at lowering the cylinder temperature/pressure as well as the residence time spent at elevated temperatures. This was achieved by intake air cooling, exhaust gas recirculation (EGR), combusting diesel-water emulsions and delaying the fuel injection. These approaches are, however, associated with a loss of thermal efficiency (lower peak combustion pressure) and higher PM emissions due to a decreased soot oxidation (*Lapuerta et al., 2008; Maricq, 2007; Majewski & Khair, 2006; Tsolakis, 2006*). The injection timing and exhaust recycle ratio will consequently be a compromise between NO$_x$ reduction and the engine efficiency/PM emission, a dilemma commonly referred to as the NO$_x$/PM trade-off. Some of the fuel penalty induced by delayed fuel injection can be restored by the good fuel atomisation obtained with high injection pressures (*Majewski & Khair, 2006*). Advanced strategies such as early fuel injection combined with EGR or late fuel injection in the presence of high swirl may to some extent overcome the NO$_x$/PM trade-off at the operating conditions of light-duty vehicles, i.e. engine speeds and loads < 30-50 % (*Johnson, 2008*). The use of emission control devices is, however, expected to be necessary in order to comply with the stringent legislation being introduced the coming years. The relative low temperature of the diesel exhaust gas stream favours catalytic reactions, but the high oxygen content makes the non-selective catalytic reduction process (NSCR), employed by the three-way catalyst in Otto engines, unfeasible (*Majewski & Khair, 2006*). The current focus is on the urea-based selective catalytic reduction (SCR) technology, which has been commercially available for heavy-duty applications since 2005, but lean NO$_x$ traps (LNT) – i.e. repeated cycles of NO$_x$ sorption (oxidizing atmosphere) and release/conversion (reducing atmosphere) performed by alkaline/alkaline earth catalysts, precious metal catalysts and hydrocarbon SCR - are being considered for application in light-duty vehicles (*Johnson, 2008*).

Selective Catalytic Reduction (SCR) of NO$_x$ with ammonia/urea has been used on stationary applications for several years, while the adaptation to the transient operating conditions of more mobile NO$_x$ sources (ships & ferries) is a more recent achievement. Mobile SCR systems for both heavy and light duty automotive engines are currently being developed or are at an early stage of commercialisation in Europe and the United States (*Majewski & Khair, 2006*). This technology offers a high cleaning efficiency within a wide

temperature range at the expense of a limited fuel penalty (*Johnson, 2008; Maricq, 2007*). A 32.5 wt.% aqueous urea solutions ($CO(NH_2)_2$) is preferred as reactant for mobile applications due to safety concerns regarding ammonia storage (*Majewski & Khair, 2006; Neeft et al., 1996*). The injected urea decomposes and hydrolyses above 160 ^{o}C (equation 2-3) in the exhaust, forming NH_3 and $\cdot NH_2$ that reduce present NO_x to N_2 (equation 4-6), whereas it may foul and deactivate the catalyst below this temperature (*Majewski & Khair, 2006*).

$$CO(NH_2)_2 \Leftrightarrow 2\ \cdot NH_2 + CO \tag{2}$$

$$CO(NH_2)_2 + H_2O \Leftrightarrow 2\ NH_3 + CO_2 \tag{3}$$

$$\cdot NH_2 + NO \Leftrightarrow N_2 + H_2O \tag{4}$$

$$4\ NO + 4\ NH_3 + O_2 \Leftrightarrow 4\ N_2 + 6\ H_2O \tag{5}$$

$$2\ NO_2 + 4\ NH_3 + O_2 \Leftrightarrow 3\ N_2 + 6\ H_2O \tag{6}$$
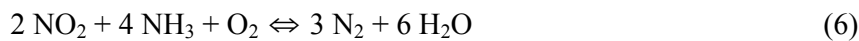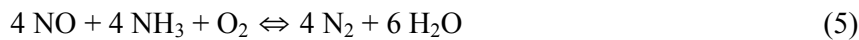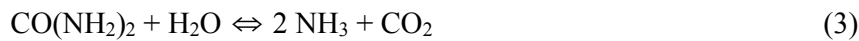
The reactant dosage is controlled by the engine speed, load and a pre-programmed map of NO_x emissions vs. speed/load. This approach has been reported to obtain ~ 80 % NO_x reductions, equation 2-5, while improved performances is expected when fast response NO_x and NH_3 sensors downstream of the SCR catalyst becomes available (*Majewski & Khair, 2006*). A nationwide reactant distribution system is, however, required and concerns about the drivers motivation to replenish the reactant in a timely manner has furthermore been expressed (*Majewski & Khair, 2006; Maricq, 2007*).

The SCR catalyst consists of a metallic/ceramic substrate onto which a high surface area coating/washcoat, consisting of base metal oxides such as Al_2O_3, SiO_2 TiO_2, CeO_2, ZrO_2, is applied alongside the active catalytic compound. The SCR catalysts currently used in Europe are based on vanadium (V_2O_5) as active catalyst compound and have an operating temperature window of 250-450 ^{o}C (*Johnson, 2008; Neeft et al., 1996*). Lower temperatures are associated with a low catalyst activity and the formation of deactivating side products, while temperatures above this window can cause a loss of surface area as well as undesired SO_2 oxidation yielding sulphate particulates in the exhaust (*Neeft et al., 1996*). Base metal oxides, such as WO_3, are often added to the catalyst formulation to suppress SO_2 oxidation at elevated temperatures and extend the catalyst lifetime (*Majewski & Khair, 2006*). Installation of an

oxidative catalyst upstream benefits the SCR catalyst performance by maximizing the NO_2 fraction and the removal of HC's that could decrease the catalyst light-off temperature, this would in particular benefit the catalyst performance at the to low exhaust temperatures during engine start-up (*Majewski & Khair, 2006*). Zeolite SCR catalysts with a higher thermal stability (operating window 350-600 ^{o}C) and an excellent selectivity towards NO_x (and not NH_3) at high temperatures can be made form aluminosilicate minerals, but insufficient low temperature efficiency is an issue (*Johnson, 2008; Majewski & Khair, 2006*).

Another promising technology is the lean NO_x trap, that absorbs NO_x onto the washcoat during lean operating conditions, while desorption and hydrocarbon SCR takes place during rich operation yielding a < 70 % NO_x reduction (*Johnson, 2008*; *Majewski & Khair, 2006*). The trap regeneration and hydrocarbon SCR reaction requires either fuel injection into the exhaust or a tight integration with the engine, i.e. periodic short pulses of fuel-rich exhaust, probable only feasible in conjunction with electronic fuel injection systems (*Majewski & Khair, 2006*). Sulphur poisoning of the catalyst may occur, even when ultra low sulphur diesel is used, necessitating periodic high temperature desulphating (*Majewski & Khair, 2006*). Lean NO_x traps have been classified as a promising technology, but thermal durability, limited NO_x removal efficiencies and the potential for sulphur poisoning provides challenges (*Majewski & Khair, 2006; Maricq, 2007*). The technology has, however, facilitated the implementation of a limited deNO$_x$ capability in today's oxidative catalysts (*Majewski & Khair, 2006*).

1.5.2 PM control

The PM composition of diesel engine exhausts depends on the fuel/lube-oil properties as well as the processes taking place in the engine cylinder (combustion, partial combustion and quenching) and exhaust (nucleation, condensation and emission control). Initial efforts for PM reductions included stricter fuel specifications, attention to lube oil consumption and engine design initiatives to improve mixing in the cylinders (*Majewski & Khair, 2006*). Subsequent initiatives included even stricter fuel specifications, additional engine design optimisations, flow-through diesel oxidation catalyst targeting gaseous hydrocarbons before condensation and recently the introduction of diesel particulate filters.

Improved fuel properties (i.e. lower sulphur & aromatic content, higher cetane number and lower density) and thereby decreased PM emission can be obtained by hydrodesulphurisation and hydrotreating of the fuel. The content of sulphur and aromatics in the fuel are correlated to the extent of H_2SO_4 and soot particulate formation respectively. High fuel cetane numbers implies swift fuel evaporation and ignition, thereby lowering the extent of diffusion combustion and PM formation (*Majewski & Khair, 2006*). The following engine design initiatives reduce PM emission through engine cylinder mixing (fuel atomisation/evaporation and swirl) and an improved soot conversion (extended residence time at high temperatures and an increased oxygen availability): (*Majewski & Khair, 2006; Maricq, 2007*)

- Manifold and intake port design (Swirl)
- Turbo charging (Oxygen availability and mixing)
- Charge air cooling and thereby higher air density (Oxygen availability)
  - The lower peak temperature furthermore reduces NO_x formation.
- Stronger engines with increased compression ratios (More heat for evaporation and shorter ignition delay)
- Higher fuel injection pressures (Increased atomization)
- Advanced injection timing (longer mixing time)
- Electronic injection control (Injection timing and profile)

The implementation of costly engine modifications such as high compression ratios, high injection pressures, electronic injection control, turbo charging and EGR have been more favourable in the expensive and durable heavy-duty engines and have therefore taken place earlier in these engines than in light-duty passenger cars (*Neeft et al., 1996*).

Diesel oxidation catalysts (DOC's) were used to clean exhausts in underground mining operations as early as the 70es and were introduced for automotive vehicles during the 90es - some EURO 2 cars, practically all EURO 3 cars, American heavy-duty busses and to a limited extent American trucks (*Majewski & Khair, 2006*). DOC's utilise the amble supply of oxygen in the diesel exhaust, to convert CO, HC, PAH, odour and the heavy-hydrocarbons, that otherwise would become the SOF of the PM, into CO_2 and water vapour. (*Kittelson, 1998; Majewski & Khair, 2006; Neeft et al., 1996*). Most commercial DOC's are optimised

for PM emission reductions, but a certain extent of HC and CO functionality is furthermore necessary in the case of European passenger cars (*Kittelson, 1998; Majewski & Khair, 2006; Neeft et al., 1996*). HC and CO conversion efficiencies in excess of 90 % can be obtained, while the PM reduction depends on the SOF fraction and thereby the driving cycle. The low loads and exhaust temperatures (< 300-350 ^{o}C) encountered in the European light-duty ECE + EUDC driving cycles produce a large SOF fraction enabling PM reductions up to 70 %, while the higher loads and exhaust temperatures (400-500 ^{o}C) experienced during heavy-duty driving cycles produce lower SOF fractions and PM reductions up to 25 % (*Majewski & Khair, 2006*). The low exhaust temperatures in light-duty vehicles, especially during cold-starts, may, however, render catalysts inactive (T < $T_{light-off}$). This may to some extent be overcome by placing the catalyst as close to the exhaust manifold as possible. Commercial light-duty European DOC's usually employ medium to high load platinum formulations (~ 10 g Pt/ft^3) optimised for HC light-off (*Majewski & Khair, 2006*). The high temperatures in heavy-duty exhaust may, however, also cause SO_2 oxidation and subsequent H_2SO_4 particulate nucleation. Commercial heavy-duty DOC's limit SO_2 oxidation through the application of lower platinum catalyst loadings, more selective but less active catalysts (palladium & rhodium), non-sulphating washcoats (TiO_2, SiO_2, ZrO_2) or alumina washcoats with sulphate inhibitors (V_2O_5) (*Majewski & Khair, 2006*). Commercial DOC's may also include catalytic active washcoats (CeO_2) or a limited (~15 %) NO_x reduction potential (Hydrocarbon SCR through HC release from a zeolite washcoat). Major sources of precious metal catalyst poisoning are additives from unburnt deposited lube oil (P, Zn, Ca and S) and fuel (S).

Diesel Particulate filters (DPF) were first introduced to off-road applications (mining & tunnelling equipment) during the 1980es and 1990es. During the late 90es heavy-duty highway vehicles (buses) were furthermore targeted in European, American and Asian cities. The first successful modern application of particulate filters for automobiles was in 2001 (Peugeot 607 (light-duty) and a Navistar 275 hp heavy-duty engine, (*Majewski & Khair, 2006*)). The stringent EURO 4 PM emissions limits are expected to increase the penetration of DPF's within the automotive sector (*Majewski & Khair, 2006*). Diesel Particulate filters provide an efficient way to control the submicron solid PM emissions (70-95 % reduction), but have a lower effectiveness against liquid particulates partially present in the gas-phase at

the conditions experienced by the filter (*Majewski & Khair, 2006*). The filters mainly capture accumulation and coarse mode particles, by inertial deposition, flow-line interception or diffusional deposition, thereby lowering the PM mass emitted but not necessarily the particle number (*Kittelson, 1998; Maricq, 2007*). The most common filter layout is the wall flow monolith, illustrated by figure 7, in which the opposing ends of the channels are blocked, thereby forcing the exhaust through the channel walls, while the particulates are retained (*Neeft et al., 1996*).
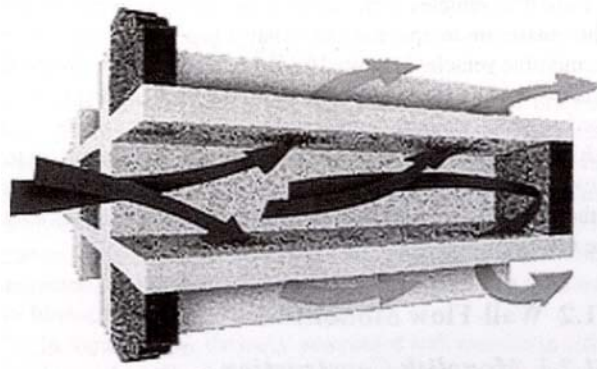

Figure 7: Flow in monolith filer *(Majewski & Khair, 2006)*

Nucleation of nanoparticles (condensed hydrocarbons (SOF) and H_2SO_4) and thereby an increased particle number concentration may furthermore take place downstream of the particle filter, especially in the presence of SO_2 and an oxidative catalyst, at high loads or low ambient temperatures, due to catalytic SO_2 oxidation, a high semi-volatile concentration and a limited particle surface area available for condensation (*Johnson, 2008; Majewski & Khair, 2006; Maricq, 2007*)**.** The application of a catalyst coating (oxidation catalyst and filter) capable of capturing sulphur has been reported to reduce the concentration of ultrafine particles below ambient levels (*Kittelson et al., 2006*). Noise reductions, similar to those of a silencer, are furthermore obtained with a particulate filter (*Neeft et al., 1996*). Filter materials include silicon carbide (both light-duty & heavy-duty applications), aluminium titanate (emerging within light-duty applications) and cordierite (heavy-duty applications) that are able to withstand the exhaust temperatures during normal operation as well as during filter regeneration (*Neeft et al., 1996*). Filter regeneration (soot oxidation by O_2 and NO_2) is performed either continuously or periodically (usually at least once a day, *Majewski & Khair, 2006*) in order to avoid excessive backpressures, while retained ash will accumulate and must

be removed by washing or air backflow usually once a year (*Majewski & Khair, 2006*). Filter regeneration may take place at medium to high-load conditions during the normal engine driving cycle (passive regeneration) or require additional measures (active regeneration) such as exhaust throttling, exhaust gas recirculation, auxiliary burners, electrical heating, post injection of fuel or microwave irradiation (*Johnson, 2008; Majewski & Khair, 2006; Neeft et al., 1996*). The approaches for active filter regeneration may induce a fuel penalty of up to 3 % and may in special cases even cause filter cracking/melting due to steep temperature gradients, caused by regeneration of excessive soot loads at insufficient exhaust flow rates – i.e. low speeds (*Johnson, 2008; Majewski & Khair, 2006; Neeft et al., 1996*). The temperature at which a reasonable filter regeneration rate is obtained depends on the soot loading, PM composition and the presence of catalysts (fuel-borne or filter incorporated) (*Majewski & Khair, 2006*). The regeneration temperature in the presence of catalysts may be as low as 300-400 $^{\circ}$C compared to the 550-650 $^{\circ}$C required to oxidise soot in standard uncatalytic filters (*Majewski & Khair, 2006*). Catalyst formulations often consist of a combination of transition metals (Platinum, palladium or rhodium) and rare earth metals (Cerium) (*Majewski & Khair, 2006; Neeft et al., 1996*)

1.5.3 Integrated NO$_x$ and PM systems

Engine calibration in terms of the NO$_x$/PM trade-off combined with either SCR or a particulate control device should be able to pass the stringent EURO 5 requirements. Integrated NO$_x$ and PM control systems are, however, still expected to enter service from 2008 (light-duty) and 2009 (heavy-duty) (*Johnson, 2008*). It is generally preferable to position the NO$_x$ system after the filter, in order to obtain as much passive NO$_2$-based filter regeneration as possible and thereby reduce the fuel penalty. However, a location in front of thefilter may be necessary in light-duty applications in order to obtain a suitable operation temperature (catalyst light-off). Regeneration of filters located up-stream may furthermore deliver very hot gas to the NO$_x$ system, raising durability concerns.

1.6 Biodiesel: Engine performance, emissions and interactions with control options

1.6.1 Engine performance and emissions

Numerous studies concerning the tailpipe emission from biodiesel fuelled engines have been published in the literature. The published data (often expressed as % difference from reference fuel) can be inconclusive or even contradictory due to differences in biodiesel and petrodiesel properties (especially cetane numbers), engine types (heavy-duty, light-duty or non-road), test cycles (engine speed and load), the dilution ratio of the exhaust and the absence of engine recalibration to its original power output (lower heating value of biodiesel) (*Lapuerta et al., 2008; Majewski & Khair, 2006*). Most studies have furthermore been performed on engines designed and calibrated for conventional diesels and not engines designed and calibrated for biodiesel combustion (*Majewski & Khair, 2006*). The following general trends have, however, been observed for pure biodiesel (*Majewski & Khair, 2006; Neeft et al., 1996*):

- An increasing ~ 10% NO_x concentration
- A decreasing ~ 50 % CO concentration
- A decreasing ~ 70 % HC concentration.
- A decreasing ~ 25-50 % PM concentration (mass) during hot-start driving cycles
  - *- Lower in carbon particulates*
  - *- Lower in sulphate particulates*
  - *- Higher in SOF particulates (may constitute up to 90 %)*
- An increased PM concentration during cold-start driving cycles

The higher NO_x emissions of pure biodiesel, as well as biodiesel blends, have been ascribed to a faster injection and an advanced ignition yielding higher cylinder pressures, heat release rates and the longer time spent at elevated temperature and pressure before the cooling during the expansion stroke. The lower compressibility (faster propagation towards injectors), higher viscosity (reduced back-flow at piston clearance), higher density (more mass injected) and lower heating value (overcompensation by the electronic control unit) of biodiesel have

been used to explain this phenomena in the case of pump-line nozzle fuel injection systems - Prevalent in the early 90'es. (*Kim et al., 2008; Lapuerta et al., 2008; Majewski & Khair, 2006; Mccormick et al., 2001; Szybist et al., 2007; Tsolakis, 2006)*. The common-rail engines, widely used today, are also associated with increased NO_x emission when using biodiesel, but this is ascribed to a reduction in heat dissipation by soot radiation as no injection advance due to biodiesel properties take place in these engines (*Kim et al., 2008; Lapuerta et al., 2008*). Biodiesel are furthermore associated with higher cetane numbers, but this property decreases the premixed combustion, due to a swift evaporation and ignition, thereby reducing pressure/temperature gradients and lowering NO_x formation *(Lapuerta et al., 2008)*. Today's engines employs a delayed start of ignition in order to control NO_x emissions, the use of biodiesel in such an engine will counter this delay and re-centre the combustion process.

The impact of biodiesel on emission and PM composition will depend on the biodiesel properties as well as engine layout and driving cycle. The utilisation of biodiesel is, however, generally associated with decreasing emissions of particulate matter and products of incomplete combustion (HC and CO). The reduced particulate matter emissions has been ascribed to the absence of sulphur (sulphate particulates) and soot precursors (aromatics) in the fuel, the higher oxygen accessibility in the flame (a higher oxygen content of the fuel) and an improved soot oxidation due to a more amorphous soot structure/increased reactivity and the advance of the combustion process (*Lapuerta et al., 2008; Mccormick et al., 2001; Szybist et al., 2007*). The fuel-incorporated oxygen prevents carbon atoms from participating in soot precursor reactions, through the formation of either CO or CO_2 by decarboxylation of the ester group (*Szybist et al., 2007*). The obtained particulate matter will consequently mainly consist of SOF, which due to the absence of sulphur species, may be successfully targeted by oxidizing catalysts to obtain further reductions in PM emissions (*Majewski & Khair, 2006*). Local quenching of the flame at low load conditions may, however, yield SOF-rich PM emissions from biodiesel higher than the emission of reference fuels (*Arai et al., 2008*). The PM particle size distribution depends on the combustion process as well as the extent of dilution and the method of analysis, making comparisons difficult. A characteristic left-shoulder peak (20-46 nm) in the particulate number distribution have, however, been reported for biodiesel combustion by some authors - *Arai et al., 2008* (exhaust from 4-stroke DI engine fuelled with 20 % palm oil biodiesel measured after 1:100 dilution) & *Tsolakis, 2006* (exhaust

from DI engine fuelled with rapeseed methyl ester measured after 1:10 dilution). The absence of this left-shoulder peak at elevated temperatures (120 $^{\circ}$C), in the work of *Kim et al., 2008,* indicate a composition dominated by condensed hydrocarbons (Exhaust from DI common-rail engine fuelled with soybean biodiesel measured after 1:500 dilution and heating to 120 $^{\circ}$C).

The influence of the fuels chemical structure (technical grade as well as real world feedstocks) on NO$_x$ and PM emissions were investigated by *Mccormick et al., 2001* on a six cylinder, 4-stroke heavy-duty turbo-charged truck engine during US federal procedure transient tests. No significant differences in emissions were observed for methyl and ethyl esters of the same fatty acid, but essentially constant low PM emissions were obtained for neat biodiesels with a density below 0.89 g cm^{-3} and a cetane number above 45, compared to a 300 ppm sulphur certification fuel. Biodiesel outside these fuel specifications caused increased PM emissions. The majority of the investigated biodiesels caused increased NO$_x$ emissions compared to the certification petrodiesel, but nearly saturated esters (<1.5 doable bonds) did reduce NO$_x$ emissions. Saturated esters with long carbon chains generated the lowest NO$_x$ emissions, but these fuels are also associated with poor cold flow properties. Decreased NO$_x$ emissions were obtained in the case of fuels with high cetane numbers (>68), which were inversely correlated with the density and iodine number of the fuels.

1.6.2 Biodiesel interaction with emission control technologies/devices

The performance of emission control devices may be significantly affected by the changed emission concentration and characteristics facilitated by a shift of fuel source (such as petrodiesel to biodiesel). The changes and potential benefits or problems in diesel particulate filter performance will be of particular interest to this work.

Several authors have reported decreasing balance point temperatures during biodiesel combustion - i.e. the temperature at which a constant pressure drop is obtained due to equilibrium between particulate deposition and oxidation. This point needs to occur at a temperature within the typical duty cycle of a diesel vehicle, to minimize the need for active regeneration (fuel penalty). This characteristic temperature is usually obtained by increasing the engine load, and thereby exhaust temperature, in steps, making it a function of the engine

load-performance as well as the particulate reactivity. Some disagreement does, however, exist concerning the actual extent of the balance temperature decrease facilitated by biodiesel.

Szybist et al., 2007 observed a balance temperature decrease from 320 to 290 ^{o}C (catalytic filter) using ULSD and B100 (soy-based biodiesel) and only a minor decrease with B20 in a Cummins turbo-diesel engine. *Tatur et al., 2007* also report of no significantly changed filter regeneration performance using an undefined B20. *Boehman et al., 2005* observed a balance point temperature decrease from 335 ^{o}C to 308 ^{o}C (catalytic filter) using LSD and B20 but no change with ULSD and B20 (315 ^{o}C) in a 6-cylinder Cummins turbodiesel engine. While *Williams et al., 2006* report of a 112 ^{o}C and 45 ^{o}C balance temperature decrease (catalytic filter) with B100 and B20 soy-based biodiesel respectively, compared to 2007 ULSD certification fuel in a 6-cylinder Cummins ISB DI engine. *Williams et al., 2006* and *Boehman et al., 2005* furthermore report of a significant increase in regeneration rate (transient development in backpressure of a preloaded filter at 348-357 ^{o}C and 480 ^{o}C respectively) even at low biodiesel blend ratios (B5-B20). Different explanations have been suggested for the increased particulate reactivity/lower regeneration temperature. *Szybist et al., 2007* and *Boehman et al., 2005* note that the balance point temperature coincided with the maximal NO_2 concentration – NO_2 is a more aggressive soot oxidiser than O_2 at low temperatures (*Williams et al., 2006*). Maximal conversion of exhaust NO to NO_2, and thereby subsequent soot oxidation, can be obtained by a precious metal catalyst located upstream of the particulate filter. *Boehman et al., 2005* demonstrated, by TGA/differential scanning calorimetry, an increased oxidative reactivity of soot (40-50 ^{o}C lower ignition temperature) from B20 blends compared to ULSD and a low sulphur diesel. This increased particulate reactivity has been attributed to a more amorphous and disordered soot nanostructure, compared to the typical shell-core structure of petrodiesel and an increased surface oxygen functionality (*Boehman et al., 2005; Szybist et al., 2007*). *McCormick, 2008* found that the majority of the increased regeneration rate at 460 ^{o}C, were due to an increased soot reactivity, with only a minor contribution from the lower engine soot output.

Conclusions

The substitution of fossil petroleum-derived diesel with biodiesel can potentially increase energy renewability, reduce political dependability on oil-producing nations and benefit public health (lower CO, HC and PM emissions). A limited availability of resources as well as a lower energy content, poor cold flow properties and an increased degradation of rubber fittings have, however, so far limited the penetration of biodiesel to low percentage blends with petroleum-derived diesel.

Current and future European legislation, concerning emissions from the transport sector, focuses on fuel quality as well as engine emissions and calls for further reductions in the emissions of NO_x and PM from diesel vehicles. Engine design optimisation, implementation of emission control devices or fuel substitution is already taking place, and is expected to become even more pronounced as future emission legislation is implemented. SCR catalysts (urea or hydrocarbon) and NO_x adsorbers are currently being developed for application on cars/trucks, while diesel oxidation catalysts and particulate filters are commercially available.

The use of biodiesel/biodiesel blends may generate slightly increased NO_x emissions (≤ 10 %), due to an advanced injection/combustion and reduced heat dissipation by soot radiation. Lower PM emissions are, however, also obtained, due to the absence of sulphur and soot precursors in the fuel, the advanced combustion process and higher oxygen accessibility in the flae (fuel oxygen). The generated PM is, furthermore, rich in condensed hydrocarbons compared to conventional petrodiesel.

The use of biodiesel/biodiesel blends have furthermore been reported to benefit the regeneration of diesel particulate filters (i.e. lower regeneration temperatures), through either an increased particulate reactivity, an increased NO_2 concentration (benefits the oxidation) or a decreased particle concentration (lower deposition flux to overcome). The exact importance/extent of the different mechanisms does, however, remain unsettled. Some of the biodiesel ash species may, however, cause a long-term catalyst potential deactivation (i.e. higher regeneration temperatures) through ash deposition, but this is another issue to be investigated.   .

Bibliography

Arai M.; Saito, T.; Furuhata, T. Effect of Biodiesel Fuel on Direct Injection Diesel Engine Performance. *Journal of Propulsion and Power* **2008**, 24(3), 603-608

Boehman, A.L.; Song, J.; Alam, M. Impact of Biodiesel Blending on Diesel Soot and the Regeneration of Particulate Filters. *Energy & Fuels* **2005**, 19(5), 1857-1864.

Dieselnet - http://www.dieselnet.com/ Ecopoint Inc: Bramalea, ON, 2008.

Directive 98/70/EC of the European Parliament: The Quality of Petrol and Diesel Fuels. **1998**.

A Comprehensive Analysis of Biodiesel Impacts on Exhaust Emissions; Environmental Protection Agency (EPA): Washington DC, 2002.

International standard EN 14214: Automotive fuels. Fatty acid methylesters (FAME) for diesel engines. Requirements and test methods: **2003.**

International standard EN 590: Automotive fuels. Diesel. Requirements and test methods. **2000.**

Johnson, T. Diesel Engine Emissions and Their Control. *Platinium Metals Review* **2008**, 52(1), 23-57.

Kim, M.Y.; Yoon, S.H.; Hwang, J.W.; Lee, C.S. Characteristics of Particulate Emissions of Compression Ignition Engine Fueled With Biodiesel Derived From Spybean. *Journal of Engineering for Gas Turbines and Power* **2008**, 130 (5).

Kittelson, D.B. Engines and Nanoparticles: A Review. *Journal of Aerosol Science* **1998**, 29(5-6), 575-588.

Kittelson, D.B.; Watts, W.F.; Johnson, J.P.; Rowntree, C.J.; Goodier, S.P.; Payne, N.J.; Preston, W.H.; Warrens, C.P.; Ortiz, M.; Zink, U.; Goersmann, C.; Twigg, M.V.; Walker, A.P. Driving Down On-Highway Particulate Emissions. *SAE Technical paper 2006-01-0916, SAE World Congress & Exhibition*, Detroit, MI, April 2006.

Lapuerta, M.; Armas, O.; Rodriguez-Fernandez, J. Effect of biodiesel fuels on diesel engine emissions. *Progress in Energy and Combustion Science* **2008**, 34(2), 198-223.

Majewski, W.A.; Khair, M.K. Diesel Emissions and Their Control, SAE International, 2006.

Maricq, M.M. Chemical characterisation of particulate emissions from diesel engines: A review. *Aerosol Science* **2007**, 38 (11), 1079-1118.

Mccormick, R.L Quality, Stability, Performance, and Emission Impacts of Biodiesel Blends. *U.S. DOE office of Vehicle Technologies "Mega" Meret Review*, Bethesda, MD, February 2008.

Mccormick, R.L.; Graboski, M.S.; Alleman, T.A.; Herring, A.M.; Shaine Tyson, K. Impact of Biodiesel Source Material and Chemical Structure on Emissions of Criteria Pollutants from a Heavy-Duty Engine. *Enviromental Science Technology* **2001**, 35(9), 1742-1747.

Neeft, J.P.A.; Makkee, M.; Moulijn, J.A. Diesel particulate emission control. *Fuel Processing Technology* **1996**, 47(1), 1-69.

Ning, Z.; Cheung, C.S.; Liu, S.X. Experimental investigation of the effect of exhaust gas cooling on diesel particulate. *Journal of Aerosol Science* **2004**, 35 (3), 333-345.

Szybist, J.P.; Song, J.; Alam, M.; Boehman, L. Biodiesel combustion, emissions and emission control. *Fuel Processing Technology* **2007**, 88 (7), 679-691.

Tatur, M.; Nenjundaswamy, H.; Tomazic, D.; Thornton, M. Biodiesel Effects on the Operation of U.S. Light-Duty Tier 2 Engine and Aftertreatment Systems. *Diesel Engine-Efficiency and Emissions Research (DEER) conference*, Detroit, MI, August 2007.

Tsolakis, A. Effects on Particle Size Distribution from the Diesel Engine Operating on RME-Biodiesel with EGR. *Energy & Fuels* **2006**, 20 (4), 1418-1424.

Williams, A.; McCormick, R.L.; Hayes, R.; Ireland, J. Biodiesel Effects on Diesel Particulate Filter Performance. *Milestone Report NREL/TP-540-39606* **2006**.

Yokoi, T.; Shinzawa, M.; Matsumote, Y. Measurement repeatability improvement for partcile number size distributions from diesel engines. *JSAE Review* **2001**, 22(4), 545-551.

Zevenhoven, R. Non-ideal gases in diesel engine processes. *First Biennial Meeting and General Section Meeting of The Scandinavian-Nordic Section of the Combustion Institute*, Gothenburg, April 2001.

Appendix I

EN 590 (European requrements for conventional diesel with up to 5 % biodiesel)

EN 14214 (International requrements for biodiesel)

Proporty	Unit	EN 590	Test method	EN 14214	Test method
Cetane index	-	≥ 46.0	EN ISO 4264	≥ 51.0	EN ISO 5165
Density (15 ^{o}C)	Kg m^{-3}	820-845	EN ISO 3675 EN ISO 12185	860-900	EN ISO 3675 EN ISO 12185
Viscosity (40 ^{o}C)	mm^2 s^{-1}	2.00-4.50	EN ISO 3104	3.5-5.0	EN ISO 3104
Flash point	^{o}C	> 55	EN ISO 2719	> 101	ISO CD 3679e
Oxidation stability		≤ 25 g m^{-3}	EN ISO 12205		
Lubricity^a	μm	≤ 460	EN ISO1 2156-1		
Copper strip corrosion (3 hrs at 50 ^{o}C)		Class 1	EN ISO 2160	Class 1	EN ISO 2160
Distilation temperature at which 95 V7V % is recovered	^{o}C	≤ 360	-		
Aciud value	Mg KOH/g			≤ 0.5	EN 14104
Iodine value	-			≤ 120	EN 14111
Oxidation stability (110 ^{o}C)	hrs			≥ 6	EN 14112
Fatty acid methyl ester	V/V %	≤ 5	EN 14078		
Ester content	Wt. %			$\geq 96,5$	EN 14103d
Ash	Wt. %	≤ 0.01	EN ISO 6245		
Sulfated ash	Wt %			≤ 0.02	ISO3987
Carbon residue (at 10 % distilation residue)	Wt. %	≤ 0.3	EN ISO 10370	≤ 0.3	EN ISO 10370
Alkali metals (Na + K)	mg kg^{-1}			≤ 5	EN 14108 EN 14109
Phosphorus	mg kg^{-1}			≤ 10	EN 14107p
Polycyclic aromatic hydrocarbons	Wt. %	≤ 11	EN ISO 12916		
Sulphur	mg kg^{-1}	≤ 50 ≤ 10 (2009)	EN ISO 20846, EN ISO 20884	≤ 10	-
Water	mg kg^{-1}	≤ 200	EN ISO 12937	≤ 500	EN ISO 12937
Total contamination	mg kg^{-1}	≤ 24	EN ISO 12662	≤ 24	EN ISO 12662
Methanol	Wt %			≤ 0.2	EN 14110l
Linolenic acid methylester	Wt %			≤ 12	EN 14103d
Polysaturated methylester (≥ 4 double bonds)	Wt %			≤ 1	EN 14103
Monoglyceride	Wt %			≤ 0.8	EN 14105m
Diglyceride	Wt %			≤ 0.2	EN 14105m
Triglyceride	Wt %			≤ 0.2	EN 14105m
Free glycerine	Wt %			≤ 0.02	EN 14105m EN 14106
Total glycerine	Wt %			≤ 0.25	EN 14105m

^{a} corrected wear scar diameter (wsd 1,4) at 60 ^{o}C

Appendix II

REBECa – WP IV – Formation and transformation of particles and other pollutants from engines using biofuel
Diesel engine setup - Design, construction and commissioning

Brian Brun Hansen

September 2011

Department of Chemical Engineering
Technical University of Denmark
Building 229
DK-2800 Kgs. Lyngby
Denmark

Contents

1. Introduction

Recent years have seen a growing concern regarding CO_2 emissions as well as street-level air quality, in particular particulate emissions from the transport sector. This has sparked initiatives such as the use of biodiesel or biodiesel/diesel blends in the highly effective diesel engine and the introduction of diesel particular filters (DPF). However, a better understanding of the interaction between emissions (NO_2, particulate reactivity, particulate composition etc.) and particulate filter performance/regeneration is desired in order to optimize both their short and long-term interaction.

The experimental setup has been constructed in order to supply the necessary experimental facilities for work package IV of the REBECa project (Renewable Energy in the transport sector using Biofuels as Energy Carriers). The project is funded by the Danish Board of Strategic Research and managed by the National Environmental Research Institute (DMU). The WP IV project have been conducted as a post.doc study, with associated B.Sc and M.Sc projects, focussing on emissions from biodiesel engines and their interaction with diesel particulate filters.

This design report will document the ideas and principles behind the constructed experimental setup (diesel engine with filtration). First the requirements to the setup will be presented, followed by an introduction to the setup, safety assessment and finally description of commissioning experiments performed by B.Sc student Helga Hubeck-Graudal, B.Sc student Vinni Rønde and M.Sc student Joachim Bachmann Nielsen. Appendices will contain manuals and, specifications and lists of components.

2. Requirements

The experimental setup is located in the eastern process hall of building 228 (DTU), alongside CHEC's other pilot scale test facilities.

The requirements of the experimental setup have been compiled through a literature review[1] and communication with project chemist Henrik Christensen (Dinex A/S). The perspective is to study the emissions obtained with different diesel fuels as well as performance of a catalytic diesel particulate filter at different particulate concentrations, particulate properties and NO_2 concentrations.

To sum up the required features are:

- Generation of a representative diesel engine exhaust
  - *Gaseous (O_2, CO, CO_2, NO_x, SO_2) and particulate concentrations and properties similar to reported values*
- The setup must be able to preheat the exhaust before the particulate filer
  - *This makes it possible to make a decoupling of engine and DPF performance*
- The setup must be able to dilute the exhaust before the particulate filer
  - *Simulation of different emission levels/engine optimisations*
- The setup must be able to add NO_2 to exhaust before particulate filer
  - *Simulation of upstream oxidation catalyst to increase NO_2 concentration*
- Flexibility must exist regarding the exhaust flow
  - *Exhaust can either pass a particulate filter, be led directly to the stack or a combination thereof*
- Representative sampling and measurement of (O_2, CO, CO_2, NO, NO_2, gaseous HC, PM, particle size distribution) before and after filter and monitoring/measurement of filter temperature and pressure drop (loading)

3. Description of setup

The main components of the diesel engine experimental setup are illustrated in the process and instrumentation diagram (PI) in Figure 1. A list of the components can furthermore be found in Appendix I.
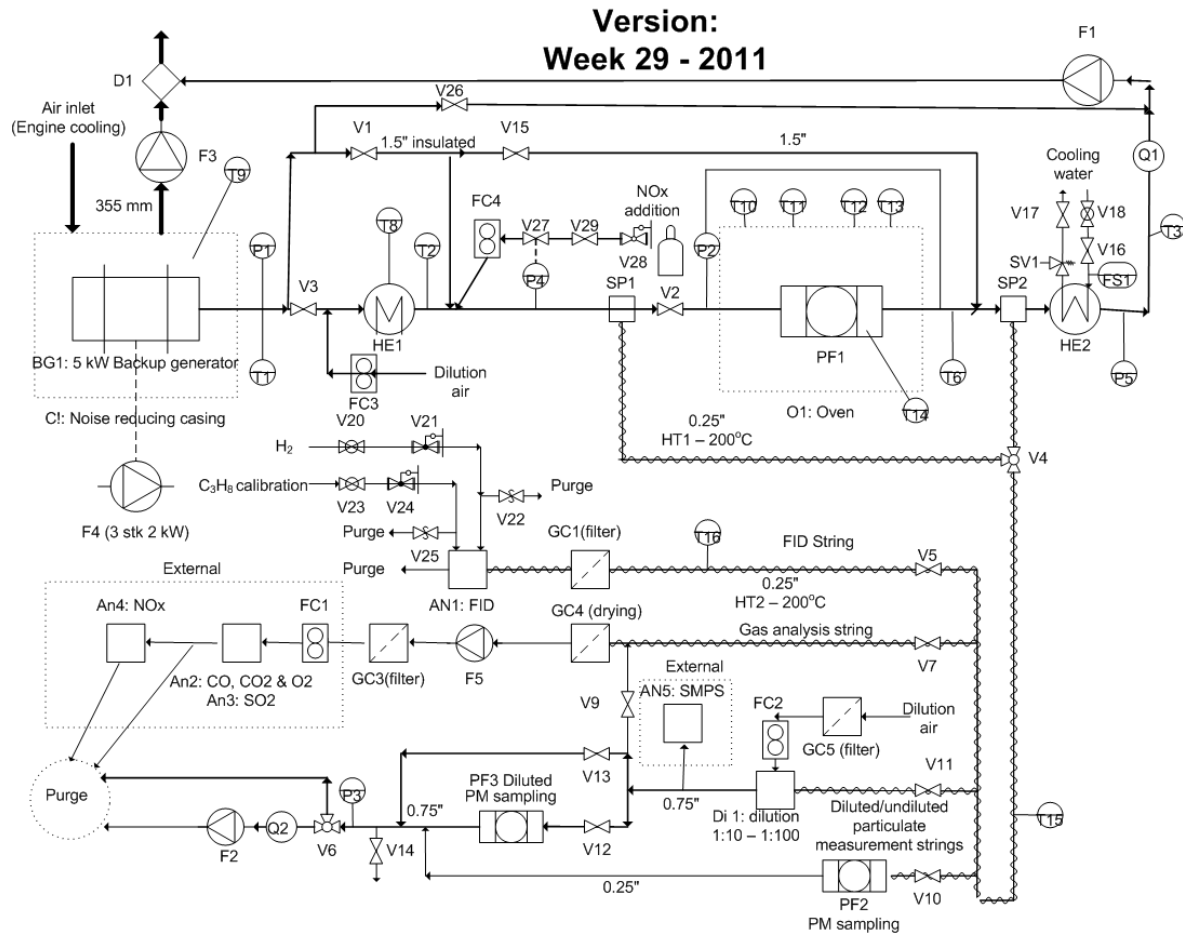
Figure 1: *PI diagram for diesel engine experimental setup (For list of components see Appendix I).*

The diesel engine (BG1: backup generator) is located in a ventilated, noise-reducing casing (C1). Cooling air is withdrawn from outside the building and discharged to the atmosphere alongside the exhaust by a fan (F3). A one-way/check valve (D1) prevents reflux of the exhaust back to the engine/process hall. 3 2 kW ventilators (F4) placed outside of building 228 are used to vary the engine load between 40 and 120 %. The generated exhaust can be heated (electrical pre-heater HE1), diluted and NO_x can be added before it passes through a

particulate filter (PF1), which is located in a three-stage oven (O1) that can ensure a constant filter temperature. During start-up it is possible to bypass the filter (valves 2 & 15) until the desired exhaust temperature is obtained. The development in pressure and temperature across the filter (T14 and P2) is monitored in order to study the particle retention and possible onset of regeneration. The exhaust is subsequently cooled (HE2) and the flow rate measured by a venture nozzle (v1). Dilution of the exhaust gas can be obtained by partial by-pass of the exhaust (V26 – leading to the stack) and the addition of dilution air (FC3). Figure 2 illustrates the engine box, cooling air piping etc.

Figure 2: *Diesel engine, noise reducing casing, cooling air pipes and oven with DPF inside.*

Withdrawal of exhaust gas samples can be performed before (SP1) and after (SP2) the filter by using a heated three-way valve (Valve 4). The sample stream is led to the sample rack (Figure 3), trough heat-traced sample lines, where it can be distributed to gas phase analysis (2 strings) or particulate analysis (3 combinations).

- FID string: The concentration of volatile hydrocarbons in the gas phase is measured by a flame-ionizing detector (FID) after filtration (GC1) is performed to remove particulate matter. The line is heat-traced and its temperature is kept at 200 $^{\circ}$C (labview specification of set point for T16) in order to prevent hydrocarbon condensation. H_2 and C_3H_8 are supplied to the FID at 1 bar and 2 bars respectively. Overpressure valves (V22 and V25), upstream of the FID will open in case of failure of V21 or/and V24 and thereby protect the FID from excessive pressures.

- Gas phase composition string: The concentration of CO, CO_2, O_2, SO_2, NO and NO_x in the gas phase is measured after filtration, drying and cooling. Drying by water condensation is avoided in order to retain NO_2 in the gas phase – instead a water permeable membrane (Permapure LCC) is used.

- Particulate collection from exhaust: The undiluted exhaust is led through valve 10 (valve 11 closed) and the particulate matter is collected on filter PF2 after the pump (F5) is started. The sampling time, flue gas flow rate (**Q2**) and filter temperature are recorded/noted. In order to avoid particle condensation the piping is heat-traced (sP = 200 $^{\circ}$C, controlled though labview specification of set point for T15).

- Particulate collection from diluted exhaust. The exhaust is diluted 1:5 (valve 11 open and 10 closed) and the particulate matter is collected on filter PF3. The sampling time, the flue gas flow rate (**Q**2) and the dilution ratio (using the CO_2 string) are recorded.

- Particle size measurement: By starting the flow of dilution air (FC2) and partially opening valve 11, a fraction of the exhaust is diluted up to 1:100. A small fraction of the diluted exhaust is sent to the scanning mobility particle sizer (either as a side-stream from the diluted or though valve 14). The remainder of the diluted stream is led directly to purge (V6), in order to avoid excessive pressure in the gas clock (Q2). The dilution ratio is determined based on the detected CO_2 concentration before (V7) and after (V11 and V9) dilution.
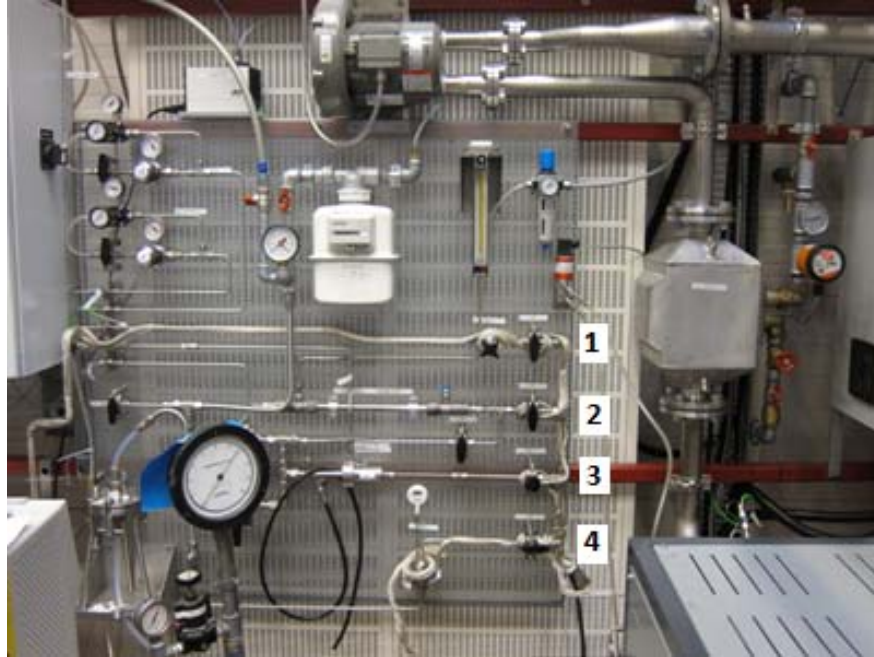
Figure 3: 1) FID string, 2) gas analysis string, 3) SMPS/dilution string and 4) PM collection string [2].

Selected data for the experimental setup is presented in table 1.

Table 1: Main data for experimental setup.

Property	
Exhaust flow	30 Nm^2/hr
Max. exhaust temperature	250 ^{o}C
Max HE1 out temperature*	700 ^{o}C
Engine	4 stroke
Engine load options	0, 40 and 80 %
DPF	Dinex catalytic
	Dinex non-catalytic
DPF dimension	D = 80 mm L= 130 mm

Ensure that the set point of the pre-heater is well below this value

3.1 Engine modifications

The 6Kw diesel backup generator (Table 2) purchased from Eurocommerce APS has been modified in a number of ways to perform better as part of the experimental setup.

- The ignition is controlled from a central setup panel
- The engines turns off in case of lack of cooling water (FS1) or excessive engine box temperatures (T9)
- The load is controlled from the same panel (3 ·2 kW fans)
- A larger more durable car battery that can be continuously charged has replaced the original internal battery.
- An on/off switch has been installed on top of the engine

Table 2: Main data for the 1 cylinder diesel engine.

Property	
Maximal load	6 kW
Maxiaml conmtinous laod	5 kW
Power	10 HK
Frequency	50 Hz
Cooling	Air
Stroke	4
Size	418 cc
RPM	3000

3.2 Filter design

The cylindrical diesel particulate filter has been designed to obtain a gas velocity inside the filter in the range of 2-4 m/s and a space time (τ^{-1}) of 100000 h^{-1}. The filter dimensions (Ø80) available from Dinex A/S also influenced the design.

The filter has been designed based on an estimated flue gas flow rate of 27 Nm^3/h, which corresponds to 66 m^3/h at 673 K. For a filter diameter of 80 mm this corresponds to a velocity of 3.7 m/s, which is within the acceptable range. In order to obtain a space time of 100000 h^{-1} a volume of 0.66 L and a length of 133 mm is necessary.

4. Safety assessment

In this section the safety considerations concerning the experimental setup will be presented, together with initiatives to prevent/minimize safety episodes. In order to achieve this the operation manual (Appendix II) should be followed closely.

4.1 Discharge to the environment

The 30 Nm^3/hr diesel exhaust containing CO, SO_2, NO_x (< 1000 ppm) and PM are diluted 1:100 by the cooling air stream and discharged from the roof of building 228. The majority of the soot PM will normally be captured by the particulate filter. The small amounts of exhaust from the sample lines are furthermore led to an existing purge system.

4.2 Consumption from building supply

The following main consumption from the building supply have been identified

- Cooling water for HE2 (~ 750 l/hr)
- Dilution air to be added to the exhaust line (< 30 Nm^3/hr)
- Driving air for ejector pump (< 60 Nm^3/hr)
- Electricity for oven (2.6 kW) and pre-heater (5 kW)

The following gas cylinders has been connected to the setup

- H_2 (40 ml/min for FID) – shared with high pressure reactor (045-12)
- C_2H_8 (25 l/hr for FID calibration)
- NO_2 (added to exhaust in selected experiments)

4.3 Main operational risks

1. **Excessive noise**

   The loudest part of the setup (the engine) is located in a noise-reducing casing

2. **Steam development in HE2**

   Flow switch (FS1) turns off engine and pre-heater (HE1) in the absence of cooling water. A safety valve (SV1) triggers at 10 bar to avoid excessive pressure build-up in the cooling system.

3. **Evaporation and ignition of diesel**

   A temperature guard in the noise reducing casing (T9) turns off the engine (and ther the heat source) if the temperature surpasses 45 ^{o}C – i.e. comes within 10 ^{o}C of the flash point of diesel. The engine is furthermore turned of in the case of a power outage.

4. **Overheating of exhaust pre-heater (HE1)**

   A temperature guard (T8) was established to turns of HE1 if the temperature of its outer surface exceeds a given temperature (to prevent it from breaking due to overheating). However, this system does not respond swift enough to save the pre-heater in the absence of flow, so a flow switch should instead be installed (yet to be established). The operator must furthermore be aware that the inlet temperature does not surpass 400 ^{o}C.

5. **Exhaust leaks to surroundings**

   Leaks of exhaust containing CO, PM, SO_2 and NO_x to the surroundings is prevented by operating the system at an under pressure – controlled by F1 and P1.

   No_x addition can furthermore only take place if under pressure is present (otherwise P4 triggers safety valve V27).

5. Test experiments

The standard operating procedure for the setup can be found in appendix II and the STA analysis procedure in appendix III.

5.1 Commissioning experiments

The commissioning experiments performed by *Hubeck-Graudal & Rønde, 2011*[2] and *Nielsen, 2011*[3] identified the following issues, which were subsequently addressed, and the resulting setup is the one described in this report.

- Damage to ΔP2 due to water condensation (New elevated ΔP2 location now used)
- The side stream pump previously used at F1 were not able to generate sub pressure (Replaced)
- Internal back-up generator battery drained fast (Replaced with external car battery)
- FID overheating (Metal lid has been loosened)

5.2 Selected experimental data

Selected exhaust and DPF data from the studies of *Hubeck-Graudal & Rønde, 2011*[2] and *Nielsen, 2011*[3] are shown below (Fuel types: Q8 ultra low sulphur diesel, Emmelev rapeseed methyl ester & DAKA tallow methyl ester):

- Filter efficiency
  Soot ~ 90 % (overall efficiency very dependent on SOF– figure 4)
  Gaseous HC conversion at 250 $^{\circ}$C ~ 50 %
  CO conversion at 250 $^{\circ}$C ~ 90 %

Figure 4: PM samples collected before and after DPF while running with DAKA biodiesel at 80 % load [2].

- Temperature at which regeneration starts:

  Petrodiesel (40 % load) $\sim$ 380 ^{o}C

  Biodiesel (80 % load) $\sim$ 360-370 ^{o}C

- Breakeven temperatures/soot loadings (deposition equals conversion):

  ULSD (80 % load 50 % exhaust dilution) $\sim$ 500 ^{o}C and 125 mbar

  RME (80 % load 50 % exhaust dilution) $\sim$ 475 ^{o}C and 120 mbar

  RME (80 % load 50 % exhaust dilution) with 400 ppm NO_2 $\sim$ 435 ^{o}C and 80 mbar

- Engine exhaust:

  Temperature 0 % load $\sim$ 100-110 ^{o}C

  Temperature 40 % load $\sim$ 150-160 ^{o}C

  Temperature 80 % load $\sim$ 235-250 ^{o}C

  Exhaust flow (All loads) $\sim$ 30 Nm^3/h

- Exhaust composition (ULSD)

  PM:– 0.05 (80 % load) g/Nm^3

  - PM size: 50-300 nm

  O_2: $\sim$ 18 % (0 % load) - $\sim$ 12 % (80 % load)

  CO_2: $\sim$ 2.5 % (0 % load) - $\sim$ 7 % (80 % load)

  CO $\sim$ 800 ppm (0 % load) - $\sim$ 500 ppm (80 % load)

  SO_2: $\sim$ 30-45 ppm

NO_x: ~ 100 ppm (0 % load) - ~ 500 ppm (80 % load)

NO_2: ~ 50 ppm (0 % load) - ~ 100 ppm (80 % load)

5.3 Further issues

To improve the operation of the diesel engine test rig the following modifications is recommended:

- Bypass and dilution degree

  In order to control the fraction of exhaust being bypassed and thereby the dilution degree, the bypass string should be separated from the exhaust string and have its own pump and a valve which can be used for adjustments of the bypass flow.

- Noise from ejector pump

  The connection between the output from the ejector pump and the air pipe from the engine box cooling is a source of considerable noise both next to the experimental setup and to the surrounds of building 228 (through the stack on the roof). Installation of a silencer should be considered.

- Improvement of drying (string to gas analysis)

  A heat-traced filter should be placed before the permapure in order to avoid soot build up in the permapure and thereby a decreased of activity.

- Drainage options to remove water condensation in the pipes

  Drainage options after the DPF and after the ejector pump should be upgraded with on/off valve and hoses leading the water to the floor/drainage

- HE1 overheating

  In order to avoid overheating of HE1 a flow switch could be installed between V3 and HE1, which would shut down HE1 in the absence of a minimum flow. This would require an upgrade of the Eurotherm control cabinet.

6. Conclusions

This report documents the design, construction and commissioning of the diesel engine setup. This setup enables studies of gaseous and particulate engine emissions as well as the interaction with flue gas cleaning units operations (particulate filter). More specifically gaseous O_2, CO, CO_2, NO_x, NO, SO_2 and hydrocarbons can be detected and particulate concentration, composition (soot and SOF), size and reactivity (ignition temperature in STA or filter regeneration temperature) can be studied. Further features are the possibility of diluting, preheating and adding NO_2 to part of the exhaust.

7. References

(1)   Hansen, B.B.; Jensen, P.A.; Jensen, A.D. *Emissions from Engines using Biodiesel – Literature survey*; CHEC report 1002; Department of Chemical and Biochemical Engineering, Technical University of Denmark: Lyngby, Denmark, 2010.

(2)   Hubeck-Graudal, H.; Rønde, V.K. *Emissions from Biodiesel Engines with Particulate Filters*, B.Sc. Thesis; Department of Chemical and Biochemical Engineering, Technical University of Denmark: Lyngby, Denmark, 2011.

(3)   Nielsen, J.B. *Filtration of diesel exhaust gas*, M.Sc. Thesis; Department of Chemical and Biochemical Engineering, Technical University of Denmark: Lyngby, Denmark, 2011.

8. Appendices

Appendix I – List of components

Further details can be found in the folders associated the setup (briefly described in appendix IV).

An1:   Mess & Analysentechnik Thermo FID (incl membrane pump)

An2-4   Central gas analysers (CO, CO_2, O_2, SO_2, NO, NO_2)

An5   TSI Scanning mobility particle analyser (Mobile unit)

BG1   6 kW backup generator

C1   Noise reducing casing

D1   Check valve to avoid exhaust backflow into C1 and process hall

Di1   Dilution tunnel

F1   Exhaust fan (1 " Ellehammer ejector) – controlled by primary air flow

F2   Sample string pump (60 l/hr)

F3   Fan for engine casing (C1) cooling (Lindab AXC 355 mm - 3000 Nm^3/hr)

F4   Fans to supply engine load (3 a 2 kW)

F5   Pump for central gas analysis (60 l/hr)

FC1   Flowmeter (60 l/hr) for gas analysis (part of central gas panel)

FC2   Flowmeter dilution air for sample string (SMPS or PM)

FC3   Flowmeter dilution air for exhaust (<30 Nm^3/hr)

FC4   Flowmeter NO_2 addition (< 1000 ml/min)

FS1   Flow switch cooling water

GC1   Gas conditioning (filter) before FID (200 ^{o}C)

GC3   Gas conditioning (filter) before gas analysis

GC4   Gas conditioning (drying by perma pure LCC) before gas analysis

GC5   Gas conditioning (filter) for dilution air to Di1

HE1   Exhaust pre-heater "Farnam Custom Heat torch 200"

            (controlled based on T2 and desired temperature)

HE2   Exhaust cooling (app 5 kW)

HT1   Heat-traced sample piping –zone 1 (controlled by T15 and labview)

HT2   Heat-traced sample piping – zone 2 (controlled by T16 and labview)

O1   3-stage oven "ENTECH ESTF 90/11 – III" for heating of filter (PF 1)

ΔP1	Exhaust under pressure indicator (0; – 100 mbar)
ΔP2	Pressure drop across particulate filter (0; – 200 mbar)
ΔP3	Under pressure particulate sample string
ΔP4	Under pressure at NO_2 addition (Failure < 20 mbar = V27 close)
ΔP5	Under pressure at flow measurement (**Q1**)
PF1	Diesel particulate filter (Dinex, D = 80 mm, L = 132 mm)
PF2	PM sampling (filter) of exhaust (47 mm Pallflex Tissuequartz)
PF3	PM sampling (filter) of diluted exhaust (142 mm Pallflex Tissuequartz)
SP1	Sampling point before PF1 (Pipe facing exhaust flow)
SP2	Sampling point after PF1 (Pipe facing exhaust flow)
SV1	Safety valve in case of steam development in HE2 (10 bar)
T1	Engine out temperature
T2	Temperature between pre-heater and filter
T3	Exhaust temperature before flow measurement (**Q1**)
T5	Diluted filter temperature (Not established)
T6	Temperature after DPF (PF1)
T8	Temperature of HE1 surface (Safety)
T9	Temperature guard engine box (Safety)
T10	Temperature (Oven zone 1)
T11	Temperature (Oven zone 2)
T12	Temperature (Oven zone 3)
T13	Oven over temperature (Safety)
T14	DPF temperature
T15	Temperature of heat traced piping – zone 1
T16	Temperature of heat traced piping – zone 2
V1	By-pass valve pre-heater (HE1)
	DN 50 Butterfly valve BVFA series (Uni-valve) - T tolerance 600 ^{o}C
V2	Valve before PF1
	DN 50 Butterfly valve BVFA series (Uni-valve) - T tolerance 600 ^{o}C
V3	Valve before pre-heater (HE1)
	DN 50 Butterfly valve BVFA series (Uni-valve) - T tolerance 600 ^{o}C
V4	Heated 3-way valve from either SP1 or SP2 to sample strings

V5	Heat-traced valve to FID
V6	Valve to bypass **Q2** at high flow rates
V7	Valve to gas analysis
V9	Valve to gas analysis (after dilution)
V10	Valve to sample filter collecting from undiluted exhaust
V11	Valve before sample dilution (Di1), partially open for high degrees of dilution
V12	Valve to sample filter collecting from diluted exhaust
V13	Valve for diluted sample string
V14	Valve for a small side-stream of diluted exhaust to SMPS (not used)
V15	By-pass valve PF1 and oven
	DN 50 Butterfly valve BVFA series (Uni-valve) - T tolerance 600 ^{o}C
V16	Valve for cooling water to HE2
V17	Valve for cooling water exiting HE2
V18	Ball-valve to control cooling water to HE2
V20	Open/close H_2 supply from gas storage to FID
V21	Reduction valve H_2 supply to FID
V22	Overpressure valve H_2 line to FID (> 1 bar)
V23	Open/close calibration gas supply from gas storage to FID
V24	Reduction valve calibration gas supply to FID
V25	Overpressure valve calibration gas line to FID (> 2 bar)
V26	Exhaust by-pass valve before air injection
	DN 50 Butterfly valve BVFA series (Uni-valve) - T tolerance 300 ^{o}C
V27	Magnetic valve to cut off NO_2 if $\Delta P4$ fails
V28	Reduction valve NO_2 string
V29	Open/close NO_2 supply from inner wall of 228
Q1	Exhaust flow rate passing or bypassing DPF
Q2	Flow rate of PM sampling stream

Labview data logging

An1:   Mess & Analysentechnik Thermo FID (incl membrane pump)

An2-4   Central gas analysers (CO, CO_2, O_2, SO_2, NO, NO_2)

ΔP2   Pressure drop across particulate filter (4-20 mA)

ΔP5   Under pressure at flow measurement (**Q1**)

T1   Engine out temperature

T2   Temperature between pre-heater and filter

T3   Exhaust temperature before flow measurement (**Q1**)

T6   Temperature after DPF (PF1)

T14   DPF temperature

T15   Temperature of heat traced piping – zone 1

T16   Temperature of heat traced piping – zone 2

Q1   Exhaust flow rate passing or bypassing DPF

Appendix II – Standard operating procedure ver. 1.7

Start-up

- Check the oil and diesel levels and the "breaker" is on
  - Diesel indicator on top of generator (next to diesel tank)
  - Yellow oil-stick inside engine room of generator
  - "breaker" is located in the upper right corner of the engines front panel
- Check that the 2 handles on the venture flowmeter points towards the central pipe
- Start the pc and labview (data logging)
  - Double click "start page" icon on desktop
  - Click white arrow to start
  - Data collection:
    Choose location of file, name, sampling frequency and press start
  - In the screens menu choose "biodiesel"
  - Check that the maximum engine temperature is set to "45 ^{o}C" and max HE1 shell temperature is set to "0 ^{o}C"
- Turn on the electrical cabinet (right side of the cabinet)
  - Press "reset" on the front of the cabinet (blue button)
- Open the diesel supply
  - switch next to glass cylinder inside engine room (upper left side)
- Turn on the on/off switch on top of the engine
  - turn so it points left towards the wall
- Start the exhaust fan (F1)
  - Slowly increase the feed airflow to the ejector pump until a slight under-pressure (app 10 mbar) is obtained (see pressure indicator next to engine box)
- Start the engine box ventilation (green switch on the front of the electrical cabinet).
- Set V1-V3 and V15 to bypass (i.e. no flow through HE1 and oven)
- Check that the cooling water is running
  - Orange bar on flowswitch next to cooler - HE2
- Check that startup battery is connected and is not being charged
- Start the engine (ignition-switch on electrical cabinet)
  - Turn from off, to ignition, to on (for a few seconds)
  - If the engine doesn't start allow the switch to fall back into ignition and try again.
- Set the engine load
  - Turn on 1, 2 or 3 ventilators (front of electrical cabinet)

Use of pre-heater

- Check that the exhaust temperature does not exceed 425 C
- Ensure that exhaust passes through the preheater
- In labview – biodiesel screen – insert max HE1 temperature = 350 ^{o}C and click "ok"
- Approach the desired output temperature is small steps (labview - biodiesel screen – green box)
  - be aware that the maximum is 675 ^{o}C (material specifications)

- Before shutting down the pre-heater, insert max HE1 temperature = 0 $^{\circ}$C and click ok to "reset He1", change desired temperature to 0 $^{\circ}$C and allow exhaust to continue to pass through in order to "cool"

Use of pre-heater + dilution

- Before starting the pre-heater measure the total exhaust by passing it all through (u1), slightly open the by-pass string (V26) until the flow passing though the filter is down to the desired level. And then start addition of dilution air (FC3) until the flow passing the filter is back to the original level.
- Only then turn on the pre-heater and do this in small increments of the desired output temperature.
- Check the dilution ratio obtained by measuring gas phase concentrations and comparing with an undiluted exhaust.
- When shutting down the experiment remember the procedure described under "shot-down" i.e. continue engine operation, but at the same time add dilution air, when this is done close V3 so only dilution air passes through the pre-heater and continue until it is "cooled" down.

Diesel particulate filter

- Turn on the 3 stage oven in which the filter is located
  - The oven panel is next to the cooler (HE2)
  - press "power"
  - Set the temperature of all 3 zones to the temperature of the exhaust
  - press "heat"
- Change the valve settings so the exhaust enters the particulate filter
- The pressure drop across the filter (dP) can now be seen in labview
  - Observe it increase over time as soot deposit
  - Be aware that the pressure drop is temperature dependent
- Filter regeneration can be obtained by bypassing the exhaust and heating the oven.
  - Follow T_{filter} in labview and pass exhaust through the filter every now and then to check dP2
- Filter regeneration can also be obtained by preheating the diluted exhaust (see pre-heater section).
  - Follow dP2 development as well as filter temperature

Sampling

- Insert pre weighed filter in either PF2 or PF3 (
  - if particulate emissions is to be collected.
  - ensure that PF2 is heattraced
- Start the heat-tracing of the sampling lines
  - Choose the "eurotherm" screen in labview
  - Set T15 and T16 to desired temperature
    200 $^{\circ}$C for lines and 50 $^{\circ}$C for the filters (check the actual filter temperature)
- Set the 3-way valve (V4) to either sampling site 1 or 2 (before or after filter)
- Ensure that the exhaust passes through the filter (PF1) when sampling from site 1

Gaseous emissions

- Start the air flow to the permapure and open this analysis string
  - Open valve before permapure
  - Set the dry airflow to the permapure by the flowmeter
  – Open valves in central gas analysis panel
  - Start pump leading to central gas analysis
  - Open flowmeter in central gas panel (aim for 1 l/min)
  – Check that to condensation take place in the piping after the permapure.

Particulate emissions

- Remember that this measurement is highly dependent on heat-tracing and deposition in the piping (flush piping with ethanol and dry with air)
- Insert pre weighed filter in either PF2 or PF3 before starting heat-tracing
- Check the filter temperature with a thermometer
- Note the time and airflow in the lab journal
- Open first valve in sample string
- Start the exhaust flow
  - by starting the pump for PF2 – ensure that the gas flow pass through the gas clock
  - or the dilution airflow for PF3 – ensure that the gas flow bypasses the gas clock.
- When sampling is complete note the time and airflow in the lab journal

FID

- Open the H_2 and FID calibration gas cylinders (gas central 27 and next to gas central 9) as well valves next to the wall and on the rack. Ensure a calibration gas pressure of 2.5 bar, a H_2 pressure of 1 bar and a sample pressure of 1 bar.
- Start the FID and allow the auto calibration to take place

SMPS

- Bypass the gas clock (can't handle high flow rates)
- Start the CPC and SMPS located on a trolley and allow them to warm up while the sampling port is in contact with the atmosphere
- Set the correct flow rate on the CPC display and the DMA model, nozzle size and sheat flow rate on the SMPS (selected based on particle size to be determined)
- Set the SMPS display to "analog"
- Open software on PC and make a SMPS file and enter DMA, impactor, flow rates etc
- When the equipment is warmed up open the dilution string.
- Start the dilution by increasing the flow rate of air into the dilutor
- Connect a side stream from the dilutor to the SMPS and start the measurement by the software

Shut-down

- Ensure that the temperature guard of the preheater (HE1) is set to 0 C, click "ok" and the red light will appear. Set the HE1 target temperature to 0 C.

- Turn off any engine load (1-3 ventilators)
- Continue engine operation, but at the same time add dilution air, when this is done close V3 so only dilution air passes through the pre-heater
- Turn off engine
- Continue cooling air addition until the pre-heater is cooled down and only then stop it
- Stop labview
  - Press "stop all" on any screen
- Turn off the switch on top of the engine (points towards you)
- Close the diesel supply (switch next to glass cylinder inside engine)
- Open drain-valve underneath HE2 (careful may be hot) and in the bypass pipe string and allow condensation to drain. Then run dilution air through the system to dry.
- Stop dilution air addition and close drain-valves

23/5-2011
Brian Brun Hansen

Appendix III – STA procedure

- Initial temperature: 30 °C

- Heating sample to 450 °C at 10 K/min (100 % N_2)

- Isotherm at 450 °C for 15 min (100 % N_2)

- Cooling sample to 120 °C (100 % N_2)

- Heating sample to 750 °C at 10 K/min (90 % N_2, 10 % O_2)

Heating the sample at a rate of 10 K/min in nitrogen up to 450 °C will release the SOF particulate fraction and heating at a rate of 10 K/min in 10 % oxygen up to 750 °C will subsequently combust the soot fraction. The filter material present alongside the sample during this analysis will only show a minimal weight change during this time (2 % loss at 750 °C).

Appendix IV – Content of Biodiesel folders

Location: Can be found at the technician associated with the setup

Folder "Biodiesel ombygning"

- Meetings, plans and mails
- Ejector (F1)
- Valves (V26)
- Flowmeter/flowswitch (FC4)
- Pressure transmitter (P5)
- Magnet valves (V27) - empty
- NO-NO2 addition - empty
- Addition of pressurised air - empty
- PI diagram
- Budget

Folder "Biodiesel"

- Meetings & plans
- Design criteria/components
- Details design & PI diagram
- Ordering parts/brochures (empty)
- Construction/Workshop drawings
- Timetable/budget
- HAZOP
- Manuals
- Invoice/suppliers

Folder "Biodiesel komponenter"

- HE2 Gascooler/flowswitch
- F1 pump (now replaced)
- Preheater (HE1)
- Filters (GC1, PF1, PF2. PF3)
- Engine/backup generator (BG1)
- Oven (O1)
- Flow measurement (**Q1**)
- Noise reducing casing (C1)
- Thermo elements
- Diluter (Di1)
- Valves, manometer & pressure transmitter
- Electricity, montage, list of components
- Heattracing
- Construction
- PI diagram and timetable
- Gas sampling

- Gas conditioning (GC4)

Appendix III

FILTERING OF DIESEL EXHAUST GAS

—————

A MASTER'S THESIS

FROM

CHEC

AT

THE DEPARTMENT OF CHEMICAL AND
BIOCHEMICAL ENGINEERING

TECHNICAL UNIVERSITY OF DENMARK

WRITTEN

BY

JOACHIM BACHMANN NIELSEN

—————

Supervisors

Prof Anker Degn Jensen

and

Assoc Prof Peter Arendt Jensen

and

Postdoc Brian Brun Hansen

←——————→

SPRING
2011

Abstract

The performance of a catalytic diesel particulate filter has been investigated as a result of combusting both petrodiesel and vegetable diesel in a 6 kW back-up generator. Unfiltered diesel exhaust yielded a total PM emission of 58 mg/m^3 and 26 mg/m^3 for the combustion of petrodiesel and vegetable diesel respectively.

For experiments involving filtering of the diesel exhaust in a DPF it was proven possible to relate a given mass of deposited soot per pressure drop exhibited, however, this requires an assumption of unchanged porosity of deposited filter cake independent of temperature and loading. It was possible to achieve balance point operation of the DPF for temperatures above 475°C implying that the catalytic rate of soot oxidation is not sufficient to ensure regeneration of the DPF and the non-catalytic soot oxidation by O_2 becomes increasingly important for increased mass of soot deposited.

A lower mass of soot deposited in the DPF was required in order to achieve balance point operation for the combustion of vegetable diesel compared to petrodiesel. This may be due to a low soot concentration in the vegetable diesel exhaust.

A lower mass of soot deposited in the DPF was required in order to achieve balance point operation for filtering of vegetable diesel exhaust with the addition of ~400 ppm NO_2 upstream of the DPF than for filtering of exhaust with no NO_2 addition. This expresses increased soot reactivity towards oxidation by NO_2.

Isothermal loading allowed for an estimate of the order of vegetable diesel soot oxidation by O_2 with respect to mass. The estimated order was n = 0.6 for conditions where the contribution to soot oxidation from the catalytic rate was negligible compared to a dominating rate by which soot enters the DPF.

Neglecting the catalytic rate of soot oxidation by O_2 the activation energy for vegetable diesel oxidation was determined indirectly from the pressure drop measurements yielding a value of 108 kJ/mol. Equally the activation energy for vegetable diesel soot exposed to ~400 ppm NO_2 was determined as 48 kJ/mol emphasizing increased reactivity of soot towards oxidation by NO_2 compared to O_2.

Problem Statement

Project title: Filtering of diesel exhaust gas

Project type: Msc

ECTS: 30

Period: 01/02-2011 to 30/06-2011

Supervisors: Anker Degn Jensen

                       Peter Arendt Jensen

                       Brian Brun Hansen

Introduction

Recent years have seen a growing concern regarding CO_2 emissions as well as street-level air quality – especially particulate emissions from the transport sector. The diesel engine is more efficient than the gasoline engine which generally means a lower contribution of CO_2 to the atmosphere. However, diesel engines contribute with an increased level of particulate matter in the exhaust gas compared to similar gasoline engines. Over the recent years legislations have enforced the use of diesel particular filters (DPF) and the threshold limit value for emissions of particulate matter (PM) has been continuously lowered. In order for diesel engines to stay competitive with similar spark ignition engines it is therefore of great interest to investigate parameters that will cause an increased operational efficiency of the filter without compromising fuel consumption. Biodiesel is becoming increasingly attractive when discussing topics such as environmental impact; however, biodiesel greatly differs from petro diesel by having different physical and chemical properties for instance higher viscosity and higher oxygen content.

Of great relevance to the operation of the DPF is the regeneration by which entrapped soot is ideally completely oxidized. The regeneration of the DPF depends on many factors such as fuel type and temperature. The use of a proper catalyst will ideally lower the temperature needed for regeneration of the filter, and a break even temperature (BET) at which soot entrapment and oxidation occur at the same rate, is therefore of great relevance as this allows for a continuous regenerating trap (CRT), which ideally requires no maintenance. The presence of NO_2 enhances the filter performance by lowering the BET, however, it is desired to keep the final NO_x emissions low. Findings in the literature concerning the interaction between engines run on biodiesel and particulate filters suggest an improved filter performance. This feature may be attributed to the higher oxygen content in biodiesels compared to petro diesels.

Project Description

It is the aim of this project to look into DPF regeneration through a study of filter performance, particulate properties (concentration, reactivity and size) and gas phase composition. Differences between biodiesel and petro diesel are compared. This project finally contains a modeling of the filter regeneration.

Contents

A series of experiments are set up for a catalytic (CeO_2) wall flow monolith DPF connected to the exhaust of a four stroke diesel back up engine. Filter performance is investigated by changing the following parameters:

- Fuel – Petro diesel fuel and biodiesel (animal and vegetable)
- Temperature – Filter temperature and pre heated exhaust temperature
- Gas flow and particle concentration level particle concentration
- Engine load
- NO_x concentration – addition of NO_2 upstream of the filter

During the experiments the pressure drop across the filter is constantly monitored as this expresses the level of deposition. The composition and reactivity of PM deposited onto the filter is determined by the use of TGA. Break even temperatures for regeneration are ideally found. Emissions are at all times continuously monitored. When experiments have been conducted a mathematical model simulating the behavior of the catalytic DPF is developed.

Dates

This project consists of several reports, which are handed in for feedback over the course of the project duration. Important dates are outlined below:

Literature survey (1st report)   04/03-2011

Experimental investigation (2nd report)   15/04-2011

Discussion of experimental results (3rd report)   03/06-2011

Master Project (final report)   30/06-2011

Preface

This is a master's thesis written at CHEC within the Department of Chemical and Biochemical Engineering at the Technical University of Denmark in the period 1st of February to the 30th of June 2011.

I would like to express my sincere gratitude to Professor Anker Degn Jensen, Associate Professor Peter Arendt Jensen and Postdoc Brian Brun Hansen for their guidance on theoretical as well as practical implications in this project. I would like to thank technicians Carsten Nørby and Nikolaj Vinterberg Nissen and Research Technician Anders Tiedje for their practical support.

_____

Joachim Bachmann Nielsen
S062145

30th of June 2011

Department of Chemical and Biochemical Engineering

DTU, Denmark

Table of Contents

1 Introduction

Recent years have seen a growing concern regarding CO_2 emissions as well as street-level air quality. The diesel engine is more efficient than the gasoline engine which generally means a lower contribution of CO_2 to the atmosphere. However, diesel engines contribute with an increased level of particulate matter in the exhaust gas compared to similar gasoline engines. Over the recent years legislations have caused a demand for the use of diesel particular filters (DPF) and the threshold limit value for emissions of particulate matter (PM) has been continuously lowered. In order for diesel engines to stay competitive with similar spark ignition engines it is therefore of great interest to investigate parameters that will cause an increased operational efficiency of the filter without compromising fuel consumption. Biodiesel is becoming increasingly attractive when discussing topics such as environmental impact; however, biodiesel greatly differs from petro diesel by having different physical and chemical properties for instance higher viscosity and higher oxygen content.

Of great relevance to the operation of the DPF is the regeneration by which entrapped soot is ideally completely oxidized. The regeneration of the DPF depends on many factors such as fuel type and temperature. The use of a proper catalyst will ideally lower the temperature needed for regeneration of the filter, and a break even temperature (BET) at which soot entrapment and oxidation occur at the same rate, is therefore of great relevance as this allows for a continuous regenerating trap (CRT), which ideally only requires occasional removal of accumulated ash. The presence of NO_2 enhances the filter performance by lowering the BET, however, it is desired to keep the final NO_x emissions low. Findings in the literature concerning the interaction between engines run on biodiesel and particulate filters suggest an improved filter performance. This feature may be attributed to the higher oxygen content in biodiesels compared to petro diesels. Also the PM emission is generally lower for the combustion of biodiesels; however, the NO_x emission can be more than 10% higher than for the combustion of petro diesels and may aid in PM oxidation.

This study initially contains a literature study where the basics of diesel engine theory are presented and current properties and differences among different diesels are highlighted. Furthermore diesel emissions are presented and different measures for emission control are discussed. The literature study concludes with a presentation of current findings on the kinetics of soot oxidation by O_2 and NO_2.

A description of the experimental setup used is given followed by preliminary experimental observations and considerations. The latter highlights current uncertainties and limitations imposed by the experimental setup.

Experimental results from the conduction of experiments involving loading of a DPF until ideally balance point operation is achieved are discussed. The results are in an extended data treatment discussed with emphasis on kinetics and models describing filter performance. Results obtained are compared with the literature and findings conducted on similar experimental setup by bachelor students Hubeck-Graudal and Rønde (2011).

2 Literature Study

The following is a literature study which covers the basics of diesel engine theory and highlights current properties and differences among different diesels. Diesel emissions are presented and different measures for emission control are discussed. Furthermore current findings on the kinetics of soot oxidation by NO_2 are highlighted. The findings are briefly summarized in a conclusion.

2.1 Internal Combustion Engines

The internal combustion engine is best described as an engine where typically air used as an oxidizer is mixed with fuel in a combustion chamber. The force exerted by the expanding gasses from the combustion of the fuel is used to power the engine. When dealing with automotive engines designed for road use the force exerted is directly applied to the displacement of a piston. Other types of internal combustion engines include gas turbines and jet engines; however, these are beyond the scope of this study. For automotive use generally two types of internal combustion engines are used namely the diesel and the gasoline engine. Both engines share some common design features but differ in advantages and disadvantages.

2.1.1 Diesel Engine

The diesel engine was patented in 1892 by Rudolf Diesel (Dabelstein et al. 2000). His goal was to create an engine with efficiency as close to the carnot cycle as possible, hence he aimed at creating an engine with the highest theoretical efficiency (Dabelstein et al. 2000). In modern day Europe more than half of the new cars sold are powered by diesel engines mainly due to the superior fuel efficiency of diesel engines compared to gasoline engines of similar power. The common efficiency of the engine in modern cars running on gasoline is typically 26-30% whereas for diesel the efficiency is approximately 45% (Schejbal et al. 2009).

The diesel engine generally works by injection of fuel into the combustion chamber after the air inside the chamber has been compressed. The compression increases the temperature above the auto-ignition point of the diesel fuel and air mixture and fuel is combusted without the need for a spark plug. Diesel engines generally have longer durability, lower greenhouse gas emissions (GHG) emissions and offer safer fuel handling (Chen et al. 2011); however, particulate matter (PM) emissions are higher for diesel engines compared to gasoline engines (see section 2.3.3.1). The diesel engine operates with excess oxygen at all engine operating conditions (Lox 2008). There is naturally aspirated (NA) and turbo charged (TC) engines depending on whether the air-intake is compressed or not (Lox 2008).

2.1.2 Four Stroke Diesel Engine

Relevant for this study is the four stroke diesel engine. This engine follows a four stroke cycle. The name of the engine implies that there is one power stroke for every four piston displacements per cylinder. The engine cycle can be seen in Figure 1

below. The two stroke diesel engine and other variants also exist; however, the four stroke engine is superior for use in passenger cars and trucks due to better fuel efficiency. The two stroke engines are however smaller and hence they are often used where weight and size is an important factor such as in lawn mowers for instance (Majewski and Khair 2006).
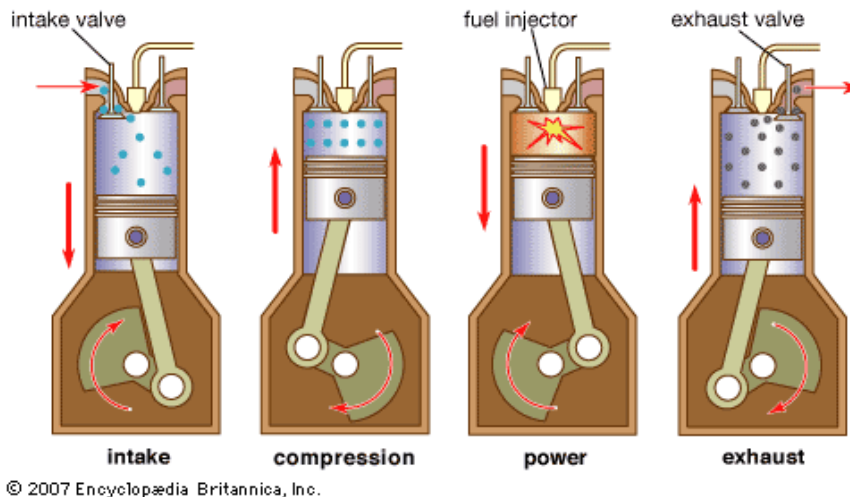
Figure 1 Combustion cycle of a four-stroke diesel engine (Encyclopædia Britannica Online 2007)

For diesel engines, fuel is added just before the piston reaches the top dead center (TDC). The four strokes are explained in the following (Majewski and Khair 2006):

Intake: The intake stroke is an isobaric expansion. The volume of the combustion chamber is increased by movement of the piston. The opening of a valve ensures an inflow of air while keeping the pressure constant. The intake valve is closed when the piston has reached the bottom-dead-center (BDC).

Compression: Assuming no energy loss in the engine the compression stroke is an adiabatic compression, where air inside the chamber is compressed thus reducing the volume and increasing the pressure. Due to the adiabatic conditions the temperature inside the chamber increases typically to between 700-900°C and pressures in excess of 10 bar may be experienced.

Power: The diesel fuel is injected into the chamber before the piston reaches the top dead center (TDC), and the heated conditions ensure ignition of the fuel. The expanding gasses resulting from the combustion displace the piston in the power stroke after reaching TDC.

Exhaust: The exhaust stroke is the movement of the piston to the TDC while the exhaust valve is open. The products from the combustion leave through the exhaust. Typical exhaust temperatures range from 200-450°C.

The moving piston transfers reciprocal motion to rotational motion through the crankshaft. One four stroke combustion cycle yields two crankshaft rotations. The valve control of the engine is controlled by the position of the crankshaft.

Figure 2 shows the pressure inside the combustion chamber of a diesel engine during the transition from the compression to the power stroke. Figure 2 shows the ignition delay which is the period between the beginning of the injection mode and the start of ignition. The ignition delay depends on conditions such as temperature, engine design and the ignition quality of the fuel (Dabelstein et al. 2000). Generally a short ignition delay yields favorable engine operating conditions such as higher efficiency, lower noise and exhaust emissions. The combustion is a combination of premixed and diffusion controlled combustion (Majewski and Khair 2006). Figure 2 also shows the event of prolonged ignition delay which may result in an inappropriate steep pressure increase. This is unfavorable as NO_x emissions may increase and the event is generally accompanied by high noise (Dabelstein et al. 2000).
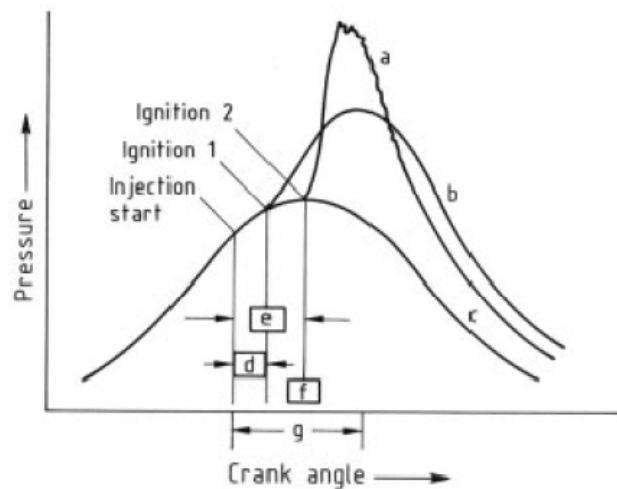
Figure 2 Combustion in a diesel engine a) noisy combustion; b) normal combustion; c) without combustion; d) ignition delay 1; e) ignition delay 2; f) top dead center (TDC); g) injection period (van Setten et al. 2001)

There are generally two types of four stroke diesel engines. There is the direct injected (DI) and the indirect injected (IDI) diesel engine. The IDI engine is

characterized by injection of a fuel into a prechamber where fuel and air mixture commences oxidation before finally entering the combustion chamber. The DI diesel engine does not utilize a prechamber and fuel is directly injected into the combustion as the name implies. The IDI engines generally exhibit lower noise and both a lower pressure and temperature inside the combustion chamber. The former may lead to greater passenger comfort and the latter generally leads to a lower NO_x formation (see section 2.3.5). Greater pumping losses are however attributed to the IDI engines. Furthermore the increased surface area from the pre chamber leads to increased heat losses. These factors contribute to DI diesel engines having greater fuel economy with up to as much as $10 - 15\%$. Modern cars are now primarily DI engines due to this (Majewski and Khair 2006). The compression ratio for DI engines can be as high as 20:1 (Dabelstein et al. 2000). The clearance volume is the volume of the engine cylinder that is not swiped by the piston and therefore equals the volume inside the cylinder when the piston is at top dead center. This volume is related to the compression ratio (see Figure 3).
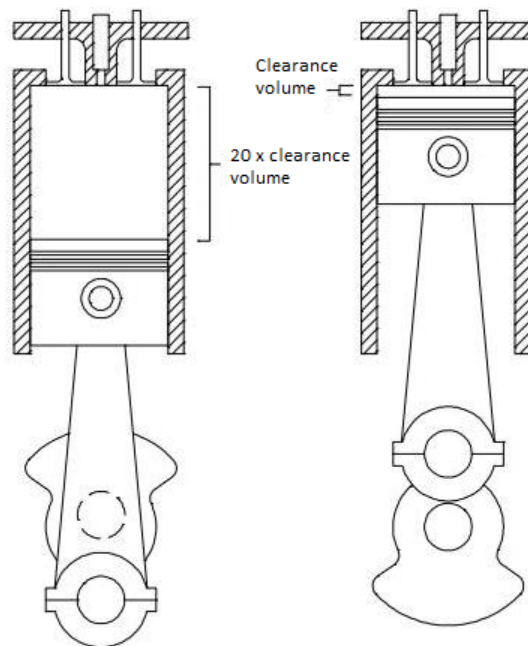
Figure 3 Schematic representation of the clearance volume for a cylinder with a compression ratio of 1:20

2.1.3   Back-Up Generator

Back-up generators (BUGs) may be preferred for laboratory experiments due to reduced level of complexity and cost compared to automotive engines. However, on-

road testing of automotive diesel engines is also widely used together with test-benchs. Comparative studies on BUGs and automotive engines are limited. Shah et al. (2004) conducted comparative measurements on elemental carbon (EC), organic carbon (OC) and PM emissions for a series of BUGs and Heavy Heavy-Duty Diesel Trucks (HHDDT). The fraction of EC stems from pyrolyzed fuel whereas he OC fraction stems from unburned fuel, lubricating oil and combustion byproducts. It was observed that the fraction of EC/OC was greater for BUGs than for the diesel trucks. The difference was more pronounced with increased engine load. This behavior is believed to be attributed to the steady state operation of BUGs. A more dynamic engine operation of the HHDDTs is attributed as the driver must occasionally throttle to maintain a constant driving speed. For different engine loads and operation modes the PM emission from the BUGs were generally 1.2 – 7 times higher than for the HHDDTs. Increased particle emissions per distance travelled were observed during driving simulating urban traffic compared to driving at highway cruise speeds (Shah et al. 2004).

2.2   Fuel and Oil

Different requirements exist for gasoline and diesel fuels (Dabelstein et al. 2000). The latter must ignite more easily, which is achieved by having a high cetane number and hence a high ignition quality. Factors such as density of the fuel affects the fuel consumption and cold flow properties, lubricity, viscosity and stability affect mainly the reliability of engine performance. The volatility of the diesel fuel does not greatly affect the exhaust emission which is the case for gasoline engines (Dabelstein et al. 2000). The different aspects affecting diesel engine operation are briefly discussed in the following.

2.2.1   Diesel Fuel Properties

Important fuel properties are presented and briefly discussed in the following.

2.2.1.1   *Ignition Delay*

As mentioned earlier a shorter ignition delay is favorable. This is achieved by having a higher ignition quality of the fuel indicating a higher cetane number (CN). The cetane number is a comparative measurement of the ignition quality. It is determined by comparison with reference values for a specific engine and fuel operation at both CN = 0 and CN = 100. Ignition delay can be improved by additives (Dabelstein et al. 2000).

2.2.1.2   *Density*

The density of the diesel fuel is mainly an indicator of the mass of fuel that is introduced to the combustion chamber for a given injection volume. Higher densities lead to an enrichment of the fuel-air mixture and hence a higher power output. Higher densities may however also increase particulate matter (PM) emissions and

cause black smoke. The maximum allowed density for diesel fuels is 845 kg/m^3 in Europe (Dabelstein et al. 2000).

2.2.1.3 Sulfur Content

Many studies have revealed an increase in PM emissions when sulfur is present in the fuel. This is due to the formation of sulfates (typically sulfuric acid, boiling point=337°C (Lide 2010)) that are trapped in the diesel particulate filter (DPF) and are often released during regeneration of the filter (see section 2.3.6). The particles may however disrupt filter performance. Furthermore, the combustion of fuel with sulfur content may yield the formation of sulfuric acid which can contribute to engine corrosion and thereby deteriorate the engine. The sulfur content in fuel is however mainly determined by tax incentives. Given countries as Germany for instance have a widespread availability of sulfur free fuels due to high taxations (Dabelstein et al. 2000).

2.2.1.4 Phosphorous and Alkali Metals

Phosphorus and alkali metal content is mainly found in biodiesels and lubrication oils and often in low quantities; however, both phosphorus and alkali metal deposits in exhaust after-treatments systems and engine respectively can be disruptive due to accumulation (Almeida 2008).

2.2.1.5 Cold Flow Properties

Cold flow properties become increasingly important when the engine is operated in colder climates. The Cold Flow Plugging Point (CFPP) indicates the operability limit expected for a diesel fuel in modern engines. The cloud point of the fuel indicates the temperature at which wax crystal may start to form and does not by itself indicate an operability limit of the fuel (Dabelstein et al. 2000).

2.2.1.6 Viscosity

If the viscosity of the fuel becomes too low, wear in the injection pump may be attributed. If the viscosity of the fuel becomes too high it may obstruct the injection process and hence greatly affect the mixing. In Europe the viscosity of diesel fuel must comply with ISO standards indicating limits on viscosity of 2.0 – 4.5 mm^2/s at 40°C (Dabelstein et al. 2000).

2.2.1.7 Volatility

Diesel fuels generally have a greater boiling range than gasoline, however, the latter depends to a greater extend on having a proper volatility in order to ensure lower exhaust emissions. Volatility affects properties such as viscosity, flash point, autoignition temperature, cetane number, density and cold flow properties (Dabelstein et al. 2000).

2.2.1.8 Fuel Stability

The stability of the fuel affects safe storage and transportation. Also the potential for deposits and corrosion in engine parts is of great concern. European ISO standards dictate a minimum flash point of 55°C for diesel as a safety measure (Dabelstein et al. 2000).

2.2.1.9 Engine Emissions due to Fuel Properties

As mentioned earlier, diesel properties may affect emissions of both gaseous components and PM. The European Programmes on Emissions, Fuels and Engine Technologies (EPEFE) conducted a series of experiments to investigate the effect on emissions. The results are summarized below in Table 1 and Table 2. Generally the presence of monoaromatics has no measurable impact on emissions and studies on the effect of polyaromatics were provided with insufficient data to draw any conclusion on the importance of this factor. The lowering of sulfur content and density however were verified to have a reducing effect on PM emissions. An increase in ignition quality from only CN=50 to CN=55 proved in the EPEFE investigation to lower both CO, hydrocarbon and NO_X emissions as well as PM emissions. Table 1 and Table 2 show smaller differences between the results obtained for light- and heavy-duty vehicles. This may be attributed to the generally higher exhaust temperatures of heavy-duty vehicles.

Table 1 Summary of effects of diesel fuel properties on emissions in light-duty vehicles (Dabelstein et al. 2000)

	Change	CO	HC	NO_x	PM
Reduce sulfur	2000 to 500ppm	no effect	No effect	No effect	-2 to -10%
Reduce density	850 to 820kg/m^3	-2 to -10%	-2 to -10%	No effect	< -20 %
Increase cetane number	50 to 55	-10 to -20%	-10 to -20%	-2 to +2%	-2 to -10%

Table 2 Summary of effects of diesel fuel properties on emissions in heavy-duty vehicles (Dabelstein et al. 2000)

	Change	CO	HC	NO_x	PM
Reduce sulfur	2000 to 500ppm	no effect	No effect	No effect	-10 to -20%
Reduce density	850 to 820kg/m^3	No effect	No effect	-2 to -10%	-2 to -10%
Increase cetane number	50 to 55	--2 to -10%	-2 to -10%	-2 to -10%	-2 to -10%

2.2.2 Diesel Fuel Components

Diesel is generally composed of a mixture of many distillation products from an oil refinery. The diesel fuel may be a mixture of hydrocarbons with different structural moieties such as *n*-paraffins, isoparaffins, olefins, naphtenes and aromatics which all affect fuel properties and engine operability. The effect of the aforementioned hydrocarbon groups on ignition quality, cold flow properties, calorific value, density and smoking tendency are summarized in Table 3 below. Generally the use of *n*-

paraffins yields a good ignition quality with a favorable low smoking tendency. The cold flow properties however are poor and the volumetric calorific value is low indicating low fuel efficiency. Generally the combination of paraffinic and aromatic substructures in the fuel molecules can reduce cold flow issues while still maintaining sufficient combustion properties (Dabelstein et al. 2000).

Table 3 Properties of various hydrocarbon groups with regard to their suitability as diesel fuels (Dabelstein et al. 2000)

	Ignition quality	Cold flow properties	Volumetric calorific value	Density	Smoking tendency
n-paraffins	Good	Poor	Low	Low	Low
Isoparaffins	Low	Good	Low	Low	Low
Olefins	Low	Good	Low	Low	Moderate
Naphtenes	Moderate	Good	Moderate	Moderate	Moderate
Aromatics	Poor	Moderate	High	High	High

2.2.3 Diesel Additives

The general definition of additives is the concentration of a given substance to be less than one percent (Dabelstein et al. 2000). Additives are added to the fuel in order to improve fuel performance as this may effectively differentiate the fuel on the market. The most important additives are discussed in the following.

Ignition improvers: Additives may be added to the diesel in order to achieve a favorably higher cetane number. The additives work by assisting in the formation of free radicals that can accelerate the fuel combustion chain reaction. Ignition improvers may be alkyl nitrates, ether nitrates, alkyldiglycol nitrates and organic peroxides (Dabelstein et al. 2000).

Detergents: Detergents are primarily added to reduce the effect of deposit formation inside the engine, where deposits may inhibit valve mobility and lower the efficiency of the spray nozzle to finely disperse the fuel. In the event of the latter increased fuel consumption and PM emissions may be observed due to complete reaction to a lesser extent. Effective detergents are amines, imidazolines, amides, succidinimides, polyalkyl succinimides or amines and polyetheramines (Dabelstein et al. 2000).

Flow improvers: The presence of high molecular mass *n*-paraffins exhibit bad low temperature performance and wax crystals may be formed at lower temperatures which can clog the engine. Flow improvers such as ethylene-vinyl acetate may be added normally in concentrations of 50-500ppm in order to improve cold temperature performance. Wax Antisettling Additives (WASA) typically added in concentrations of 100-500 ppm may also be added in order to lower the settling time of potentially formed wax crystals. Finally cloud point depressants may also be added (Dabelstein et al. 2000).

Lubricity additives: Low sulfur fuel has generally lower lubricity. This can result in engine wear. Fatty acid derivatives may be added in the range of 50-200mg/L in order to achieve high lubricity of the fuel mixture (Dabelstein et al. 2000).

Foaming depressants: During filling of the fuel tank air bubbles may enter the mixture and cause foaming. This is undesired as it hinders the fuelling process. Added in concentrations of typically 10-50ppm, poly-siloxanes depress foam formation and accelerate foam decomposition (Dabelstein et al. 2000).

Antioxidants: Undesired oxidation of the fuel during storage may cause corrosion effects and sediment formation. The later may clog the fuel filter. Trialkylamines added in the concentration of 50 ppm are very efficient in preventing undesired aging of the fuel. Corrosion inhibitors mainly work by lowering the acidity of the fuel and these may also be added. Due to differences in fuel compositions a multifunctional mixture at a concentration of 100 ppm is typically added to the fuel to reduce aging and corrosion effects (Dabelstein et al. 2000).

Dehazers: During oil distillation and later fuel handling water droplets may enter the mixture. Quaternary ammonium salts added in concentrations of 5-50 ppm are effective dehazers functioning by lowering the surface tension of the water droplets (Dabelstein et al. 2000).

Antistatic additives: In order to avoid the potential dangers of electrostatic discharges igniting fuel fumes during rapid pumping the addition of typically 5 ppm antistatic additives may prevent this (Dabelstein et al. 2000).

2.2.4   Biodiesel

Vegetable oils are becoming increasingly important as alternatives to diesel fuel as they are renewable in nature, are easily produced locally and are environmentally friendly (Laza et al. 2011). Vegetable oils however have a high viscosity and to achieve desired combustion performance and prevent clogging of the engine, treatment of the oil is needed (Laza et al. 2011). Blending of oils with lower alcohols or esterification are two pathways that result in increasing the volatility of the fuel. Blending vegetable oil with higher alcohols (C3-C4) in order to reduce viscosity can be advantageous as there is no need for emulsifier or surfactant (Laza et al. 2011). Furthermore the addition of alcohols to the blend contributes to an increased oxygen concentration which reduces PM emissions (Laza et al. 2011). Blending vegetable oil with higher alcohols shows that for increasing concentrations of the latter a decreased viscosity, CFPP, CN and heating value is achieved (Laza et al. 2011). Both vegetable oils and animal fats mainly consist of triglycerides. A lowering of viscosity and increased volatility can be achieved by treating the triglycerides to form

alkylesters and glycerol. The process generally used is catalyzed basic transesterification with methanol whereby glycerol is separated out (Majewski and Khair 2006):
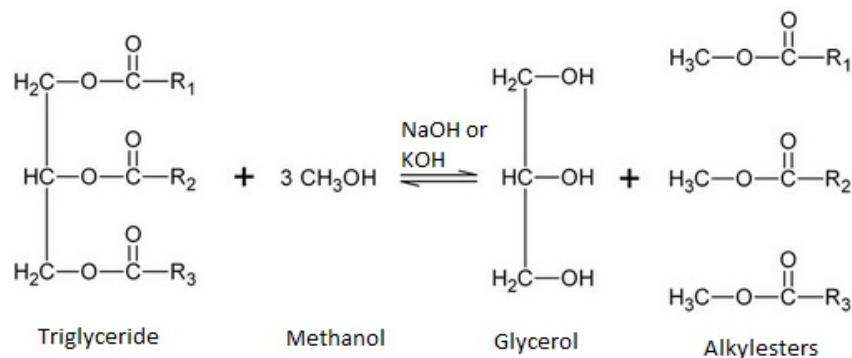
Figure 4 Catalyzed basic transesterification of a triglyceride

2.2.4.1 Properties

Biodiesels generally differ from petro diesels in many properties. Often biodiesels are mixed with petro diesel to satisfy engine specifications where B20 biodiesel implies a blend with 20% biodiesel content and a pure biodiesel is B100.

Sulfur: The sulfur content depends on the feedstock used. Vegetable oils typically contain no sulfur whereas the animal fats typically contain up to 50 ppm. Over the recent years however successful efforts have been made to lower the sulfur content of petro diesels by desulfurization (Majewski and Khair 2006). Ultra-low-sulfur diesels offered contain down to 10 ppm of sulfur (Majewski and Khair 2006).

Polynuclear aromatic hydrocarbons: Biodiesels contain no aromatics and no polynuclear aromatic hydrocarbons (PAHs). This is desired in terms of toxicity compared to petro diesels which may contain up to 40% aromatics. The high concentration of non cyclic aliphatics in biodiesel however reduces the heating value, which obviously is less desired (Majewski and Khair 2006).

Cetane number: Biodiesels contain approximately 11% oxygen whereas petro diesels have no oxygen content. This facilitates easier combustion and generally higher cetane numbers of up to CN=60 are observed (Majewski and Khair 2006). Generally the cetane number for vegetable oils is lower compared to animal fats (Madsen et al. 2009).

Lubricity and volatility: Biodiesels generally have better lubricity which in itself is advantageous; however, an increased viscosity may cause increased engine wear. The components found in biodiesels generally have a lower volatility than those of

fossil diesels. Handling of vegetable oil is generally safer than diesel fuel as the flash point of the former is higher (Laza et al. 2011). Peterson et al. (Peterson et al. 2010) attributed the lower volatility to cause an increased engine oil dilution, which may lead to increased engine wear and may deteriorate the engine if the dilution of engine oil is not monitored.

Biodegradability: The biodegradability of biodiesels is favorable in an environmental sense; however, the fuel is thus susceptible to degradation and water absorption which are unfavorable characteristics (Majewski and Khair 2006).

Fatty acids: Animal fats have a high content of saturated fatty acids whereas vegetable oils predominantly contain a high content of mono- and poly-unsaturated fatty acids. The higher content of unsaturated fatty acids in vegetable oils generally yields a lower viscosity and risk of blocking of the fuel filter compared to animal fats (Madsen et al. 2009).

2.2.4.2   *Effect on Emissions*

Biodiesel and biodiesel blends generally produce less soot when combusted and the temperature required for oxidation of deposited soot inside a DPF is also generally lower compared to the combustion of petro fuels (Peterson et al. 2010)(Boehman et al. 2005). The lower amount of particulate matter produced during combustion of biodiesels increases the time it takes to load the DPF (see section 2.4.1)(Peterson et al. 2010). The generally higher content of unsaturated fatty acids in vegetable oils compared to animal fats may yield a higher NO_x and PM emission (Madsen et al. 2009).

Peterson et al. (2010) reported that combustion of B20 in a light-duty diesel engine yielded an increased amount of oxygenated species in the exhaust such as formaldehyde and acetaldehyde. This trend is argued to be attributed to the higher oxygen content in biodiesels compared to petro diesels (Peterson et al. 2010; Boehman et al. 2005). Also after introduction to a diesel oxidation catalyst (DOC) and subsequent filtration the combustion of B20 showed a sharp increase in water and carbon dioxide emitted, thus implying that the products produced after the DOC are more reactive compared to the combustion of petro diesel. The higher oxygen content in the exhaust possibly aids in faster regeneration of DPF (Peterson et al. 2010; Boehman et al. 2005). Biodiesel fueling also alters the nanostructure and oxidation reactivity of primary soot particles which yields a more amorphous soot structure (Boehman et al. 2005).

The increased oxygen content of biodiesels is believed to cause a generally higher NOx emission compared to the combustion of petro diesels. The combustion of B100 can lead to an increase in NOx emissions of over 10%, and the combustion of B20 typically leads to an increased NOx emission of 2-4% (Majewski and Khair 2006).

With the use of a diesel oxidation catalyst NOx present in the exhaust serves as a contributor to regeneration of the diesel particulate filter (see section 2.4.2)

2.3 Exhaust Emissions

Diesel droplets sprayed inside the combustion chamber do not exert complete mixing with the present oxygen and hence incomplete reaction is inevitable (van Setten et al. 2001). Incomplete combustion of fuel leads to gaseous emissions of unburned hydrocarbons, alcohols, aldehydes, CO and PM. Hydrocarbons different from those present in the fuel may also be emitted due to locally high flame temperatures of excess 1400°C (Lox 2008).

A general reaction scheme for the complete combustion of fossil fuel is shown below in (2.1). The generalized reaction scheme assumes that the petro fuel mainly consists of C and H (Lox 2008).

$$C_mH_n + (m+n/4)O_2 \rightleftarrows mCO_2 + (n/2)H_2O \qquad (2.1)$$
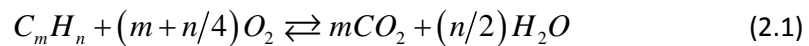
Emission of PM is greater for diesel engines compared to gasoline engines and the emission is generally attributed to the more incomplete reaction occurring when diesel fuel is injected into the combustion chamber is not as finely dispersed as for a spark ignition engine with premixed gasoline. Emissions of CO and hydrocarbons are generally significantly lower for diesel engines than for gasoline engines (Majewski and Khair 2006). NO_x emissions from diesel engines are generally higher than for gasoline engines using a three-way catalyst for reduction (Majewski and Khair 2006). The composition of a large number of volatile and semi-volatile particles in diesel exhaust is still not resolved (Dwyer et al. 2010b). This is especially true during DPF regeneration (Dwyer et al. 2010b). The oxygen is typically available at 5-10% in the diesel exhaust (D. B. Kittelson et al. 2006).

2.3.1 Legislations

PM and NO_x emissions have over the years become increasingly discussed subjects together with Green House Gas (GHG) emissions (Majewski and Khair 2006). Emissions are regulated by tail pipe emission standards of mainly diesel PM, NO_x, HC and CO. Emissions are measured during test cycles of a vehicle reflecting normal driving. The tests currently used for European legislations include the New European Driving Cycle (NEDC) for LDD vehicles and the European Stationary Cycle (ESC) and European Transient cycle (ETC) for HDD vehicles. The NEDC involves both urban driving and high speed driving. The definition of light-duty vehicles is passenger cars with a gross weight of <1305kg and vans weighing <3500kg. Heavy-duty vehicles are trucks and buses travelling at speeds of >25km/h and weighing >3500kg (van Setten et al. 2001). The European methodology for quantifying PM emissions is known as the Particle Measurement Programme (PMP). Particles smaller than 20 nm are not included in the PMP (Dwyer et al. 2010b).The EU emission standards for relevant

emissions are shown below in Table 4 and Table 5 which also include future emission standards that are to be met (Dieselnet 2011):

Table 4 EU emission standards for DI diesel passenger cars (Dieselnet 2011)

Stage	Date	CO (g/km)	HC+NOx (g/km)	NOx (g/km)	PM (g/km)	PN (#/km)
Euro 1	1992.07	2.72	0.97	-	0.14	-
Euro 2	1996.01	1.0	0.9	-	0.10	-
Euro 3	2000.01	0.64	0.56	0.50	0.05	-
Euro 4	2005.01	0.50	0.30	0.25	0.025	-
Euro 5a	2009.09	0.50	0.23	0.18	0.005	-
Euro 5b	2011.09	0.50	0.23	0.18	0.005	$6.0 \cdot 10^{11}$
Euro 6	2014.09	0.50	0.17	0.08	0.005	$6.0 \cdot 10^{11}$

Table 5 EU emission standards for HDD engines (Dieselnet 2011)

Stage	Date	CO (g/kWh)	HC (g/kWh)	NOx (g/kWh)	PM (g/kWh)
Euro I	1992 (>85kW engine)	4.5	1.1	8.0	0.36
Euro II	1998.10	4.0	1.1	7.0	0.15
Euro III	2000.10	2.1	0.66	5.0	0.10
Euro IV	2005.10	1.5	0.46	3.5	0.02
Euro V	2008.10	1.5	0.46	2.0	0.02
Euro VI	2013.01	1.5	0.13	0.4	0.01

A standard for particle number emissions from passenger cars is to be defined no later than the start of Euro 6. The changed focus to particle number emission is due to the potential health effects associated with nano-sized particles (see section 2.3.3).

Legislations generally apply to new cars only; however, fiscal and tax incentives may promote retrofitting of older vehicles with measures to enhance emissions control (Lox 2008).

The Environmental Protection Agency (EPA) regulates the U.S. emissions. Mass-based air pollutions regulations for PM are mainly governed; however, particle number and surface area of emitted particles may be of greater importance due to adverse health effects that may be related (D. B. Kittelson et al. 2006). As the composition of emitted particulate matter depends highly on the sampling method

and temperature the US EPA has defined the diesel particulate as material collected from diesel exhaust gas on a polytetrafluoroethylene-coated glass fiber filter at 45-52°C (van Setten et al. 2001). Dwyer et al. (2010b) emphasizes the need for better understanding of the quality and errors associated with measurement technologies in the future as the European and USA test cycles sometimes show very different results.

2.3.2   Greenhouse Gas Emissions

Emissions from the transportation sector are an important contributor to the total green house gas (GHG) emission. In 2005 the transport sector contributed to 27% of the US national GHG emission (Graham et al. 2008). Generally CO_2 emissions dominate the species of GHG emitted by a diesel engine without after-treatment of the exhaust. For a heavy duty vehicle without after-treatment Graham et al. (Graham et al. 2008) reported that CH_4 emissions account for 0-0.11% and N_2O emissions account for 0.16 – 0.27% of the CO_2 equivalent GHG emissions. It was further reported that N_2O emissions are increased by both the use of a diesel oxidation catalyst and a diesel particulate filter as exhaust after treatment, however, the CH_4 emission remained unchanged. Graham et al. (2008) reported that the use of natural gas compared to diesel fuel can reduce GHG tail pipe emissions by 10-20% on a CO_2-equivalent basis. For biodiesel blends with up to 20% biodiesel content the CH_4 and N_2O emissions have been reported to be reduced by 18% and 10% respectively if no exhaust after treatment is used. However, the CH_4 and N_2O emissions remained unchanged when a diesel oxidation catalyst was used (Graham et al. 2008). During active DPF regeneration of an HDD vehicle Graham et al. (Graham et al. 2008) reported an increase in CO_2 emissions, a 36-72% increase in N_2O emissions and no change in CH_4 emissions.

2.3.3   Particulate Matter

Diesel particulates diminish visibility, interfere with the global heat balance and may settle on plants to interfere with photosynthesis. However, mostly discussed are the effects on human health (van Setten et al. 2001). Particle emissions from diesel engines typically cover the wide size range 3 to 10,000 nm. Scientific studies on the topic of health effects by particulate matter reveal a link between exposures to fine particles less than 2.5μm to adverse health effects (D. B. Kittelson et al. 2006). It is further suggested that ultrafine particles less than 100 nm are detrimental to human health (D. B. Kittelson et al. 2006)(Lee et al. 2008). Smaller particles have higher particle deposition efficiency in human respiratory tracts and the deposition in the alveolus is highest for ~20nm particles (D. B. Kittelson et al. 2006). Toxic compounds may be carried by adsorbtion onto the smaller soot particles and thereby also cause health effects if inhaled (van Setten et al. 2001). Diesel PM is believed to cause asthma, persistent bronchitis and lung cancer (van Setten et al. 2001). The suspected carcinogenic properties are related to polynuclear aromatic hydrocarbons (PAH) (Lox 2008), however, this may lack reliable data (van Setten et al. 2001).

PM consists mostly of carbonaceous soot and a volatile organic fraction (VOF) of hydrocarbons that have condensed on the soot (see Figure 6)(Walker 2004). The total particulate matter (TPM) is generally classified as a contribution from the solid fraction (SOL), soluble organic fraction (SOF) and sulfates (SO_4) described below (Majewski and Khair 2006). Diesel PM is defined as the non-volatile part of the exhaust at a temperature of 52°C(Majewski and Khair 2006).

Table 6 Definitions of solid fraction (SOL), soluble organic fraction (SOF) and sulfates (SO_4).

SOL	Elemental carbon and ash
SOF	Organic material from fuel and engine lubrication oil
SO_4	Sulfuric acid and water

The particulate matter consists not only of carbonaceous materials but also ash. The ash content varies greatly with the type of fuel used. The ash present is typically metal oxides formed in the combustion chamber as additives from engine lubrication oil may be burned. Sulfates or phosphates may also be the result of this. As the lubricating oil wears the engine, oxides of metal such as iron, copper, chromium and aluminum may also be carried into the combustion chamber by the lubrication oil. Metal oxides from catalytic fuel additives also contribute to the ash formation. Finally corrosion of the exhaust gas manifold and subsequent exhaust gas system may also contribute to the presence of iron oxides in the ash (van Setten et al. 2001).

SOF concentration is strongly dependent on operating conditions and ranges from 10-50% of total PM (Majewski and Khair 2006). The SOF concentration is generally lower for higher engine loads and temperatures (Majewski and Khair 2006). PAHs are contained in the SOF and are highly undesired emissions due to mutagenic and carcinogenic behavior of some PAHs. The PAHs are found in the fuel but may also be generated during combustion. The PAH concentration in diesel PM is typically around 0.5% of TPM. Dioxins may also be present in the SOF and are suspected of having carcinogenic effects as well as increased resistance to biological breakdown (Majewski and Khair 2006).

The main contributor to sulfate particulate emissions is hydrated sulfuric acid while sulfate salts are only present in smaller concentrations. Sulfate particles are formed even though sulfuric acid and water are undersaturated in the gas phase. Nucleation of the most stable sulfate particles are formed at a molar ratio of H_2O to H_2SO_4 of 8:3. The sulfate particles typically consist of 8000 molecules of H_2O and 3000 molecules of H_2SO_4 (Majewski and Khair 2006).

The reactions leading up to the soot formation are extremely complex (van Setten et al. 2001). The main constituent of soot is ethyne which through polymerization eventually forms polycylic structures. The latter are called platelets which stacked together yield crystallites. Turbostratic particles are formed when the crystallites stack together in a random formation around a center and they are

typically 1-2nm in diameter. These steps are called nucleation. The nucleation and the subsequent steps for soot formation are shown in Figure 5 below. Coagulation and surface growth yields 10-30nm spherical primary soot particles. Chainlike aggregates may form these and even larger agglomerates are the result of coalesced soot aggregates (van Setten et al. 2001).
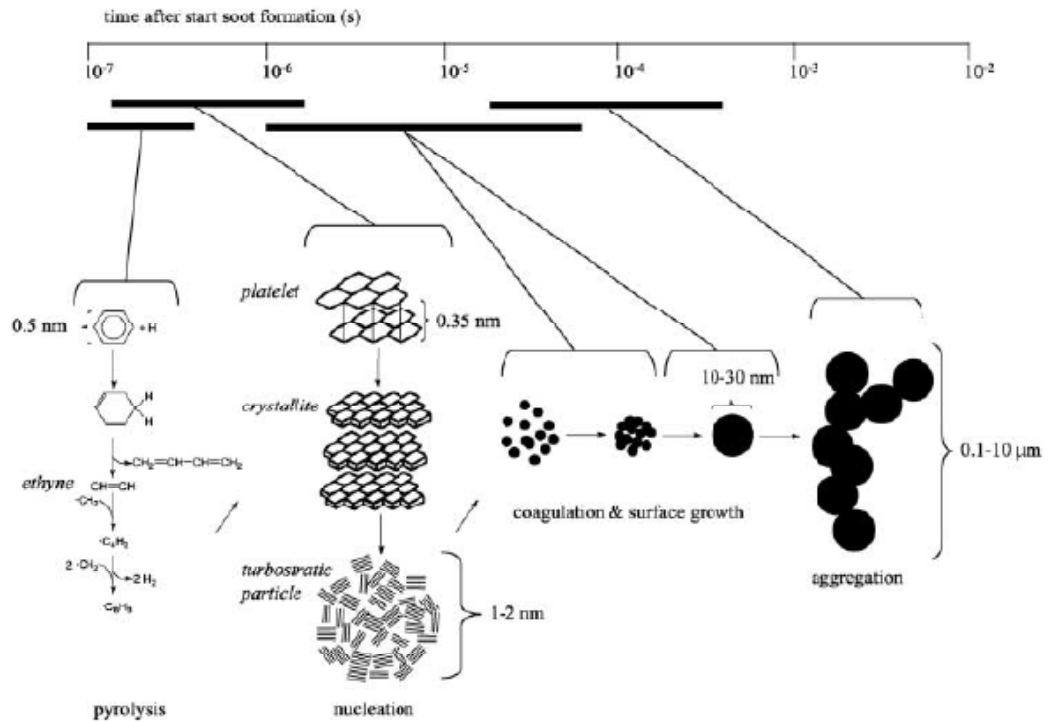

Figure 5 Schematic mechanism of the formation of soot particles (van Setten et al. 2001)

Figure 6 shows the structure of a typical chainlike aggregate onto which hydrocarbons and sulfuric acid droplets may be adsorbed (van Setten et al. 2001).
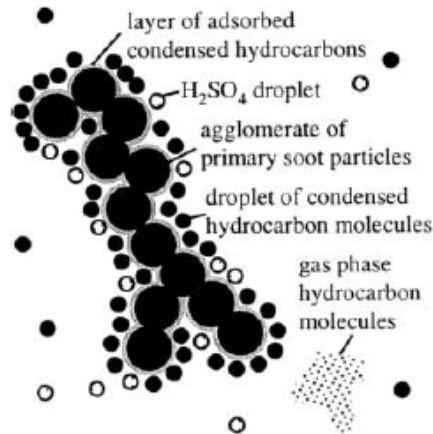
Figure 6 Schematic structure of a chainlike aggregate of primary soot particles and associated compounds (van Setten et al. 2001)

The PM emission is reduced if complete combustion occurs to a greater extend. This is generally achieved by a reduced fuel/air ratio, increased time for combustion, increased fuel-air mixing and higher temperatures. A fuel with a higher cetane number promotes shorter ignition delay with better mixing of fuel and air which leads to reduced PM emissions. Engine design factors such as injection rate and design also affect PM emission level (Majewski and Khair 2006)(van Setten et al. 2001).

2.3.3.1 Size Distribution

The typical size distribution of aerosols from a diesel engine exhaust is shown below in Figure 7. The size distribution is described by mainly three size ranges all often exhibiting local extremes. These size ranges are characterized by nuclei mode (3-30nm), accumulation mode (30-500nm) and coarse mode (larger than 1µm) particles. The nuclei mode particles are mainly volatile organic compounds, sulfuric acid droplets (van Setten et al. 2001) and other sulfates and metallic and carbonaceous compounds (Majewski and Khair 2006). The particles are formed during dilution and cooling of the exhaust gas. Typically the nuclei mode particles contribute to less than one percent of the total aerosol particle mass but up to 90% of the particle number. The accumulation mode particles are primarily carbonaceous agglomerates onto which materials may be adsorbed. The accumulation mode contributes to the majority of the total mass of aerosols. The coarse mode particles are mainly the result of reentrained particular matter deposited on engine and exhaust surfaces. The coarse mode particles typically contribute to 1-20% of the total particle mass (D. B. Kittelson et al. 2006).
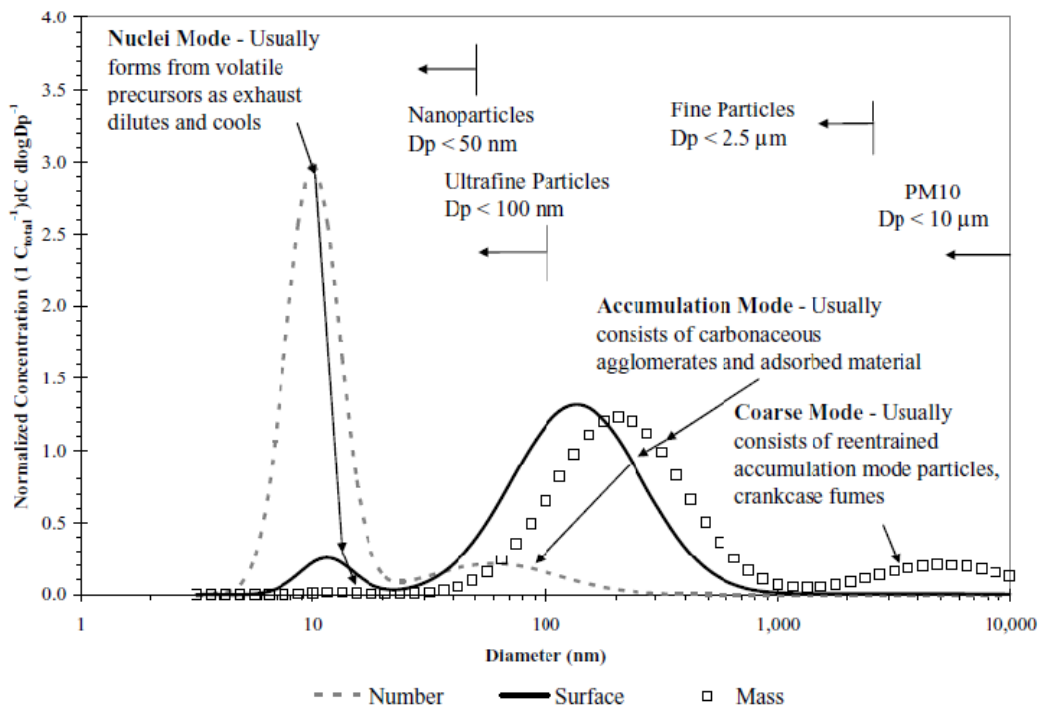
Figure 7 Typical PM size profile of the emissions from a diesel engine indicating the nuclei, accumulation and coarse mode size regions (D. B. Kittelson et al. 2006)

The size distribution from spark ignition engines exhibits similar shape as that from diesel engines, however, less material is present in the accumulation mode region (D. B. Kittelson et al. 2006). Lee et al. (2008) reported that particle number emissions from diesel passenger vehicles with particulate filters are lower than for gasoline passenger vehicles; however, the PM mass has similar values. Particle emissions from the combustion of diesel fuels are generally higher during cold engine start up (Lee et al. 2008). Caroca er al. (2010) reported that for a Euro 5 common rail automotive diesel engine operating under normal conditions the particle number and mass size distributions prior to a DPF were similar for operation with either petro- or bio-diesel fuels. The combustion of the biodiesel fatty acid methyl ester (FAME) lead to a reduction of particle number up to 80% and reduction in mass up to 90% under normal operating conditions compared to standard diesels. During active regeneration of DPF the particle number reportedly increased by 1 order of magnitude with a substantial shift towards larger particle diameters (Caroca et al. 2010).

2.3.4 Hydrocarbons

Hydrocarbons (HC) are either products of incomplete fuel combustion or recombined intermediate compounds exhibiting different structure than that of the fuel. Combustion of engine lubrication oil also contributes to some of the hydrocarbon

emission. Factors such as mixing and engine design play a great role in the nature and quantity of hydrocarbons emitted. Furthermore the type of fuel used plays a major role (Majewski and Khair 2006). Hydrocarbons generally condense through nucleation or adsorption in the exhaust gas. The former yields the formation of new particles while the total particle number remains unchanged if hydrocarbons adsorb onto already existing particles. If less surface area is available for adsorption in the exhaust gas the emission of accumulation mode may be lowered as nucleation of the formed hydrocarbons is favored. This however may yield a dramatic increase in particle number (van Setten et al. 2001).

Gaseous hydrocarbons in diesel exhaust are typically emitted in concentration of 20-300 ppm; however, liquid hydrocarbons are also emitted as PM. The latter fraction generally adsorbs onto soot or other PM (see section 2.3.3). The difference in volatility of different hydrocarbons makes it difficult to make a clear distinction between volatile and particulate HC emissions. Polynuclear aromatic hydrocarbons can be found in both the gas phase and in the PM and are often highly undesired due to potential carcinogenic effects. Many hydrocarbons can undergo photochemical reactions with NO_x in the atmosphere and thus contributes smog formation and ground level ozone. Legislations regulating the HC emission concern only the volatile gaseous HCs (Majewski and Khair 2006).

2.3.5 Nitrogen Oxides

NO_x concentration in diesel exhaust is typically in the range of 50-1000ppm. It is important to limit the NO_x emission as this is a precursor for smog and acid rain and it may disrupt the ozone layer (Majewski and Khair 2006). NO is colorless and odorless while NO_2 is a brown colored gas with an unpleasant smell which means that locally high emissions in urban areas is undesired (Majewski and Khair 2006). Many ways exist to reduce NO_x emission from diesel engines. Selective catalytic reduction (SCR) or NO_x absorption is generally used.

Nitrogen containing constituents of the fuel contribute to NO_x formation; however, thermal NOx formation is the dominant cause for emissions due to low fuel-N content (Lox 2008)(Majewski and Khair 2006). NO generally constitutes more than 70% of the total NO_x in DI diesel engines. Combustion of standard diesels generally yields raw exhaust concentrations of NO_2 at 5-15% of total NO_x, or less than 50ppm (Kandylas et al. 2002a)(Schejbal et al. 2010). Thermal NO formation inside the combustion chamber is well understood and follows the extended Zeldovich mechanism (see reactions (2.2) to (2.4)). The homogenous reaction between N_2 and O_2 proceeds at high temperatures above 1500°C because of the high activation energy required for reaction (2.2).

$$N_2 + O \rightleftarrows NO + N \qquad (2.2)$$

$$N + O_2 \rightleftarrows NO + O \qquad (2.3)$$

$$N + OH \rightleftarrows NO + H \tag{2.4}$$

Gaseous radicals (OH, N, O and NO) are often formed in the flame region during combustion due to locally higher temperatures. OH, N and O are very reactive radicals due to their unpaired electrons and may proceed in various reactions during the combustion process, whereas NO is rather stable in comparison. The NO formation is highly temperature dependant. The NO formation favors high temperatures and pressures (Majewski and Khair 2006)(Turns 2006). In the presence of excess oxygen NO_2 is formed by NO. The residence time for NO inside the combustion chamber therefore affects NO/NO_2 ratio. As the formed NO leaves though the exhaust manifold no additional NO_2 is readily formed. The subsequent treatment of the exhaust with a DOC contributes to an increased NO_2 fraction (see section 2.4.2).

The topic of NO_x emissions is relevant to discuss as hardly any published data on the reactivity of NO_2 with soot under real engine conditions exists. NO_2 readily oxidizes carbon at lower temperatures than oxygen.

2.3.6 Sulfur Oxides

During combustion the presence of sulfur will lead to the formation of SO_2 which is a colorless gas with a characteristic odor. Approximately 2% is further oxidized to SO_3. The latter reacts rapidly with water and forms droplets of sulfuric acid (van Setten et al. 2001).

$$SO_3 + H_2O \rightarrow H_2SO_4 \tag{2.5}$$

The sulfur used to mainly come from the fuel; however, as low-sulfur fuels have become widely available over the recent years, the sulfur content of engine lubrication oil has become an important determinant for sulfur oxide emissions. The formed sulfuric acid is responsible for sulfate PM emissions (see section 2.4.2) (Majewski and Khair 2006). Tail pipe emission of SO_x may contribute to acid rain and is therefore undesired.

2.3.7 Carbon Monoxide

The odorless and colorless carbon monoxide gas is highly toxic as it inhibits oxygen uptake by occupation on hemoglobin in the blood stream which may lead to suffocation. CO is the product of incomplete combustion of hydrocarbons. However due to large excess of air in the lean fuel mixture of the diesel combustion chamber the CO emission is generally extremely low as formed CO is readily oxidized by the excess oxygen in the gas phase. The CO concentration in the diesel exhaust is typically 10-500ppm (Majewski and Khair 2006).

CO is readily oxidized to CO_2 over a diesel DOC (see section 2.4.2). The reaction scheme is shown below:

$$2CO + O_2 \rightleftarrows 2CO_2 \qquad\qquad (2.6)$$

2.4   Emissions Control

For diesel engine exhausts it is desired to reduce the emission of a wide span of compounds (see Table 4 and Table 5). Generally PM is reduced by trapping particles in a filter. The use of an oxidation catalyst reduces the emission of hydrocarbons and CO. NO_x emissions are generally lowered by use of Selective Catalytic Reaction (SCR) or NO_x trapping. Changes in engine design and for example exhaust gas recirculation ratio (EGR) affects various emissions; however, exhaust gas after treatment is a necessity as trade-off effects between emissions are often observed. Trade-off effects are observed between NO_x and PM tail pipe emissions thus complicating matters of emissions control as a way of reducing the NO_x emission is by increasing EGR or retarding injection timing; however, this will contribute to an increase in formed particulate matter (van Setten et al. 2001). A general schematic of an exhaust after-treatment system is shown in Figure 8 below:
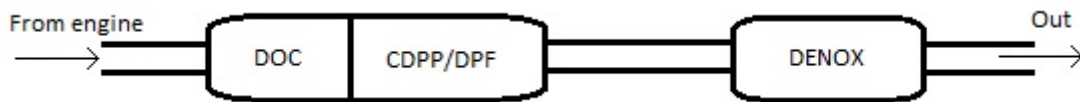
Figure 8 Typical exhaust after-treatment system for diesel cars and trucks. DOC: Diesel Oxidation Catalyst. CDPF/DPS: Catalytic or non-catalytic Diesel Particulate Filter. DENOX: NO_x removal often in the form of SCR or NO_x trapping

A modular design containing the DOC and PDF combined as one unit is popular for retrofitting of old busses and trucks (van Setten et al. 2001). Figure 8 only shows elements relevant for emissions control. If for instance a turbo charger is used it must be positioned upstream of the DPF as ceramic filter flakes or larger particle deposits can potentially be reentrained into the exhaust stream and may destroy a turbocharger downstream of the filter (van Setten et al. 2001). Positioning a turbocharger upstream of the DPF will however contribute to a lowering of the DPF temperature which is generally undesired as higher temperatures facilitate soot oxidation which is needed for the regeneration of the filter (see section 2.4.3) (van Setten et al. 2001). Filter regeneration is the removal of deposited soot by oxidation with either oxygen or NO_2.

2.4.1   Filtration

The DPF functions by trapping soot and thereby reduces PM emissions. Filter deposits cause an increase of filter back-pressure which at higher levels increases fuel consumption and reduces available torque (Yamamoto et al. 2010).Trapped soot is oxidized to regenerate the filter. This process occurs either actively or passively (see section 2.4.3.3). Silicon carbide (SiC) is the preferred filter material as it offers superior physical properties (van Setten et al. 2001). It has a higher thermal

conductivity and melting point than cordierite (α-$Mg_2Al_4Si_5O_{18}$ (Montanaro et al. 1994)) which is generally seen in older vehicles. Montanaro et al. (1994) reported that temperature rather than heat treatment duration is a critical parameter for cordierite stability. The higher thermal conductivity of SiC aids the conductive heat transfer and thereby reduces the temperature of local hot spots that may arise during filter regeneration which may be due to inhomogeneities in soot loading. This reduces the potential for damage done to the filter (Lox 2008). Thermal properties for cordierite and silicon carbide are shown below in Table 7:

Table 7 Structural properties of cordierite and silicon carbide (van Setten et al. 2001)

	Melting point T_{mp} (°C)	Heat Capacity C_p (J/g/°C)	Thermal Expansion Coefficient α (µm/m/°C)	Thermal Conductivity κ (W/m/°C)
Cordierite	1200	0.6	1.0	<0.5
Silicon Carbide	1650	0.75	4.6	11

The filter is generally coated with a catalyst to promote soot oxidation at lower temperatures for the regeneration of the filter (see section 2.4.3.2).

2.4.1.1 Filtration Issues
Generally either fouling or filter damage are the two types of failure that may be observed in a DPF (van Setten et al. 2001).

2.4.1.1.1 Mechanical Damage
Mechanical damage to the filter can be due to vehicle vibrations and mechanical stress (van Setten et al. 2001). Excessive temperature excursions can melt the ceramic filter material. It is proposed by Chen et al. (2011) that these temperature excursions are a dynamic effect following rapid changes in the driving mode during active regeneration of the DPF. Changes in driving mode affect factors such as feed temperature, oxygen concentration and filtration velocity (Chen et al. 2011). Rapid shifts from normal driving to idle during active regeneration of the filter can cause transient temperature excursions with high peak temperatures sufficient to melt the filter material (Chen et al. 2010)(Chen et al. 2011). The shift to idle causes a rapid increase in the feed oxygen concentration and a decreased flow rate. If the latter is faster than the rate at which the feed temperature increases high temperature excursions may be observed (Chen et al. 2011).

A catalytic coating of a DPF may lose efficiency over time as catalyst is lost due to dissolution in water or if high temperatures are achieved the catalyst may evaporate to leave the filter. Sintering of the catalytic material may also reduce available surface area (reduce the number of active sites) and thus greatly affect

catalyst efficiency. If a fuel borne catalyst is used the catalytic efficiency does not depend on catalyst loss or altering of the catalyst structure to the same degree as the catalyst is easily replenished.

2.4.1.1.2   Fouling

Accumulated ash will slowly reduce filter performance as the deposited ash is not removed during regeneration. The filter thus needs to be cleaned periodically. The cleaning however may be troublesome as high temperatures may have caused the ash to adhere to the surface (van Setten et al. 2001).

A catalyst inside a catalytic particle trap may be deactivated in many ways. SO_3 can deactivate the use of catalytic traps. The presence of higher sulfur content in the fuel which leads to a higher SO_3 concentration in the exhaust gas has shown to increase the temperature required for regeneration of the filter. The inhibition may however be reversible depending on the nature of the filter material. The use of metal oxide catalysts as a means of lowering the temperature required for catalytic soot oxidation has shown to cause SO_3 depositions that are not reversible during normal filter regeneration (van Setten et al. 2001). An example on irreversible filter deposition is the reaction between Al_2O_3 which is typically found in the wash coat and SO_3 (Görsmann 2005):

$$Al_2O_3(s) + 3SO_3(g) \rightarrow Al_2\left(SO_4\right)_3(s) \tag{2.7}$$
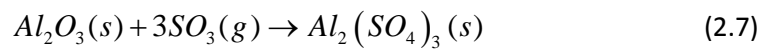
2.4.1.2   *Wall Flow Monolith*

The filter typically used for diesel particulate filters is a wall flow monolith. The monolith has typically a honeycomb structure of square channels, typically 1-2 mm across where the ends of each channel are alternately plugged (see Figure 9). This ensures that the exhaust gas is forced to flow through the porous filter walls, where soot is deposited (Kim et al. 2010). DPF filtration efficiency can be as high as 99% for particulate mass (Yamamoto et al. 2010)(van Setten et al. 2001). An illustration of the closed end wall flow monolith is shown below in fig and a cross sectional view of a soot loaded monolithic channel is seen in Figure 10.
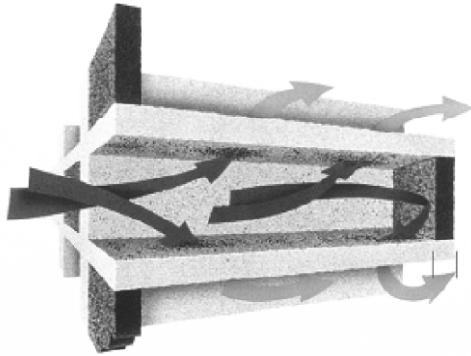
Figure 9 Schematic representation of the mode of operation of a wall-flow diesel particulate filter (D. B. Kittelson et al. 2006)
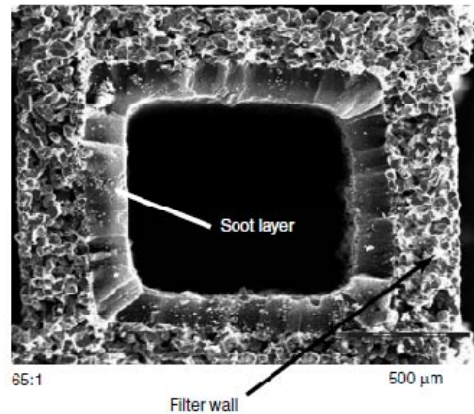

Figure 10 Scanning electron microscopy image showing the layer of trpped diesel particulate matter in a channel of a modern wall-flow diesel particulate filter. The loading corresponds to 10 g particulates L^{-1} geometric volume of filter (Lox 2008)

Filtration of particles in a DPF is normally characterized by two subsequent phases. Initially nano-sized particles are first trapped in the filter pores. This gradually lowers the porosity and hence the permeability of the filter. This first stage is called depth filtration (Bensaid et al. 2009). As soon as the filter pores have become impermeable (maximum packing density has been achieved) a soot layer will build up on the filter walls. This second step is known as cake formation (Bensaid et al. 2009). During cake formation the pressure drop over the filter increases linearly with time (Bensaid et al. 2009)(Bensaid et al. 2010).

It is generally observed that soot does not deposit evenly along the axial component (along the filter walls) of the filter. A minimum soot layer thickness is often observed at around the half of the monolith channel length (Bensaid et al. 2009). Bensaid et al. (2009) reported that also great differences in soot deposition in the radial component (cross section of the filter) may be present. This results in different soot loading of the monolith channels.

The porous wall resistance of the filter is controlling the filtration rate during depth filtration. During cake formation the local resistance of the deposited soot is controlling the filtration rate. The filter resistance typically increases a hundredfold over time and it is during the initial phase of filtration, that the resistance increases at its highest rate (Soldati et al. 2010). Bergmann et al. (2009) reported for a modern DPF equipped diesel passenger car travelling at 100 km/h the filtration efficiency during 3 min on a clean filter was on average 67%. As soot deposits would build the efficiency increased quickly to >99%.

During soot deposition in the DPF the flow is largely changed and the filter back-pressure increases as soot is deposited (Yamamoto et al. 2009). The flow pattern of particles inside the monolith channels are dominated by mainly three mechanisms,

which are drag force, Brownian motion and particle inertia (Liu et al. 2009). Liu et al. (2009) concluded that the most primary determinant of particle motion and deposition is drag force. The importance of the Péclet number (Pe) and Reynold's number (Re) is also stressed. An increase in Pe lowers the effect of Brownian motion. For an increase in Re the effect of particle inertia is enhanced (Liu et al. 2009).

$$Pe = \frac{LV}{D_m} \tag{2.8}$$

$$\mathrm{Re}_p = \frac{\rho VL}{\mu} \tag{2.9}$$

L is monolith channel length, V is linear velocity, D_m is the mass diffusion coefficient, ρ is gas density and μ is the viscosity. The gas flow during normal engine operating conditions exhibits laminar flow as Re<2000 (Liu et al. 2009). During cake formation the flow through the filter cake can generally be described by Darcy's law (see section 2.5.4)(van Setten et al. 2001).

2.4.1.3   Other Filters

An alternative to the closed end monolithic filter is an open filter. These filters can function by deep-bed filtration and ceramic foams or woven ceramic fibers are often used. The deep-bed filters are called open filters due to their way of trapping PM. PM is led through open passages in the filter material and the deposition may occur by inertial interception with the filter material where a particle travelling in an air stream through the filter passageways collides with the filter material as the flow pattern is constantly changed. PM may also be trapped due to simple Brownian diffusion onto the filter material or simply as flow line interception where a particle following a flow line near the filter material is collected by simply touching the filter material. In deep bed filtration the exhaust gas is let through a filtration medium much thicker than the walls in a wall flow monolith thus they are more suited for catalyst support. The larger connected filter structure in deep-bed filters offers better conductive heat transport than wall flow monoliths and therefore also lower temperatures and less thermal stress. The open structure however means that deep-bed filters are less suited for periodic regeneration events as deposited particles may easier be reantrained into the gas stream. Furthermore sudden changes in exhaust flow rate can result in reentrainment of particles. Even though deep-bed filters offer great potential for catalyst support they may still cause issues for an operation with continuous regeneration. The filter generally only becomes efficient after initial particle deposition and if the continuous regeneration at even low temperatures oxidizes deposited soot rapidly an effective initial soot deposition is never achieved (van Setten et al. 2001).

2.4.2 Diesel Oxidation Catalyst

A diesel oxidation catalyst functions by oxidizing gaseous compounds typically in a flow through operation prior to the DPF (D. B. Kittelson et al. 2006). The cell density of the majority of modern flow through oxidation catalysts produced has a cell density of 62 cells/cm^2 (Lox 2008). Precious metals such as Pt supported on metal oxides are often used as catalyst in DOCs (Issa et al. 2008). The platinum loading of modern DOCs can be as high as up to 10g/L (Lox 2008). The flow inside the DOC channels exhibit laminar flow at all engine operation conditions (Lox 2008).

The VOF of soot in the exhaust is removed with high efficiency in a DOC, however, the carbonaceous core of the PM is not converted (Walker 2004). Table 8 below shows the conversion of CO, HC, NO$_x$ and PM after the use of a combined system with a DOC and subsequent use of DPF for a HDD engine in this case operated over the European Stationary Cycle. The use of a DOC almost completely eliminates the presence of CO and HC by the complete oxidation to CO_2 and H_2O. A substantial fraction of PAH is also removed in the DOC (Lox 2008).

Table 8 Conversion of CO, HC, NO$_x$ and PM when using a CR-DPF system on a HDD engine over the European Stationary Cycle (D. B. Kittelson et al. 2006)

	CO	HC	NO$_x$	PM (mass)
Conversion (%)	98.70	98.20	2.10	95.10

The main advantage of using the DOC however is the effect on NO oxidation to NO_2 (reaction (2.10)) (D. B. Kittelson et al. 2006).

$$NO + \tfrac{1}{2}O_2 \rightleftarrows NO_2 \qquad\qquad (2.10)$$
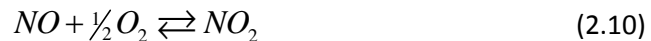
Formed NO_2 is used for oxidation of deposited soot in the DPF and NO is formed (D. B. Kittelson et al. 2006).

The DOC should produce a surplus of NO_2 in order to compensate for periods where the exhaust gas temperature is too low for regeneration; however, large emissions of NO_2 in the vicinity of the vehicle is not desired as NO_2 has an unpleasant smell. The DOC unit does not contribute to a net NO$_x$ increase and emitted NO will eventually be oxidize to NO_2 in the atmosphere (van Setten et al. 2001).

Sulfur present in fuel and engine lubricant forms SO_2 during combustion. The emitted SO_2 is also further oxidized in the DOC to form SO_3 (see reaction (2.11)). During normal vehicle operation the conversion of SO_2 is less than 50% (D. B. Kittelson et al. 2006).

$$SO_2 + \tfrac{1}{2}O_2 \rightarrow SO_3 \qquad\qquad (2.11)$$

The reaction proceeds at temperatures above 300-350°C (D. B. Kittelson et al. 2006)(van Setten et al. 2001). If the exhaust temperature never exceeds 300°C the

SO_3 would never be a problem. This however is inevitable and thus the oxidation catalysts can be tailored to have a lower activity by using rhodium, palladium or V_2O_5 alloyed with platinum (van Setten et al. 2001)(Kim et al. 2003). The compromised activity thus requires higher temperatures for the SO_2 oxidation to proceed (van Setten et al. 2001).

SO_3 forms sulfates on the surface of the DPF and can lead to inhibition of catalyst coating in both DOC and DPF, faster deposit build up and increased PM emissions during regeneration (van Setten et al. 2001). Fouling of the DOC is undesired. Deposits reduce the available catalytically active surface area and thus reduce efficiency. Other deposits such as different carbon species only occur to a minimal extend compared to sulfur oxides (Lox 2008). Emitted sulfates are typically <30nm in size and hence the use of a DOC in the presence of sulfur contributes to an increased emission of nucleation mode particles (D. B. Kittelson et al. 2006).

2.4.3   Soot Oxidation

The temperature of a DPF under normal driving conditions is typically in the range of 200-450°C (Issa et al. 2008). At real driving conditions the average exhaust temperature of a light-duty vehicle is frequently lower than 200°C (Lee et al. 2006). Having oxidation of deposited soot occur within the exhaust temperature range of a typical duty cycle or requiring a minimum of active regenerations is a critical requirement for DPFs. Catalytically coated DPF, fuel-borne catalysts and a DOC upstream of the DPF all contribute to a lowering of the temperature required for soot oxidation (Boehman et al. 2005). For diesel exhaust emissions generally two gasses can sufficiently facilitate the oxidation of soot, namely O_2 and NO_2 (Jeguirim et al. 2009).

It is generally understood that the reactivity of soot depends on the initial structure of the deposited carbon material. Disordered amorphous carbon mainly has a higher rate of oxidation and requires a lower activation energy (lower temperature needed for regeneration) than carbon in graphite structure (Song et al. 2007).

Not only the initial carbon structure of the soot may determine reactivity towards oxidation but the presence of specific surface groups may also enhance oxidation (Song et al. 2007). The oxidation may cause structural and micro-porosity changes which alter the reactivity during oxidation; however, the intrinsic rate of oxidation remains unchanged (Song et al. 2007).

Biodiesel fueling also alters the nanostructure and oxidation reactivity of primary soot particles which yields a more amorphous soot structure that enhances the rate of soot oxidation. This implies that there is a structural relationship between soot nanostructure and oxidation reactivity (Boehman et al. 2005).

Chemisorbed oxygen groups such as carboxyls, lactone and carbonyls are believed to enhance soot reactivity as these groups may provide a means of lowering the energy requirement for oxidation through an intermediate pathway (Song et al.

2007). Carboxylic and lactone groups begin to decompose already at temperatures as low as 250°C (Song et al. 2007).

The structure of soot from the combustion of B100 is generally more ordered in structure than Fischer-Tropsch (FT) fuel (zero oxygen content synthetic fuel) and Song et al. (2007) determined it was 5 times more reactive. Song et al. (2007) emphasize that the oxygen content of the diesel and hence the amount of oxygen groups present in the formed soot is the more important factor determining soot reactivity than the initial carbon structure. Experiments have also shown that different engine conditions can produce soot with different reactivities (Song et al. 2007).

2.4.3.1   Non-Catalytic Soot Oxidation

The non-catalytic activity of soot is determined by properties such as structure, impurities and temperature. The structure of the carbon expresses the surface area concentration of active sites which are readily attacked by atmospheric oxygen. Setten et al. (2001) has suggested a unified mechanism for the non-catalytic combustion of soot with oxygen. It involves the oxidation to form ketone surface complexes on the edges of the soot structure. A semiquinone is eventually formed resulting in a lowering of the connecting C-C bond. The complex then decomposes to form CO/CO_2 (van Setten et al. 2001).

2.4.3.2   Catalytic Soot Oxidation

Soot oxidation is promoted at lower temperatures if catalyzed. The catalyst may be present as a fuel additive or incorporated into the DPF.

2.4.3.2.1   Catalytic Fuel Additives

Using catalytic fuel additives yields a deposited soot layer in which the catalyst is incorporated. This provides direct contact with the soot. If the fuel-catalyst solution is injected upstream of the DPF the operation is called quasicontinuous regeneration or passive-active regeneration. Using a diesel already containing a catalytic additive may provide the means of a passive regeneration strategy (van Setten et al. 2001). The catalytic activity of fuel additives is enhanced by the presence of volatile components in the soot (Stratakis et al. 2003).

For the addition of cerium the initiation of soot oxidation occurs at lower temperatures for higher cerium concentrations. It is suggested that this effect is due to faster catalytic oxidation of adsorbed hydrocarbons (Stratakis et al. 2003). Experiments with a mixed platinum-cerium catalyst fuel have been conducted not only showing a decreased temperature required for initiation of soot oxidation but also an increase in fuel efficiency by 5-7% and a reduction of PM by 10-25% (van Setten et al. 2001).

Copper and iron have shown to spontaneously initiate regeneration at temperatures lower than 200°C. This however may result in undesired high local
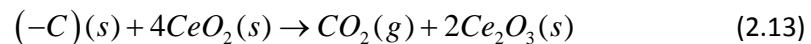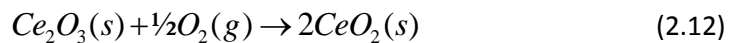
temperatures that may compromise the filter as the catalyst is not necessarily distributed evenly across the filter (van Setten et al. 2001).

2.4.3.2.2 Catalytic Diesel Particulate Filter - CDPF

A catalytic diesel particulate filter is a DPF with catalytic material supported on the filter. The process of catalytically combusting deposited soot is problematic as the catalyst requires direct contact with the soot. Fuel additives offer better contact with the deposited soot as the catalyst is deposited inside the soot structure (van Setten et al. 2001).

2.4.3.2.3 Ceria

Ceria is a commonly used catalyst for the use in DPFs as its oxygen storage capacity allows it to assist in the oxidation of deposited soot at temperatures lower than those required during non-catalyzed oxidation. Ceria aids the soot oxidation through redox reactions where a reduced form of ceria is oxidized by the presence of oxygen in a gas-solid reaction (see reaction (2.12)). The oxidized form then oxidizes carbon in a solid-solid reaction (see reaction (2.13)) (Issa et al. 2008).

$$Ce_2O_3(s) + \frac{1}{2}O_2(g) \rightarrow 2CeO_2(s) \tag{2.12}$$

$$(-C)(s) + 4CeO_2(s) \rightarrow CO_2(g) + 2Ce_2O_3(s) \tag{2.13}$$

In a reducing atmosphere the general formula may be described as Ce_{2-x} where $0 \leq x \leq 0.5$ (Issa et al. 2008). It has generally been reported that reduction of ceria is a slow process compared to the oxidation by oxygen from the gas phase which is generally very fast, hence mostly the CeO_2–form exists in the filter. This effect may be attributed to the fact that carbon adsorbs metal bound oxygen faster than molecular oxygen; however, solid-solid interaction during the reduction of ceria is not clear as only few studies on this matter have been conducted (Issa et al. 2008).

Experiments conducted on the kinetic behavior of differently formulated carbon black/CeO_2 mixtures in a fixed bed reactor yielded an increased rate of carbon oxidation when the mass fraction of CeO_2 is increased and if the carbon black/CeO_2 mixture achieved more intimate contact (Issa et al. 2008).

Ceria also plays an important role in reduction of the SOF. The dominant mechanism by interaction with HCs is the cracking into light HCs. The catalyst present in the coating of a catalytic DPF, typically consisting of a noble metal such as Pt, is then responsible for the oxidation of the gaseous light HCs (Majewski and Khair 2006)

CeO_2 based catalysts utilize mainly active oxygen from the vicinity of the catalyst surface. Harada et al. (2010) found that a ZrO_2 based catalyst may be superior to the conventional CeO_2 based catalysts due to an oxygen ion transfer inside the catalysts which promotes the reaction rate and yields a lowering of DPF regeneration time by

33%. Furthermore a ZrO_2 based catalyst also has high thermal stability (Harada et al. 2010).

2.4.3.3 DPF Regeneration

Regeneration of the filter may occur actively or passively (see sections 2.4.3.3.1 and 2.4.3.3.2). Generally four demands are to be met for the regeneration of the DPF. These demands are as follows (van Setten et al. 2001):

- Exhaust gas temperature must reach a maximum at a minimum of additional fuel consumption.
- No additional noise during regeneration
- No additional formation of byproducts
- The operator of the vehicle should not actively initiate the regeneration

An increased loading time reduces the number of regenerations required and thus increases the overall life expectancy of the DPF.

Exhaust emissions generally increase during regeneration events (Dwyer et al. 2010a). Dwyer et al. (2010a) reported for experiments conducted on a EURO 4 LDD vehicle a large increase in volatile particles were emitted between 5 and 10 nm during regeneration. Lee et al. (2008) reported that the effect of DPF regeneration was larger on particle number concentration than on PM mass and the occurrence and duration of DPF regeneration is a key factor in effecting nano-sized particle emissions.

The combustion of soot deposited on the filter surface during regeneration of a DPF may proceed in three different modes (Martirosyan et al. 2010):

- A moving hot zone emanating from a single ignition point
- Hot zones generated at several ignition points
- Uniform combustion all over the surface

2.4.3.3.1 Active DPF Regeneration

Actively promoting regeneration requires an increased energy consumption to promote higher temperatures that facilitate soot oxidation. A lowering of the frequency required for active regeneration would hence improve fuel economy (Harada et al. 2010). Each active regeneration cycle typically requires 1000 km of road driving before commencing. The regeneration operation is typically only a few minutes. The maximum allowable back-pressure together with the maximum tolerated exothermic heat release during combustion of the deposited soot layer determine the time before each regeneration event (Lox 2008).

Soot can be indirectly ignited by heating of the exhaust gas temperature or filter or directly ignited heating the soot directly (van Setten et al. 2001). Additional fuel burning for heating of the exhaust gas is typically up to five times more energy

efficient than electrical heating, however, the fuel burner is more complex and can cause issues such as soaking the DPF with fuel if flame ignition fails and thus cause a runaway reaction. Also transient conditions in the exhaust make it difficult to control the amount of fuel needed for additional combustion in a fuel burner (van Setten et al. 2001).

Indirect heating can also be achieved through means of engine controlled heating with a throttling of the inlet gas stream. Diesel engines normally run with an excess of air so a reduction in this through throttling will still ensure a diesel combustion to the same extend but with a lower exhaust oxygen content. The reduced gas volume yields less potential for absorption of heat generated and the temperature will thus increase. Even though inlet gas throttling causes increased temperatures the reduced oxygen content may make soot combustion more difficult. Inlet throttling furthermore greatly reduces engine efficiency. Throttling of the inlet gas stream can be controlled by changing the EGR. Another means of engine controlled heating is fuel injection timing by which additional fuel is injected at the top end of the expansion stroke. At this point no additional work can be generated and the injected fuel is combusted leading only to a heat increase. This is generally the preferred method for temporarily increasing the exhaust temperature as it does not affect drivability (van Setten et al. 2001). Bergmann et al. (Bergmann et al. 2009) reported for experiments conducted on a modern DPF equipped diesel passenger car that during active regeneration by post-injection and EGR shut off the total PM number emission of nucleation mode particles was 3-4 orders of magnitude higher compared to those emitted at the same speed without regeneration. The level of accumulation mode particles was reported the same. The particles emitted during the regeneration were mainly volatile and they are suggested to originate from accumulated sulfur compounds (Bergmann et al. 2009).

Microwave heating of the DPF has been proposed for initiation of active regeneration; however, problems such as usage of often inappropriate filter materials and generation of local hot spots due to uneven microwave heating may result in physically damaging the filter (Pallavkar et al. 2009). Only off-line regeneration with microwave heating has proven to work efficiently as the oxygen concentration in the exhaust stream is too low during on-line operation (Pallavkar et al. 2009).

The filter may be directly heated by use of internal incorporation of electrical heating elements inside the filter. A 100% regeneration at a fuel efficiency loss of only 1% has been reported (van Setten et al. 2001). The low efficiency loss can be attributed to the fact that not all the flue gas has to be heated.

Experiments have also been conducted with aerodynamic regeneration where a back pulse through the filter is applied at time intervals and particulate matter is collected. These systems are however highly impractical (van Setten et al. 2001).

2.4.3.3.2   Passive DPF Regeneration - Continuously Regenerating Trap

NO_2 for the passive regeneration of the DPF is generated either in the DOC, in the catalytic coating of DPF or by a combination of both (Schejbal et al. 2010). The soot oxidation follows the general reaction scheme (D. B. Kittelson et al. 2006):

$$(-C)(s) + 2NO_2(g) \rightarrow 2NO(g) + CO_2(g) \qquad (2.14)$$
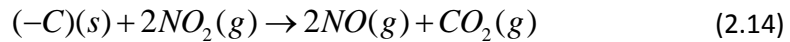
Jeguirim et al. (Jeguirim et al. 2009) proposed a mechanism by which NO_2 oxidizes soot in the form of two parallel reactions. The one reaction is a direct C-NO_2 reaction which is catalyzed by the presence of water and the other is a cooperative C-NO_2-$O2$ reaction catalyzed by Pt/Al_2O_3 (see (2.18) and (2.19) for similar non-catalyzed reaction) The presence of water in the exhaust stream is often readily available. The oxidation of soot by NO_2 occurs at typical exhaust temperatures of diesel engines at around 250-400°C (Jeguirim et al. 2009).

The dominant factors for the efficiency of a continuously regenerating trap (CRT) system are the NO_x/soot ratio and the exhaust gas temperature (Kandylas et al. 2002b). Kim et al. (2010) reported that a continuous regeneration of DPF is possible at an m_{NO2}/m_{soot} ratio between 7 and 8 at exhaust gas temperatures of 250-350°C. Passive DPF regeneration is difficult to achieve in LDD vehicles due to a generally low operating temperature and NO_x/PM ratio hence an active regeneration strategy is preferred (Walker 2004)

The use of plasma for continuous filter regeneration has been proposed. This strategy functions by electrically accelerating electrons in the exhaust gas and thereby increasing the potential for formation of free and more reactive radicals and it may also increase the vibrational energy of gas molecules thereby increasing the temperature. Free radicals of oxygen are more reactive towards soot oxidation thus regeneration may be initiated. Even though use of plasma can reduce NO_X to N_2 the energy requirement for this reaction exceeds the energy released during the engine operation and hence N_2 formation becomes impossible. It may also prove troublesome having an uncontrolled combination of free radicals in the exhaust gas which may react to form undesired and/or unknown byproduct. A net increase of NO_x or increased formation of PM may also be the result (van Setten et al. 2001).

By letting the exhaust gas passing catalytically covered electrodes as a means of filtration, near continuous electrochemical regeneration has been reported with a loss of fuel efficiency of only 1%. More research however still has to be conducted on the subject (van Setten et al. 2001).

2.5   Models and Kinetics Describing Filter Performance

Diesel filter performance has been widely investigated by modeling approaches. Modeling of flow patterns inside a DPF and soot deposition profiles are mainly modeled using numerical approaches. The catalytic as well as the non-catalytic soot oxidation inside a DPF has been extensively investigated together with the effects of

different gaseous components and different carbon microstructures. Finally the oxidation of soot and carbon in general by NO_2 has been widely investigated; however, there is a limited number of published data on the effect of NO_2 on soot reactivity.

Several gaseous species can contribute to a gasification of soot, however, mainly NO_2 and O_2 are of relevance. The latter is due to its abundance (typically 10% in the exhaust gas) and the former is due to its highly oxidative properties. Other nitrogen oxides may also gasify soot, and the relative magnitude of the reaction rates are listed below (Stanmore et al. 2008).

$$NO_2 > N_2O \approx NO \approx O_2 \qquad (2.15)$$

Soot oxidation by NO_2 occurs either by a direct reaction between C-NO_2 and a cooperative reaction C-NO_2-O_2 (Jeguirim et al. 2005). Furthermore, a catalyst such as Pt will also enhance the rate at which the cooperative reaction occurs (Jeguirim et al. 2007). The direct reaction schemes are listed below in (2.16) and (2.17), and the cooperative reaction is listed in (2.18) And (2.19) (Jeguirim et al. 2007)(Jeguirim et al. 2009). The only nitrous species formed after reaction with NO_2 is generally NO (Stanmore et al. 2008).

$$C + 2NO_2 \rightarrow CO_2 + 2NO \qquad (2.16)$$

$$C + NO_2 \rightarrow CO + NO \qquad (2.17)$$

$$C + NO_2 + \tfrac{1}{2}O_2 \rightarrow CO_2 + NO \qquad (2.18)$$

$$C + NO_2 + \tfrac{1}{2}O_2 \rightarrow CO + NO_2 \qquad (2.19)$$

For both the direct and the cooperative mechanism either CO or CO_2 is formed. In the case of the cooperative mechanism NO_2 is adsorbed onto the soot surface forming both oxygen and nitrogen surface complexes such as –C(O) and –C(ONO$_2$). The presence of oxygen in the gas phase has shown to enhance the NO_2 adsorption. This feature is believed to be attributed to chemisorption of O_2 which yields oxygen complexes onto which NO_2 mainly adsorbs (Jeguirim et al. 2004). The presence of water has shown to increase the overall oxidation rate; however, the global mechanism by which the reaction occurs remains unchanged (Jeguirim et al. 2005). Water is believed to enhance only the direct C-NO_2 reaction by the formation of nitric (HNO_3) and nitrous (HNO_2) acids which serve as intermediates (Jeguirim et al. 2005). Water thus acts like a catalyst for the reactions (2.16) and (2.17).

Jeguirim et al. (2004) reported that gasification by NO_2 of diesel soot occurred at temperatures down to 120°C. Azambre et al. (2006) equally found that gasification starts at 110°C from experiments involving Temperature Programmed Desorption

(TPD). Gasification by NO_2 occurs more readily at lower temperature than O_2 or NO (Choi et al. 1998). The main products of oxidation by NO_2 for temperatures 200-355°C are CO_2 and NO in a molar ratio of 1:2 with small presence of CO and N_2 (Stanmore et al. 2008). For temperatures up to 400°C an increased CO yield has been observed. Reaction order with respect to NO_2 was unity for temperatures above 300°C.

2.5.1   Non-Catalytic Soot Oxidation by O_2

The non-catalytic soot oxidation rate can generally be described as an nth order reaction with respect to oxygen partial pressure (P_{O2}) where the rate constant is expressed by an Arrhenius expression (van Setten et al. 2001):

$$r_{ox} = N_T k(T) p_{O_2}^n, \ \ where \ \ k(T) = k_0 \exp\left(\frac{-E_a}{RT}\right) \tag{2.20}$$

The total number of active carbon sites N_T may be assumed proportional to the actual surface area S_a. N_T then becomes the following, where λ is the surface concentration of active sites and $S_{a,0}$ is the initial surface area (van Setten et al. 2001):

$$N_T = \lambda \frac{S_a}{S_{a,0}} \tag{2.21}$$

The actual surface area depends on the pore structure and the combustion regime in which soot oxidation occurs.

The non-catalytic soot oxidation by O_2 typically proceeds at a rate with orders of 0.76-94 at temperatures around 500°C (Stanmore et al. 2001).The order of the reaction depends on the ratio at which CO/CO_2 is formed (Stanmore et al. 2001).

2.5.2   Kinetics of Soot Oxidation by NO_2

Limited studies on the kinetics of soot oxidation by NO_2 have been conducted. The majority of studies implement numerical simulation and most experiments conducted in order to investigate the kinetics involve the combustion in a fixed bed reactor and not in an actual DPF.

With a setup where soot is oxidized by NO_2 in a fixed bed reactor, measured values of both CO and CO_2 allowed Jung et al. (2008) to determine the parameters necessary for describing the rate of carbon consumption by the direct mechanism with NO_2. A simple n[th] order expression for the carbon mass (m) consumption per n[th] order of remaining mass is shown below, where the overall rate constant can be expressed by an Arrhenius expression:

$$-\frac{1}{m^{n_c}} \frac{dm}{dt} = k(T) \cdot P_{NO_2}^{n_{NO_2}}, \ \ where \ \ k(T) = A \cdot \exp\left(\frac{-E_a}{RT}\right) \tag{2.22}$$

The order of the remaining mass n_c for the fixed bed experiments conducted by Jung et al. (2008) was $n_c = 0.75 \pm 0.01$ at temperatures between 350-400°C in both the presence of oxygen and water. The order of remaining mass depends on the oxidized soot particles and thus depends highly on the conditions of the experiment. One would expect for the combustion of spherical soot particles the behavior of a shrinking core combustion where ideally $n_c = \frac{2}{3}$ (Jung et al. 2008). For temperatures ranging from 270-450°C Jung et al. (2008) found a reaction order of unity with respect to NO_2.

Jeguirim et al. (2009) proposed a model for the direct soot oxidation by NO_2 based on experiments conducted in a fixed bed reactor. The rate of carbon mass (m) consumption is shown below in (2.23) as function of the contribution for both the formation of CO and CO_2 as two additive terms.

$$-\frac{1}{m}\frac{dm}{dt} = k_{CO_2} P_{NO_2}^{\alpha} + k_{CO} P_{NO_2}^{\alpha} \tag{2.23}$$

k_{CO_2} and k_{CO} are the kinetic rate constants for reaction (2.16) and (2.17) respectively. The rate expression is a function of the partial pressure of NO_2 (P_{NO2}) with the reaction order α. Jeguirim et al. (2009) argued that the reaction order of the reaction in the absence of water is unity. For a water content of the gas stream between 5-10% at 300-400°C the reaction order was found to be α = 0.6. It is worth noticing that the order of the carbon mass is unity thus implying that the active surface area is proportional to remaining mass for the given conditions.

Jung et al. (2008) investigated the effect on the activation energy for the overall reaction rate (2.22) by varying oxygen, water and NO_2 concentrations. The results are summarized in the table below:

Table 9 Activation energy of carbon – NO_2, O_2, H_2O oxidation (Jung et al. 2008)

NO_2 900 ppm and O_2 5%			
H_2O (%)	0	2	5	10
E_a (kJ/mol)	62	41	38	38
NO_2 900 ppm and H_2O 5%			
O_2 (%)	0	2	5	10
E_a (kJ/mol)	38	41	39	39
O_2 5% and H_2O 5%			
NO_2 (ppm)	0	200	500	900
E_a (kJ/mol)	155	41	36	42

It is clearly seen that the presence of water lowers the activation energy by ~20kJ/mol. Increasing the water concentration from 5 to 10% has no effect on the activation energy thus emphasizing how water works as a catalyst for the oxidation of carbon by NO_2. The presence of water at 300°C has been reported by Jeguirim et

al. (2005) to increase the rate of soot oxidation by NO_2 up to three times faster than for a reaction with no water present . In an atmosphere of 900 ppm NO_2 the addition of oxygen has hardly any influence on the activation energy. For a constant oxygen and water concentration the addition of NO_2 greatly lowers the activation energy; however, an increase in NO_2 from 200 to 900 ppm has hardly any effect on the activation energy (Jung et al. 2008).

A term including the cooperative mechanism for soot oxidation by NO_2 and O_2 can also be included in the overall rate expression. The overall rate of carbon oxidation per initial carbon mass is then given by the added contribution from the direct and the cooperative soot oxidation described as (Jeguirim et al. 2007).

$$r = r_{dir} + r_{coop} \tag{2.24}$$

Assuming first order kinetics the rate of direct soot oxidation is (Jeguirim et al. 2007):

$$r_{dir} = k_{CO_2} P_{NO_2} + k_{CO} P_{NO_2} = k_{dir} P_{NO_2} \tag{2.25}$$

For the rate of the cooperative reaction Jeguirim et al. (Jeguirim et al. 2007) proposed the following expression:

$$r_{coop} = k_{O_2,CO_2} P_{NO_2} X_{O_2}^{0.3} + k_{O_2,CO} P_{NO_2} X_{O_2}^{0.3} \tag{2.26}$$

k_{O_2,CO_2} and $k_{O_2,CO}$ are the kinetic rate constants for (2.18) And (2.19) respectively. The temperature dependence of the rate constants follow an Arrhenius expression. X_{O2} is the volume fraction of oxygen in the gas phase.

Only the cooperative contribution to the reaction rate in (2.24) is affected if the soot oxidation is catalyzed by the presence of catalytic fuel additives or a catalytic DPF. The catalyzed rate expression then becomes (Jeguirim et al. 2007):

$$r^{cat} = r_{dir} + r_{coop}^{cat} \tag{2.27}$$

Jeguirim et al. (2009) proposed a rate expression for both the catalyzed and non catalyzed soot oxidation by NO_2 based on experiments conducted in a fixed bed reactor. The catalyst used in their investigation was Pt/Al_2O_3. The rate expressions are presented below in reactions (2.28) and (2.29) and the dependence on both the molar fraction of NO_2 (x_{NO2}) and oxygen (x_{O2}) in the gas phase is clearly seen.

$$r = 0.48 \exp\left(\frac{-26700}{RT}\right) x_{NO_2}^{0.6} + 1395 \exp\left(\frac{-47800}{RT}\right) x_{NO_2} x_{O_2}^{0.3} \ [s^{-1}] \tag{2.28}$$

$$r^{cat} = 0.51 \exp\left(\frac{-26800}{RT}\right) x_{NO_2}^{0.6} + 51.4 \exp\left(\frac{-52200}{RT}\right) x_{NO_2}^{0.4} x_{O_2}^{0.3} \ [s^{-1}] \quad (2.29)$$

It is important to note that the above equations were derived as a result of combustion in a fixed bed reactor, and differences may be present compared to combustion in an actual DPF used for automotive use (Jeguirim et al. 2009). The reaction order with respect to NO_2 for experiments conducted on real CRT systems was found to be unity by Kandylas et al. (2002a).

2.5.3 Activation Energies and Soot Reactivity

In this section activation energies for soot and factors contributing to different reactivity towards oxidation are presented. The activation energies for soot oxidation by either NO_2 or O_2 are summarized in Table 10 below.

The reactivity of soot towards oxidation is highly dependent on the type of soot. The reactivity of diesel soot obtained from idle and full load engine conditions and carbon black have proven to show similar reactivity towards oxidation by either NO_2 or NO_2/O_2 (Setiabudi et al. 2004). For reaction with O_2 alone the soot from idle engine operation was more reactive than the soot from full engine load which again was more reactive than CB (Setiabudi et al. 2004). Choi et al. (1998) found that graphite requires higher temperatures for gasification by NO_2 than for the gasification of carbon black or activated carbon. Soot obtained from a HDV and a LDV engine has been exposed to 375°C in an atmosphere containing 150ppm NO_2, 45ppm NO, 10% O_2 and 3% by Messerer et al. (2006) et al. Results indicated that the rate of carbon mass conversion was three times higher for the combustion of HDV soot compared to LDV soot (Messerer et al. 2006).

Different experimental methods have been conducted in order to obtain kinetic data for soot oxidation involving TGA, fixed bed experiments and full scale experiments on DPF where monitoring of pressure drop provides an indicator of the extend of reaction. From sensitivity analyses on a one dimensional generalized DPF model Law et al. (2004) found that the activation energy is the most important factor in the regeneration process.

Activation energies for non-catalyzed oxidation of diesel soot by oxygen range from 80-200 kJ/mol (Choi et al. 1998)(Setiabudi et al. 2004). The activation energy for gasification by H_2O and CO_2 typically range from 170-200 kJ/mol. An activation energy for soot oxidation by NO_2 of 50 kJ/mol has been observed for temperatures 200-300°C (Stanmore et al. 2008). For experiments conducted with a real DPF and a fuel additive of the catalyst ceria Stratakis et al. (2003) determined an apparent activation energy for the catalytic soot oxidation of 80 – 130 kJ/mol for temperatures ranging from 420 – 490°C.

Messerer et al. (2006) argued that the rate of soot oxidation may be described as two additive parallel reactions from the oxidation by O_2 and NO_2. The reaction with NO_2 is believed to follow a Langmuir Hinshelwood mechanism where the

activation energy for the chemical reaction with NO_2 is 100-110 kJ/mol but due to a lower activation energy required for the adsorption the observed overall activation energy for soot oxidation by NO_2 is 60-80 kJ/mol. This emphasizes the difficulties related to determining overall kinetics as one may need to distinguish between different reaction steps. The assumption of an overall reaction accounting for both the adsorption of oxidative species and subsequent chemical reaction combined is for simplicity therefore applied in this study.

Table 10 Typical activation energies for both catalyzed and non–catalyzed soot oxidation by O_2 and for soot oxidation by NO_2. Temperatures range from 200-500°C and different soots have been used in order to investigate the activation energies. Equally the method for determining the activation energies include TGA and indirect measurement by pressure drop monitoring on a full-scale DPFs.

Oxidant	Catalyst	Activation energy / [kJ/mol]
O_2	None	80-210
O_2	Ceria	80-130
NO_2	None	27-80

The great span in activation energies emphasizes how difficult it is to compare these as factors such as type of soot and experimental conditions affect the results greatly.

2.5.4 Particle Flow and Deposition

The flow inside the monolith channels is generally assumed to be laminar under normal engine operation. Liu et al. (2009) conducted numerical studies on the trajectories of particles inside a monolith filter in order to predict a particle deposition profile. The forces acting on the particles were assumed to be dominated by drag force and Brownian motion (Liu et al. 2009). Of relevance is the flow of gas and particles in the monolith channels but also the flow across the filter walls. The flow across the filter walls changes with different levels of particle deposition, hence an expression for pressure drop over the filer changes over time. The total pressure drop over the DPF $\left(\Delta P_T\right)$ can be expressed as the sum of the clean filter pressure drop $\left(\Delta P_c\right)$, The pressure drop due to wall flow filtration $\left(\Delta P_w\right)$ and the pressure drop due to cake filtration $\left(\Delta P_s\right)$ when a deposited layer has formed (Pallavkar et al. 2009):

$$\Delta P_T = \Delta P_c + \Delta P_w + \Delta P_s \qquad (2.30)$$

The clean filter pressure drop is measured experimentally. Darcy's law can generally be applied for the pressure drop across the porous filter wall and filter cake. The pressure drop across the filter cake of thickness w_p can be expressed as:

$$\Delta P_s = \frac{\mu U H w_p}{4 L k_p} \qquad\qquad (2.31)$$

The gas viscosity is denoted μ, inlet monolith cell linear gas flow velocity is U and the cell height and length are H and L respectively. k_p denotes the soot layer permeability and is generally assumed to be constant as the pressure drop during cake filtration shows linear dependence on soot layer thickness (Pallavkar et al. 2009). The pressure drop due to wall flow filtration can be expressed as the sum of pressure drop due to gas flow through the filter wall where soot particles are deposited and frictional loss due to gas flow throught he monolith channel.

$$\Delta P_w = \frac{\mu U H w_w}{4 L k_w} + \frac{2 \mu F U L}{3 H^2} \qquad\qquad (2.32)$$

F is the friction factor for the filter walls. The filter permeability k_w decreases during deposition until the filter wall has reached saturation and cake filtration follows (Pallavkar et al. 2009).

Many models describing particle and gas flow behavior from numerical studies with CFD have been proposed. CFD is used to describe the three-dimensional flow pattern inside the monolithic channels of a wall flow DPF. Balances on conservation of energy, momentum and mass together with an expression for the pressure drop similar to expressions (2.30) through (2.32) all have to be setup. It is beyond the scope of this report to go into extensive details with the actual numerical studies conducted on the field of flow through monolith channels.

2.6 Summary

The diesel engine is more fuel efficient than the gasoline engine; however, particle emissions are much larger. Emission of nano-sized particles is believed to have a severe affect on human health. Many ways exist to promote a low particle emission such as different engine design, different fuel and different types of engine exhaust after-treatment systems. Generally the particle emission from biodiesel fired engines is lower than for the combustion of petro diesels. Furthermore the higher oxygen content of typically up to 10% in biodiesels results in an increased reactivity towards oxidation of the formed soot. The sulfur content of the fuel used is of great importance, as this is oxidized in the engine to form sulfates which increase the total particulate matter emitted. Furthermore sulfates can have a disruptive effect on exhaust after-treatment systems. It is not only desired to limit the emission of PM but also many gaseous compounds such as CO, NO_x and volatile hydrocarbons. The European legislation governing emission standards is constantly lowering the emission limits.

Diesel exhaust is typically treated in a diesel oxidation catalyst (DOC) where CO and volatile carbons are almost fully oxidized to CO_2 and water. A diesel particulate filter (DPF) (typically a wall-flow monolith) ensures up to 99% entrapment of PM on a mass basis. The exhaust gas is finally treated to reduce NO_x emissions typically by selective catalytic reduction or NO_x absorption.

The temperature of the DPF under normal driving conditions ranges from 200-450°C. Soot deposited in the DPF is either removed by a passive or an active regeneration strategy. Typically heavy-duty diesel vehicles can adopt passive regeneration of the filter where high exhaust temperatures facilitate a continuous oxidation of deposited soot. For light vehicles an active regeneration strategy is used, where the exhaust temperature is increased at intervals to promote complete oxidation of deposited soot. The temperature required for oxidation of soot by oxygen can be lowered by using a catalyst such as ceria through either coating of the DPF or as a fuel additive. Furthermore the presence of NO_2 can non-catalytically oxidize deposited soot at even lower temperatures down to 250°C. The presence of sulfates in the exhaust increases the temperature required for oxidation of soot.

Only a limited number of kinetic studies on soot oxidation by NO_2 have been conducted. The oxidation of soot by NO_2 can occur by both a direct mechanism and a cooperative mechanism involving oxygen. The rate of soot oxidation by NO_2 generally exhibits first order behavior. A catalyst such as Pt can catalyze the reaction and the presence of water and oxygen can further enhance the rate of soot oxidation.

3 Experimental setup

The experimental setup is in the following briefly presented and discussed with emphasis on apparent uncertainties and potential for errors. The experimental setup is shown in a P&I diagram below in Figure 11 (a larger version of the P&I diagram together with pictures of the experimental setup can be seen in Appendix I – P&I and Setup). An operational procedure for the setup is presented in more detail in Appendix T - Procedure.
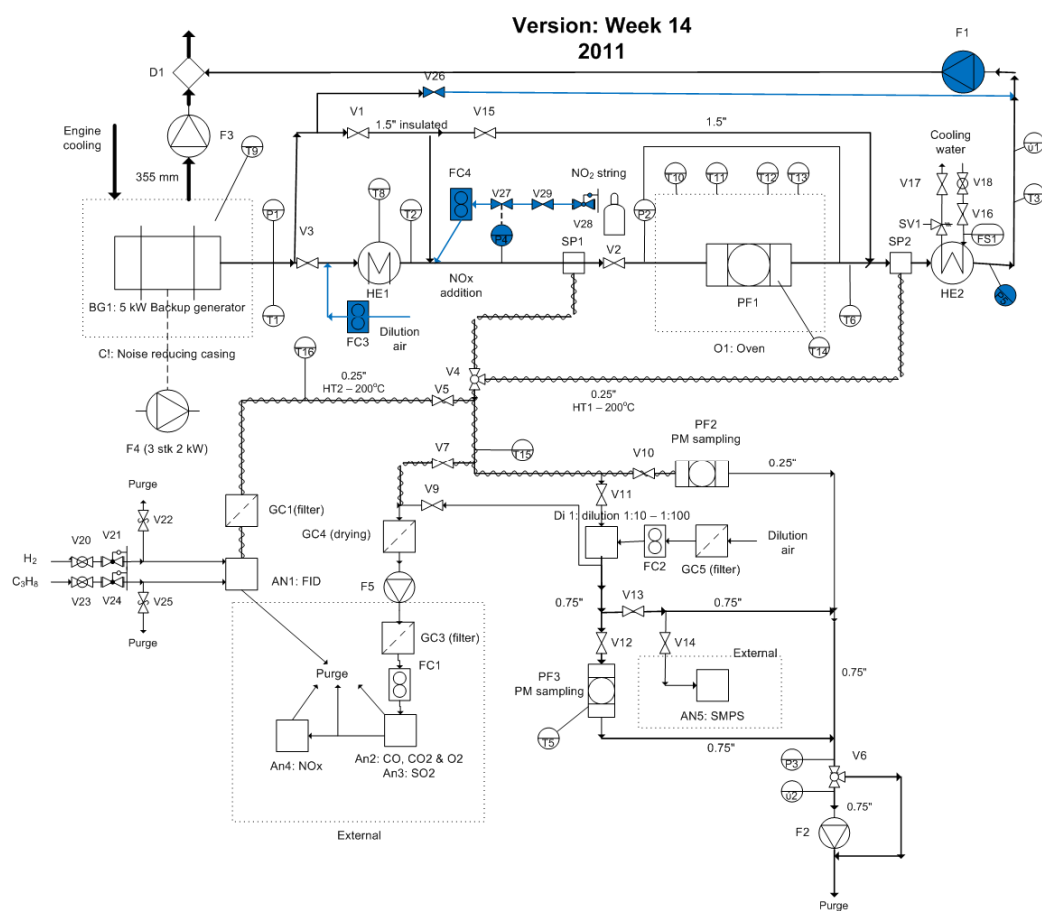
Figure 11 P&I diagram showing the experimental setup. Elements marked with blue color indicate alterations that have been implemented different from experiments previously carried out by DTU students Hubeck-Graudal and Rønde in the fall of 2010 (Hubeck-Graudal et al. 2011)**. (larger version of the P&I can be seen in Appendix I – P&I).**

The exhaust gas exiting the engine may pass a preheater (HE1) and a DPF mounted in an oven (PF1). The exhaust is subsequently cooled to near room temperature in HE2 prior to measurement of the volumetric flow rate in the venturi meter (U1). Different configurations such as bypassing the preheater or the DPF and the potential for

diluting the gas stream as well as introduction of NO_2 is discussed in more detail in the following paragraphs. The potential for sampling a part of the exhaust stream for analysis upstream or downstream of the DPF is also further discussed. A LabVIEW Program logs data from the gas analyzers and FID. Selected temperature sensor and pressure gauge readings are further logged in LabVIEW.

The pump marked F1 ensures an under pressure in the exhaust system. The setting is manually regulated. For flow through operations with the DPF the backpressure onto the engine will inevitably increase due to accumulation of deposited soot inside the filter. In order to avoid this transient behavior a regulation of the setting for F1 will ensure a constant sub atmospheric pressure. Introduction of NO_2 through FC4 requires a gauge pressure of -20 mbar or lower in order to reduce the potential for accidental harmful leakages when NO_2 is present in the piping at greater concentrations. For this reason the pressure at the engine exhaust exit (P1) is regulated in order to achieve -30 mbar (±10 mbar).

Valves for drainage are opened (not shown on Figure 11) when the engine is not running, as water inevitably accumulates due to condensation of water formed during the combustion.

3.1 Engine

The engine is a four stroke back-up generator fuelled with diesel. The engine can be operated a different loads; however, only 80% load is used for the purpose of this investigation, as this provides sufficiently high soot content of the exhaust in order to conduct experiments which require loading of the DPF within a reasonable time frame and higher engine temperatures will more closely resemble the temperature of an automotive engine. The engine runs at a fixed RPM which means that the volumetric flow rate of the exhaust is unchanged for all experiments conducted. Relevant data for the engine is seen in Table 11 below. Detailed specifications for the engine can be seen in Appendix A – Engine .

It is finally worth mentioning that the engine is situated inside a sound reducing casing in which the temperature is monitored and a safety switch will turn off the system (engine shut down) if the temperature exceeds 45°C. This is in order to reduce the potential for ignition of fuel fumes as the flash point of diesels may be as low as 55°C (Dabelstein et al. 2000).

Table 11 The engine is from PowerGenerator and engine specific data such as type, RPM, displacement volume, number of cylinders and fuel used re listed. Detailed list of specifications can be seen in Appendix A – Engine

Engine	RPM	Maximum effect / [kW]	Displacement volume / [L]	Cylinders	Fuel
4 stroke	3,000	6	0.418	1	Diesel

Hubeck-Gradual and Rønde (2011) experienced difficulties keeping the engine running when fueled with biodiesels. The spontaneous engine failures were believed

to be attributed to increased back pressure on to the engine when fueling with biodiesel. Only the combustion of biodiesels proved troublesome engine operation and one may attribute these observations to the different characteristics of biodiesels compared to petrodiesels such as different fluid properties (see section 2.2.1). The setting for pump F1 remained unchanged for experiments conducted on loads of 0 - 80 % and for both fueling with petro- and biodiesel. This stresses the importance of keeping the pressure downstream the engine at a desirably low level which may change depending on fuel type and engine load. For the experimental conditions in this study spontaneous engine failures have not been observed.

3.1.1 Fuels and Oils

A petro diesel and biodiesel is used during the experimental work. For preliminary testing of the experimental setup only petro diesel is used as one may assume that general trends observed will comply for different types of diesel. During the main experimental work a petro diesel from Q8 and a vegetable diesel from Emmelev A/S will be used. Relevant specifications for the diesels used are shown in Table 12 below. Extended information about the diesels used can be seen in Appendix B - Diesels.

Table 12 Fuel specific data for the diesels used. See Appendix B - Diesels for extended details (Q8 2008)**.**

	Petrodiesel	Vegetable Diesel
LHV / [kJ/kg]	42,800	37,301
Cetane number	≥51	56.6
Density (15°C) / [kg/m^3]	830	883.0
Viscosity (40°C) / [mm^2/s]	2.8	4.413
Sulphur / [mg/kg]	≤10	2.1
Phosphorous / [mg/kg]	0	3.1

The lubrication oil used is a Q8 Formula V Long Life 5W-30. Inorganic contents of the oil can be seen in Table 13 below and extended details can be seen in Appendix B - Diesels. Only one type of lubrication oil is used for all experiments conducted in order to limit the potentially variable impact on emissions. The miscibility of the lubrication oil and the diesel inside the engine cylinder provides a potential for contamination of the diesel with inorganics present in the oil. Contamination of the engine oil (dilution by diesel) may however also occur. For these reasons the oil is drained from the engine when a different diesel is used and the oil batch is therefore only used in connection with a given diesel. This helps to ensure that running the engine on different diesels will not affect the emissions or the engine performance; however, each batch of lubrication oil is recycled meaning that over time the oil performance will decrease. After approximately 100 hours of operation the oil must be renewed. Ideally one would want to renew the oil as often as possible in order to eliminate this

trend. Recycling of the lubrication oil can affect engine performance as the oil affects the ease of piston movement inside the engine cylinder and thereby affects the combustion process. As lubrication oil also affects the emissions changes in composition may also alter the emissions.

Table 13 Inorganic contents of the lubrication oil Q8 Formula V Long Life 5W-30. See Appendix B - Diesels for extended details .

Content	Minimum Value	Maximum Value
Ca + Mg / [wt%]	0.134	0.162
Phosphorous / [wt%]	0.052	0.065
Sulphur / [wt%]	N/A	0.3
Zinc / [wt%]	0.055	0.070

3.2 Preheater

The preheater (HE1) is a 5.5kW (3 x 240V) flow through heating pipe HT 200 from Farnam Custom Products (see Appendix C - Preheater for detailed specifications). The preheater provides the main means of regulating the temperature of the particulate filter (PF1) as the flow through heating pipe is designed to rapidly heat a gaseous medium. Changing the temperature of the DPF with the surrounding oven only will ensure neither a sufficient nor a controlled regulation of the exhaust temperature as it passes the DPF due to the high volumetric flow rates. The heat pipe is customized to handle a maximum inlet temperature of 450°C and a maximum outlet temperature is 704°C. In the case of overheating (shell temperature exceeds 350°C) the heating element will be turned off automatically. The preheater is regulated by simple on-off control. A set point is entered in LabView and due to its simple control system fluctuations up to 60°C above the set point may be experienced after stabilization of the controller (see Appendix C - Preheater). The temperature of the gas downstream of the preheater averages a temperature up to 40°C higher than the set point. The deviation from the set point may depend on temperature and gas flow rate.

A preheater is not used for automotive use; however, other means of heating the exhaust are used such as post combustion (see section 2.4.3.3.1) in order to satisfy regeneration of the DPF. Using a flow through heat exchanger as a means of preheating the exhaust before entering the DPF is advantageous for experimental use as the temperature can be easily controlled. As a preheater is not used for automotive use it is important to determine the potential changes to gas composition of the exhaust and soot reactivity it may impose. The effect of preheating on emissions is investigated and discussed in section 8.

3.3 DPF and oven

The DPF is located inside an oven which is electrically heated by three heating elements (PF1); however, the preheater (HE1) must be used in connection in order to achieve a satisfiable temperature increase of the entire gas stream and the catalytically coated filtermaterial which is passed inside the DPF. The temperature of the inside of the filter is logged at T14.

The DPF is a SiC filter with a wash coat of TiO_2 produced by Dinex A/S. The filter is coated with the catalysts CeO_2 and Pt. The coatings as well as dimensions of the DPF resemble that of what one would find in a modern diesel powered automotive vehicle for road use but has been attempted scaled down with respect to engine exhaust flow rate. The maximum tolerable temperature of the filter is 625°C. Detailed specifications on the DPF and oven can be seen in Appendix D - DPF and Oven.

The pressure drop over the DPF is measured at P2. Pressure drops over 150mbar should be avoided due to conclusions drawn from previous studies by Hubeck-Graudal and Rønde (Hubeck-Graudal et al. 2011), were exposure of the pressure sensors to high pressure resulted in abnormal readings persisting post measurement.

3.4 Analysis

The exhaust is analyzed either prior to or after filtration in PF1. This is carried out by regulating the setting of the three way valve V4.

3.4.1 Gas analysis

Gas analyzers are marked An1, An2 and An3 on Figure 11. The gasses used for calibration have an uncertainty of ±2%. Gas data is obtained on a dry basis. The gas stream is stripped from water and filtered for PM before it is sent through the analyzers. This is important in order to avoid deposits and corrosion inside the gas analyzers. Water is removed using a Perma Pure MD^{TM} gas dryer (see Appendix E - Perma Pure) which functions by osmosis of gaseous water molecules through a selective membrane to a dry purge gas in counter flow. Only water is removed during the Perma Pure drying and the gas composition is thus unaltered. Another means of removing water from the stream is through condensation; however, this method would provide a means of also selectively removing NO_2 as condensed water readily absorbs NO_2 to form nitric acid. This effect would lower the NO_2 concentration detected in the gas analyzers. The presence of condensed water anywhere in the system thus results in NO_2 readings lower than the actual gas phase concentration. Proper drainage of piping is therefore carried out prior to initiation of experiments. Before the gas stream is sent through the gas analyzers it passes a particulate filter which must be replaced when filled; however, deposition of smaller particles are also observed downstream of the filter and therefore the piping leading to the analyzers is also cleaned with ethanol and pressurized air on a regular basis. All of the data

from the gas analyzers is accounted for with a 45s time delay due to transport delays (see Appendix L – Time Delay).

3.4.2 FID

Opening of V5 sends some of the exhaust through a Flame Ionization Detector (FID) (see Appendix F - FID for specifications). From an external gas storage H_2 is supplied at 1bar through V20 as flame resource and CH_4 is supplied at 2 bar through V23 for calibration. The FID apparatus automatically calibrates and regulates the required inflow and the hydrocarbon content of the exhaust is continually logged as an ethane equivalent mass per volume or ppm. The exhaust gas is heat traced (set point given for T16) in order to maintain a minimum of 150°C prior to entering the FID. This ensures no condensation of hydrocarbons prior to the measurement as this would reduce the actual hydrocarbon level registered. A heat tracing temperature of excess 200°C is however undesired as the valves in the system may not tolerate higher temperatures. Uncertainties related to the measurement with the FID are further discussed in section 4.3 as a result of preliminary experimental investigation

3.4.3 Soot sampling and sampling filter

Particulate matter is collected at PF2 on a sampling filter. The piping upstream of the filter is heat traced (T15) to ensure a filtration temperature of around 50°C (the US EPA reference temperature is 45-52°C (van Setten et al. 2001)). The heat tracing upstream of the sampling filter is heat traced at 180C. When sampling of soot is initiated by opening of V10 the sampling time is manually logged together with the gas flow passing a gas meter which has an error in accuracy up to 1%. The sample filter has 99.9% retention of solid PM (see Appendix G - Sampling Filter) and no soot is visible on the backside of the filter. The mass of sampled PM is determined on a decimal scale (Sartorius AC210S) with a readability and standard deviation of 0.0001 g. A sampling of 50mg of soot therefore has a determined weight with an accuracy of 2%. Uncertainties related to the sampling are further discussed in section 4.2 as a result of preliminary experimental investigation

3.5 NO_2 addition

NO_2 is supplied as a pure gas from a gas cylinder and added to the setup downstream of HE1 and upstream of PF1. When NO_2 is added to the exhaust a sub atmospheric pressure must be maintained at all times to eliminate the risk of potential accidental leakages. If the gauge pressure exceeds -20mbar the NO_2 gas supply is automatically shut off. The NO_2-string is heat traced at 40°C in order to eliminate the potential for condensation due to the low vapor pressure at ambient pressure and the gas cylinder is equally heated to 30°C. Due to the low vapor pressure of NO_2, the gas is supplied at a gauge pressure of 0.2-1.2 bar.

NO_2 is added upstream sampling point SP1 at a very close distance not allowing for an accurate measurement of the amount of NO_2 added. For this reason the NO_2

concentration after addition of NO_2 to the exhaust is measured at SP2 downstream of the DPF.

3.6   Dilution

The exhaust gas can be diluted by addition of atmospheric air upstream of the preheater. When the exhaust is diluted prior to entering the DPF a given portion of the exhaust prior to mixing can be bypassed to the ventilation (opening of V26) in order to maintain a constant volumetric flow through the filter. The exact dilution ratio can be determined from measured gas concentrations. The latter is further discussed in section 5.2. Uncertainties and design limitations are discussed in section 4.1 as a result of preliminary experimental observations.

3.7   STA

The apparatus used for Simultaneous Thermogravimetric Analysis (STA) provides both a mass loss (TGA) and calorimetric (DSC) signal as a function of temperature for heating/cooling of a given soot sample. The mass loss at given temperatures provides important information such as volatile hydrocarbon content of the soot and soot reactivity if the sample is heated in an inert or an oxidative atmosphere (10% O_2) respectively. The equipment used is a NETZSCH STA-449F1 and a NETZSCH STA-409C (specifications can be seen in Appendix H - STA). The crucibles used for measuring on the soot samples are Al_2O_3. The method adopted for using the STA can be seen in section 5.1.

4 Preliminary Experimental Observations and Considerations

In the following preliminary observations and considerations will be presented together with a discussion on which factors that may contribute to an increased uncertainty or inaccuracy in measurements obtained. Initially limitations due to the experimental setup are briefly outlined and discussed. Preliminary results are presented with regards to PM sampling, volatile hydrocarbons, the potential for deposition of PM upstream of the sampling/analysis, the effect of different backpressure onto the engine and finally the uncertainties observed with TGA.

4.1 Limitations due to Experimental Setup

The experimental work has been limited by many factors such as the limited availability of technicians who may help finalizing the setup or fix potentially faulty equipment. This may impose certain time limitations which may limit the total number of experiments one can conduct. Factors which provided a limitation to the diversity of experiments conducted are briefly presented in the following and involve

- Uncontrolled valve regulation
- Inaccurate flow rate measurement

4.1.1 Leaking Valves

The butterfly valves marked V1, V2, V3, V15 and V26 did all prove leaking behavior when in a closed position. The valves are specially designed for temperatures up to 300-500°C and therefore have no gasket. It desired to be able to ensure proper closing of valve V15 in order to ensure that a controlled flow rate is passing the DPF. Furthermore it is also desired to ensure both proper closing and regulation of the amount of gas potentially being bypassed through V26. The current valve V26 lets approximately 50% of the exhaust pass through when in a closed position meaning that it is not possible with the current setup to regulate the magnitude of the bypass. This means that during experiments involving deposition of soot in the DPF the valve V26 should remain untouched as minor changes from a closed position may lead to an undesirably large flow being bypassed. The degree of dilution is determined by measuring the gas phase composition (described in section 5.2).

4.1.2 Inaccuracy in Venturi Meter Readings

The venturi meter U1 has proven to give abnormal readings such as an increased flow rate registered when the bypass valve V26 is opened. This is believed to be attributed to the bypass stream passing near the downstream side of the venturi meter at too close a distance potentially causing flow and pressure disturbances large enough to yield faulty flow readings. It is also believed that the flow rate reading from U1 while not bypassing through V26 is prone to be inaccurate due to the closely connecting piping from the bypass string and lack of straight piping downstream of the venturi meter. Furthermore the venturi meter was last calibrated prior to implementing the bypass string and this may therefore contribute inaccuracy

in the flow meter readings. The rotameter FC3 used to control the volumetric flow rate of air potentially added to system did however prove a directly proportional dependence between the flow setting and the flow rate reading on U1 (see section 5.2.1). The inaccuracy and faulty reading when running the setup in a bypass configuration of the DPF means that the only way of estimating the volumetric flow rate passing the DPF is when a flow rate of added dilution air is known together with the dilution ratio determined from gas composition data (see section 5.2).

4.2   PM Sampling and Sampling Filter

The PM sampling may be attributed to uncertainties related to both the sampled soot and the sampling filter. Potential contributors to uncertainty in measured mass of sampled PM may be:

- Ash content in sampled soot may yield faulty values of sampled mass
- Differences in sampling flow rate may contribute to different retention of sampled PM
- Uncontrolled sampling filter temperature may allow for undesired passage of volatiles through the sampling filter

Each of the above is discussed in the following.

4.2.1   Ash Content

Sampled soot is closely incorporated into the upper layer of the filter meaning that removal of soot from the filter after sampling is impossible without also removing filter material. For this reason it is impossible to experimentally determine the ash content of the soot experimentally after for example conducting TGA. Hubeck-Gradudal and Rønde (Hubeck-Graudal et al. 2011) did however analytically estimate an ash content of the soot from both petrodiesel and vegetable diesel by using data for the inorganic content of both the diesels and the lubrication oil yielding near similar contributions from ash per energy of fuel combusted of ~0.5 mg/MJ which is equal to <0.5 weight% of the PM. It may therefore be reasonable to assume that the contribution from ash is negligible in measurement of mass of sampled soot.

4.2.2   Sampling Flow Rate

During sampling the gas flow having passed the gas meter is occasionally logged together with the time in order to ensure that sampling occurs with a constant flow passing the sampling filter. The flow rate of gas passing the sampling filter is determined as the slope of the curve expressing gas meter readings as a function of time. The correlation coefficient for linear regression of the collected data points helps ensuring that sampling occurs at a constant rate. Correlation coefficients of R^2>0.98 indicate a satisfiable steady filtration flow, however, great differences in sampling flow for different samplings have been observed (see Appendix J – Sampling Data). The flow rate passing the sampling filter will inevitably depend on the pressure

registered at the point from which the sample is taken. The correlation coefficient mentioned in the above provides an indicator of potential uncertainty in registered PM concentration of the exhaust. The flow rates during sampling ranged from 3.1-4.6 l/min with a standard deviation of 11.7%. The pressure exhibited during filtration on the sampling filters are unmeasured, however, the deviation in flow rates could potentially contribute to differences in retention of PM especially the smaller SOF molecules due to changes in pressure drop over the sampling filter. The SOF contributes to the majority of the nuclei mode particles of the total PM (Majewski and Khair 2006) indicating that if the sampling filter allows the passage of particles within the smaller size range the level of SOF registered may actually be lower than the actual value.

4.2.3   Sampling Filter Temperature

The temperature of the sampling filter is measured as the external temperature of the metal casing containing the sampling filter. The actual filter temperature is therefore expected to be higher than this measured temperature. The sampling string leading up to the sampling filter is heat traced at a temperature of up to 180°C in order to avoid condensation of both water and volatile hydrocarbons. The sampling filter temperature measured did at no time exceed 100°C despite the considerably higher heat tracing temperatures. In order to sample soot at a temperature between 50-100°C it is necessary to assume that the sampled gas is immediately cooled when passing the sampling filter. For this reason it is likely to believe that the potential for a temperature gradient across the span of the filter may be present as the sampled gas is led from a pipe with a diameter of 15mm through a filter with a diameter of 47mm. The potential for uncontrolled temperature of the sampling filter will result in greater inaccuracy when determining SOF content of sampled PM. The ignition temperatures obtained on sampled soot should ideally not depend on potential uncontrolled deviations in the temperature of the sampling filter as temperatures in excess of the ignition point are not obtained prior to sampling.

In order to verify that the filter temperature measured actually resembles the filter temperature a thermo couple has been inserted into the bottom of the filter casing for temporarily measuring the temperature immediately downstream of the filter. The temperature was measured for flow conditions passing the filter similar to those experienced during soot sampling. Furthermore an actual filter was inserted into the sampling chamber and the sampling string upstream of the filter was heat traced to 200°C. Both the external temperature measured as the temperature of the casing and the temperature immediately downstream of the filter was measured for a gas flow both heated solely by the heat tracing and additionally heated prior to entering the sampling string by having an air flow added through FC3 similar to the exhaust flow rate heated in the preheater with a set point of 500°C. The temperatures registered are presented in Table 14 below.

Table 14 Temperature of the sampling filter registered as either the external temperature of the casing or measured immediately downstream of the filter.

	Temperature of the casing / [°C]	Temperature immediately downstream of the filter / [°C]
T15=200°C, HE1= 0	60	88
T15=200°C, HE1=500°C	67	97

From the table above it is seen that preheating of the gas prior to entering the heat traced sampling contributes equally to an increased temperature registered as the external casing temperature and the temperature immediately downstream of the sampling filter. The data indicates that for the temperatures registered externally the actual temperature of the sampling filter is at least 30°C higher. Ideally one would want to continuously measure the temperature immediately downstream of the filter during sampling. For the samplings conducted the temperature would never exceed 65°C registered as the external casing temperature indicating that the filter temperature ideally never exceeded 100°C. Hubeck-Gradual and Rønde (2011) argued that externally measured temperatures of the sampling filter up to 100°C had no impact on the mass of sampled soot; however, their sampling may also be attributed to a great deal of uncertainty especially with regards to the mass of SOF sampled.

Heat tracing should not exceed 200°C during sampling of soot as the filter temperature may exceed 100°C which was the highest temperature Hubeck-Gradual and Rønde (2011) tested for, thus potentially cause an increased potential for evaporation of SOF that will not be sampled on the filter. If the latter is the case the sampled mass will be lower than the actual mass of PM (measured at the reference temperature of 52°C).

4.3 FID and Volatile Hydrocarbons

Measurement of volatile hydrocarbons in the FID may be attributed uncertainties. The most important potential contributors to uncertainty may be:

- The temperature upstream of the FID if too low may allow for condensation of volatiles and thereby yield faulty HC readings
- Uncertainty in the measurement by the FID

Each of the above is discussed in the following

4.3.1 Temperature

For preliminary experiments on petrodiesel combusted at an engine load of 80% FID readings showed a hydrocarbon content of the unfiltered exhaust around 120 ppm (ethane basis). Subsequent heating of the DPF to 500°C for 24 hours while simultaneously having a slow flow of air passing through the filter may have

contributed to a removal of PM downstream the DPF as sampling from this position would never exceed a hydrocarbon content of 32 ppm in following experiments. This gives reason to believe that deposited PM downstream the filter has been removed to some extent by either evaporation or oxidation due to the exposure to temperatures up to 500°C. The SOF contained in deposited PM may evaporate and cause faulty FID readings higher than the actual hydrocarbon content of the exhaust. This emphasizes the need for thorough heat treatment of piping upstream of sampling points for the FID as well as for sampling for the gas analyzers and the sampling filter. The piping downstream of the preheater and upstream of the DPF is easily exposed to temperatures of up to 500°C as it is immediately downstream of the heating elements, however, the internal bypass is more difficult to expose to higher temperatures which indicates that more accurate readings are inevitably obtained when sampling from a flow through operation with the DPF.

The piping immediately downstream of the engine and upstream the preheater together with the string bypassing the preheater will never achieve temperatures higher than the exhaust temperature (up to ~275°C). For this reason PM may potentially deposit over time, however, FID readings conducted on exhaust either bypassing or flowing through the preheater showed similar values. The exhaust temperatures exceeding 250°C at all times during steady operation for the combustion of petrodiesel at 80% load exceeds the temperature required in order to evaporate SOF present in potentially deposited PM (see section 8.1.3). This may explain the coinciding values for the identical FID readings for bypassing and flow through operation with the preheater turned off. The heat tracing immediately upstream of the FID should not exceed 200°C as the valves may not handle higher temperatures. Ideally one might want a heat tracing of up to at least 300°C in order to ensure more accurately that no condensation of SOF upstream of the FID takes place. The heat tracing upstream of the FID was initially set to 150°C due to previous studies conducted at this temperature; however, the heat tracing was later raised to 200°C in order to potentially obtain higher accuracy due to the abovementioned reasons. See section 4.4 for further discussion on deposition in the piping.

4.3.2   Uncertainty of Measurement

When leading atmospheric air through the system at a volumetric flow rate of 27.7 m^3/h near the typical exhaust flow rate a reading of ~7 ppm was registered in the FID indicating a base line that needs to be subtracted from measured data. This amount of volatile hydrocarbons may be attributed to an evaporation of condensed hydrocarbon along the inside of the pipe walls from the engine outlet to the FID inlet despite ensuring a heat tracing of the string (200°C). This indicates how difficult it is to obtain clean pipes. The calibration gas used for calibration of the FID contains 0.999% methane (±2% uncertainty) equal to 4995 ppm on an ethane basis. This value is a factor 10^2 higher than the actual level of volatile hydrocarbons measured in the exhaust (shown in Table 24) meaning that increased uncertainty will be attributed to

these readings. Furthermore one may attribute an uncertainty of 1-2% to the measurement by the FID apparatus. For this reason the low base line value of 7 ppm is not necessarily an accurate measure of the amount of SOF present in the piping when only atmospheric is led through as measurement on unfiltered diesel exhaust would yield <50 ppm of HC (see section 8.1.5).

4.4   Deposition in Piping

Reentrainment of PM deposited along the inside of the walls of the piping leading up to analysis may give faulty values of soot concentration of the exhaust exceeding the actual value; however, the deposition of PM prior to sampling of soot may also contribute to a lowering of the actual PM concentration registered. Equally the release of larger soot agglomerates deposited inside the engine may contribute to variations in PM emissions registered over time. For this reason Yokoi et al. (2001) argued that a preconditioning operation at higher temperatures is essential in order to obtain stable measurements on PM emission such as both total mass and size distribution.

In the following the flow behavior of different strings in the experimental setup is investigated and finally the potential for deposition of particulates along pipe walls is assessed.

4.4.1   Flow Behavior

In order to estimate the potential for soot deposition upstream of the sampling filter as a measure of uncertainty related to this measurement it is necessary to have an understanding of the flow conditions exhibited.

The experimental setup consists of two types of piping. Both larger pipes upstream and downstream of the DPF and smaller pipes with an internal diameter of 1.5 mm in the sampling string as well as the string upstream the analyzers. The Reynold's number is calculated for the flow conditions in each type of piping and shown in Table 15 below. The Reynold's number is a dimensionless number relating inertial forces to viscous forces (given in equation(2.9)).

Table 15 Reynold's numbers calculated for a 200°C exhaust flow through the sampling pipe at a flow rate of 0.2m^3/h and the larger exhaust pipe at a flow rate of 30m^3/h.

Pipe	Re
Sampling	$1.3*10^3$
Exhaust pipe	$6.7*10^3$

From the Reynold's numbers presented in the table it can be seen that the flow is turbulent in the larger exhaust pipes both upstream and downstream of the DPF. For temperatures higher than 200°C one would expect an increased tendency

towards turbulent flow. The flow through the sampling pipes however can be assumed to be laminar as Re<2100 (Clement 2004). Re is calculated for an average flow created by the sampling pump meaning that for situations where both the FID pump and the pump used for the gas analyzers contribute to an increased flow the Reynolds number would increase indicating an increased tendency towards turbulent flow. Due to the laminar flow experienced when sampling soot only there is an increased potential for deposition of PM along the pipe walls (see section 4.4.2).

4.4.2   Deposition Efficiency along Pipe Walls

For a steady laminar flow in a cylinder particles may be deposited on the wall by Brownian diffusion assuming that particles in contact with the wall interface immediately adhere to the surface. For isothermal conditions, neglecting axial diffusion and assuming that the concentration of particles along the inside of the cylinder wall is equal to zero the fraction of particles deposited on the wall can be calculated as a function of a dimensionless tube length given by (Livbjerg 2006):

$$\varepsilon = \frac{D_p Z}{Q}$$

(4.1)

where D_p is the diffusion coefficient of the particles, Z is the pipe length and Q is the volumetric flow rate of the flowing fluid (gas). The fraction of particles deposited on the inside of the pipe wall can be read from Figure 44 provided in Appendix N – Deposition.

As only laminar flow will be experienced in the sampling string the deposition efficiency for this string is investigated. For a 10 nm particle (typically the most abundant particle size from the number distribution as seen on Figure 7 and this is also supported by findings by Hubeck-Graudal and Rønde (Hubeck-Graudal et al. 2011)) travelling in the sampling string at a volumetric flow rate equal to the suction provided by the sampling pump only and at a temperature equal to 200°C the fraction of deposited particles onto the wall given by the dimensionless tube length for a 1m string equals 0.8%. For larger particles the diffusion coefficient decreases thus resulting in a lower degree of potential for particle deposition along the walls. The contribution to the total mass of PM form the nuclei mode particles typically equals less than one percent indicating that for the given conditions the rate of mass lass due to PM deposition along the walls of the sampling string is negligible. However it has been visually verified that deposition does occur.

4.5 Effect of backpressure

Different engine backpressures may potentially affect the degree of dilution when diluting the exhaust prior to filtration in the DPF. Different backpressures may also affect engine performance and thereby affect the volumetric flow rate of the

exhaust. Each of the mentioned effects are discussed in the following in order to give an estimate of the potential contribution to uncertainties.

4.5.1 Effect on Dilution

For increasing preheater temperatures the pressure drop across the preheater will increase. This effect is seen as the manually logged engine back pressure at P1 increases for increased preheater temperatures. At conditions where V26 is not fully closed in a fixed position an increase in the stream bypassed is therefore inevitably observed for increased preheater temperatures. Likewise will an increased bypass be observed for increased loading of the DPF. This trend will remain despite maintaining a constant engine out pressure at P1 by continuously regulating the setting on F1 as the position of the latter facilitates in generating a sub atmospheric pressure in both the bypassed and the non-bypassed string. This means a fixed valve setting on V26 yielding a dilution ratio determined under non-preheated conditions may yield an increased dilution when the preheater is heated. This effect is presented in Table 16 where the degree of dilution is presented for both a non-preheated and a preheated exhaust stream under fixed conditions for air addition and the setting on V26.

Table 16 Differences in the degree of dilution for different temperatures of the preheater. Some of the exhaust is bypassed with identical valve settings and setting for F1. $1-\eta$ is the degree of dilution (see section 5.2).

$1-\eta$ (no preheating)	$1-\eta$ (HE1 set point = 500°C)	Difference / [%]
0.505	0.569	13.0

Furthermore increased deposition in the DPF will over time also contribute to variations in the dilution rate (see section 8.2.3).The above indicates that the gas phase composition needs to be regularly monitored during deposition in the DPF as the dilution ratio may change over time. Furthermore this emphasizes difficulties in obtaining similar degrees of dilution for different experiments.

4.5.2 Effect on Engine

Different engine out pressures will affect engine performance. Generally an increased backpressure onto the engine causes an increased resistance that needs to be overcome during the exhaust stroke which ultimately leads to increased energy loss and fuel consumption. The energy loss may be registered as an increased temperature of the exhaust.

A changed engine backpressure may affect the volumetric flow rate of the exhaust. In case of an increased backpressure onto the engine residual exhaust gas contained in the clearance volume of the cylinder will increase.

Assuming ideal gas behavior the molar increase of residual gas at increased pressure can be explained by the ideal gas law where a pressure increase greater

than a potential temperature increase results in an increased amount of residual gas for a constant volume.

By applying the ideal gas law the molar amount of gas contained in the clearance volume is proportional to a pressure increase and inversely proportional to a temperature increase. A loaded DPF may exhibit a pressure drop of 0.2 atm. Neglecting a potential temperature increase an increased engine back pressure of 200mbar results in a $^{0.2atm}/_{1atm} = 20\%$ increased molar amount of residual gas in the clearance volume compared to unhindered engine operation at atmospheric conditions at the exhaust manifold. During the intake stroke the increased amount of residual gas will expand and results in a reduced air intake equal to 20% of the clearance volume. Assuming a typical diesel engine compression ratio of 1:20 the reduction in volumetric exhaust flow rate is easily calculated from the displacement volume as:

$$\frac{1}{20-1} \cdot 20\% = 1.1\% \tag{4.2}$$

For the experimental setup used with the back-up generator operating at a fixed RPM the volumetric flow rate of the exhaust is therefore expected to remain constant with a deviation of a less than 1% for all engine operations as the magnitude of the air intake is main contributor to the magnitude of the exhaust.

4.6 TGA Uncertainties

For TGA experiments conducted by Hubeck-Graudal and Rønde (2011) a constant heating rate of 10K/min was used. They argued that a lower heating rate of 2K/min had only a negligible effect on the TGA measurements. The conclusion was based on experiments conducted by DTU student Martin Jakobsen as part of a master's study (Hubeck-Graudal et al. 2011); however, Jakobsen only compared the effect of different heating rates for the heating of diesel soot in an inert N_2 atmosphere. No experiments were conducted on the effect of TGA readings when heating at different heating rates in an oxidative atmosphere.

Sampling filter mass contributes to more than half of the sampled mass analyzed during TGA. Hubeck-Graudal and Rønde (2011) investigated the contribution to mass loss due to the presence of filter material in the samples used for TGA. A heating of only filter material in the TGA apparatus during conditions similar to TGA experiements conducted with sampled soot showed a mass loss of 1-2%. The filter mass loss was therefore accounted for in the TGA analyses conducted by Hubeck-Graudal and Rønde (2011).

Greater accuracy on determination of soot reactivity is ideally obtained if a greater mass of sampled soot is analyzed in TGA. Removal of the SOF prior to measurement of a soot sample through TGA thus potentially increases the accuracy of data obtained regarding temperature at which oxidation occurs most rapidly. Two

soot samples from the same soot sampling batch (combustion of petrodiesel at 80% load) have been used in order to determine if a removal of the SOF prior to measurement through TGA is of any relevance (see Appendix R – TGA Data). Pretreatment of one of the soot samples by heating in an inert N_2 atmosphere to 300°C prior to TGA yielded a temperature at which oxidation occurs most rapidly at a value of ~20°C lower than for the untreated sample, which undergoes SOF removal during the initial part of the TGA analysis (procedure as described in section 5.1). A reason for this behavior may be due to an increased deactivation of the latter sample due to an initial heating in an inert atmosphere up to 450°C which is 150°C greater than the temperature achieved prior to TGA with the pretreated sample. The removal of SOF prior to TGA did not facilitate a greater accuracy of the results obtained; however, no repetition has been carried out.

The NETZSCH STA-90C showed increased fluctuations in the mass loss signal. The values for SOF obtained as a result of using TGA are however not clearly indicative of the actual SOF value as a stable mass loss signal during both the isotherm and cooling provided in the analysis was not always obtainable. The latter may be related to the relatively low mass of soot analyzed due to the high content of filter material present. TGA data is provided in Appendix H - STA. Conduction of TGA on soot sampled at identical conditions at different times did however prove lack of repeatability. This contributes to increased uncertainty in the results obtained from the TGA data. Data obtained from TGA is further discussed in section 8.1.

4.7   Conclusions to Preliminary Observations

The valves located on the main exhaust piping proved leaking behavior when in a closed position. This together with an inaccuracy in the venturi meter readings at U1 provides a bypass that is not easily controlled when diluting the exhaust during experiments involving flow through operation with the DPF.

The experimental setup provides potential for a lot of uncertainties. Sampling on the sampling filter has shown great deviation in the flow at which sampled exhaust passes the filter. Furthermore the temperature of the sampling filter is potentially more than 30°C higher than what is registered as the external filter casing temperature. Measurements involving the use of the FID may be subject to great uncertainties due to calibration with a gas containing HC with a concentration a factor 10^2 greater than the concentration of HC measured during experiments. Furthermore the base line measurement contributes to nearly a quarter of the registered HC level. A great contributor to uncertainties and inaccuracies related to HC content and sampled soot mass may be the potential for deposition of PM along the pipe walls; however, preliminary calculations suggest that less than 0.1% of the soot aerosols are deposited upstream of the sampling/analysis. Visual inspection of the sampling pipes did however show considerable accumulation of deposited PM.

4.7.1 Potential Future Analysis

In order to obtain better accuracy in the FID readings a higher heat tracing temperature of up to 300°C is ideally desired. Also the calibration gas used for calibration should ideally contain volatile hydrocarbon content closer to the actual level registered during the combustion. General hydrocarbon emissions range from 20-300 ppm (Majewski and Khair 2006).

TGA on the same soot sample in order to prove repeatability of the analysis yielded coinciding values; however, it may still be desired to conduct TGA on the same soot sample with soot from the center of sampling filter only and soot near the edges in order to finally conclude if differences in flow pattern or temperature exist across the sampling filter which may yield different results with regards to the composition observed.

After sampling of soot a collection of the filter in a sealed atmosphere such as a plastic bag could undergo gas chromatography mass spectroscopy (GCMS) in order to indicate the composition of volatiles potentially evaporated from the sample immediately after sampling and hence potentially give a better estimate of the volatility of the SOF.

Finally the use of two filters stacked during sampling could help giving an indicator if some of the PM is not retained in one filter only; however, no quantitative conclusions can be derived from this as PM potentially capable of passing one sampling filter may also potentially pass more filters.

The addition of pure NO_2 is troublesome in the sense that heat tracing and additional safety precautions need to be taken into account. It may be worth considering the use of NO_2 diluted in N_2 in order to potentially ensure supply of the gas with a higher pressure and heat tracing and gas cylinder heating will not have to be used. In order to justify the use of dilute NO_2 one needs to take into account the additional gas volume added to the exhaust in order to obtain similar NO_2 concentrations as when pure NO_2 is added. Only 0.1L/min of pure NO_2 gas supplied at ambient conditions yields an addition of >1000ppm NO_2 for the exhaust indicating that using a gas with 10% NO_2 may contribute to a <1% increase of the volumetric flow rate of the exhaust.

5   Experimental Method and Assumptions

In the following the applied method when analyzing sampled soot in TGA is presented. Furthermore the calculations adopted and appertaining assumptions required in order to investigate the behavior of the DPF are presented.

5.1   TGA Method

Hubeck-Graudal and Rønde (2011) proposed a method for conducting TGA measurements on collected soot. The method involves heating in an inert atmosphere to promote devolatilization and evaporation of condensed hydrocarbons (SOF). The sample is subsequently heated in an oxidative atmosphere resembling that of a diesel exhaust gas in order to determine the temperature at which the soot is ignited and thereby the reactivity. The method will be used in this investigation and is as follows:

- Initial temperature: 30°C
- Heating to 450°C at 10°C /min (100% N_2)
- Isotherm at 450°C for 15 min (100% N_2)
- Cooling to 120°C (100% N_2)
- Heating sample to 750°C at 10°C /min (90% N_2, 10% O_2)

From the mass loss signal as a result of heating in an atmosphere containing oxygen the rate of mass loss expresses the rate of oxidation. No predefined standard for determination of soot reactivity or soot ignition temperature exists. For the purpose of this study the reactivity of the sampled soot determined is the temperature from the TGA at which oxidation occurs most rapidly denoted T_{max}. This serves as a comparative measurement of the reactivity of sampled soot and results obtained may be compared to results from Hubeck-Graudal and Rønde (Hubeck-Graudal et al. 2011).

5.2   Flow Calculations

The flow rate can only be determined as long as the gas stream is diluted with a known dilution ratio and the volumetric flow rate of the added air is known. Below in Figure 12 a schematic of the exhaust system including the engine outlet and the air addition inlet as streams entering and the outlet for the external bypass and flow through the filter (DPF) indicate outgoing streams. The addition of air happens downstream of the outlet for the external bypass and therefore one may assume, that during engine operation the force exerted by the exhaust gas is so great that all of the added air will be forced downstream. Dilution of the exhaust by air addition occurs by bypassing an amount of exhaust equal to the amount of air added thus keeping the volumetric flow rate through the DPF unchanged. Figure 12 shows molar flow rates and the molar fraction of a given species (for example CO_2) for each stream.
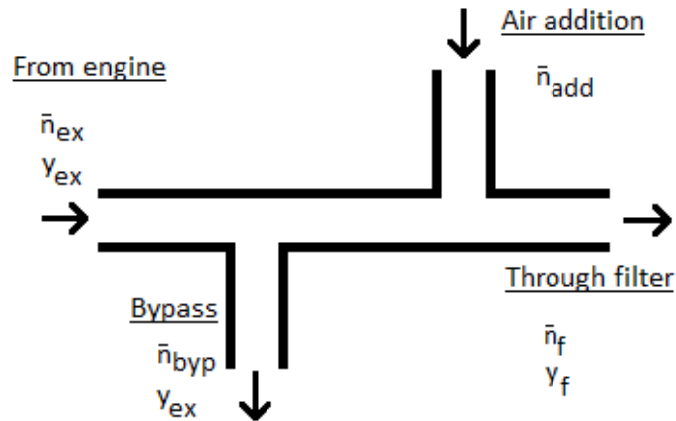
Figure 12 Shchematic representation of the gas going in and out in order to dilute the exhaust prior to filtration in the DPF. Molar flow rates are represented as $\dot{n}$ and molar fractions as y.

The most accurate way of determining the dilution ratio of the exhaust gas is by looking at data from the gas analyzers. Assuming that that the addition of air contains zero carbon dioxide the concentration of this species serves as an indicator of the dilution ratio of the exhaust gas. The degree of dilution is expressed by (1-η) where η is given as the ratio between the CO_2 concentration (y^{CO2}) registered in the diluted and the undiluted exhaust gas. A component balance yields the volumetric flow rate through the DPF calculated as the following where ambient conditions are assumed (see Appendix O - Flow Calculations for derivation):

$$Q_{filter} = \frac{Q_{add}}{1-\eta}, \ where \ \eta = \frac{y_f^{CO_2}}{y_{ex}^{CO_2}} \tag{5.1}$$

5.2.1   Corrected Flow

The venturi flow meter used has been calibrated for gas flows exhibiting a pressure of 1 atm and the volumetric flow rate logged is therefore based on this design pressure. For any volumetric flow rate logged at a different pressure the measured flow rate needs to be corrected in order to achieve the actual flow rate. In order to compare flow rates obtained at different pressures the actual volumetric flow rates must be correlated in relation to a standard pressure. The flow rate logged at U1 is used only for calibration of the rotameter FC3. Assuming ideal gas behavior and isothermal conditions volumetric flow rate is inversely proportional to the pressure and may be expressed as (see Appendix P – Corrected Flow for details)

$$Q_{corrected} = Q_{U1} \sqrt{\frac{P_{actual}}{P_{atm}}} \tag{5.2}$$

U1 does not provide an accurate measure of the flow rate when V26 is opened for a bypass configuration (see section 4.1.2). V26 is opened for bypass when it is desired to dilute the exhaust by adding dilution air through FC3. The rotameter (FC3) used for measuring the added volume of dilution air therefore needs to be calibrated in order to determine the accurate volumetric flow rate of added air. Due to the potential for leaking valves (see section 4.1.1) the external bypass valve V26 is sealed shut and V1, V2 and V3 are closed assuming added air through FC3 will only travel upstream in the exhaust system bypassing the DPF internally during flow meter calibration. The flow rate registered at U1 therefore equals the volumetric flow rate of air added. For varying settings on FC3 the volumetric flow rate registered at U1 has been logged together with pressure readings at P5 upstream of the venturi meter. For identical settings on FC3 the setting on F1 has been regulated in order to generate different sub atmospheric pressures at U1 with the pressure registered at P5. For each measurement the actual corrected volumetric flow rate has been calculated and can be seen in Appendix K – Flow Meter Calibration. Linear regression on the corrected volumetric flow rates as a function of flow meter setting coincide for different data series collected with different pressures registered at P5. This implies validity of the calculation used for determining the corrected volumetric flow rate independent of pressure (see section 5.2.1) and a correlation coefficient of $R^2 >$ 0.99 indicates that the setting on FC3 may be used in order to determine the volumetric flow rate added with reasonable accuracy.

The setting on the flow meter FC3 should ideally remain constant during filter cake formation when doing experiments involving loading of the DPF, however, despite ensuring a near constant engine out pressure the setting on FC3 has proven to not remain constant. For changes in pressure drop over the DPF of up to 100 mbar a reduction in added air flow up to 2.1m^3/h has been observed. The setting on FC3 should not be altered during DPF filtration in order to keep the amount of externally varied parameters to a minimum. The dilution ratio will be further affected by changing the setting on FC3. For all experiments involving dilution of the exhaust a dilution of ~50% would require an addition of 14m^3/h air through FC3 indicating a total flow through the DPF of 28m^3/h.

5.2.2 Flow through the DPF

The pressure drop registered over the DPF depends on the actual volumetric flow through the filter. Furthermore the latter is dependent on both pressure and temperature. The temperature of the gas passing the DPF is for simplicity assumed uniform along the DPF at a value equal to the filter temperature logged at T14. The

pressure of the flowing gas inside the DPF is also assumed uniform along the DPF and may therefore be calculated as:

$$P_{filter} = P_{afterDPF} + \frac{\Delta P_{filter}}{2} \tag{5.3}$$

In order to account for the effect on registered pressure drop over the DPF for different flow rates the registered value for ΔP_{filter} should ideally be correlated as a function of the flow rate through the DPF, Q_{filter}. For a flow of atmospheric air through a loaded DPF the pressure drop registered for variations in flow rate at a constant filter temperature equal to ambient temperature have been logged (see Figure 45 in Appendix Q – Flow through DPF). One may assume that the pressure drop is directly proportional to the flow rate only in accordance with Darcy's law (previously described in the literature study) assuming negligible changes in the friction factor. A linear regression on the data yields a correlation coefficient R^2=0.97; however, for simplicity it is assumed that the pressure drop over the DPF is directly proportional to the flow rate. The pressure drop over the DPF for a different volumetric flow rate passing the DPF can therefore be calculated as:

$$\Delta P_{filter,1} = \Delta P_{filter,2} \frac{Q_{filter,1}}{Q_{filter,2}} \tag{5.4}$$

Assuming ideal gas behavior the flow rate of the gas passing the DPF is inversely proportional to the pressure P_{filter} and directly proportional to the temperature T_{filter}. Combination of (5.1) with the volumetric flow rate of gas passing the filter the latter becomes:

$$Q_{filter} = \frac{Q_{add}}{1-\eta} \frac{T_{filter}}{T_{ambient}} \frac{P_{atm}}{P_{filter}} = \frac{Q_{add}}{1-\eta} \frac{T_{filter}}{298K} \frac{1013mbar}{P_{filter}} \tag{5.5}$$

6 Conclusions from previous studies on identical setup

DTU students Hubeck-Graudal and Rønde (Hubeck-Graudal et al. 2011) carried out experiments on the setup described in this study with identical diesels. Only minor alterations have been implemented in this study such as adding the potential for NO_2 addition prior to the DPF inlet, adding of new piping allowing for bypass regulated through V26 and a much stronger pump to ensure sub atmospheric engine out pressure has been mounted. Results obtained in the study by Hubeck-Graudal and Rønde (2011) are therefore valid and relevant for this study. Their results and conclusions are summarized below:

NO_x emissions: For the combustion of the different diesels the petrodiesel combustion gave the highest NO_x emissions (505ppm at 80% engine load); however, the combustion of vegetable diesel showed the highest peak concentration of NO_2 specifically (100ppm at 80% engine load). The higher NO_x emission from the combustion of petrodiesel is believed to be attributed to higher engine exhaust temperatures for the combustion of this fuel as higher combustion temperatures generally facilitate increased NO_x emission (see section 2.3.5). For increased engine load (0 - 80% load) increased engine out temperatures were observed together with increased emission of both NO and NO_2.

PM and HC emissions: Combustion of vegetable diesel showed the highest level of PM emission up to 0.56 g/m^3 at an engine load of 80%. At all engine loads the combustion of biodiesels (both vegetable diesel and animal fat) yielded soot having a lower fraction of carbonaceous core and thereby a higher fraction of SOF. This corresponds with an observed faster soot accumulation in the DPF when running the engine on petrodiesel due to the SOF not being trapped inside the DPF at heated conditions. Gaseous hydrocarbon emissions registered were higher for the combustion of petrodiesel which is believed to be attributed to a more volatile SOF observed in TGA results for the engine loads 0% and 40%. For an engine load of 80% the results however were ambiguous.

Soot reactivity: Combustion of vegetable diesel yielded soot more reactive than the soot from combustion of either animal fat or petrodiesel. Soot reactivity decreased for increasing engine loads (0 - 80% load). At a load of 80% the combustion of petrodiesel required the highest BET of 380°C for catalytically assisted regeneration of the DPF. The method used for determining the BET was based on the assumption that only the catalytic oxidation of soot by oxygen would facilitate a depletion of the deposited soot.

7 Experimental Strategy

Petrodiesel and vegetable diesel have been used for the experiments conducted in this study. Ideally also animal fat was considered to be a potential fuel; however, due to time limitations this diesel has been omitted from the experimental part of this study. The experimental setup is shown in a P&I diagram in Appendix I – P&I. For all experiments involving engine operation the engine load is kept constant at 80% (~4.8kW). For all of the final experiments the exhaust is led through the DPF in order to sample emitted PM and determine gaseous composition through sampling at SP1 (unfiltered exhaust). The experimental procedure involves a study on unfiltered emissions and the behavior of the DPF. A detailed procedure for operating with the engine and the appertaining experimental setup can be seen in Appendix T - Procedure.

Initially a study on the emissions from the aforementioned diesels is carried out. Sampled PM is analyzed in order to determine reactivity, SOF content and emission concentrations. This includes weighing of the soot samples and subsequent TGA (see section 5.1 for procedure). The results are compared among the vegetable diesel and the petrodiesel. Preliminary samplings on soot from petrodiesel are used in order to investigate the potential effect of preheating and diluting the exhaust. One may assume that trends observed and uncertainties remain unchanged for the different types of diesel.

Finally balance points for the DPF-operation are determined for both vegetable diesel and petrodiesel as the pressure drop over the DPF at which the rate of soot deposition equals the rate of soot oxidation. Equally with the addition of NO_2 added upstream of the DPF similar investigation is carried out for vegetable diesel combustion also. The temperature dependence of balance points is investigated by changing the preheater setting and monitoring the filter temperature inside the DPF. The experimental matrix can be seen in Table 17, Table 18 and Table 19. A single loading of the DPF where no regenerative behavior is expected (filter temperature T = 250°C) is carried out for both diesels in order to determine deposited mass of soot per pressure drop over the DPF. Furthermore a single loading of the filter with a preheater set point of 400°C is carried out in order investigate the rate of catalytic soot oxidation separately for vegetable diesel combustion only. Experiments involving filtering of the exhaust with DPF include a 50% dilution of the exhaust with atmospheric air. The dilution is not changed due to limitations in the experimental setup and V15 is sealed shut to ensure no internal bypass through leaking valve (see section 4.1). In order to keep a constant filter back pressure the pump F1 downstream of the filter is used to manually regulate the flow and for all conditions ensure an engine out pressure lower than -20 mbar.

Table 17 Schematic representation of experiments conducted involving DPF filtration of the exhaust from the combustion of petrodiesel. No NO$_2$ is added prior to the DPF inlet. The * indicates repetition of the experiment.

Diesel	HE1 set point / [C]	Dilution / [%]	Engine load / [%]	Comments
Petrodiesel	250	50	80	Measure ΔP_{DPF} during linear deposition profile
	500*	50	80	Measure ΔP_{DPF} until balance point
	525	50	80	Measure ΔP_{DPF} until balance point
	475	50	80	Measure ΔP_{DPF} until balance point

Table 18 Schematic representation of experiments conducted involving DPF filtration of the exhaust from the combustion of vegetable diesel. No NO$_2$ is added prior to the DPF inlet

Diesel	HE1 set point / [C]	Dilution / [%]	Engine load / [%]	Comments
Vegetable diesel	250	50	80	Measure ΔP_{DPF} during linear deposition profile
	400	50	80	Measure ΔP_{DPF} during linear deposition profile
	500	50	80	Measure ΔP_{DPF} until balance point
	475	50	80	Measure ΔP_{DPF} until balance point
	450	50	80	Measure ΔP_{DPF} until balance point

Table 19 Schematic representation of experiments conducted involving DPF filtration of the exhaust from the combustion of vegetable diesel. NO$_2$ is added prior to the DPF inlet

Diesel	HE1 set point / [C]	Dilution / [%]	Engine load / [%]	NO$_2$ added / [ppm]	Comments
Vegetable diesel	500	50	80	400	Measure ΔP_{DPF} until balance point
	450	50	80	400	Measure ΔP_{DPF} until balance point
	400	50	80	400	Measure ΔP_{DPF} until balance point

8 Experimental Results and Discussion

In the following results obtained from both experiments involving sampling of PM and flow through operation of the DPF in order to determine a BET are presented and discussed accordingly. Initially soot characteristics and emissions are investigated. Finally the DPF behavior is discussed with regards to results obtained.

8.1 Sampling Results – SOF, Soot Reactivity and Emissions

In the following an investigation on soot characteristics and emissions is conducted. The aim is to estimate the amount of soot emitted in order to estimate a rate of soot oxidation in DPF experiments. Equally the PM emission is compared to real engine emissions. Gaseous emissions and soot characteristics such as SOF and reactivity are compared for vegetable diesel and petrodiesel and the effect of preheating the exhaust is investigated. The reactivity of the soot potentially serves as a measure of the ease of DPF regeneration; however, the amount of soot emitted may also be equally important.

Soot reactivity, SOF content and the PM concentration of the exhaust is obtained from data on mass of sampled soot and subsequent TGA. In the following data is presented for the combustion of both petrodiesel and vegetable diesel at an engine load of 80% load only. Data presented for diluted exhaust is correlated in order to expresses the equivalent value for PM concentration in an undiluted case and flow rates are similar to those for undiluted exhaust. The engine out pressure remained at -20 to -30 mbar at all times with a temperature of at least 250°C indicating stable engine operation. For all samplings on the sampling filter the heat tracing upstream of the filter was heat traced at 180°C and the filter temperature measured remained in the range of 55-65°C (measured as the external temperature on the filter casing). In the following section only results obtained from sampling on unfiltered exhaust are presented and discussed according to two different sampling procedures, bypass of the DPF with sampling at SP2 or a flow through configuration of the DPF with sampling upstream of the DPF at SP1. The latter case involved prior to each experiment a preconditioning treatment of the main pipes by sending through atmospheric air for ~20 minutes heated to around 500°C and the sampling pipe was cleaned with ethanol and dried with pressurized air. The reactivity, SOF content and the mass of sampled PM has shown great variability in obtained results. The sampling point and a preconditioning treatment of the setup have shown to greatly affect the obtained results.

8.1.1 Sampling points

Conduction of experiments where the DPF was bypassed involved investigating the effect of preheating on the sampled mass and SOF. The data obtained from sampling at SP2 in a bypass configuration can be seen in Figure 13 and data obtained from sampling at SP1 can be seen in Figure 14.
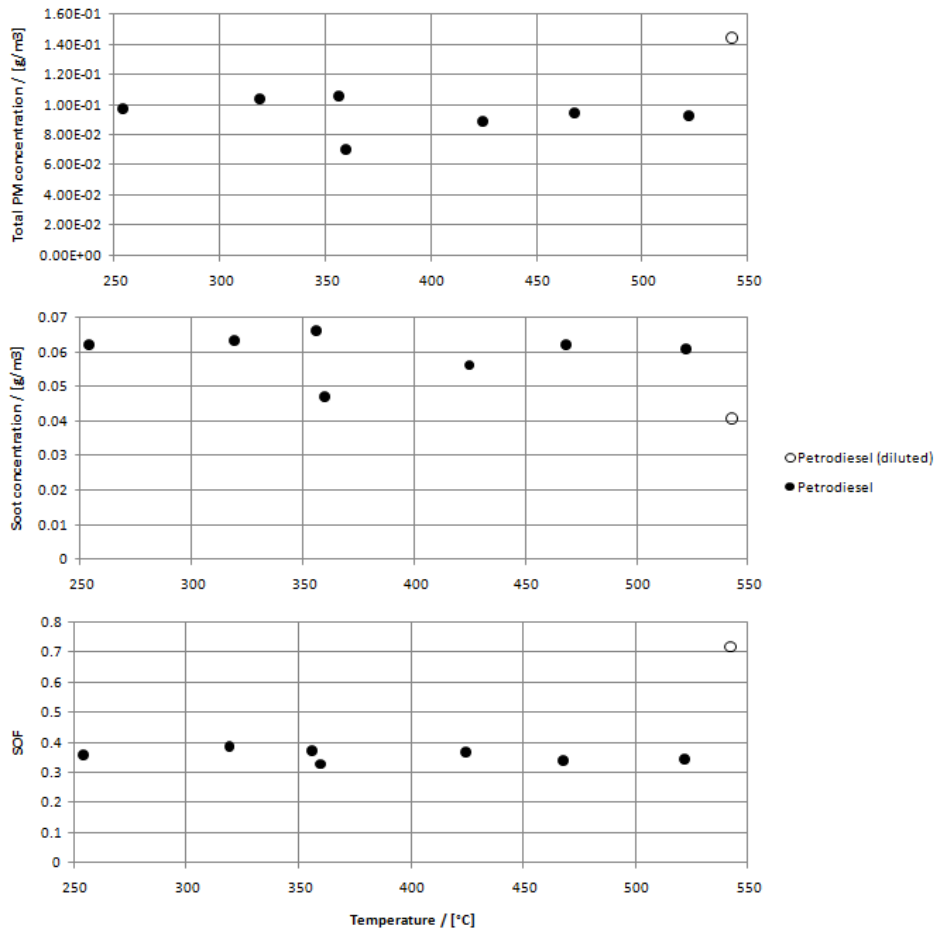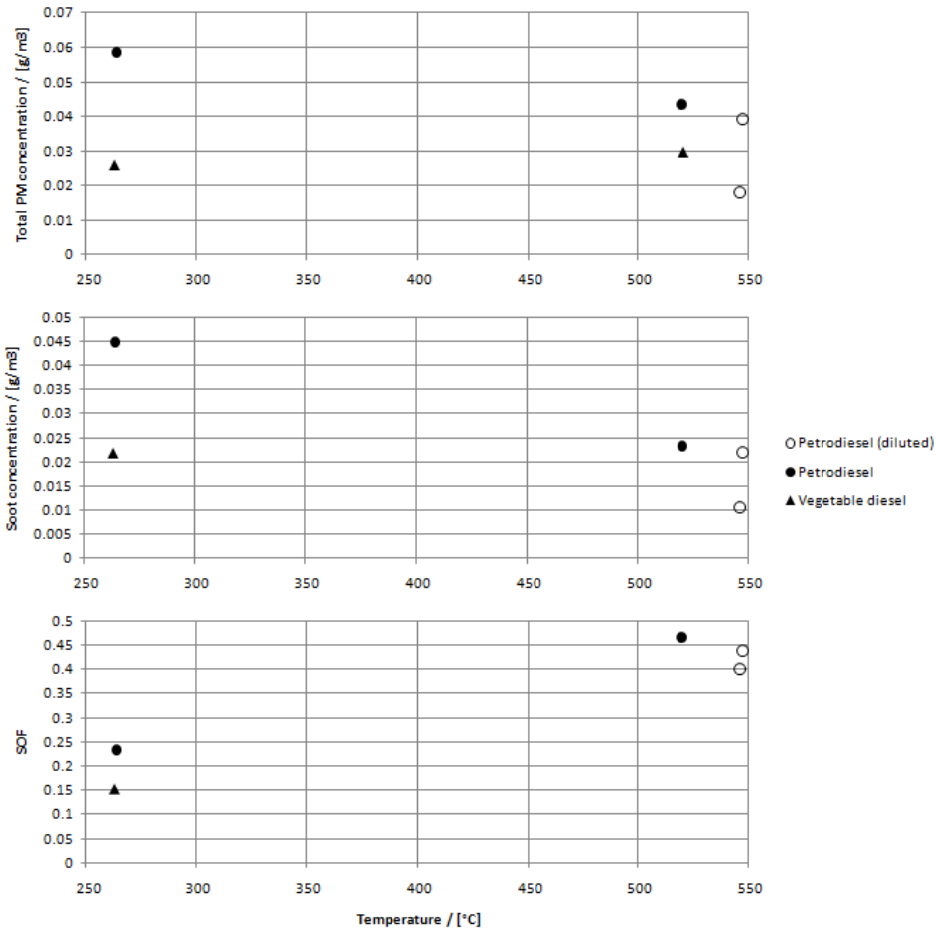
Figure 13 Emission of PM as a function of the highest temperature exhibited by the exhaust prior to sampling. The SOF is determined from TGA. All of the data is from the combustion of petrodiesel at 80% load. Exhaust is sampled at SP2 in a bypass configuration of the DPF.

Figure 14 Emission of PM as a function of the highest temperature exhibited by the exhaust prior to sampling. The SOF is determined from TGA. All of the data is from the combustion of petrodiesel at 80% load. Exhaust is sampled at SP1 in a flow through configuration of the DPF post cleaning with ethanol of the sampling and preconditioning operation with elevated temperatures.

For sampling results from SP2 (see Figure 13) preheating did not show any noticeable effect on the magnitude of the SOF registered for sampling on undiluted exhaust; however, for sampling on diluted exhaust both the total PM concentration as well as the magnitude of the SOF showed higher values. The contribution to PM concentration from the carbonaceous soot core for sampling from SP2 is however lower than for the undiluted exhaust both non-preheated and preheated up to more than 500°C. The soot concentration derived from soot sampled at SP2 in the bypass configuration expresses values for total PM larger than for PM sampled at SP1 prior to the DPF inlet (see Figure 14); however, the mass of carbonaceous soot core

sampled show values more similar therefore contributing to a higher magnitude of SOF registered when sampling in a bypass configuration of the DPF.

For the experiments involving sampling at SP2 no preconditioning heat treatment or cleaning of the piping bypassing the DPF was conducted hence there is an increased potential for reentrainment of previously deposited PM along the pipe walls. Furthermore the temperature of the piping downstream of V15 is uncontrolled meaning that SOF may condense prior to sampling of the soot if the temperature drops below the SOF evaporation temperature (see section 4.2). Preheating of the exhaust may lead to temperatures that exceed the temperature required for SOF evaporation and thus contribute to evaporation and thereby a reentrainment of previously deposited SOF along the pipe walls. This may explain the effect of an increased SOF registered when bypassing the DPF. One may finally conclude that huge uncertainties are involved in sampling after a bypass configuration of the DPF and emphasizes the necessity for a preconditioning treatment of the string upstream of the sampling filter. Sampling of unfiltered exhaust should therefore be achieved by sampling at SP1 prior to leading the exhaust through the DPF. For this reason data presented in the following is derived from sampling in the latter configuration only and data from Figure 14 only will be discussed.

8.1.2 PM Emissions

Increased temperatures experienced by the exhaust prior to sampling of PM results in a reduction of the total PM emitted for petrodiesel soot but an increase for soot from vegetable diesel combustion (see Figure 14). This apparent relation is unexpected as one would expect the soot from both vegetable diesel and petrodiesel to behave similarly. However, lack of data points and the potential for uncertainties may be attributed to the obtained values (see section 4.2).

TGA data for sampled soot (later described in section 8.1.4.1) did show a temperature at which soot oxidation occurs most rapidly (T_{max}) above 570°C; however, as this is not an accurate measure of the exact and lowest temperature at which soot can undergo combustion in an atmosphere containing 10% oxygen one would expect the potential for oxidation of the soot to some extend when preheating the exhaust. One must also take into account the fluctuations observed by the preheater as an average preheater temperature of 550°C may include fluctuations of up to over 600°C for the exhaust temperature (see section 3.2). Due to lack of data it is not easily concluded whether the effect of diluting the exhaust by ~50% atmospheric air has any considerable effect on the extent to which the total PM concentration is reduced due to preheating as the oxygen concentration is effectively increased from 11% to near 16%.

Below in Table 20 the total PM concentration as well as contribution to total PM concentration from carbonaceous soot core is summarized for both petrodiesel and vegetable diesel. The values are for non-preheated exhaust only and for simplicity

those are the values used when it is desired to get an estimate of the rate at which soot enters the DPF for experiments involving loading of the DPF (see section 8.2).

Table 20 The table shows the total PM concentration as well as contribution from carbonaceous soot core. The data is for an engine load of 80%. The sampling filter was 55-65°C and the heat tracing upstream the sampling filter was 180°C. The results are for non-preheated exhaust only

Diesel	PM concentration with no preheating / [g/m^3]	Contribution to total PM from carbonaceous soot core / [g/m^3]
Petrodiesel	$5.84*10^{-2}$	$4.48*10^{-2}$
Vegetable diesel	$2.58*10^{-2}$	$2.19*10^{-2}$

From the data obtained petrodiesel showed a total PM concentration in the exhaust almost twice as large as for the combustion of vegetable diesel. The uncertainties related to determining the SOF and the total PM concentration previously described may however describe this behavior as experiments conducted by Hubeck-Graudal and Rønde (2011) on similar diesels showed near the opposite trend with a total PM emission from petrodiesel of $1.2*10^{-1}$g/m^3 and $4.5*10^{-1}$g/m^3 for vegetable diesel both values greater than values obtained in this study; however, also greater amounts of SOF were observed by Hubeck-Graudal and Rønde (2011). Generally one would expect a lower total PM emission from the combustion of biodiesel. Due to the increased uncertainties potentially attributed to the actual SOF registered the mass of carbonaceous soot core also presented in the table below is believed to be of greater accuracy. For the purpose of this study it is necessary to know the mass of carbonaceous soot core emitted as the SOF is either readily combusted or in gaseous form when the exhaust is filtered by the DPF at elevated temperatures. Therefore the contribution from carbonaceous soot core is a relevant measure in order to investigate the behavior of DPF during loading with soot.

8.1.2.1   *Comparison with Standard PM Emissions*
In order to compare diesel powered engines standard PM emissions a comparison of different units is required. Different units describing PM and gaseous emissions are used in the literature. The Euro standards use "g/km" whereas laboratory scale experiments often use "ppm". On road testing results may express emissions as "g/km". In order to compare emissions it is desired to convert the units. When the RPM, vehicle speed and cylinder volume is known the units for emission of both gaseous species and PM can be readily converted between ppm, g/km and g/h. An excel sheet has been made for that purpose and the method adopted is shown in Appendix M - Conversion of Units. The above implies that some assumptions regarding vehicle speed and cylinder volume may be required in order to express the PM emission in a comparable form.

Great differences are often seen in typical exhaust emissions found in the literature. Furthermore often lack of information is given in order to ensure comparable data. Van Setten et al. (van Setten et al. 2001) listed for a typical 1998 passenger car diesel engine and a typical heavy-duty truck typical exhaust emissions for different engine loads and RPM. The type of diesel used is unclear. This data is presented in Table 21 below together with Euro 3/III standards and the total PM emissions from the back-up engine used for the studies in this experimental investigation (engine operation at 80% load with petrodiesel and non-preheated exhasut). The Euro standards presented indicate what were achievable PM emission limits for unfiltered exhaust prior to year 2000 (Majewski and Khair 2006).

The units have been converted in order to express mass of soot emission per exhaust volume assuming a vehicle speed of 90 km/h for the conversion of units from the Euro 3 standards and an exhaust flow rate equal to the value for the passenger given ($2.4 \cdot 10^2 \; ^{Nm^3}/_h$). In order to convert the Euro III standards for heavy-duty vehicles an effect and an exhaust flow rate equal to the value for the truck given ($1.2 \cdot 10^3 \; ^{Nm^3}/_h$) is assumed.

The PM emission from the back-up generator is calculated from the data given for petrodiesel PM emission in Table 20 assuming an exhaust flow rate of 30 Nm^3/h. The difference in data presented emphasizes difficulties associated with comparing PM emissions; however, the main purpose in the following is a comparison to the back-up generator used in these experiments only. The total emission expressed as mass per exhaust volume serves as directly comparable measure of the degree to which the DPF is exposed to soot as the DPF used in the experiments conducted has been scaled according to the magnitude of the volumetric flow rate.

Table 21 Typical exhaust emission of PM for a range of different diesel engine operating at different conditions (van Setten et al. 2001)**. Selected Euro emission standrrds are also included** (Dieselnet 2011) **The emission from the backup generator used in this study is also included based on emission for petrodiesel given in Table 20. The units for emissions have been converted according to the method described in section 8.1.2.1.**

Engine	RPM	Effect / [kW]	Speed / [km/h]	Exhaust flow rate / [Nm^3/h]	Total PM emission / [g/h]	Total PM emission / [g/Nm^3]
Passenger car	4000	-	-	2.4*10^2	0.7	2.9*10^{-3}
Truck	2000	210	-	1.2*10^3	16.8	1.4*10^{-2}
Euro 3 (LD vehicle)	-	-	90	2.4*10^2	4.5	1.9*10^{-2}
Euro III (HD vehicle)	-	210	-	1.2*10^3	21	1.8*10^{-2}
Back-up generator	3000	4.8	-	3.0*10	1.8	5.8*10^{-2}

The data presented in the Table 21 above indicates that the PM emission from the back-up generator exceeds both the vehicular emissions as well as Euro 3/III standards. The back-up generator seemingly exposes the DPF to more than ~3 times the amount an automotive vehicle prior to year 2000 would do. This indicates that the DPF performance experienced in the experiments conducted in this study should be worse than for filtering on real automotive engine exhaust.

It has not been proven possible to fully regenerate the DPF at temperatures as high as ~500°C (see section 8.2.3) which would be required for the emission from a real automotive diesel engine involving operational cycles with active DPF regeneration. The data in the table above however represents only the emissions from higher engine loads and taking into account the assumptions required for the conversion of units it is difficult to fully compare the emission from the backup generator used in this study to real automotive engines. The emission from back-up generators in general was previously described in section 2.1.3 and different studies on back-up generators also showed an increased PM emission compared to real automotive engines. For this reason the emission from the back-up generator used in this study is possibly best compared to the emission from a HDD-vehicle. Due to generally higher exhaust temperatures from heavy duty vehicles a passive regeneration strategy of the DPF can be applied.

8.1.3   SOF

Sampled diesel PM at a configuration with no dilution or preheating has been analyzed in a TGA in order to determine the temperature at which the SOF evaporates and the fraction of the soluble organics. The data is presented in the table below for both the combustion of petrodiesel as well as vegetable diesel. The point of evaporation is in this context defined as the point on the mass loss curve from TGA that expresses a mass loss occurring most rapidly.

Table 22 The SOF and temperature required for evaporation as a result of TGA on sampled soot. The data is for non-preheated exhaust only with an engine load of 80%. The sampling filter was 55-65°C and the heat tracing upstream the sampling filter was 180°C. Data for preheated exhaust resulting from combustion of vegetable diesel is not included due to failed TGA operation and time did not allow for a repetition. TGA data from which evaporation temperatures have been read are shown in Appendix H - STA.

	SOF evaporation temperature / [°C]		SOF	SOF
Diesel	No preheating	Preheater set point = 500C	No preheating	Preheater set point = 500C
Petrodiesel	155 – 185	155	0.23	0.47
Vegetable diesel	155 – 185	-	0.15	-

For soot sampled on both non-preheated and preheated exhaust the SOF showed temperatures lower than 185°C required for evaporation. The exact value is not easily obtained as the point on the mass loss curve obtained from the TGA which

shows the steepest slope as the point of evaporation is not always clear. The latter may depend on the smoothing of the mass loss curve (dm/dt) required hence the SOF evaporation temperature is sometimes best described as a visually estimated interval. Mass loss curves can be seen in Appendix H - STA.

The temperature required for evaporation of SOF from petrodiesel soot is seemingly identical for vegetable diesel soot for non-preheated exhaust. The evaporation temperature for the preheated petrodiesel soot is seemingly unaffected by preheating with respect to SOF evaporation temperature. Due to the difficulty in obtaining an excat value for the temperatue at which the SOF evaporates it is difficult to conclude on the values presented as ideally more sampled data is desired. However, The SOF evaporation temperature may be unaffected by preheating judging from the relatively small temperature range in which evaporation temperatures have been found. This may indicate that the composition of the SOF is unaltered as a result of preheating of the exhaust. Equally diluted preheated exhaust expresses coinciding values for evaporation temperature with data from undiluted exhaust which indicates that the composition of the SOF is unaltered as a result of diluting the exhaust (TGA data for the SOF evaporation is provided in Appendix H - STA)

For the combustion of petrodiesel the amount of SOF showed an increase from 0.23 to 0.47 (see Table 22) as the result of an increase from no preheating of the exhaust to a preheating of above 500°C. This together with the trend of seemingly a reduction of total PM as a function of preheating the exhaust for the combustion of petrodiesel may indicate that the amount of volatile hydrocarbons condensed on the soot remains unchanged as a result of preheating thereby causing a reduction in soot concentration only. This is contrary to what one would expect as SOF consisting of more easily oxidized hydrocarbons would be oxidized to a greater extent than soot if oxidative conditions are exhibited due to high temperature exposal of the exhaust passing the preheater.

For the combustion of vegetable diesel the SOF was registered at a much lower value than for petrodiesel soot. The lower SOF registered in vegetable diesel compared to petrodiesel soot is contrary to what has previously been observed by Hubeck-Graudal and Rønde (2011) who registered a SOF value for petrodiesel of 0.45-0.65 and for vegetable diesel 0.7-0.9. They also observed highest deviation in obtained SOF values for the engine load of 80% contrary to 0% and 40% engine load. The much greater values obtained by Hubeck-Graudal and Rønde (2011) emphasizes the uncertainties involved in investigating the SOF especially under conditions with high exhaust temperatures such as during high engine load or when preheating the exhaust. Typical SOF content of the total PM ranges from 10-50% (Majewski and Khair 2006). Generally lower SOF is experienced for higher engine loads (Majewski and Khair 2006).

The uncertainties involved in determining the SOF content may be attributed to uncertainties attributed to the sampling (see section 4.2) such as uncontrolled

temperature of the sampling filter which under higher temperatures may allow for the passage of uncondensed SOF thus resulting in lower values of SOF registered. The uncertainties may also be attributed to evaporation of previously condensed SOF in the pipes upstream of the filter as a result of potentially improper cleaning prior to sampling. Finally transient engine operation and transient patterns in emissions may also contribute to uncertainties associated with determining the SOF. Considering the uncertainties attributed to the determination of the SOF the total PM concentration determined thus becomes equally uncertain

8.1.4   Soot Reactivity

In the following the effect of preheating on soot reactivity is investigated. This is carried out by looking at the temperature at which the soot allows for combustion in TGA and the data obtained from the mass loss curve to further estimate an apparent activation energy which also serves as a measure of the ease of soot combustion.

8.1.4.1   Temperature Required for Oxidation

In order to compare the reactivity of different soot samples towards oxidation by O_2, the point on the mass loss curve obtained from TGA at which oxidation occurs at the highest rate is used as a comparative measure of the reactivity denoted T_{max}. The data is presented in Figure 15 below as T_{max} as a function of the highest temperature experienced by the exhaust after leaving the exhaust manifold. TGA data showing the rate of mass change as a function of temperature is provided in Appendix R – TGA Data.
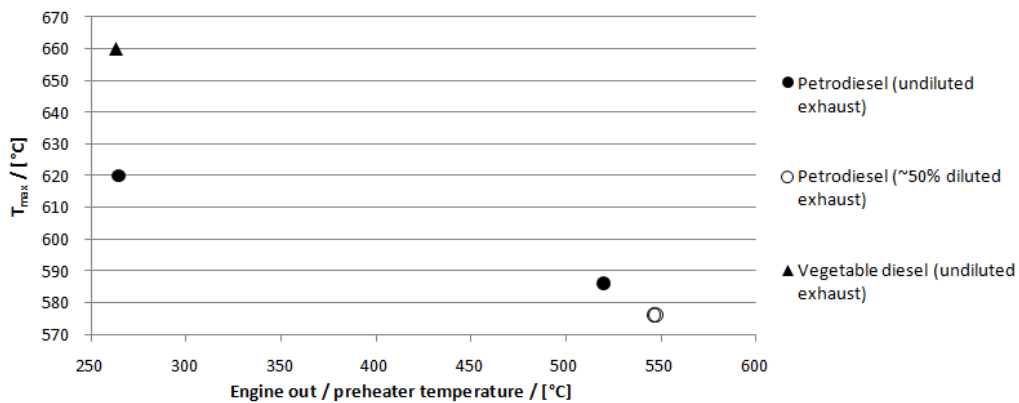

Figure 15 T_{max} for petrodiesel and vegetable soot combusted at 80% load plotted as a function of highest temperature experienced by the exhaust prior to sampling. The sampling filter was 55-65°C and the heat tracing upstream the sampling filter was 180°C.

Some uncertainty is attributed to the determination of the soot reactivity as proper averaging of the mass loss curve needs to be carried out in order to clearly identify a local maximum on the mass loss curve from the TGA. The soot reactivity is seemingly unaffected by a ~50 % dilution prior to preheating with a preheater set point of

500°C as both preheated undiluted and diluted exhaust show T_{max} of 586°C and 576°C respectively. For a non-preheated exhaust the soot seemingly requires over 40°C higher temperature in order to reach T_{max}. Due to the few data points and the uncertainties attributed to determining T_{max} it is not possible to derive a clearly defined tendency of increased soot reactivity as a function of increased temperature exposal to the exhaust. One would generally expect the opposite behavior as an exposure to higher temperatures of the soot could lead to an increased deactivation of the soot. Preliminary investigation by pretreatment of a soot sample in an inert atmosphere by heating up to 300°C prior to conducting TGA also showed an increased deactivation towards ignition (see section 4.6). The combustion of vegetable diesel showed soot requiring a temperature higher than that for petrodiesel in order to achieve ignition. Generally one would expect the opposite as the higher oxygen content of the biodiesel among other factors will contribute to an increased reactivity towards oxidation (Majewski and Khair 2006). Experiments conducted by Hubeck-Graudal and Rønde (2011) showed closely resembling values for T_{max} of the same petrodiesel and vegetable diesel at a temperature of 650-660°C.

8.1.4.2 Activation Energies

The TGA provides a mass loss signal as a function of time and temperature. Assuming a first order dependence on the mass of soot present in the crucible the rate of reaction with oxygen may follow the following expression where the rate constant follows an Arrhenius expression. Contribution to a diffusion controlled regime is neglected due to the relatively high concentration of oxygen. As the oxygen concentration during all of the experiments with TGA conducted remained constant the pre-exponential factor and the oxygen dependence is expressed through one constant k. Reaction order with respect to mass is assumed unity

$$\frac{dm}{dt} = -k \exp\left(\frac{-E_A}{RT}\right) m \tag{8.1}$$

A plot of $\ln\left(-\frac{dm}{dt} \cdot m^{-1}\right)$ as a function of 1/T ideally yields a straight line from which the slope can be read in order to yield the activation energy. Furthermore the intersection with the secondary axis may be used to express the value of k.

$$\ln\left(-\frac{dm}{dt} m^{-1}\right) = -\frac{E_A}{RT} + \ln(k) \tag{8.2}$$

The mass loss curves as a result of exposing sampled soot to TGA have been treated according to (8.2) in order to obtain a value for the activation energy for the combustion of soot in an atmosphere of 10% O_2. $\ln\left(-\frac{dm}{dt} \cdot m^{-1}\right)$ as a function of 1/T is shown in Figure 16 plotted for the interval in which oxidation by O_2 clearly

proceeds. The last part of the mass loss curve as the mass of remaining soot approaches zero has been edited away in order to obtain greater accuracy (better linear fit) in the obtained activation energy. The values of E_A are shown in Table 23.
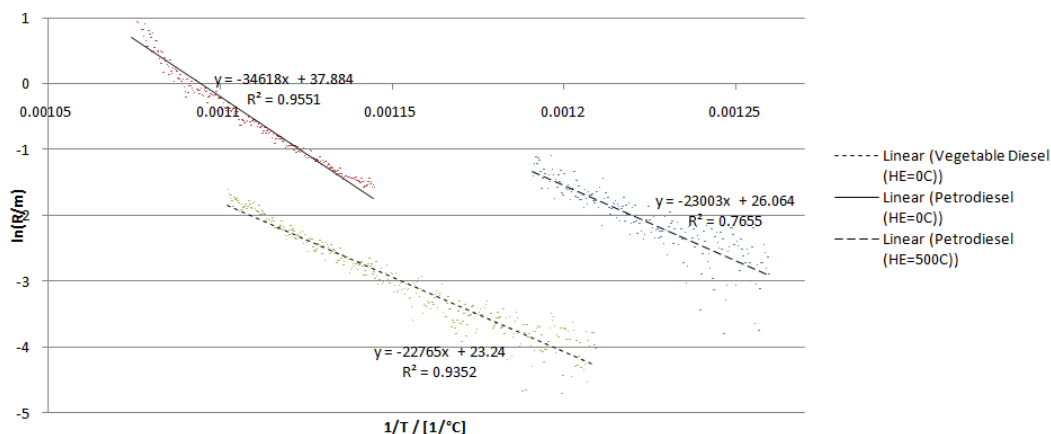

Figure 16 The plot shows extended data treatment on the mass loss signal obtained from TGA for both preheated and non-preheated petrodiesel exhaust and non-preheated vegetable diesel exhaust. The mass loss is plotted according to (8.2).

Table 23 Activation energies obtained from the slope of the graphs on Figure 16.

	Petrodiesel		Vegetable diesel	
Preheater set point / [°C]	-	500	-	500
E_A / [kJ/mol]	132	191	189	-

Only values for activation energies are shown as one may attribute greater uncertainty to the value of k. The uncertainty attributed to the value of E_A is seen from the value of the correlation coefficients also presented in Figure 16 expressing a low value of $R^2<0.9$ for preheated petrodiesel soot. The values presented in Table 23 do somewhat represent what is expected from the combustion of soot in an atmosphere containing oxygen (see Table 10). The results seemingly indicate that preheating of the soot samples yields an increase in the activation energy. This is what one would generally expect as a result of potentially increased deactivation of the soot due to exposure to higher temperatures prior to combustion. From the values presented in Table 23 soot from vegetable diesel seemingly has higher activation energy than soot from petrodiesel which is generally unexpected as one would expect an increased reactivity of the vegetable soot due to potentially higher oxygen content (see section 2.4.3). The apparent higher value of activation energy is however in agreement with the higher temperature required for ignition than for petrodiesel soot (see section 8.1.4.1) which also indicates a lower reactivity towards oxidation.

8.1.5   Gaseous Emissions

Data obtained from the gas analysis for the combustion of both petrodiesel and vegetable diesel is presented in Table 24 and Figure 17. The data is from undiluted exhaust with an engine operation at 80% load at steady state. The latter was implied by an exhaust temperature of at least 250°C.

Table 24 Gaseous emissions from the combustion of non-preheated and undiluted exhaust at an engine load of 80%. HC concentration for the combustion of vegetable diesel has not been measured as the heat tracing upstream of the FID stopped working.

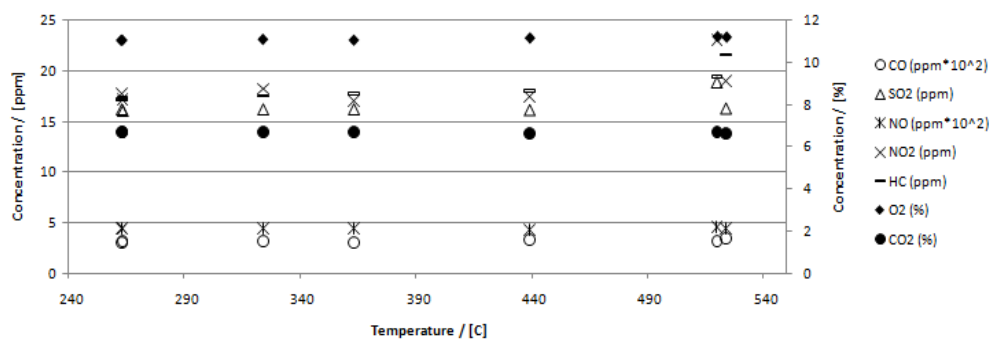| Diesel	O_2 / [%]	CO_2 / [%]	CO / [ppm]	SO_2 / [ppm]	NO / [ppm]	NO_2 / [ppm]	HC / [ppm]
Petrodiesel	11.1	6.7	313	16	442	18	17
Vegetable diesel	11.3	6.9	463	20	511	11	-

Figure 17 Gaseous emissions for the combustion of petrodiesel at an engine load of 80% as a function of the highest temperature exhibited by the exhaust prior to analysis. Exhaust gas was undiluted.

A comparison between gaseous emission form the combustion of petrodiesel and vegetable diesel (see Table 24) indicates an increased concentration of oxygenated gaseous species such as CO_2, CO and total NOx while the oxygen concentrations are near identical. Similar trend was observed by Hubeck-Gradual and Rønde (Hubeck-Graudal et al. 2011); however, NO_2 emissions up to more than 100ppm were observed. The increase in oxygenated gaseous species of the exhaust by the combustion of biodiesel may be attributed to the higher oxygen content of the fuel compared to petrodiesels. Biodiesels typically contain up to 11% O_2 (Majewski and Khair 2006). Differences in exhaust emissions may also be attributed to different combustion patterns inside cylinders. Biodiesel combustion generally emit higher emissions of NO_x (Majewski and Khair 2006). Both the petrodiesel and the vegetable diesel used for the experiments contain similar sulfur content which may be seen from similar values for SO_2 emission as well. In the table below FID readings are not included for the combustion of the vegetable diesel as the heat tracing upstream the

apparatus was not functioning and values obtained may therefore contain increased inaccuracy due to the potential for condensation of volatiles in the piping. Differences in combustion patterns inside the engine cylinder can also greatly affect the products of combustion.

For the combustion of petrodiesel the effect on gaseous emissions by changing the setting on the preheater has been investigated (see Figure 17). Concentrations of CO_2 and O_2 remained unchanged for preheating up to 500°C, and generally only negligible deviations have been observed at steady state operation with a standard deviation on measured values of 0.1% measured units. Equally the CO and NO concentrations did not show any changes due to changes in the preheater setting from zero to 500°C. The concentration of NO_2 did however show a minor increase of ~5 ppm from non-preheated exhaust to preheating up to over 500°C, however, this increase is assumed negligible taking into consideration the uncertainties related to the measurements. The concentration of volatile hydrocarbons however did show a tendency towards increased concentration for increased preheating. Measured values of volatile hydrocarbons may be attributed a great uncertainty to the measured value as an increase of only 4 ppm HC is observed for an increase in preheating from zero to excess 500°C. This value is lower than the base line of ~7 ppm observed for the FID measurements and equally great uncertainty is attributed to the calibration of the FID (see section 4.3.2). No clear tendency was observed for the magnitude of the SOF as a function of preheating; however, great uncertainties have been attributed to the magnitude of the SOF (see section 4.2 and 8.1.3).

8.2 DPF Experiments

In the following results obtained as a result of filtering the exhaust are presented and discussed. It is desired to relate a given pressure drop over the DPF to a given amount of deposited soot. For this reason the DPF is loaded at conditions where soot only is deposited but not subsequently oxidized. Equally the DPF is loaded under regenerative conditions in order to investigate the effect of soot oxidation. Balance points obtained for operation with filtering of the exhaust through the DPF serve as an indicator of DPF performance. The latter is discussed for a comparison between petrodiesel and vegetable diesel and further the effect of adding additional NO_2 upstream of the DPF. Finally a discussion on an estimated soot layer thickness for all experiments involving balance point operation emphasizes assumptions and uncertainties in regards to the discussions on the filter performance.

8.2.1 Non-regenerative Linear Loading of the DPF - Correlated Pressure Drop

The pressure drop over the DPF as a function of time is plotted together with the temperature of the DPF in Figure 18 below. The plot shows the results of combustion of petrodiesel at an engine load of 80%. The exhaust achieved a steady temperature before being sent through the DPF and the stream has been diluted (~50%) in order to determine the volumetric flow rate (see section 5.2). The valves V26 and V15 may be sealed, but then the transient behavior of the engine during start up, would result in transient conditions during the initial part of DPF filtration, as exhaust would have to pass the DPF immediately after turning on the engine.
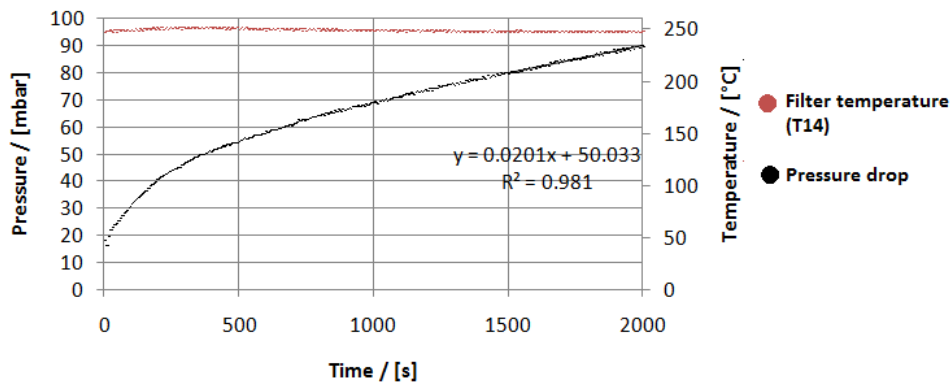

Figure 18 Deposition of soot in the DPF from the combustion of petrodiesel at an engine load of 80%. Degree of dilution was 1-η=0.51. Both the pressure drop and the filter temperature are shown as a function of temperature. Linear regression on the pressure drop curve has been carried out for the time interval 1500-2250s.

It is evident that during the linear pressure buildup the temperature of the filter remains at a constant value of 250°C. Assuming that no SOF condenses (see section 8.1.2) and the porosity of deposited soot remains unchanged the pressure increase can be assumed to be directly proportional to deposited mass of carbonaceous soot

core hence ideally also expressing a soot layer thickness. One may assume that the temperatures experienced inside the DPF are low enough to neglect the potential oxidation of deposited soot (Haralampous et al. 2004). Hubeck-Graudal and Rønde (Hubeck-Graudal et al. 2011) observed a catalytic effect for temperatures exceeding 380°C only.

After ~400 seconds of deposition the rate at which the pressure drop increases changes significantly. This may be caused by a change applied to the pump setting of F1 in order to ensure an engine out pressure of near -25mbar when exhaust is sent through the DPF. The rate at which the pressure drop changes does however decrease slightly after 400 seconds of operation until a near linear pressure buildup is experienced. Assuming that all of the soot sent through the DPF is retained the decrease in the rate at which pressure is build up may indicate a transition from depth filtration to cake filtration as the volumetric flow rate through the DPF remained near constant during the given time interval. Assuming a 100% retention of soot during wall filtration the initial 500 seconds of deposition is equal to 9.0 mg of soot. This assumption is generally not valid as soot retention during wall filtration only is much lower than during cake filtration. For this reason the mass of soot is a potential maximum. Assuming a filter wall porosity of 0.5 (Law et al. 2004) for the given geometric filter parameters (given in Appendix D - DPF and Oven) the maximum volume fraction of soot in the filter pores is <1%.

From Figure 18 the clean filter pressure drop at the given flow conditions can be seen as ~20 mbar. During the linear deposition both the dilution ratio and the flow rate through the filter remained constant with a deviation of <1%. The degree of dilution was 0.51 for the time interval 1,500-2,000 and the appertaining change in pressure drop then yields for the given flow conditions in the filter a mass of deposited soot per pressure drop during cake filtration equal to 8.9 mg/mbar (assuming a constant emission of carbonaceous soot core of 44.8 mg/m^3 for undiluted exhaust as presented in section 8.1.4.2). Equally for the combustion of vegetable diesel deposited soot per pressure drop during cake filtration has also been determined equaling 6.9 mg/mbar (a plot showing the linear deposition profile is shown in Appendix S – Vegetable Diesel DPF Loading). As the linear loading of the DPF at the conditions described is not carried out at identical exhaust flow rates due to the inaccuracies related to diluting the stream the values for mass of deposited soot per pressure are normalized with respect to a standard volumetric flow rate of 30m^3/h through the DPF. A table showing deposited soot core per filter pressure drop together with the clean filter pressure drop can be seen in Table 25 below:

Table 25 mass of deposited soot core obtained from experiments by loading the DPF with a filter temperature of ~250°C. The values are normalized for a standard exhaust flow rate of 30m³/h passing through the DPF.

Diesel	Deposited soot core per DPF pressure drop / [mg/mbar]	Clean filter pressure drop / [mbar]
Petrodiesel	16.7	10.7
Vegetable diesel	12.6	

Neglecting the mass of soot deposited due to depth filtration and assuming that deposited soot has an unchanged porosity and the mass of deposited soot at all conditions is proportional to the soot layer thickness the above can be used in order to estimate the amount of soot retained in the DPF at BET when the flow rate is normalized. The clean filter pressure drop is subtracted prior to estimating the mass of deposited soot. For heavy degrees of filter loading one may assume that the contribution to depth filtration is negligible especially under regenerative conditions where soot deposition in the filter wall is oxidized catalytically. The obtained values for mass of deposited soot per pressure drop are used in the calculation/estimation of the mass of soot deposited when a balance point of the DPF operation is observed (see section 8.2.3).

The masses of deposited soot core per DPF pressure drop shown in Table 25 indicate a difference in the characteristics of soot from petrodiesel and vegetable diesel as one would expect similar values if the soot were identical. The higher mass of soot required per pressure drop for the combustion of petrodiesel indicates a different packing of the soot compared to the vegetable diesel soot. This may indicate an increased density of the deposited soot for the combustion of petrodiesel, however, based on the experimental data obtained it is not possible to finally conclude on differences in soot density as factors such as porosity and soot layer thickness are not known. Previously described in section 2.5.4 Darcy's law is generally used to express the pressure drop over the DPF. When considering only the contribution from cake filtration it is relevant to discuss the main parameters for the soot cake that will affect the pressure drop due to a flow through the porous filter cake. Similar to Darcy's law the Kozeny-Carman equation (Clement 2004) describes the pressure drop over a filter cake as proportional to both the filter cake depth and the fluid viscosity, however, also the dependence on bed porosity is more clearly seen. The Kozeny-Carman equation is presented below for a flow through a media consisting of spherical particles of diameter d_p.

$$\frac{\Delta P}{l} = 180 \frac{v_0 \mu}{d_p^{\,2}} \frac{(1-\varepsilon)^2}{\varepsilon^3} \tag{8.3}$$

Due to similar gaseous compositions of the exhaust from the combustion of both petrodiesel and vegetable diesel the fluid viscosity μ can be assumed identical. Since the pressure drops are normalized for a standard flow rate of 30m^3/h through the filter (see section 5.2) the superficial gas velocity v_0 is also identical for the two diesels. Assuming that the average particle size is similar for soot from the two diesels (in accordance with findings Hubeck Graudal and Rønde (2011)) the Kozeny-Carman equation shows that the pressure drop registered over the DPF increases proportionally with an increased soot layer thickness, however, greater filter cake porosity may contribute to a lower pressure drop registered. As both the porosity and the soot layer thickness is not readily obtained from the experiments conducted it is not possible to draw any conclusions on the density of the deposited soot. Furthermore the difference in deposited mass per pressure drop registered for the different fuels may be attributed to the uncertainties related to determining the soot emission for both diesels and the assumption of no depletion of deposited soot for this experiment.

8.2.2 Regenerative Linear Loading of the DPF

Loading of the filter with a preheater heating with a set point of 400°C on diluted (~50%) exhaust has been carried out. The resulting pressure drop as a function of time can be seen in Figure 19 below.
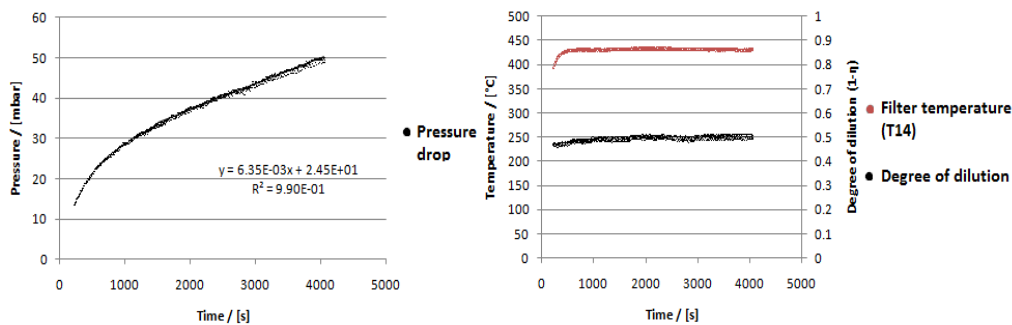

Figure 19 Left: The pressure drop over time resulting from deposition of soot in the DPF from the combustion of vegetable diesel at an engine load of 80%. Linear regression on the pressure drop curve has been carried out for the time interval 1500-4000s. Right: Degree of dilution and filter temperature as a function of time during loading.

The pressure drop achieves linear behavior after ~1000 seconds with a linear fit having a correlation coefficient of R^2=0.99. The temperature inside the DPF averaged at 432°C during the linear deposition and the degree of dilution remained near constant at around 50% dilution. The non-catalytic soot oxidation showed ignition for temperatures in excess of 600°C from TGA and one may assume the catalytic coating of the filter to be active at a temperature of 432°C as Hubeck-Graudal and Rønde (Hubeck-Graudal et al. 2011) documented catalytic activity at temperatures in excess of 380°C. From this one may assume that the catalytic oxidation rate is the dominant

contributor to soot oxidation at the conditions depicted in Figure 19. The slope of the linear fit is converted into a mass of soot deposited per time using data from Table 25. The result together with rate of deposition taking the degree of dilution into account is shown in Table 26 below. The rate of change of mass in the DPF subtracted the contribution from soot entering the DPF equals the rate of catalytic oxidation of deposited soot assuming the non-catalyzed reaction is negligible. One would expect the catalytic reaction to be more dominant during initial part of deposition as only the non-catalytic reaction depends on mass of soot deposited (further discussed in section 9).

Table 26 The table shows an estimated rate of catalytic soot oxidation for vegetable diesel soot with relevant data such as rate of deposition from Table 20 and filter temperature. The rate of change of mass in the DPF is read from the slope of the pressure drop plotted in Figure 19 and the appertaining mass of soot per pressure drop from Table 25.

Diesel	Temperature / [°C]	Rate of soot deposition / [mg/s]	Rate of change of mass in the DPF / [mg/s]	Rate of catalytic soot oxidation / [mg/s]
Vegetable diesel	432	$8.4 \cdot 10^{-2}$	$8.0 \cdot 10^{-2}$	$4.0 \cdot 10^{-3}$

The rate of soot deposition is ~20 times larger than the estimated rate of catalytic oxidation rate at the current conditions.

8.2.3 Balance Point

For the combustion of diesel with a fuel borne catalyst balance temperature experiments are typically conducted by loading a DPF at different temperatures starting at a high temperature and then gradually lowering the temperature when steady state is achieved (van Setten et al. 2001). Up to 5 hours may be needed in order to achieve steady state as can be seen from an example in Figure 20 below. The data presented clearly shows a dependence between pressure drop over the filter and the temperature:
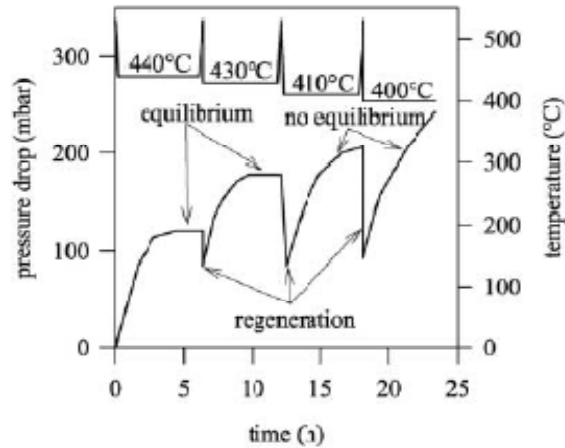
Figure 20 Result of a balance temperature experiment: positive slopes, normal operation with soot deposition; negative slopes, regeneration; horizontal line, equilibrium. A fuel borne catalyst (100 ppm cerium) was used (van Setten et al. 2001)

The above scenario is what one would expect assuming the fuel borne catalyst is evenly distributed in the deposited soot inside the DPF. The rate of catalytic soot oxidation is then a function of soot present in the filter as one may assume a fixed ratio between catalyst and soot thereby increasing the reaction interfaces between the catalyst and the soot proportionally to soot layer thickness.

During cake filtration for the experiments conducted in this project additionally deposited soot will not contribute to an increased contact area between the catalyst present in the DPF and the soot hence one would not expect the catalytic soot reaction to depend on the amount of deposited soot during cake filtration. A dependence on the amount of deposited soot was however observed for both the combustion of petrodiesel and vegetable diesel in the experiments conducted in this investigation (see section 8.2.3).

Experiments involving loading of the DPF until a balance point has been achieved and are shown below in Figure 21. Steady state data for the combustion of petrodiesel has not been obtained for preheater temperatures other than 500°C. A lowering and an increase of the DPF temperature by ~25°C did however result in an increase and a decrease of the pressure drop respectively. Steady state data for the pressure drop over the DPF has been obtained for the combustion of vegetable diesel at filter temperatures of 475 – 506°C. Equally for the combustion of vegetable diesel with the addition of NO_2 (387-403 ppm) upstream of the DPF steady states have been obtained in the temperature range 436-506 °C.
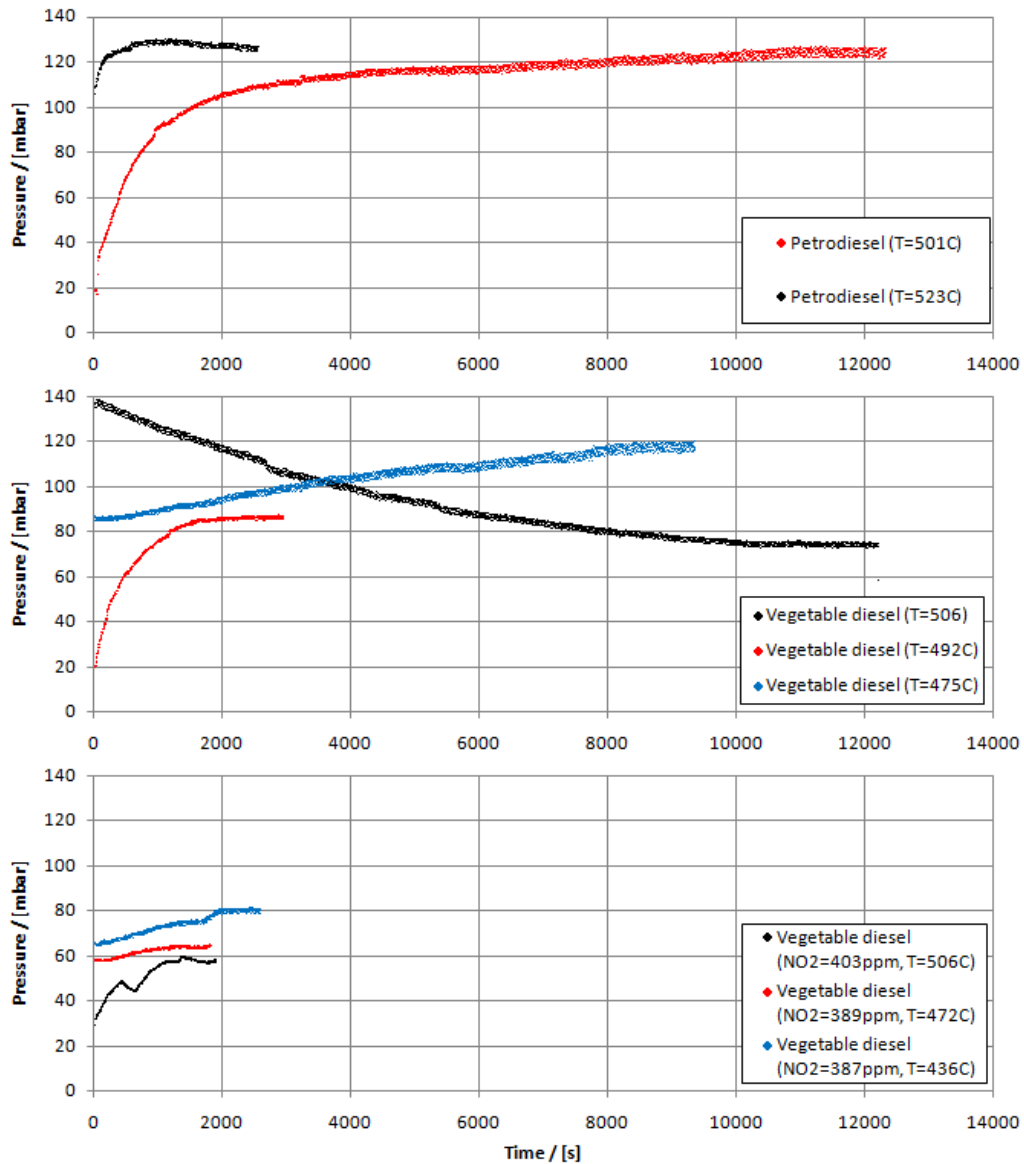
Figure 21 Actual pressure drops registered during loading of the DPF until balance point operation. Each transient depicts isothermal conditions, where the temperature presented is the value registered at the balance point. The engine load remained constant at 80% and at the balance points the degree of dilution was ~50% for all transients. Conditions such as flow rate and degree of dilution leading up to the balance point may be highly transient. Top: Combustion of petrodiesel with no NO$_2$ addition. Middle: Combustion of vegetable diesel with no NO$_2$ addition. Bottom: Combustion of vegetable diesel with NO$_2$ addition.

In order to better give a discussion on the balance point an uncorrelated pressure drop signal registered as a function of time is presented below in Figure 22 for one loading of the DPF starting on a clean filter (combustion of petrodiesel at 80% load).

The preheater heated with a set point of 500°C resulting in a filter temperature of just above 500°C (Table 27 and Table 28 in section 8.2.4 show the final results). It is from Figure 22 evident how the dilution ratio may change during the course of the experiment as the setting on F1 is changed in order to maintain a constant engine out pressure.
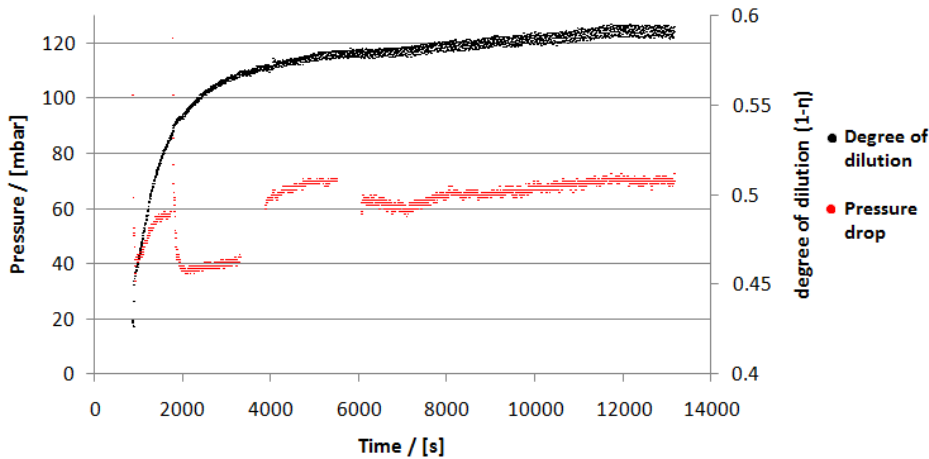

Figure 22 Measured pressure drop as well as calculated degree of dilution plotted as a function of time for an experiment involving loading of the DPF with preheated exhaust (set point of 500°C). Petrodiesel was combusted at an engine load of 80%.

Neglecting changes in flow rate through the filter and the dilution ratio it can be seen that the rate at which the DPF is loaded decreases over time until a break even configuration is potentially achieved where the rate of soot entering the DPF equals the rate at which soot is being oxidized. This implies that the regeneration of the DPF is not solely catalytically controlled as the rate depends on the amount of soot deposited during cake filtration. The rate is also not solely controlled by the non-catalyzed soot oxidation as a filter temperature of around 500°C expresses a BET lower than the ignition temperature for soot in an atmosphere of 10% O_2 which requires temperatures in excess of 600°C (see section 8.1.4). Due to dilution of the exhaust with atmospheric air the O_2-concentration was however ~16%. The results depicted in Figure 22 indicate that the rate at which deposited soot is oxidized is controlled by a combination of the catalytic reaction occurring at the filter-soot interface and the non-catalyzed oxidation occurring in the filter cake. This may indicate that despite diluting the exhaust from the backup-generator the DPF is still exposed to soot-concentrations higher than what the filter is designed for (see section 8.1.2.1) as a filter temperature of 500°C satisfies the temperature regime in which the catalyst is active.

8.2.4 Mass of Deposited Soot

In order to compare the pressure drop over the DPF for both the combustion of petrodiesel and vegetable diesel both with and without addition of NO_2 the pressure drop is correlated with the same volumetric flow rate through the DPF ($Q=30m^3/h$) by using equation (5.4). The effect on pressure drop resulting from potentially different flow rates experienced in the different experiments are therefore accounted for. The mass of deposited soot in the DPF at break even conditions is calculated using values from Table 25 with the assumptions presented accordingly in section 8.2.1. The results obtained are shown in Table 27 and Table 28 below.

Table 27 Values for BET obtained for combustion of both petrodiesel and vegetable diesel without additional NO_2 addition prior to DPF filtration shown together with degrees of dilution and appertaining values for normalized pressure drop over the DPF. The mass of deposited PM inside the DPF has been calculated according to values from Table 25. All of the data is obtained for the combustion at an engine load of 80%.

Diesel	BET / [°C]	1-η	$P_{corrected}$ (Q=30m^3/h) / [mbar]	Mass of deposited PM / [mg]	Mass of soot per geometric volume of filter / [g/L]
Petrodiesel	523	0.45	44	556	0.85
	501	0.51	46	590	0.90
Vegetable diesel	506	0.53	28	218	0.33
	492	0.51	32	268	0.41
	475	0.52	45	432	0.66

Table 28 Values for BET obtained for combustion of vegetable diesel with additional NO_2 addition prior to DPF filtration shown together with degrees of dilution and appertaining values for normalized pressure drop over the DPF. The mass of deposited PM inside the DPF has been calculated according to values from Table 25. All of the data is obtained for the combustion at an engine load of 80%.

Diesel	BET / [°C]	1-η	$P_{corrected}$ (Q=30m^3/h) / [mbar]	Mass of deposited PM / [mg]	Mass of soot per geometric volume of filter / [g/L]	NO_2 concentration / [ppm]
Vegetable diesel	506	0.51	21	124	0.19	403
	472	0.50	24	166	0.25	389
	436	0.50	31	257	0.39	387

It is not possible to determine an absolute maximum degree of loading of the filter as the pressure sensors disallow measurement of pressure drops exceeding 150mbar.

The degree of dilution (1- η) resembles better similarity for the experiments conducted on vegetable diesel; however, for the two BET's obtained for the combustion of petrodiesel the slightly larger difference in degree of dilution may be assumed to have a negligible effect on the pressure drop at the balance point also taking into account the uncertainties related to determining the soot concentration.

As the degree of dilution is a measure of the soot concentration, different degrees of dilution ideally result in different pressure drops registered at the balance point. The degree of dilution ideally needs to be identical in order to obtain comparable data. As the degree of dilution is used for determining the actual flow of exhaust passing through the DPF (see section 5.2.2) the differences in dilution therefore also indicate differences in the flow inside the DPF.

The temperature of the filter was controlled by a set point for the preheater. Due to the aggressive temperature control by the preheater (see section 3.2) the temperature of the exhaust downstream of the preheater may experience large temperature fluctuations exceeding ±50°C (see section 3.2). The filter temperature however would remain more stable but at a temperature lower than the temperature of the gas immediately downstream of the preheater. The temperature measured at T14 may therefore not necessarily be an exact measure of the temperature inside the DPF at all points, however, it does serve as a reasonable reference temperature with regards to comparison of the data obtained for different temperatures. One would expect that reactivity towards oxidation of the PM in the exhaust may suffer from an increased deactivation due to exposure to temperatures prior to filtration exceeding the actual temperature of the filter. This effect is not easily accounted for as more data from TGA on preheated soot samples ideally needs to be obtained (see section 8.1) as the TGA results were not indicative. Equally potential mass loss prior to deposition is also not accounted for.

Mass of deposited soot is relatively low compared to what the filter may potentially hold. The mass of soot deposited per geometric filter volume is equally low. Comparison with the SEM image (see Figure 10) which shows a filter with a loading of 10 g/L geometric filter volume the relatively low soot thicknesses and considerably lower filter loadings per geometric filter volume may indicate that the DPF used in the experimental work in this study was far from being fully loaded. The experimental setup did however not allow for measurements of pressure drops exceeding 150-200 mbar (see section 3.3).

8.2.4.1 *Comparison between Petrodiesel and Vegetable Diesel*
The mass of deposited PM for the combustion of petrodiesel and vegetable diesel without NO_2 addition has been plotted as a function of balance temperature in Figure 23. The mass of deposited PM has been calculated according to the assumptions presented for the deposition under non-regenerative conditions (see section 8.2.1). For similar temperatures it is clear that a lower mass of deposited PM is required in order to reach the balance point for the soot resulting from combustion of vegetable diesel compared to petrodiesel combustion. This may indicate an increased reactivity towards oxidation by the soot from the combustion of vegetable diesel. This is contrary to what was obtained from the TGA, however one would ideally expect soot from combustion of biodiesel to be more reactive towards oxidation compared to petrodiesel (see section 2.4.3). It was observed in section 8.1.2 that total PM

emission for vegetable diesel combustion was half the value for petrodiesel combustion. This may also contribute to lower mass of soot deposited at the balance point. Ideally if similar PM concentration of the exhaust from both vegetable diesel and petrodiesel combustion is achievable through dilution the mass deposited at the balance point may serve a s a better indicator of the soot reactivity.
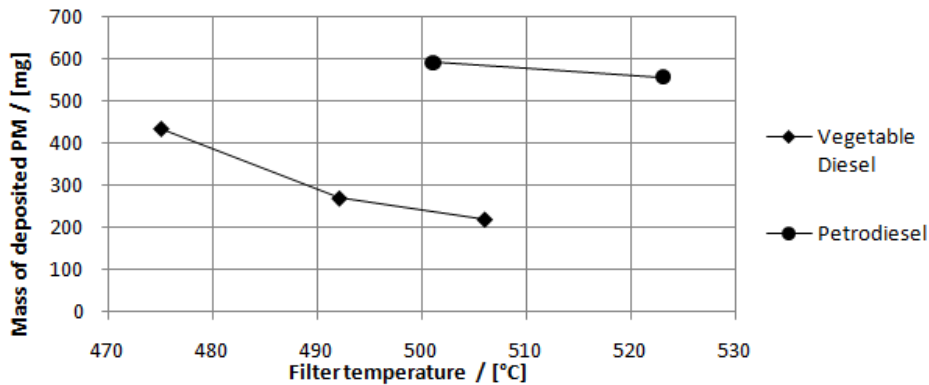

Figure 23 The values for deposited PM presented in Table 27 plotted as a function of the BET for the combustion of both petrodiesel and vegetable diesel at an engine load of 80% and no NO$_2$ addition prior to DPF filtration. The conditions given in Table 27 apply.

8.2.4.2   Effect of NO$_2$ addition

The mass of deposited PM as a result of combustion of vegetable diesel only both with and without the addition of NO$_2$ upstream of the DPF is presented in Figure 24 as a function of filter temperature. The results indicate clearly that the mass of soot required in order to achieve balance point operation for a given temperature is lower for experiments involving addition of NO$_2$. This is in agreement with what one would expect as the addition of NO$_2$ ideally increases the potential for soot oxidation. Furthermore the difference between mass required in order to achieve balance point operation is seemingly smaller for higher filter temperatures. This may be due to the increased contribution to the soot oxidation rate from the reaction with O$_2$ at higher temperatures.
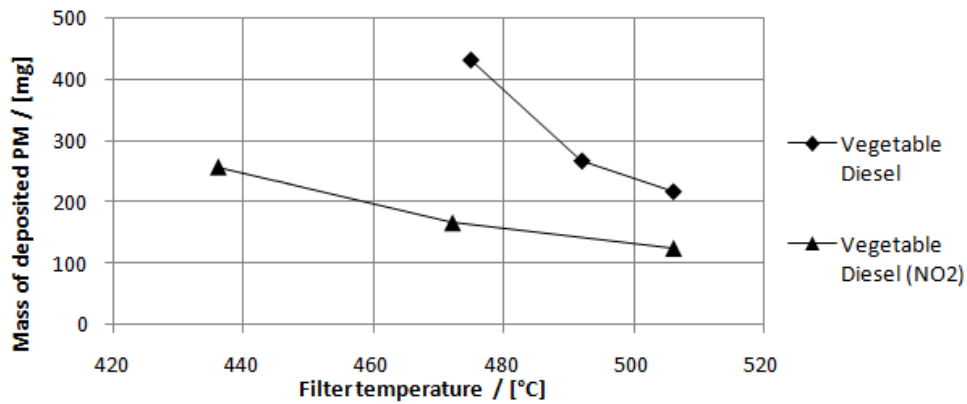
Figure 24 The values for deposited PM presented in Table 27 and Table 28 plotted as a function of the BET for the combustion of vegetable diesel at an engine load of 80% and with and without NO$_2$ addition prior to DPF filtration. The conditions given in Table 27 and Table 28 apply.

8.2.4.3 Soot Layer Thickness and Filter Interaction

The results depicted in Figure 23 and Figure 24 are based on the assumption of the mass of deposited PM being proportional to the pressure drop over the DPF thereby also neglecting the contribution to depth filtration. The contribution to the pressure drop from the latter is not easily experimentally obtained; however, one may expect the mass of soot in contact with the filter surface to remain constant independent on soot layer thickness during filter cake formation at a constant temperature. This is due to the catalytic reaction only occurring at the soot-filter interface. The filter cake may however be subject to change in character as the soot layer thickness changes during filtration as the non-catalytic contribution to soot oxidation may occur at any point were the soot is in contact with the oxygen containing exhaust. This may lead to a mechanism were deposited soot is potentially oxidized from any point in the soot layer thereby potentially causing changes in porosity. One may expect the layers of soot closest to the filter surface to have porosity greater than freshly deposited soot at the outer layers due to being exposed to the oxygen containing gas for a longer period of time. This effect may however also be countered by the potential for collapse of the pore structure due to increased pressure exerted by the upper layers of soot thus contributing to a potential for a uniform porosity of the soot. It is however not possible to finally conclude on the density and pore structure of the deposited soot from these experiments, however, it is an important parameter required for better understanding the mechanism by which the DPF regenerates.

The soot layer thickness is directly proportional to the mass of soot in the filter cake for thicknesses much smaller than the cell width. Assuming the contribution to soot deposited in the filter wall is negligible the soot layer thickness is calculated from the mass of soot m, the density of the soot ρ and total surface area of the filter walls on the cake side.

$$Z = \frac{m}{\rho_s S_w}$$
(8.4)

The soot layer thickness calculated from the deposited soot mass is presented in Table 29 below together with the mass of soot deposited per geometric filter volume. The soot layer thickness is based on the assumptions presented in the above.

Table 29 Values of soot layer thickness calculated from(8.4) using values for mass of deposited soot from Table 27 and Table 28. Soot layer thicknesses are presented together with appertaining values for BET for both the combustion of petrodiesel and the combustion of vegetable diesel with and without NO_2 addition upstream of the DPF.

Diesel	NO2 added / [ppm]	BET / [°C]	Soot layer thickness (Z) / [μm]
Petrodiesel	-	523	3.3
	-	501	3.5
Vegetable diesel	-	506	1.3
	-	492	1.6
	-	475	2.6
	403	506	0.74
	389	472	0.98
	387	436	1.5

Table 30 Geometric paramters for the DPF used in this study. Internal cell width and cell wall thickness is calculated from geometric parameters given in Appendix D - DPF and Oven.

Average pore diameter / [μm]	Internal cell width / [μm]	Cell wall thickness / [μm]
$2.0*10$	$1.5*10^3$	$5.5*10^2$

The density used for the calculation of the soot layer thickness is for carbon black (364 mg/cm^3, (Jeguirim et al. 2009)). Differences between CB and real engine soot may affect the calculated soot layer thickness. The density of the filter cake depends on the porosity and factors contributing to differences in porosity (see section 8.2.1) may affect the actual density required for estimating a soot layer thickness with greater accuracy. Great uncertainties and assumptions are however also related to the determined mass of deposited soot.

From a modeling study on deposition of nano-sized spherical monodisperse particles Elmøe et al. (2009) argued that the porosity of the filter cake formed depends solely on the Peclet number as:

$$\varepsilon = 1 - 0.15\left(1 + \frac{1.5}{Pe}\right)^{-0.5}$$
(8.5)

For nano-sized particles the Peclet number may be calculated by (Elmøe et al. 2009):

$$Pe = \frac{v_w d_p}{2D_p}$$

(8.6)

Where v_w is the filter face velocity, d_p is the average particle diameter and D_p is the appertaining diffusivity. Calculated Peclet numbers and appertaining cake porosities are presented in Table 31 below for different particle diameters including both the mass and the number based medians found for the soot emissions in previous study by Hubeck-Graudal and Rønde (Hubeck-Graudal et al. 2011).

Table 31 Peclet numbers calculated using equation (8.6) for different particle diameters are shown together with appertaining values of porosity calculated using (8.5). The diffusivity is calculated using Stokes-Einstein relation (Appendix N – Deposition) for a gas temperature of 500°C. The normalized gas flow is 30 Nm³/h. The pressure inside the filter is assumed to be ambient pressure. * is mass based median from particle size distribution by Hubeck-Graudal and Rønde (2011)**. ** is number based median from particle size distribution by Hubeck-Graudal and Rønde** (2011)**.**

Particle diameter d_p / [nm]	Peclet number Pe	Cake porosity ε
10	0.075	0.97
100*	7.5	0.86
150**	17	0.86

For the calculation of the soot layer thickness in Table 31 the porosity of the filter cake was assumed having a value of ε = 0.8 with values for soot density from studies by Jeguirim et al. (2009) and Park et al. (2004). The porosities formed by monodisperse deposition of particles at the size of PM in the exhaust from these studies indicate an increased potential for validity of the soot layer thickness calculated. Elmøe et al. (2009) argued that the porosity of the filter cake becomes constant at a distance of up to approximately the diameter of the capillary of the filtration medium onto which the particles deposit. The average pore size (20µm) greatly exceeds the calculated soot thickness indicating that porosity is not necessarily constant. Elmøe et al. (2009) further showed that cake formation resulting from deposition of nano-sized particles on the face size of the filter occurs mainly by deposition at the edges of the pores on the face side. This may contribute to an increased potential for non-uniformity of the deposited filter cake; however, this effect may be countered by the constant contribution from the catalytic reaction occurring at the filter-soot interface. This emphasizes the difficulties related to estimating the behavior of the deposited soot layer as many factors may contribute to the changes in the cake porosity.

Elmøe et al. (2009) argued that for Peclet number <0.01 the penetration of nano-sized particles through a capillary of up to a few microns may be neglected. However, for high Peclet numbers >1 as mainly experienced in the DPF for these studies penetration may not be neglected. The penetration length is however not

easily obtained; however, from the estimate of a maximum volume fraction of soot in the filter wall of <1% as shown in section 8.2.1 combined with the potential from depletion of soot deposited in the filter wall by catalytic oxidation it may be reasonable to assume that the penetration of particles into the filter wall is negligible after cake filtration has commenced.

Ideally one may be able to determine the actual amount of soot deposited at the balance point through a mass balance based on the gaseous concentrations downstream of the DPF. Sufficient data is not provided from the experiments conducted (the heat tracing upstream of the FID stopped working and therefore a lot of the data obtained on volatile hydrocarbon concentration may be unreliable). Ideally the change in CO, CO_2 and HC concentration over the DPF could be used in setting up a mass balance for estimating the mass of deposited soot being oxidized in the DPF. Neglecting the potential for uncertainties and inaccuracies the mass of deposited soot estimated from the balance may ideally coincide or exhibit similar trend as a function of changed filter temperature as the mass of deposited PM presented in Table 27. This would serve as an indicator for a porosity of the deposited soot layer independent of soot layer thickness. Deviations from the values presented in the table may indicate changes in porosity during deposition. Taking into account the uncertainties related to the experimental setup (see section 4) it may seem unlikely to obtain data accurately describing changes in the characteristics of the deposited soot layer. Ideally one would want to investigate the latter in a fixed bed experiment were the contribution from both the catalyzed and non-catalyzed oxidation of soot can also be investigated separately. For this reason modeling on the soot deposition also provides a reasonable alternative to supporting a discussion on the experimental data obtained from the DPF experiments.

9 Simple Modeling and Kinetics

In the following an expression for the overall rate is used together with a mass balance on the DPF in order to discuss parameters such as reaction order with respect to mass of soot deposited and activation energies for the catalyzed soot oxidation by O_2 as well as the non-catalyzed soot oxidation by both O_2 and NO_2. Data from isothermal loading of the DPF allows for an estimate of the order of the non-catalytic soot oxidation by O_2. Steady state data obtained from balance point operation with the DPF allows for an estimation of activation energies which are discussed in relation to DPF performance.

9.1 Overall rate expression

The oxidation of soot by NO_2 is generally believed to follow both a direct and a cooperative mechanism (see section 2.5). For both the catalyzed as well as non-catalyzed soot oxidation the literature mainly describes kinetic rates per mass of soot present. The mass of soot deposited along the filter walls inside a DPF is easily translated into a soot layer thickness if a uniform soot layer with constant density is assumed. The catalyzed soot oxidation on the other hand is more difficult to describe kinetically for both the reaction with O_2 as well as NO_2 as the mass of soot particles in contact with the catalytic filter wall or the catalytically available surface area is much harder to determine. This would require knowledge about the penetration length of deposited soot particles through the filter walls which is highly specific for the filter used and the soot. The penetration depth is best determined experimentally. For this reason the assumption of having a given number of soot mono layers in contact with only the surface of the external filter walls allows for a reasonable estimate of the catalytically reacting mass of soot bypassing the need for knowledge about penetration length. The number of mono layers needed in order to satisfy final experimental data is thus an expression for the penetration depth. Assuming an even distribution of soot particles in a single mono layer along the internal surface area of the filter one may estimate an actual penetration length if the number of mono layers is known together with internal surface area of the filter walls.

Figure 25 shows an illustration of a deposited uniform soot layer of thickness z together with a mono layer deposited evenly along the external surface area of the filter walls. The mono layer thickness is equal to the average soot particle diameter. Only the NO_2 depletion from the gas phase is of relevance as O_2 is in abundance for the reaction between soot and O_2 (typically ~10%). On Figure 25 the NO_2 concentration is shown as the only variable parameter across the filter and filter cake where the only nitrous species formed is NO. For small soot layer thicknesses the gradient of NO_2 across the filter may be neglected.
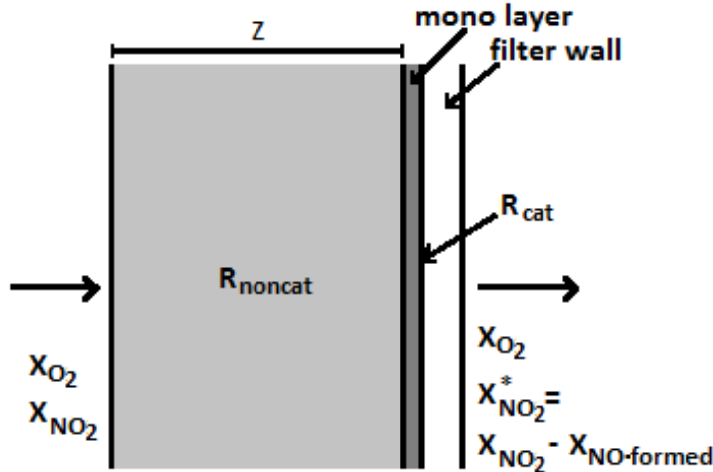
Figure 25 Representation of soot deposition along a filter wall. Arrows indicate flow direction. Non-catalyzed soot oxidation occurs with a rate of R_{noncat} in the filter cake where the catalyzed soot oxidation is represented as reaction with a mono layer with a rate of R_{cat}.

With R_{noncat} and R_{cat} denoting the rate of soot oxidation both in the soot layer and at the wall interface respectively, the total rate of soot oxidation is the sum of these contributions only.

$$R_{total} = R_{noncat} + R_{cat} \quad [{}^{mg}\!/\!_{s}]$$ (9.1)

The equation (9.1) is the general overall expression for rate of soot oxidation described in the literature (see section 2.5). R_{total} expresses the overall rate at which deposited soot is oxidized assuming the reaction is kinetically controlled. This may be a valid assumption as the transport of gaseous species through the filter is generally believed to be by means of convection primarily thereby neglecting the potential for diffusion controlled regimes as the rate depends predominantly on the available surface area of soot in contact with the gas phase. If Langmuir-Hinshelwood kinetics were to be applied one may assume that the rates of reaction may follow a similar model assuming that the rate of desorption of adsorbed reacted gaseous species is included in the rate expression in parameters such as pre-exponential factor and activation energy.

Assuming a constant density of the soot layer the mass of soot is proportional to the soot layer thickness z. Having m_i denote the mass of the soot layer at a given time and m_{mono} denotes the mass of the mono layers. The previously described expressions for both the non-catalyzed and the catalyzed soot oxidation become:

$$R_{noncat} = m_i \cdot r_{noncat} = \rho_{soot} S_w z_i \cdot r_{noncat} \quad [mg / s]$$ (9.2)

$$R_{cat} = m_{mono} \cdot r_{cat} \quad [mg / s] \tag{9.3}$$

S_w is the external surface area of the filter walls in contact with deposited soot and ρ_{soot} is the density of the soot layer. Assuming a mono layer thickness equal to the average soot particle diameter d_p and the number of mono layers $n_m \in \{0,1,2,3,...\}$ the total mass of the mono layers can be expressed as:

$$m_{mono} = \rho_{soot} S_w d_p n_m \tag{9.4}$$

For operation where exhaust is filtered through the DPF a mass balance for soot on the latter is used to express the filter behavior. Assuming 100% retention of soot, a constant addition of soot from the exhaust and a soot depletion equal to the rate at which soot is oxidized both catalytically and non-catalytically the balance becomes

$$\text{In} + \text{Produced} = \text{Out} + \text{Accumulated} \tag{9.5}$$

$$R_{dep} + \left(-R_{cat} - R_{noncat}\right) = 0 + \frac{dm}{dt} \tag{9.6}$$

The expressions for R_{cat} and R_{noncat} may exhibit varying temperature dependence depending on the presence of NO_2.

9.1.1   Experiments without NO_2

For experiments conducted with no NO_2 addition the contributions from soot oxidation rate may be expressed by rate expressions where the rate constants are expressed by Arrhenius expressions. When cake filtration has commenced one may assume that the mass of the mono layer reacting catalytically at the filter interface is constant. The mass balance for soot then becomes a function of the variable temperature of the DPF (T) and the mass of soot (m) in the filter cake. The concentration of NO_2 (<25ppm, see section 8.1.5) in the exhaust for both petrodiesel and vegetable diesel combustion is assumed to have a negligible effect on the soot oxidation for experiments without additional NO_2 addition upstream of the DPF.

$$R_{dep} - k_{noncat} \exp\left(\frac{-E_A^{noncat}}{RT}\right) m(t)^n - k_{cat} \exp\left(\frac{-E_A^{cat}}{RT}\right) = \frac{dm(t)}{dt} \tag{9.7}$$

The dependence on oxygen concentration of the gas phase is included in the constants k_{noncat} and k_{cat} in the equation as the parameter is unchanged. After a considerable pressure drop over the DPF is achieved one may assume the contribution to the total soot mass from the mass of soot in the mono layer is negligible. The mass of soot in the filter therefore becomes the total mass of soot in the DPF for a given time.

9.1.2 Experiments with NO$_2$

For the experiments with addition of NO$_2$ upstream of the DPF the mass balance (9.6) may be expressed as (9.8) below. In the expression below the contribution from both catalyzed as well as non-catalyzed soot oxidation by O$_2$ is neglected. This may however only be a valid assumption when large amounts of NO$_2$ is present in the exhaust.

$$R_{dep} - k_{NO_2} \exp\left(\frac{E_A^{NO_2}}{RT} \right) m(t)^n = \frac{dm(t)}{dt} \tag{9.8}$$

The reaction by NO$_2$ is typically described as consisting of a contribution from a term from both the direct and the cooperative mechanism (see section 2.5). For this reason the activation energy $E_A^{NO_2}$ in (9.8) may be an observed overall activation energy taking into account both the direct and cooperative mechanism. The dependence on the NO$_2$ concentration is included in the constant k_{NO_2} and equally the concentration of O$_2$ may also be included depending on the prominence of the cooperative rate of soot oxidation.

9.1.3 Assumptions

For the theory described the following assumptions were made:

- Isothermal conditions during loading.
- Uniform distribution of gas molecules in the bulk phase prior to and after filtration.
- Homogenous and unchanged soot composition.
- Oxygen concentration unchanged after filtration
- The reaction with NO$_2$ is neglected for loading of the DPF with no additional NO$_2$ added.
- No depletion of NO$_2$ is assumed due to small soot layer thicknesses
- For loading of DPF involving addition of NO$_2$ upstream of the filter the contribution from catalyzed as well as non-catalyzed soot oxidation by O$_2$ is neglected.
- The external surface area of filter cake is equal to the filter wall area
- Mass transport in the gas phase occurs by convection only.
- Penetration of soot particles into the filter wall is accounted for by assuming contact between catalytic wall and a given number of mono layers.
- Only the mono layers undergo catalytic oxidation and the catalytic reaction rate therefore becomes a function of mass and not the filter surface area.

9.2 Isothermal Loading of the DPF

For a DPF experiment without NO_2 addition depicting transient conditions during loading with a constant filter temperature the contribution to soot oxidation from the catalytic term can be assumed to be constant as one would expect the mass of soot in contact with the catalytic surface area to be independent of deposited soot layer thickness during cake filtration. The mass balance (9.7) then becomes a first order differential equation which is non-linear if $n \neq \{0,1\}$. With the constant contributions expressed in (9.9) the mass balance is expressed in (9.10):

$$c_1 = R_{dep} - k_{cat} \exp\left(\frac{-E_A^{cat}}{RT}\right) \ \wedge \ c_2 = k_{noncat} \exp\left(\frac{-E_A^{noncat}}{RT}\right) \tag{9.9}$$

$$\frac{dm}{dt} = c_1 - c_2 m^n, \ where \ c_1 \leq R_{dep} \ \wedge \ c_2 \geq 0 \tag{9.10}$$

For $c_1 \leq 0$ the rate of soot oxidation will at all times exceed the rate of deposition meaning that the DPF will fully regenerate due to the high catalytic rate of soot oxidation. For $c_1 \in]0; R_{dep}]$ the rate of soot oxidation depends also on the mass of soot present in the DPF.

The value of c_1 should ideally be known in order to potentially estimate an order of the soot oxidation for a given set of experimental conditions. For DPF operation involving transient loading the mass of soot deposited per time can be readily found by differentiation and for an estimated value of c_1 the order of the oxidation of soot with respect to mass is ideally obtained as the slope of the following linear function of ln(m):

$$y = \ln\left(-\frac{dm}{dt} + c_1\right) = n \cdot \ln(m) + \ln(c_2) \tag{9.11}$$

Without knowing the value of the catalytic soot oxidation rate the constant c_1 is unknown making it difficult to obtain an estimate of the order n.

For the limited amount of experiments conducted involving determination of the BET only one experiment would provide a transient profile of pressure drop change over the DPF at constant filter temperature and constant degree of dilution. The transient loading of the filter for the combustion of vegetable diesel at 80% engine load with preheated exhaust ensuring a filter temperature of 506°C is shown below.
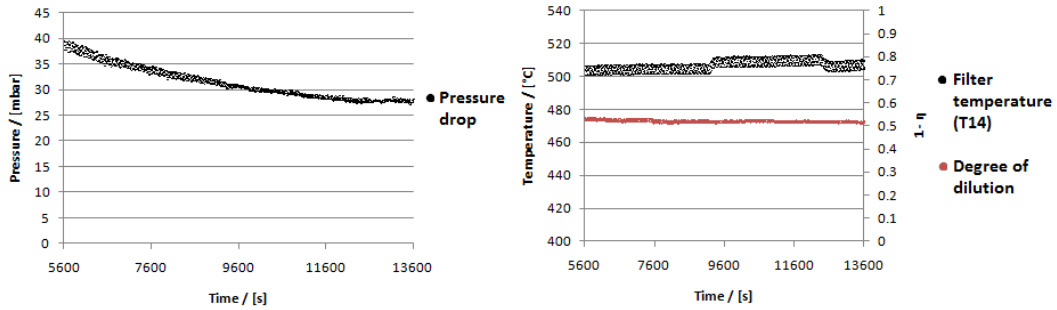
Figure 26 Left: The pressure drop over time resulting from conversion of deposited soot during DPF loading for the combustion of vegetable diesel at an engine load of 80%. Right: Degree of dilution and filter temperature as a function of time during deposition and conversion of deposited matter.

From the above figure one may see that the temperature of the filter as well as the dilution ratio and thereby the volumetric flow rate through the filter remains reasonably stable during the transient pressure profile depicted.

For an isothermal transient loading where a steady state is achieved the value of c_1 must satisfy $c_1 \in]0; R_{dep}]$. A plot showing equation (9.11) for the boundaries yields the following plot Figure 27.
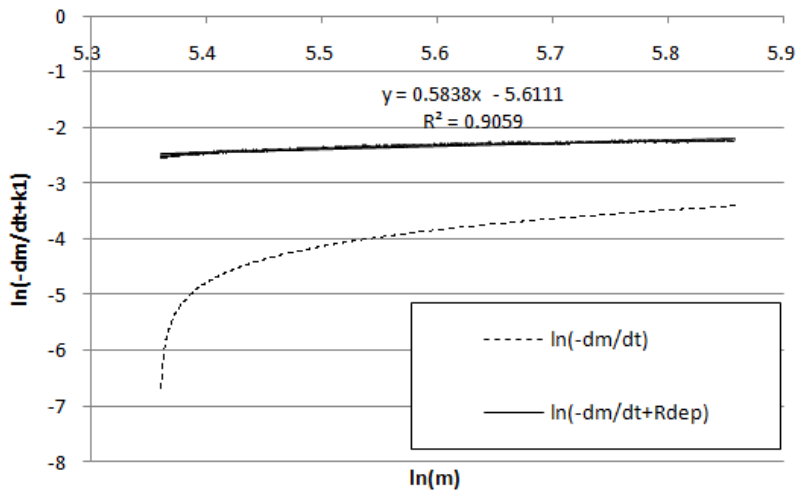

Figure 27 The transient pressure drop profile depicted in Figure 26 is converted into a mass loss signal using the values for mass of deposited soot given in Table 25 and subsequently plotted according to equation (9.11) for $c_1=0$ and $c_1=R_{dep}$.

The above plot indicates that for a value of $c_1=R_{dep}$ representing the case were the catalytic oxidation rate is zero a greater linear fit is achieved. This may indicate that the catalytic rate is much slower than the rate of deposition ($R_{cat} << R_{dep}$) but factors

such as changes in soot composition and porosity over time are not accounted for. This suggests that the rate is strongly controlled by the non-catalyzed soot oxidation.

If the rate of catalytic reaction depends on the mass of soot deposited c_1 is not constant and the plot may not yield a straight line. Equally if the porosity of the deposited soot layer does not remain constant the calculated mass of soot deposited is not directly proportional to the pressure drop over the DPF and deviations from a straight line in the above plot may also be observed.

One may not finally conclude on the exact order of soot oxidation by O_2 with respect to mass; however, for a negligible catalytic reaction and the assumption of constant soot porosity during cake filtration an order of n = 0.6 with respect to mass is read from the slope of the linear fit. The order is generally described as $n \in [0.75; 1]$ in the literature (see section 2.5).

Ideally also the value of c_2 can be read but with great inaccuracy due to the reasons mentioned in the above. As the transient is isothermal it is not possible to obtain a value for the activation energy form this data only.

9.3 Steady State Data

When steady state has been achieved the accumulation term equals zero and the mass balance then becomes the following for both with and without NO_2 addition where the variables are the temperature of the filter and the mass of soot deposited.

Without NO_2:
$$R_{dep} = k_{noncat} \exp\left(\frac{-E_A^{noncat}}{RT}\right) m^n + k_{cat} \exp\left(\frac{-E_A^{cat}}{RT}\right) \qquad (9.12)$$

With NO_2:
$$R_{dep} = k_{NO_2} \exp\left(\frac{-E_A^{NO_2}}{RT}\right) m^n \qquad (9.13)$$

In order to obtain values for activation energies for the reaction with no NO_2 addition, experimental steady state data from the DPF for different temperatures may not be sufficient as it is not possible to separate the contributions from both catalyzed and non-catalyzed soot oxidation. Ideally one would want to carry out an experiment where these contributions can be separated.

In order to separately investigate the catalytic soot oxidation in the DPF one may conduct experiments involving loading of the DPF at temperatures just above the temperature at which the catalyst is active (380°C (Hubeck-Graudal et al. 2011)) and thereby assume that the contribution from non-catalytic soot oxidation is negligible, however, the temperature range may be very slim. Furthermore the change in pressure drop experienced immediately after initiation of loading on a clean filter at sufficiently high stable temperature may express only the catalytic reaction if the soot concentration of the exhaust is known. This would require that no cake filtration occurs. Obtaining the rate of soot oxidation immediately after having exhaust pass

through the DPF is however troublesome as transient conditions may apply to temperature, pressure and flow rate immediately after initiation of filtration. For the experiments conducted in this study only a few of the filter loadings were conducted with a start on a clean DPF. Unfortunately due to highly transient conditions especially in the temperature of the preheated exhaust immediately after initiation of filtration a contribution from only the rate of catalytic soot oxidation is not obtainable. No estimates on this matter may be given from these experiments as the rate of pressure change exhibited during the initial part of filtration exceeds the rate of change one would expect from the known R$_{dep}$ (see Figure 27).

TGA may provide a way of investigating the rate of soot oxidation separately for both the catalytic and non-catalytic reaction (see section 8.1.4.2). In the former case however it may be difficult to obtain a sufficient mixing of catalyst with the soot as sampled soot is heavily incorporated into the filter material. Furthermore the chemical composition and bulk density of the soot may be substantially different from what is deposited in the DPF. The general uncertainties related to sampling of soot (see section 4.2) and the lack of repeatability on this matter may cause great uncertainties in potentially determined kinetics. Equally for determination of kinetics for non-catalytic soot oxidation similar conditions may apply.

9.3.1   Estimating Activation Energies

In section 8.2.2 it was seen that at a DPF temperature of 423°C the rate of soot deposition considerably exceeded the rate of catalytic reaction. Furthermore a better linear fit for equation (9.12) was observed under the assumption of negligible contribution from the catalytic rate of oxidation for a DPF temperature of 506°C. Assuming that $R_{cat} \ll R_{dep}$ the mass balance (9.12) becomes the following for reaction without NO_2:

$$\frac{R_{dep}}{m^n} = k_{noncat} \exp\left(\frac{-E_A^{noncat}}{RT}\right) \tag{9.14}$$

Equally for the addition of NO2 the mass balance becomes:

$$\frac{R_{dep}}{m^n} = k_{NO_2} \exp\left(\frac{-E_A^{NO_2}}{RT}\right) \tag{9.15}$$

The best linear fit of $\ln\left(R_{dep} \cdot m^{-n}\right)$ as a function of 1/T then yields an observed activation energy readily obtained from the slope when the order n is known.

$$\ln\left(\frac{R_{dep}}{m^n}\right) = -\frac{E_A}{R}\frac{1}{T} + \ln\left(k\right) \tag{9.16}$$

The slope is unaffected for different constant values of R_{dep} meaning that the observed E_A remains unchanged independent of potential changes in dilution rate. If one does not neglect the catalytic oxidation but assumes an unchanged contribution independent of the given temperature interval the observed E_A will still remain unchanged. Also if the actual mass of deposited soot is different from the one calculated and shown in Table 27 and Table 28 but the assumption of mass being proportional to pressure drop is still valid the observed E_A will also remain unchanged.

For the steady state data obtained the above yields the following plot in Figure 28 under the assumption of a reaction order of unity with respect to mass.
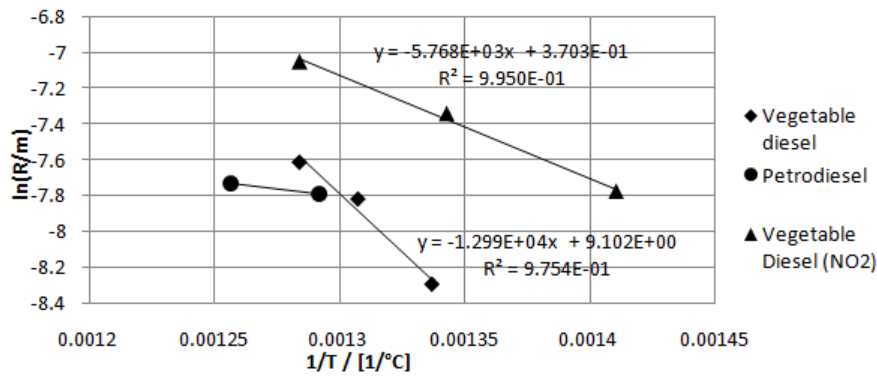

Figure 28 Mass of deposited soot as a function of DPF temperature from Figure 23 and Figure 24 is plotted according to equation (9.16) where the value of R_{dep} is given from Table 20 and appertaining degree of dilution.

The combustion of petrodiesel did not provide enough data points for a discussion on the steady state data with regards to activation energy. Soot from the combustion of petrodiesel required higher temperatures in order to achieve a balance point and due to the limitations imposed by the setup more balance points from the filtration of petrodiesel soot in an atmosphere not containing additional NO_2 may not be sufficient for the determination of activation energy as the temperature range becomes very slim. Equally the temperature range of 475 – 506°C for the balance points obtained from biodiesel soot with no NO_2 addition may also impose an increased uncertainty with regards to determining activation energy; however, due to the seemingly higher reactivity more balance points should ideally be obtainable. The low temperature range together with very few data points in Figure 28 nevertheless imposes a large uncertainty with regards to discussion on the linear behavior as generally a temperature range of over 100°C is desired (Haralampous et al. 2004).

The balance points for the vegetable diesel seemingly exhibit a linear relationship when plotted after equation (9.16). If the catalytic contribution to the

rate of soot oxidation cannot easily be neglected one may not necessarily observe a liner function in the above plot.

The observed activation energy is readily obtained from the slope of the linear fit. Equally k can also be obtained. The activation energy and k is shown in the table below based on the assumptions described in the above.

Table 32 Observed activation energies and appertaining values of k for the combustion of vegetable diesel with and without NO_2 addition. The values are obtained from the linear fit to the plots on Figure 28.

Diesel	NO_2 concentration / [ppm]	Observed E_A / [kJ/mol]	k / [s^{-1}]
Vegetable	-	108	$8.97*10^3$
diesel	386 – 402	48.0	1.45

The value of k may be affected by changes in the deposition rate and may therefore be subject to greater uncertainties than the value for E_A obtained.

The observed activation energy is for the reaction without NO_2 apparently within the range of the typical value for ceria oxidized soot (80-130 kJ/mol, see Table 10). Still the value of 108 kJ/mol is in the low range of what is generally observed for non-catalyzed soot oxidation and this value is also considerably lower than the activation energies obtained from TGA in these studies (189kJ/mol, see Table 23). This is contrary to what is expected under the assumption of a dominating non-catalyzed soot oxidation. The value of $E_A{}^{NO_2}$ is lower than $E_A{}^{noncat}$ indicating an increased reactivity of the soot towards oxidation by NO_2. The value of $E_A{}^{NO_2}$ is near what is reported in the literature (see section 2.5.3). For values of n<1 the slope of the plot in Figure 28 will be smaller thus yielding an observed lower E_A.

9.3.2 Comparison between Catalytic and Non-Catalytic Soot Oxidation Rate by both O_2 and NO_2

For the values of steady state previously discussed it is possible for known values of the activation energies of the catalyzed and non-catalyzed soot oxidation by O_2 only to estimate values for k_{noncat} and k_{cat} which cause the mass balance (9.12) to yield the best fit with experimental values if sufficient data is available. Great differences are however observed in the literature for activation energies as different soots have different reactivities (see section 2.5.3). For the limited data obtained in this study it has not proven possible to obtain an adequate fit for estimated of values of activation energies in order to obtain values for k_{noncat} and k_{cat}. The value of k_{cat} is also subject to great uncertainties as minor changes in the calculated mass of deposited soot at the balance point may alter the observed k_{cat} considerably.

For different masses of soot the parameters in Table 32 have been used to plot the rate of non-catalyzed oxidation by O_2 and the rate of oxidation by NO_2 in Figure 29 assuming first order kinetics with respect to mass. Furthermore the estimated rate of catalytic oxidation determined in section 8.2.2 is also shown.
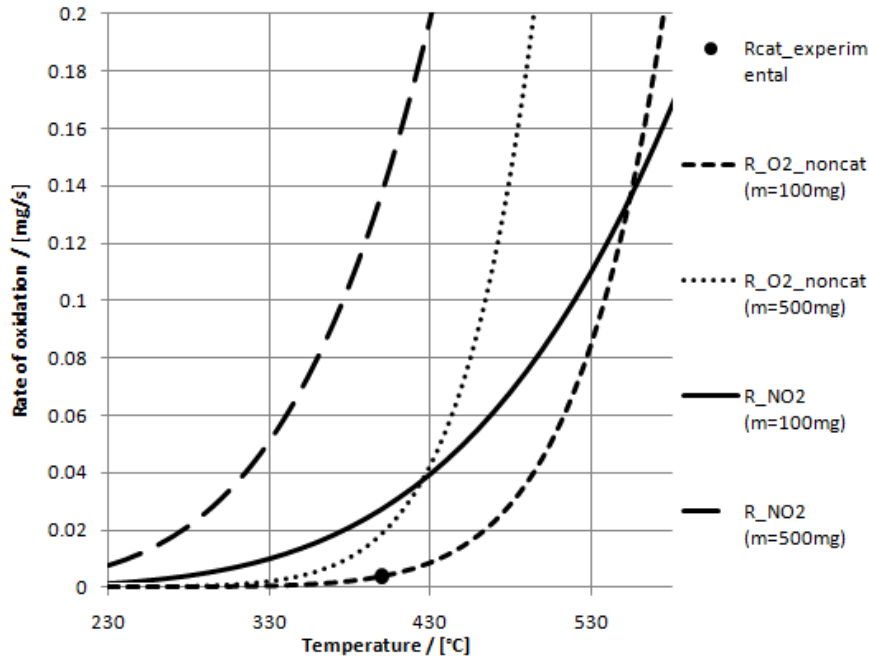
Figure 29 The rate of non-catalytic soot oxidation by O_2 and NO_2 plotted separately for different mass of soot as a function of temperature. Kinetic parameters from Table 32 have been used. The estimated rate of catalytic oxidation determined in section 8.2.2 is also shown.

The plot clearly indicates a great dependence for the non-catalyzed rate by O_2 and by NO_2 on mass of soot present in the filter. Despite uncertainties attributed to the above plot it serves as a qualitative assessment of the rates compared for the oxidation by O_2 and NO_2 as one would ideally want to obtain a great number of data points for a larger temperature range in order to obtain a greater accuracy. From Figure 29 it is also seen that the rate of soot oxidation by NO_2 (~400 ppm) exceeds the rate at which non-catalyzed reaction by O_2 proceeds for similar masses of soot for lower temperatures. For similar masses of soot it is also seen that the rate of oxidation by NO_2 becomes less dominant for increased temperatures.

From Figure 29 it is observed that masses of soot exceeding 100 mg deposited in the DPF may yield a non-catalytic oxidation rate by both O_2 and NO_2 greater than the catalytic O_2 oxidation rate for a temperature of ~400°C. For all experiments conducted in this study the mass of deposited soot has been estimated as >100 mg.

10 Conclusion

The experimental setup used in this study imposed limitations to the diversity of experiments conducted. The valves located on the main exhaust piping proved leaking behavior when in a closed position. This together with an inaccuracy in the venturi meter readings at U1 provides a bypass that is not easily controlled when diluting the exhaust during experiments involving flow through operation with the DPF. Experiments involving sampling of emitted soot is believed to contain an increased uncertainty mainly with respect to the SOF.

Non-preheated diesel exhaust yielded a total PM emission of 58 mg/m^3 and 26 mg/m^3 for the combustion of petrodiesel and vegetable diesel respectively. For comparison of the petrodiesel emission with standard emissions from automotive engines a more than 3 times greater total PM emission is observed for the back-up generator used in these studies. For non-preheated exhaust petrodiesel soot yielded a SOF of 0.23 where the vegetable diesel soot yielded a lower SOF at a value of 0.15. A lower SOF for vegetable diesel soot is generally expected. Preheating of the exhaust seemingly yielded an increase in SOF for petrodiesel soot which together with a reduction in emitted soot potentially indicates a conversion of carbonaceous soot core rendering the condensed volatiles untouched as a result of preheating. This is contrary to what one would expect and may be due to increased potential for uncertainties in measured SOF.

TGA data for petrodiesel soot from non-preheated exhaust indicated a lower temperature required for oxidation in an atmosphere containing 10% O$_2$ than vegetable diesel soot. This together with a seemingly lower activation energy determined from the mass loss signal from TGA indicates an increased reactivity towards oxidation by O$_2$ for petrodiesel compared to vegetable diesel soot which is contrary to what is expected as biodiesels generally exhibit greater reactivity of formed soot. Non-preheated exhaust yielded an activation energy of 132 kJ/mol for petrodiesel soot and 189 kJ/mol for vegetable diesel soot. Increased preheating of the exhaust to temperatures exceeding 500°C seemingly caused an increase of the observed activation energy for petrodiesel soot, however, also lower temperatures for ignition were observed indicating ambiguous results on the affect of preheating on soot reactivity.

For experiments involving filtering of the diesel exhaust in a DPF it was proven possible to relate a given mass of deposited soot per pressure drop exhibited, however, this requires an assumption of unchanged porosity of deposited filter cake independent of temperature and loading.

It was possible to achieve balance point operation of the DPF for temperatures above 475°C implying that the catalytic rate of soot oxidation is not sufficient to ensure regeneration of the DPF and the non-catalytic soot oxidation by O$_2$ becomes increasingly important for increased mass of soot deposited.

A lower mass of soot deposited in the DPF was required in order to achieve balance point operation for the combustion of vegetable diesel compared to

petrodiesel potentially indicating an increased reactivity of the former; however, lower total PM emission from the combustion of vegetable diesel may equally contribute to the lower mass of deposited soot required for balance point operation.

A lower mass of soot deposited in the DPF was required in order to achieve balance point operation for filtering of vegetable diesel exhaust with the addition of ~400 ppm NO_2 upstream of the DPF than for filtering of exhaust with no NO_2 addition. This expresses increased soot reactivity towards oxidation by NO_2.

For all DPF loadings conducted where balance point operation was achieved the mass of deposited soot would yield an estimated soot layer thickness of less than 3.5μm potentially indicating that the DPF was far from fully loaded despite difficulties in obtaining regeneration of the DPF.

Isothermal loading allowed for an estimate of the order of vegetable diesel soot oxidation by O_2 with respect to mass. The estimated order was n = 0.6 for conditions where the contribution to soot oxidation from the catalytic rate was negligible compared to a dominating rate by which soot enters the DPF. The estimated order may however be highly uncertain.

Neglecting the catalytic rate of soot oxidation by O_2 the activation energy for vegetable diesel oxidation was determined indirectly from the pressure drop measurements yielding a value of 108 kJ/mol. Equally the activation energy for vegetable diesel soot exposed to ~400 ppm NO_2 was determined as 48 kJ/mol emphasizing the increased reactivity of soot towards oxidation by NO_2 compared to O_2.

Ideally more data regarding balance points need to be obtained in order to verify the trends observed in this study. For this reason greater accuracy in obtained data is ideally needed. In order to obtain greater accuracy in obtained results the degree of dilution of the exhaust needs to be regulated more accurately. This will require replacement of the valves V15 and V26 (see Appendix I – P&I and Setup) with non-leaking valves that allow for accurately determining valve settings. The venturi meter U1 needs to potentially undergo recalibration and remounting of the piping downstream of the measurement in order obtain viable flow rate readings. The pump F1 supplying the system with a sub-atmospheric pressure should ideally only be connected to the piping downstream of the DPF and not the external bypass string as is the case with the current setup. This will allow for maintaining a more constant degree of exhaust dilution and flow through the DPF during loading as the pump setting is continuously changed.

11 References

1. Almeida, Manny. 2008. The determination of phosphorus, sulfur, sodium, potassium, calcium, and magnesium in biodiesel. *SPECTROSCOPY*: 47-50.

2. Azambre, B., S. Collura, J. M. Trichard, and J. V. Weber. 2006. Nature and thermal stability of adsorbed intermediates formed during the reaction of diesel soot with nitrogen dioxide. *Applied Surface Science* 253 (4): 2296-303.

3. Bensaid, S., D. L. Marchisio, N. Russo, and D. Fino. 2009. Experimental investigation of soot deposition in diesel particulate filters. *Catalysis Today* 147 : S295-300.

4. Bensaid, Samir, D. L. D. Marchisio, and Debora Fino. 2010. Numerical simulation of soot filtration and combustion within diesel particulate filters. *Chemical Engineering Science* 65 (1): 357-63.

5. Bergmann, Maik, Ulf Kirchner, Rainer Vogt, and Thorsten Benter. 2009. On-road and laboratory investigation of low-level PM emissions of a modern diesel particulate filter equipped diesel passenger car. *Atmospheric Environment* 43 (11): 1908-16.

6. Bird, R. B., W. E. Stewart, and E. N. Lightfoot. 2002. *Transport phenomena*. Wiley: New York,NY.

7. Boehman, Andreì L., Juhun Song, and Mahabubul Alam. 2005. Impact of biodiesel blending on diesel soot and the regeneration of particulate filters. *Energy and Fuels* 19 (5): 1857-64.

8. Caroca, Jose C., Federico Millo, Davide Vezza, Theodoros Vlachos, Andrea De Filippo, Samir Bensaid, Nunzio Russo, and Debora Fino. 2010. Detailed investigation on soot particle size distribution during DPF regeneration, using standard and bio-diesel fuels. *Industrial & Engineering Chemistry Research* 50 (5): 2650-8.

9. Chen, K., D. Luss, and K. Chen. 2011. Temperature excursions in diesel particulate filters: Response to shift to idle. *Industrial and Engineering Chemistry Research* 50 (2): 832-42.

10. Chen, K., K. S. Martirosyan, and D. Luss. 2010. Temperature excursions during soot combustion in a diesel particulate filter (DPF). *Industrial & Engineering Chemistry Research* 49 (21): 10358-63.

11. Chen, Kai, Karen S. Martirosyan, and Dan Luss. 2011. Hot zones formation during regeneration of diesel particulate filters. *AICHE Journal* 57 (2): 497-506.

References

12. Choi, K. Y., N. W. Cant, and D. L. Trimm. 1998. Gasification of carbonaceous particulates. *JOURNAL OF CHEMICAL TECHNOLOGY AND BIOTECHNOLOGY* 71 (1): 57-60.

13. Clement, Karsten H.,et al. 2004. *Kemiske enhedsoperationer*. Lyngby: Polyteknisk Forlag.

14. D. B. Kittelson, W. F. Watts, J. P. Johnson, S. P. Goodier, M. J. Payne, W. H. Preston, C. P. Warrens, et al. 2006. Driving down on-highway particulate emissions.

15. Dabelstein, Werner, Arno Reglitzky, Andrea Schütze, and Klaus Reders. 2000. *Automotive fuels*. Ullmann's encyclopedia of industrial chemistry.Wiley-VCH Verlag GmbH & Co. KGaA.

16. Dieselnet. Emission standards. 20112011]. Available from www.dieselnet.com (accessed 2011).

17. Dinex A/S. DiSiC catalyzed. 2010 [cited November 2010]. Available from www.dinex.dk.

18. Dwyer, Harry, Alberto Ayala, Sherry Zhang, John Collins, Tao Huai, John Herner, and Wilson Chau. 2010a. Emissions from a diesel car during regeneration of an active diesel particulate filter. *Journal of Aerosol Science* 41 (6): 541-52.

19. Dwyer, Harry, Alberto Ayala, Sherry Zhang, John Collins, Tao Huai, Jorn Herner, and Wilson Chau. 2010b. A study of emissions from a euro 4 light duty diesel vehicle with the european particulate measurement programme. *Atmospheric Environment* 44 (29): 3469-76.

20. Elmøe, T. D. Tobias D., Antonio Tricoli, Jan-Dierk Grunwaldt, and S. E. S. Pratsinis. 2009. Filtration of nanoparticles: Evolution of cake structure and pressure-drop. *Journal of Aerosol Science* 40 (11): 965-81.

21. Encyclopædia Britannica Online, Inc. Internal-combustion engine: Four-stroke diesel engine. 2007 [cited Accessed March 2nd 2011]. Available from http://www.britannica.com.

22. Farnam Custom Products. Heat torch 200. 2011]. Available from http://www.farnam-custom.com.

23. Görsmann, Claus. 2005. Catalytic coatings for active and passive diesel particulate filter regeneration. *Monatshefte Für Chemie - Chemical Monthly* 136 (1): 91-105.

24. Graham, Lisa A., Greg Rideout, Deborah Rosenblatt, and Jill Hendren. 2008. Greenhouse gas emissions from heavy-duty vehicles. *Atmospheric Environment* 42 (19): 4665-81.

References

25. Hansen, Brian Brun. 2011. Technical university of denmark.

26. Harada, Koichiro, Hiroshi Yamada, Kenji Okamoto, and Akihide Takami. 2010. Development of high performance catalyzed DPF with new soot burning mechanism. *Catalysis Surveys from Asia* 14 (3-4): 176-84.

27. Haralampous, Onoufrios A., Ioannis P. Kandylas, Grigorios C. Koltsakis, and Zissis C. Samaras. 2004. Experimental evaluation of apparent soot oxidation rates in diesel particulate filters. *International Journal of Vehicle Design* 35 (4): 365-82.

28. Hubeck-Graudal, Helga, and Vinni K. Rønde. 2011. *Emissions from biodiesel engines with particulate filters - bachelor's thesis.* DTU, .

29. Issa, May, Corinne Petit, Alain Brillard, and Jean-Francois Brilhac. 2008. Oxidation of carbon by CeO2: Effect of the contact between carbon and catalyst particles. *Fuel* 87 (6): 740-50.

30. Jeguirim, M., V. Tschamber, and J. F. Brilhac. 2009. Kinetics and mechanism of the oxidation of carbon by NO2 in the presence of water vapor. *International Journal of Chemical Kinetics* 41 (4): 236-44.

31. Jeguirim, M., V. Tschamber, J. F. Brilhac, and P. Ehrburger. 2005. Oxidation mechanism of carbon black by NO2: Effect of water vapour. *Fuel* 84 (14-15): 1949-56.

32. Jeguirim, M., V. Tschamber, J. F. Brilhac, and P. Ehrburger. 2004. Interaction mechanism of NO2 with carbon black: Effect of surface oxygen complexes. *Journal of Analytical and Applied Pyrolysis* 72 (1): 171-81.

33. Jeguirim, M., V. Tschamber, and P. Ehrburger. 2007. Catalytic effect of platinum on the kinetics of carbon oxidation by NO2 and O2. *Applied Catalysis B: Environmental* 76 (3-4): 235-40.

34. Jeguirim, Mejdi, Valérie Tschamber, and Jean Francois Brilhac. 2009. Kinetics of catalyzed and non-catalyzed soot oxidation with nitrogen dioxide under regeneration particle trap conditions. *Journal of Chemical Technology & Biotechnology* 84 (5): 770-6.

35. Jung, J., J. H. Lee, S. Song, and K. M. Chun. 2008. Measurement of soot oxidation with No2-O2-H2O in a flow reactor simulating diesel engine DPF. *International Journal of Automotive Technology* 9 (4): 423-8.

36. Kandylas, Ioannis P., Onoufrios A. Haralampous, and Grigorios C. Koltsakis. 2002a. Diesel soot oxidation with NO2: Engine experiments and simulations. *Industrial and Engineering Chemistry Research* 41 (22): 5372-84.

References

37. Kandylas, Ioannis P., and Grigorios C. Koltsakis. 2002b. NO2-assisted regeneration of diesel particulate filters: A modeling study. *Industrial and Engineering Chemistry Research* 41 (9): 2115-23.

38. Kim, Jong Hun, Man Young Kim, and Hyong Gon Kim. 2010. NO2-assisted sort regeneration behavior in a diesel particulate filter with heavy-duty diesel exhaust gases. *Numerical Heat Transfer; Part A: Applications* 58 (9): 725-39.

39. Kim, Myoung Rae, Do Heui Kim, and Seong Ihl Woo. 2003. Effect of V2O5 on the catalytic activity of pt-based diesel oxidation catalyst. *Applied Catalysis B: Environmental* 45 (4) (10/15): 269-79.

40. Law, M. C., A. Clarke, C. P. Garner, and C. P. Garner. 2004. The effects of soot properties on the regeneration behaviour of wall-flow diesel particulate filters. *Proceedings of the Institution of Mechanical Engineers, Part D: Journal of Automobile Engineering* 218 (12): 1513-24.

41. Laza, T., and Á Bereczky. 2011. Basic fuel properties of rapeseed oil-higher alcohols blends. *Fuel* 90 (2): 803-10.

42. Lee, H. -S, and K. M. Chun. 2006. Investigation of soot oxidation characteristics in a simulated diesel particulate filter. *INTERNATIONAL JOURNAL OF AUTOMOTIVE TECHNOLOGY* 7 (3): 261-7.

43. Lee, J. W., Y. I. Jeong, M. W. Jung, K. O. Cha, S. I. Kwon, J. C. Kim, and S. Park. 2008. Experimental investigation and comparison of nanoparticle emission characteristics in light-duty vehicles for two different fuels. *International Journal of Automotive Technology* 9 (4): 397-403.

44. Lide, David R. 2010. *CRC handbook of chemistry and physics, 2010-2011*. Boca Raton: CRC Press.

45. Liu, Yunqing, Jinke Gong, Jun Fu, Hao Cai, and Gang Long. 2009. Nanoparticle motion trajectories and deposition in an inlet channel of wall-flow diesel particulate filter. *Journal of Aerosol Science* 40 (4): 307-23.

46. Livbjerg, Hans. 2006. Aerosol equations of change.

47. Lox, Egbert S. J. 2008. *Automotive exhaust treatment*. Handbook of heterogeneous catalysis.Wiley-VCH Verlag GmbH & Co. KGaA.

48. Madsen, Anders Theilgaard, Anders Riisager, and Rasmus Fehrmann. 2009. Udfordringer og strategier ved produktion af biodiesel. *Dansk Kemi* 8 : 18-21.

References

49. Majewski, W. A., and Magdi K. Khair. 2006. *Diesel emissions and their control ; W. addy majewski and magdi K. khair.* Warrendale, Pa: SAE International.

50. Martirosyan, K. S., K. Chen, and D. Luss. 2010. Behavior features of soot combustion in diesel particulate filter. *Chemical Engineering Science* 65 (1): 42-6.

51. Messerer, A., R. Niessner, and U. Pöschl. 2006. Comprehensive kinetic characterization of the oxidation and gasification of model and real diesel soot by nitrogen oxides and oxygen under engine exhaust conditions: Measurement, Langmuir–Hinshelwood, and arrhenius parameters. *Carbon* 44 (2): 307-24.

52. Montanaro, L., and A. Bachiorrini. 1994. Influence of some pollutants on the durability of cordierite filters for diesel cars. *Ceramics International* 20 (3): 169-74.

53. Pall Corporation. Pallflex filters. 2011Available from http://www.pall.com.

54. Pallavkar, Sameer, Thomas Ho, Tae-Hoon Kim, Dan Rutman, Jerry Lin, and Thomas Ho. 2009. Active regeneration of diesel particulate filter employing microwave heating. *Industrial and Engineering Chemistry Research* 48 (1): 69-79.

55. Park, Kihong, David B. Kittelson, Michael R. Zachariah, and Peter H. McMurry. 2004. Measurement of inherent material density of nanoparticle agglomerates. *Journal of Nanoparticle Research* 6 (2): 267-72.

56. Peterson, Amy M., Po-I Lee, Ming-Chia Lai, Ming-Cheng Wu, Craig L. DiMaggio, Simon Ng, and Hiyang Tang. 2010. Effects of B20 on emissions and the performance of a diesel particulate filter in a light-duty diesel engine. *Journal of Engineering for Gas Turbines and Power* 132 (11).

57. Power Generator. Diesel generator 6.000 watt. 20112011]. Available from www.powergenerator.dk.

58. Q8. Q8 super diesel. 2008.

59. Schejbal, M., M. Marek, M. Kubíc ek, and P. Kocí. 2009. Modelling of diesel filters for particulates removal. *Chemical Engineering Journal* 154 (3-3).

60. Schejbal, M., J. Stepánek, M. Marek, P. Kocí, and M. Kubíc ek. 2010. Modelling of soot oxidation by NO2 in various types of diesel particulate filters. *Fuel* 89 (9): 2365-75.

61. Setiabudi, Agus, Michiel Makkee, and Jacob A. Moulijn. 2004. The role of NO2 and O2 in the accelerated combustion of soot in diesel exhaust gases. *Applied Catalysis B: Environmental* 50 (3): 185-94.

References

62. Shah, Sandip D., Cocker,David R., I.,II, J. W. Miller, and Joseph M. Norbeck. 2004. Emission rates of particulate matter and elemental and organic carbon from in-use diesel engines. *Environmental Science & Technology* 38 (9): 2544-50.

63. Soldati, Alfredo, Marina Campolo, and Fabio Sbrizzai. 2010. Modeling nano-particle deposition in diesel engine filters. *Chemical Engineering Science* 65 (24): 6443-51.

64. Song, Juhun, Mahabubul Alam, and André L. Boehman. 2007. Impact of alternative fuels on soot properties and DPF regeneration. *Combustion Science and Technology* 179 (9): 1991-2037.

65. Stanmore, B. R., J. F. Brilhac, and P. Gilot. 2001. The oxidation of soot: A review of experiments, mechanisms and models. *Carbon* 39 (15): 2247-68.

66. Stanmore, B. R., V. Tschamber, and J. -F Brilhac. 2008. Oxidation of carbon by NOx, with particular reference to NO2 and N2O. *Fuel* 87 (2): 131-46.

67. Stratakis, G. A., and A. M. Stamatelos. 2003. Thermogravimetric analysis of soot emitted by a modern diesel engine run on catalyst-doped fuel. *Combustion and Flame* 132 (1-2): 157-69.

68. Turns, S. R. 2006. *An introduction to combustion - concepts and applications*. 2nd edition ed.McGraw-Hill Internationals Editions.

69. van Setten, BAAL, M. Makkee, and J. A. Moulijn. 2001. Science and technology of catalytic diesel particulate filters. *CATALYSIS REVIEWS-SCIENCE AND ENGINEERING* 43 (4): 489-564.

70. Walker, A. P. 2004. Controlling particulate emissions from diesel vehicles. *Topics in Catalysis* 28 (1-4): 165-70.

71. White, F. M. 1991. *Viscous fluid flow*. New York,N.Y.: McGraw-Hill.

72. Yamamoto, Kazuhiro, Masamichi Nakamura, Hiroyoshi Yane, and Hiroshi Yamashita. 2010. Simulation on catalytic reaction in diesel particulate filter. *Catalysis Today* 153 (3-4): 118-24.

73. Yamamoto, Kazuhiro, Shingo Satake, and Hiroshi Yamashita. 2009. Microstructure and particle-laden flow in diesel particulate filter. *International Journal of Thermal Sciences* 48 (2): 303-7.

74. Yokoi, Taro, Motohiro Shinzawa, and Yasuo Matsumoto. 2001. Measurement repeatability improvement for particle number size distributions from diesel engines. *JSAE Review* 22 (4): 545-51.

Appendix A – Engine

Diesel Generator 6.000 Watt
3-Fase / El-Start / Støjdæmpet.

PowerGenerator
PURE ENERGY

Generatoren er udstyret med AVR, så alt elektrisk udstyr inkl. computere kan tilsluttes.

Støjsvag kun 64 dB(A).

16 Liters tank med niveau indikator.

4 - Takt Diesel motor med 10.0 HK.

Thermisk sikring til beskyttelse mod kortslutning eller overbelastning.

Olietryksalarm med automatisk stop.

Motorolieskift indikeres via digital time-tæller.

Lavt brændstofforbrug

Frekvens	50 Hz
Volt	230 / 400 Volt
Volt Regulering	AVR (Automatisk Volt Regulering)
Max Belastning	6.000 Watt - 30 Ampere - 10 Ampere pr. fase
Vedvarende Belastning	5.000 Watt - 21 Ampere - 7 Ampere pr. fase
12 Volt Udtag	8.3 Ampere
Motor	4 Takt - Diesel - Luftkølet
Størrelse	418 cc
HK	10.0 HK
O/Min	3.000
Støjniveau	64 dB(A)
Tank	16 Liter
Forbrug	1.76 Liter pr. time ved fuld belastning
Længde	95,5 cm
Bredde	57,5 cm
Højde	86,5 cm
Vægt	150 KG

CE EC-II Noise

24 **On-line shop www.powergenerator.dk - Tlf 64 41 59 02**

(Power Generator 2011)

Appendix B - Diesels

Q8 Super Diesel

Svovlfrit brændstof med forbedrede egenskaber til dieselmotorer.

Anvendelse
Q8 Super Diesel er en højkvalitets diesel som kan anvendes i alle diesel motorer f.eks. i personbiler, vare-biler, lastbiler og busser, hvorfra man ønsker et mindst muligt svovl- og partikelindhold i udstødningen.
Q8 Super Diesel anbefales til den krævende bilist, som ønsker at bibeholde bilens ydeevne optimalt samt opleve større køreglæde og sikrere kørsel.

Egenskaber og fordele
Q8 Super Diesel opfylder kravene til den Europæiske diesel standard **EN 590**, hvilket sikrer at produktet kan anvendes til alle typer dieselmotorer i bl.a. person-, vare-, og lastbiler.
Q8 Super Diesel er afsvovlet til under 10 ppm (0,001 %). Produktet er derved velegnet til Euro 4 diesel-motorer, hvor udstødningen er monteret med et partikelfilter og SCR-enhed, som stiller krav om brændstof med max. 10 ppm svovl.
Q8 Super Diesel er tilsat smørende additiver, som sikrer optimal smøring af brændstofsystemets pumper og dyser.
Q8 Super Diesel renser og renholder brændstofsystemet og specielt motorens indsprøjtningsdyser. Det betyder bedre brændstoføkonomi, bedre ydelse og større køreglæde.
Q8 Super Diesel skummer mindre under tankning, hvilket gør det nemmere og hurtigere at fylde tanken, uden at pistolen slår fra før tanken er fuld.
Q8 Super Diesel nedsætter risikoen for korrosion betydeligt. Desuden modvirker Q8 Super Diesel binding af vand i brændstoffet, og derved nedsættes risikoen for mikrobiologiske forekomster.
Q8 Super Diesel er i vinterperioden frostsikret ned til -24 °C og er ikke tilsat petroleum.

Begrænsning
Produktet bør ikke anvendes til fiskeri- og marineformål, da flammepunktet kan være under 61 °C, som er minimumskravet ved international marinedrift. Tilsætning af petroleum eller benzin for at forbedre kuldesik-ringen frarådes, da det kan forringe produktets egenskaber samt medføre øget brandfare.

Specifikationer: Energiministeriets bek. nr. 884 af 03/11/2003   **CEN EN 590**

Tekniske analysedata

Egenskab	Data	Enhed	Metode
Vægtfylde ved 15 °C	830	kg/m³	EN ISO 12185
Viskositet ved 40 °C	2,8	mm²/s	EN ISO 3104
Svovlindhold, max.	10	mg/kg	EN ISO 20846
Polycykliske aromatiske kulbrinter, max	11	% masse	EN 12916
Uklarhedspunkt (cloud point), max.		°C	EN 23015
1. april – 30. september	0		
1. oktober – 30. november	-7		
1. december – 31. marts	-10		
Filtreringspunkt (CFPP), max.		°C	EN 116
1. april – 30. september	-12		
1. oktober – 30. november	-18		
1. december – 31. marts	-24		
Flammepunkt, min.	56	°C	EN ISO 2719
Cetantal, min.	51	—	EN ISO 5165
Cetanindex, min.	46	—	EN ISO 4264
95% destillation, max	360	°C	EN ISO 3405
Nedre brændværdi	42.800	kJ/kg	Beregnet

(Q8 2008)

ASG Analytik-Service Gesellschaft mbH
Trentiner Ring 30 • D-86356 Neusäss / Germany

Emmelev A/S
Emmelevgyden 25
DK-5450 Otterup

your reference	:	Jensen
your order-no.	:	-
date of order	:	17.06.2010
sample receipt	:	18.06.2010
sampling	:	Customer
report date	:	23.06.2010
page	:	1 of 2
start of test period	:	21.06.2010
end of test period	:	23.06.2010
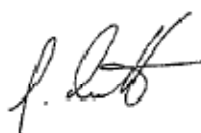
Report-No. : 183724

Sample Designation : RME MT "BRØVIG WIND"
Sample Appearance : yellowish, limpid, no free water visible, no contaminations visible, characteristic odour
Sample Container : glass bottle 1000 mL, sealed "EMMELEV"
ASG-ID : 172064

Seal : X

Parameter	Method	Result	Specification DIN EN 14214:09-02 min.	max.	Unit
Ester Content	DIN EN 14103	>99	96,5	-	% (m/m)
Density at 15 °C	DIN EN ISO 12185	883,0	860	900	kg/m³
Viscosity at 40 °C	DIN EN ISO 3104	4,413	3,5	5,0	mm²/s
Flash Point	DIN EN ISO 3679	161,0	101	-	°C
CFPP	DIN EN 116	-13	-	*	°C
Sulfur Content	DIN EN ISO 20884	2,1	-	10,0	mg/kg
Carbon residue (10%)	DIN EN ISO 10370	0,12	-	0,3	% (m/m)
Cetane number	DIN EN 15195	56,6	51,0	-	-
Sulfated Ash	ISO 3987	<0,01	-	0,02	% (m/m)
Water Content	DIN EN ISO 12937	272	-	500	mg/kg
Total contamination	DIN EN 12662	6	-	24	mg/kg
Copper Strip Corrosion	DIN EN ISO 2160	1	1		Corr.Degree
Oxidation stability at 110 °C	DIN EN 14112	6,6	6,0	-	h
Acid value	DIN EN 14104	0,336	-	0,5	mg KOH/g
Iodine value	DIN EN 14111	113	-	120	g Iodine/100g
Linolenic Acid Methylester	DIN EN 14103	9,6	-	12,0	% (m/m)
Methanol Content	DIN EN 14110	0,04	-	0,20	% (m/m)
Free Glycerol		<0,01	-	0,020	% (m/m)
Monoglyceride Content		0,29	-	0,80	% (m/m)
Diglyceride Content	DIN EN 14105	0,12	-	0,20	% (m/m)
Triglyceride Content		0,08	-	0,20	% (m/m)
Total Glycerol		0,10	-	0,25	% (m/m)
Phosphorous Content	DIN EN 14107	3,1	-	4,0	mg/kg
Metals I (Na + K)	DIN EN 14108/109	0,7	-	5,0	mg/kg
Metals II (Ca + Mg)	DIN EN 14538	<0,5	-	5,0	mg/kg

* requirements :	15.04. -	30.09.	max.	0 °C
	01.10. -	15.11.	max.	-10 °C
	16.11. -	28.02.	max.	-20 °C
	01.03. -	14.04.	max.	-10 °C

J. Bernath

ASG Analytik-Service Gesellschaft mbH
Trentiner Ring 30
D-86356 Neusäss / Germany

phone +49 (0) 821 450423-0
fax +49 (0) 821 486 25 19
e-mail info@asg-analytik.de

DGA-PL-4404.05

General Manager
Dr. Thomas Wilharm
Amtsgericht Augsburg HRB 12297

ASG Analytik-Service Gesellschaft mbH
Trentiner Ring 30 • D-86356 Neusäss / Germany

Emmelev A/S
Emmelevgyden 25
DK-5450 Otterup

your reference	: Jensen
your order-no.	: -
date of order	: 17.06.2010
sample receipt	: 18.06.2010
sampling	: Customer
report date	: 23.06.2010
page	: 2 of 2
start of test period	: 21.06.2010
end of test period	: 23.06.2010

Report-No.   : 183724

Sample Designation	:	RME MT "BRØVIG WIND"
Sample Appearance	:	yellowish, limpid, no free water visible, no contaminations visible, characteristic odour
Sample Container	:	glass bottle 1000 ml, sealed "EMMELEV"
ASG-ID	:	172064

Seal : X

Parameter	Method	Result	Unit
Calorific value, lower	DIN 51900-2	37301	J/g
Cloud Point	DIN EN 23015	-4	°C

J. Bernath

This report is related only to the samples stated above and may not be reproduced except in full, without approval
of the testing laboratory. Storage of the samples: 4 weeks from report date
Accreditation according to E N ISO/IEC 17025.

ASG Analytik-Service Gesellschaft mbH	phone	+49 (0) 821 450423-0	General Manager
Trentiner Ring 30	fax	+49 (0) 821 486 26 19	Dr. Thomas Wilharm
D-86356 Neusäss / Germany	e-mail	info@asg-analytik.de	Amtsgericht Augsburg HRB 12297

Table 33 Specifications for the lubrication oil Q8 Formula V Long Life 5W-30

Property	Minimum Value	Maximum Value	Method
Density (15°C) / [kg/m3]	844	854	D 4052
Viscosity (100°C) / [mm^2/s]	11.5	12.5	D 445
Viscosity (30°C) / [mm^2/s]	N/A	6,600	D 5293
Flash point (COC) / [°C]	200	N/A	D 92
Pour point / [°C]	N/A	-36	D 97
Nitrogen / [wt%]	0.096	0.116	D 5291(C)
Ca + Mg / [wt%]	0.134	0.162	D 4961 / D 6443
Phosphorous / [wt%]	0.052	0.065	D 4961 / D 6443
Sulphur / [wt%]	N/A	0.3	-
Zinc / [wt%]	0.055	0.070	D 4951 / D 6443

Appendix C - Preheater

Below the gas temperature immediately after passing the preheater with a set point of 500°C is shown. The preheater is regulated through simple on-off control and due to the very powerful heating elements.
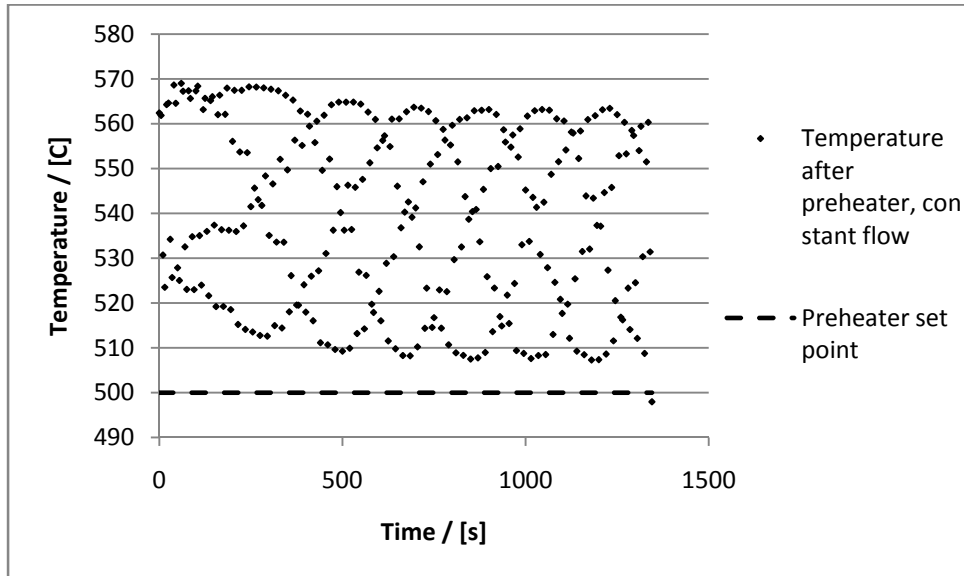
Figure 30 Temperature of the gas leaving the preheater with a gas flow of ~30m³/h. The set point for the pre heater is 500°C.

HEAT TORCH™ HT200

Shown with optional inlet & exhaust fittings

Wattage	Min. SCFM Req.
1.0kW	9.6
4.0kW	9.6
5.0kW	12.4
6.0kW	14.8
7.0kW	17.0
8.0kW	19.3
9.0kW	21.4
10.0kW	23.5
11.0kW	25.5
12.5kW	28.4

Airflow (SCFM)	0.5kW-4.25kW Pressure Drop (psig)	4.5kW-8.5kW Pressure Drop (psig)	8.75kW-12.5kW Pressure Drop (psig)
10	.36	.72	1.1
20	.75	1.5	2.3
30	1.7	3.4	5.1
40	3.0	6.0	9.0
50	4.7	9.4	14
60	6.8	14	20
70	9.2	18	28
80	12	24	36
90	15	30	45
100	19	38	57

- The Heat Torch™ 200 inline heater is engineered to satisfy the most demanding requirements. It is contained in a 2" diameter stainless steel pipe and is available in three sizes. The 5" long heater body is for power ratings from 1000 to 4250 watts (with power increments of 250 watts). The 9" long is for power ratings of 4500 to 8500 watts (with standard power increments of 500 watts). The 13" long heater is for power ratings from 9000 to 12500 watts (with standard power increments of 1000 watts).

- The Heat Torch™ 200 has an allowable air flow ranging from 9.6 to 100 SCFM . Maximum air input temperature is 250°F (121°C) with 1300°F (704°C) the maximum output temperature. Standard inlet fitting is a 1" NPT female. Standard outlets are 1 1/4" female NPT fitting or no exhaust fitting.

Wattage & Voltage Options
120V, single phase, 1.0kW-2.5kW
240V, single phase, 1.0kW-8.5kW
240V, three phase, 4.5kW-12.5kW
480V, single phase, 4.5kW-12.5kW
480V, three phase, 1.5kW-12.5kW

Fitting Options
Inlet Fitting:
1F- 1" FNPT

Exhaust Fitting:
1 1/4F- 1 1/4" FNPT
NF- No Fitting

Other Options
Thermocouple Fitting
Thermocouple
Flexible Conduit

Specifications
Category:	Inline Heaters, Process Heaters, Open Coil Heaters
Max. wattage:	12.5kW
Max. exhaust air temp.:	1300°F
Max. inlet air temp.:	250°F
(consult factory for higher inlet temp.)	
Max. SCFM:	100
Pressure Rating:	120 psig
Mounting:	Horizontal/Vertical
Leads:	12 gauge (12" long)
Heater Body:	Stainless Steel
Inlet Fitting:	Stainless Steel
Exhaust Fitting:	Stainless Steel
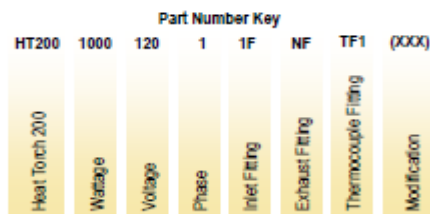
Wattage	Heater Body Dim. A	Exhaust Fitting	Dim. B
1.0kW-4.25kW	5.0	1 1/4F	1.13
4.5kW-8.5kW	9.0	NF	0.10
8.75kW-12.5kW	13.0		

Part Number Key
HT200	1000	120	1	1F	NF	TF1	(XXX)
Heat Torch 200	Wattage	Voltage	Phase	Inlet Fitting	Exhaust Fitting	Thermocouple Fitting	Modification

(Farnam Custom Products)

Appendix D - DPF and Oven

Table 34 Specifications for the DPF (Dinex A/S 2010)

Filter Type	Wall Flow Monolith
Produced By	Dinex A/S
Filter material	SiC
Catalytic coating	TiO2 + CeO2 (11g/l filter volume) + Pt (1.8 wt%)
Average pore diameter	20 μm
Cell density	150 CPSI
Filter width / cross sectional diameter	80 mm
Filter Length	130 mm
Cell Wall Thickness	0.55 mm
Maximum Temperature	625 °C

Figure 31 Oven in which the DPF is located

Appendix E - Perma Pure

Figure 32 Perma Pure MD^{TM}

Appendix F - FID

Table 35 Specifications for Flame Ionizing Detector

Model	Thermo FID, ES
Produced By	Mess & Analystechnik GmbH

Figure 33 Picture of the Thermo FID produced by Mess & Analystechnik GmbH

Appendix G - Sampling Filter

A Tissuquartz Filter is used for soot sampling

PALL Life Sciences

Pallflex® Filters
Emfab™, Fiberfilm™, and Tissuquartz™ Filters

Emfab – preferred filters for diesel exhaust and stack emission testing
Pure borosilicate glass microfibers reinforced with woven glass cloth and bonded with PTFE
- Withstands folding for weighing and transport.
- Every filter flushed with DI water to remove water-soluble residue.
- Low moisture pickup eliminates lengthy desiccations.
- Low air resistance.

Fiberfilm – economical filters for air monitoring applications
Pure borosilicate glass fibers with fluorocarbon coating
- Unique combination of heat-resistant borosilicate glass fibers and moisture-resistant fluorocarbon (tetrafluoroethylene, TFE) coating.
- Moisture variations in air or gases during air sampling will not cause chemical reactions on the filter.
- Low moisture pickup eliminates lengthy desiccations.
- Low air resistance.
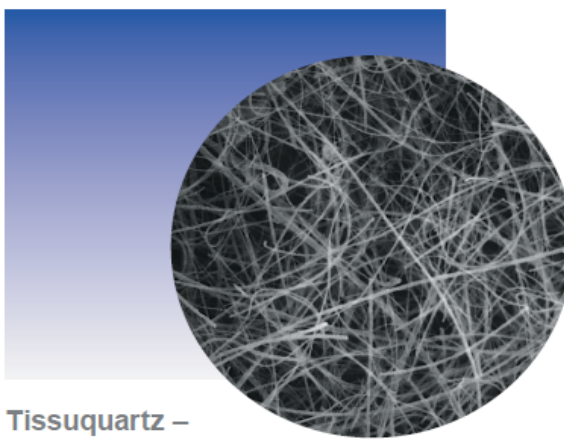
Tissuquartz – uniquely designed for air monitoring in high temperatures and aggressive atmospheres
Binder-free pure quartz
- Heat treated for reduction of trace organics and superior chemical purity.
- High temperature use up to 1093 °C (2000 °F).
- High flow rate and filtration efficiency.

Applications
- Emfab Filters – Low air resistance for use in critical aerosol sampling tests that demand filter purity and non-hygroscopic properties such as diesel exhaust, stack emission control, and ambient air monitoring for particulate concentration.
- Fiberfilm Filters – Suitable for high temperature and hot gas air monitoring applications. Heat-treated (HT) version available for reduction of trace organics.
- Tissuquartz Filters – High temperature use for analysis of acidic gases and stack sampling aerosols. Ultra-pure soft water processing reduces residual ion content. (Contact Pall Life Sciences for typical values.)

Specifications

Description	Emfab Filters	Fiberfilm Filters	Tissuquartz Filters
Filter Media	Borosilicate microfibers reinforced with woven glass cloth and bonded with PTFE	Heat resistant borosilicate glass fiber coated with fluorocarbon (TFE)	Pure quartz, no binder
Diameter	12 - 142 mm [and 8 x 10 in. (20 x 25 cm)]	25 - 100 mm [and 8 x 10 in. (20 x 25 cm)]	25 - 142 mm [and 8 x 10 in. (20 x 25 cm)]
Typical Thickness	178 µm (7 mils)	203 µm (8 mils)	432 µm (17 mils)
Typical Filter Weight	5.0 mg/cm²	3.4 mg/cm²	5.8 mg/cm²
Typical Water Flow Rate at 0.35 bar (5 psi)	32 mL/min/cm²	220 mL/min/cm²	220 mL/min/cm²
Typical Air Flow Rate at 0.7 bar (10 psi)	68 L/min/cm²	180 L/min/cm²	73 L/min/cm²
Maximum Operating Temperature – Air	260 °C (500 °F)	315.5 °C (600 °F)	1093 °C (2000 °F)
Typical Aerosol Retention*	99.9%	96.4%	99.9%
pH in Boiled Water Extract	Not available	Not available	6.5 - 7.5

Following ASTM D 2986-95A 0.3 µm (DOP) at 32 L/min/100 cm² filter media

(Pall Corporation 2011)

Appendix H - STA

Table 36 Specifications for STAs used

Produced By	Netzsch	Netzsch
Model	449FI Jupiter	409C
Measuring Principle	TGA and DSC	TGA and DSC
Temperature Range	25 - 1550 °C	-
Heating Rate	0.1 - 50 °C/min	-

Figure 34 Netzsch 449FI Jupiter capable of doing TGA and DSC

Figure 35 Netzsch 409C capable of doing TGA and DSC
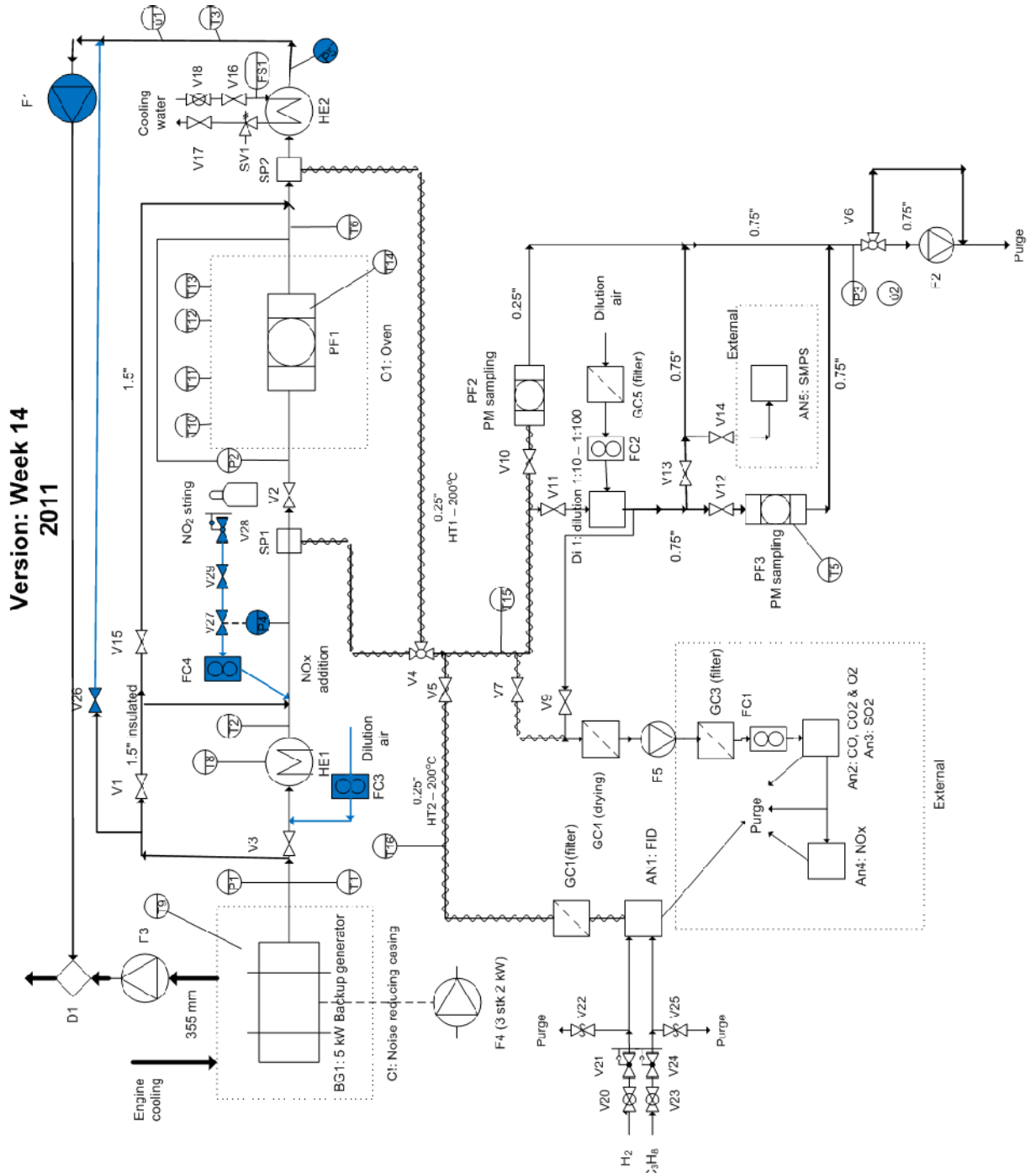
Appendix I – P&I and Setup

P&I Diagram

Figure 36 P&I diagram showing the experimental setup. Elements marked with blue color indicate alterations that have been implemented different from experiments previously carried out by DTU students Hubeck-Graudal and Rønde in the fall of 2010 (Hubeck-Graudal et al. 2011)**.**

Setup

Figure 37 The experimental setup shown with the casing surrounding the engine to the right.
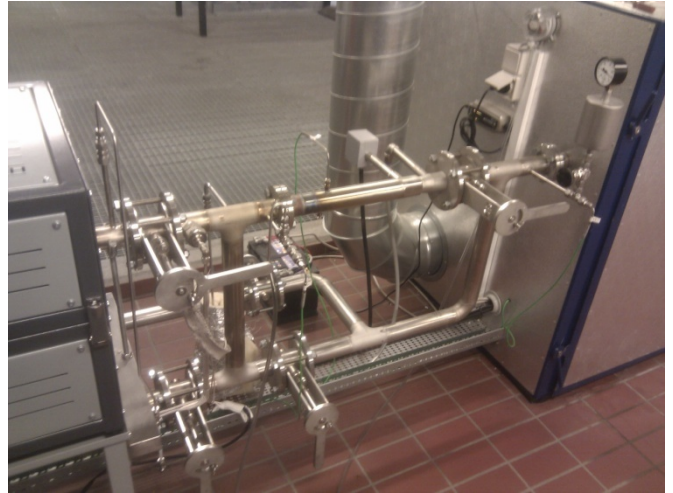
Figure 38 The piping connecting the engine outlet to the DPF.

Figure 39 The heat exchanger HE2 is seen at the bottom center. Downstream of HE2 the horizontal piping contains the venturi meter U1.
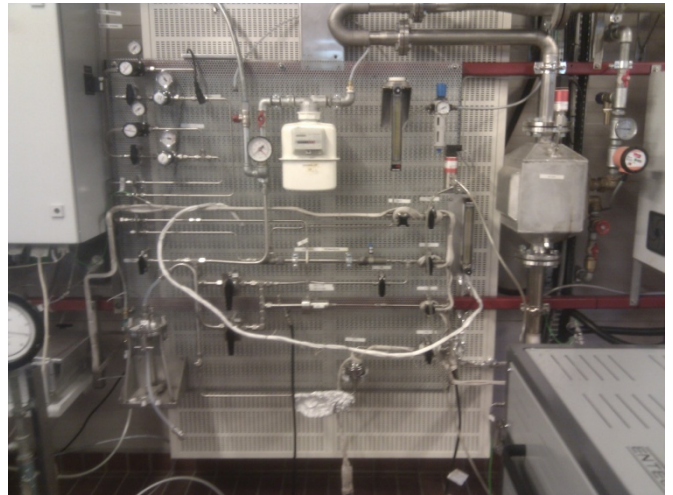
Figure 40 The panel containing all the piping downstream of the sampling points SP1 and SP2.

Appendix J – Sampling Data
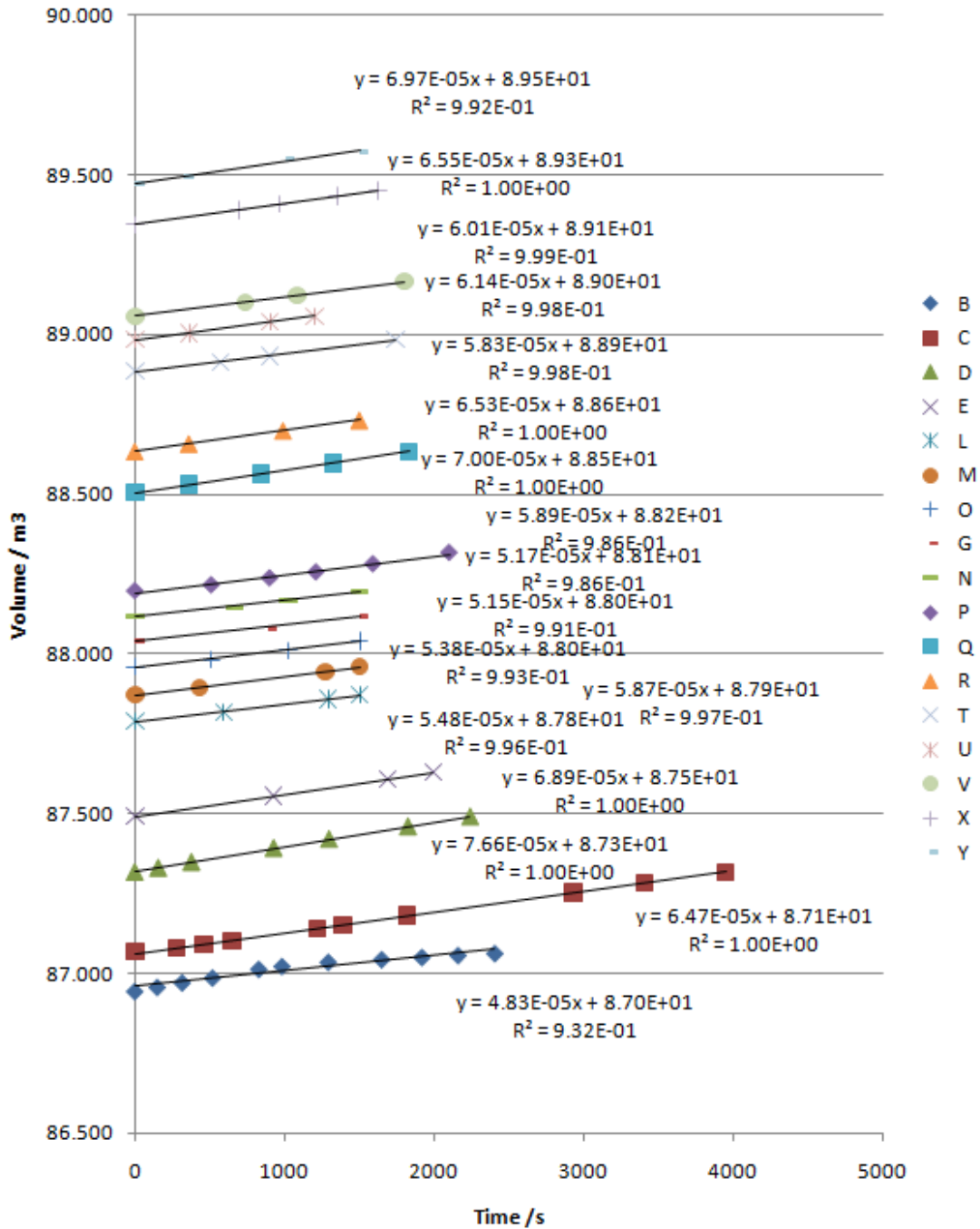
Figure 41 Data obtained during sampling of soot on the sampling filter. The plot shows gas meter readings as a function of time for all samplings conducted. The filter temperature ranged from 50-75C and the pressure at the sampling point may be different due to changes in the setting on F1.

Appendix K – Flow Meter Calibration
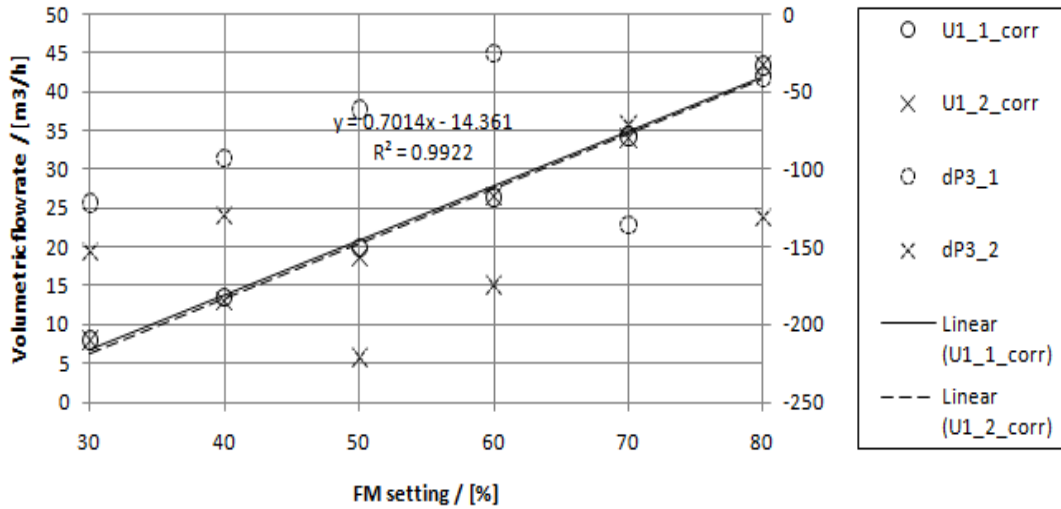
Figure 42 Corrected flow rates plotted together with actual flow rates measured at U1 for different pressures registered at P5. A linear regression on the corrected flow rates as a function of the flow meter setting is also shown.

Appendix L – Time Delay

The time delay experienced when gas is sent from the experimental setup to the gas analyzers. The gas needs to travel a distance of excess 10 m making the time delay significant. The distance from the sampling point to the FID inlet is no larger than 3 m and due to the fact that no need rapid changes in volatile hydrocarbon readings are needed due to the uncertainties associated with these the time delay for the string leading to the FID is neglected.

The time delay from the sampling point to the gas analyzers is determined by initially letting atmospheric air through FC3 and therefore ~0% CO_2 is registered in the gas analyzers. With the engine running at 80% load the valve V3 is changed from a closed to an open position and an increase in CO_2 concentration is observed 45 seconds later indicating the time delay. All data containing results from the gas analyzers have been adjusted for with this delay.
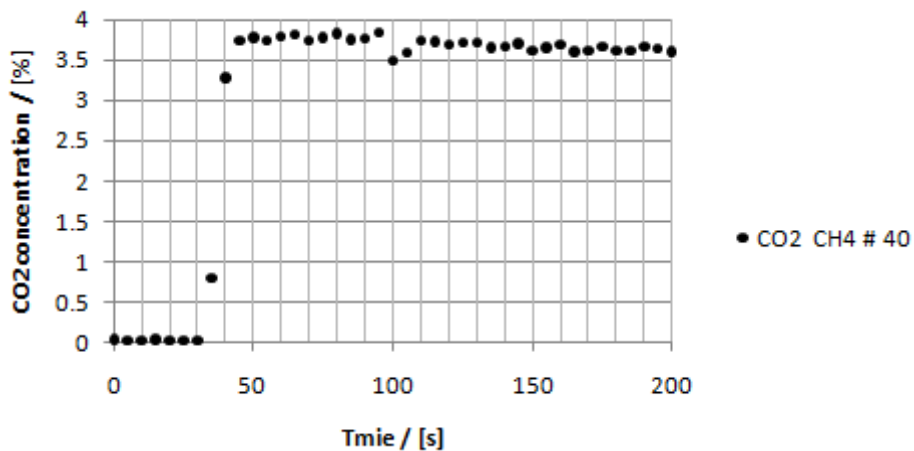

Figure 43 The plot shows measured CO_2 concentration as a function of time. The plot shows time delay experienced on measured values in the gas analyzers as sampled gas is transported from the sampling point. With the engine running at 80% load the valve V3 is changed from a closed to an open position at time = 0 seconds.

Appendix M - Conversion of Units

Following an average diesel soot composition of $C_{12}H_{23}$ the simplified reaction scheme for complete combustion becomes:

$$C_{12}H_{23} + 17.75O_2 \rightarrow 12CO_2 + 11.5H_2O \tag{A.1}$$
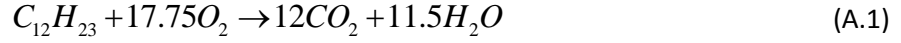
It is seen that the post combustion volume is increased by (11.5+12)/17.75 = 23.5/17.75 gas molecules per molecule of O_2 consumed. With an oxygen content of atmospheric air around 21% the post combustion volume assuming complete combustion becomes:

$$79\% + 21\% \cdot \frac{23.5}{17.75} = 106.8\% \tag{A.2}$$

From the above one can easily see that the main contributor to the exhaust gas flow rate is the volume of the air intake. A four stroke engine has two crankshaft rotations per combustion cycle hence the engine displacement volume (V_c) can express the intake volume (V_{intake}) as the following assuming ideal gas behavior and assuming that the volumetric contribution from the injected fuel can be neglected:

$$V_{int\,ake} \Big/ \min ute = V_{cylinder} \frac{RPM}{2} = n_{int\,ake} \left(\frac{RT}{P} \right)_{inlet} \frac{1}{\min ute} \tag{A.3}$$

The amount of gas molecules in the exhaust is calculated from n_{intake} and the contribution from increase in post combustion volume:

$$n_{out}^{gas} = n_{int\,ake}^{gas} \cdot 1.068 \tag{A.4}$$

The molar emission of gas molecules per minute is readily converted to emission per kilometer travelled by division with the vehicle velocity.

Appendix N – Deposition

Particle Diffusivity

In order to determine the diffusion coefficient of the soot particles a given particle size needs to be considered. Assuming the soot particles are spherical the Stokes-Einstein relation can be used in order to determine the diffusion coefficient for diffusion in a slow flowing fluid. The diffusion coefficient for a spherical particle with radius r in a fluid with viscosity μ and temperature T the Stokes-Einstein relation states (Bird, Stewart, and Lightfoot 2002):

$$D_p = \frac{k_B T}{6\pi\mu r} \tag{A.5}$$

The Boltzmann constant is $k_B = 1.381 \big/ K$.

Viscosity

The viscosity of the gas can be calculated after Sutherland's formula expressing the temperature dependence (White 1991).

$$\frac{\mu}{\mu_0} = \left(\frac{T}{T_0}\right)^{3/2} \frac{T_0 + S}{T + S}$$

(A.6)

The Sutherland constant for air is S=120. From the equations above it is seen that increased temperatures and smaller particles yield increased diffusivity.

Fraction of Particles Deposited on Wall

The fraction of particles deposited on the wall as a function of dimensionless tube length can be seen below
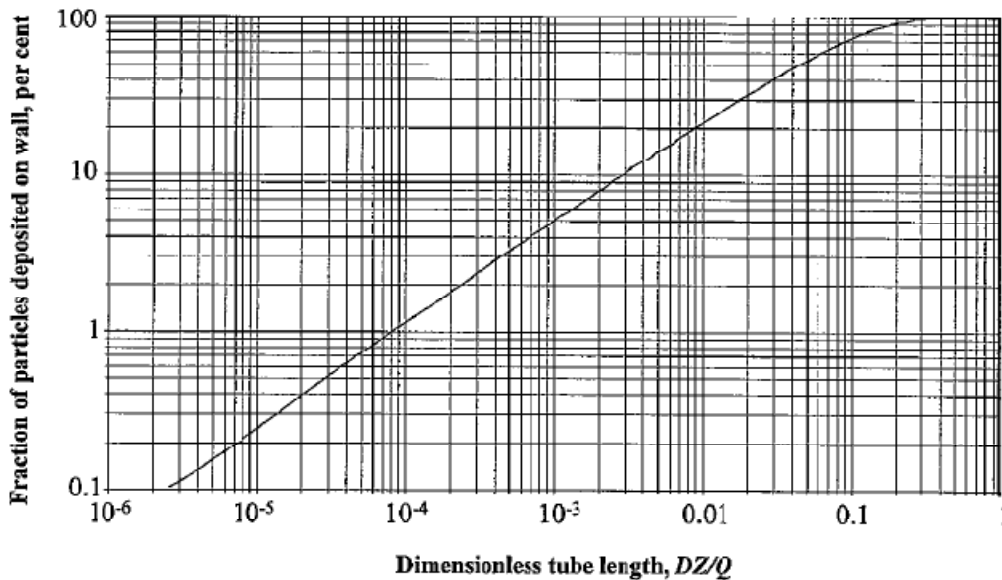
Figure 44 Deposition efficiency as a function of the dimensionless tube length, ε. Q is the volumetric gas flow rate (m³/s), D is the diffusion coefficient (m²/s) for the particle size fraction considered, and Z is the tube length (m) (Livbjerg 2006).

Appendix O - Flow Calculations

The degree of dilution is defined as:

$$\eta = \frac{y_f^{CO_2}}{y_{ex}^{CO_2}}$$

(A.7)

Setting up a component balance for CO_2 yields the following, where $\dot{n}$ is the molar flow rate:

$$IN = OUT$$

(A.8)

$$\dot{n}_{add} \cdot y_{add}^{CO_2} + \dot{n}_{ex} \cdot y_{ex}^{CO_2} = \dot{n}_{byp} \cdot y_{ex}^{CO_2} + \dot{n}_f \cdot y_f^{CO_2}$$

(A.9)

As the air addition happens downstream of the bypass outlet one may assume that little or no added air exits the system through the bypass. Assuming that all of the added air is forced downstream of the inlet, the molar flow rate of the bypassed stream is easily determined as:

$$\dot{n}_{byp} = \dot{n}_{ex} + \dot{n}_{add} - \dot{n}_{f} \qquad (A.10)$$

Insertion of (A.10) into (A.9) yields an expression for the molar flow rate through the filter as a function of known parameters:

$$\dot{n}_{f} = \frac{\dot{n}_{add}}{1 - \eta} \qquad (A.11)$$

The volumetric flow rate of the stream passing through the DPF is measured after a heat exchanger exhibiting near ambient temperatures. Assuming similar temperature and pressure for the added air, the total molar flow rates may then be replaced by volumetric flow rates thus becoming:

$$Q_{filter} = \frac{Q_{add}}{1 - \eta} \qquad (A.12)$$

Appendix P – Corrected Flow

For an incompressible horizontally flowing fluid where friction by viscous forces can be neglected Bernoulli's equation (A.13) states that an increase in pressure P results in a decrease in the linear flow rate v according to:

$$\frac{\rho}{2} v^2 + P = \text{constant} \qquad (A.13)$$

The assumption of incompressible fluid is generally also valid for slow flowing gasses. Based on the Bernoulli principle a venturi meter utilizes the pressure increase when a flowing fluid is led through a narrowing on its passage. The pressure increase results in an acceleration of the fluid. Applying the Bernoulli equation to the pressure prior to and after a narrowing of a tube with known cross sectional areas the volumetric flow rate in a simplified form becomes

$$Q = k \frac{\sqrt{\Delta P}}{\sqrt{\rho}} \qquad (A.14)$$

where k is constant as a function of cross sectional area prior to and after the narrowing and also the coefficient of discharge, which is function of the Reynolds's number taking into account for inertial forces associated with the contraction of stream lines. The density ρ remains constant for incompressible fluids, however, in order to account for changes in the overall pressure of a flowing gas the change in density needs to be considered. The venturi meter U1 expresses registered volumetric flow rates calculated for a flowing gas at atmospheric pressure and ambient temperature. In order to account for changes in pressure the volumetric flow needs to be corrected. Assuming the changes in the pressure drop ΔP in the venturi meter are negligible the following is obtained for two gasses with different densities:

$$\frac{Q_1}{Q_2} = \frac{\sqrt{\rho_2}}{\sqrt{\rho_1}} \qquad (A.15)$$

Assuming ideal gas behavior and isothermal conditions at U1 the above is transformed into:

$$\frac{Q_1}{Q_2} = \frac{\sqrt{\dfrac{M \cdot P_2}{R T_2}}}{\sqrt{\dfrac{M \cdot P_1}{R T_1}}} = \sqrt{\frac{P_2}{P_1}} \tag{A.16}$$

In order to correct the flow measurement at U1 which is calculated on the assumption of atmospheric pressure, the corrected and real volumetric flow rate becomes:

$$Q_{actual} = Q_{measured}\sqrt{\frac{P_{atm}}{P_{actual}}} \tag{A.17}$$

In order to compare volumetric flow rates obtained for different pressures the flow rate is correlated in order to obtain the volumetric flow rate at a standard atmospheric pressure. Assuming ideal gas behavior and isothermal conditions volumetric flow rate is inversely proportional to the pressure and the correlated flow rate thus becomes:

$$Q_{corrected} = Q_{U1}\sqrt{\frac{P_{atm}}{P_{actual}}} \cdot \frac{P_{actual}}{P_{atm}} = Q_{U1}\sqrt{\frac{P_{actual}}{P_{atm}}} \tag{A.18}$$
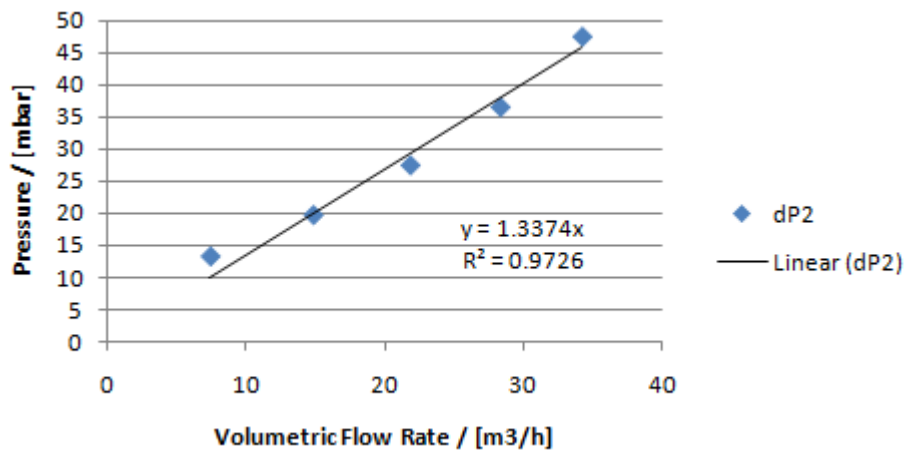
Appendix Q – Flow through DPF

Figure 45 The pressure drop registered over the DPF (dP2) as a function of volumetric flow rate of air added. The loading of the filter remained fixed.

Appendix R – TGA Data
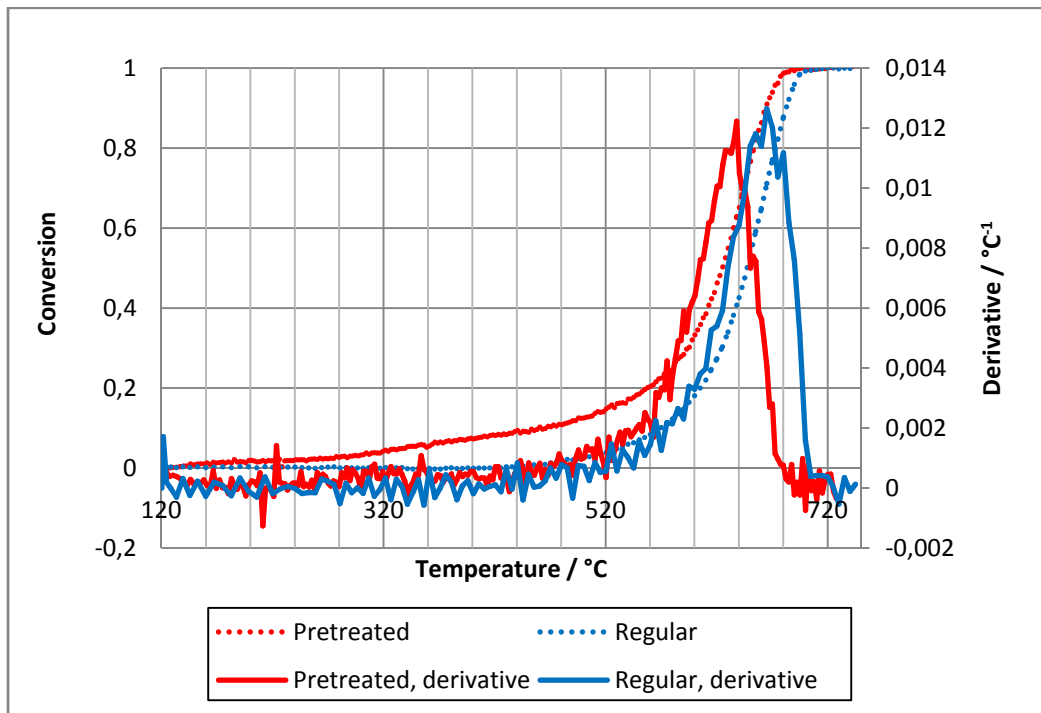
Pretreatment of TGA Samples

Figure 46 The plot shows both conversion as well as the derivative of the conversion as function of temperature for two identical soot fractions (petrodiesel combusted at 80% load) investigated in NETZSCH STA-449FI. One sample is pretreated by removal of volatiles through heating in an inert N_2 atmosphere to 300°C (5°C/min) prior to STA. The pretreated sample is heated from ambient temperature to 750°C (10°C/min) in 10% O_2 and 90% N_2. The untreated sample marked 'regular' is within the STA apparatus initially heated to 450°C (10°C/min) in 100% N_2, kept isothermal at 450°C for 15 min, cooled to 120°C and finally heated to 750°C (10°C/min) in 10% O_2 and 90% N_2.
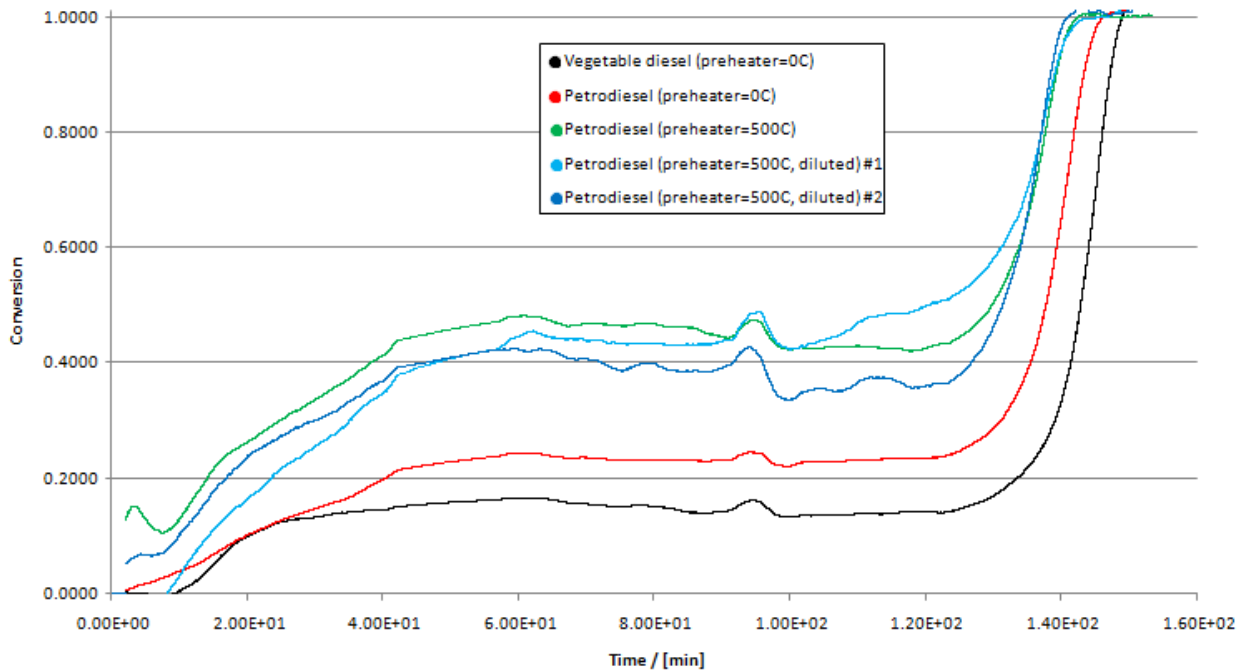
Conversion

Figure 47 The plot shows conversion as a function of time for different runs in STA. The obtained mass loss signal has been averaged for a full interval of 4 min evenly around each data point. Each soot sample is initially heated to 450°C (10°C/min) in 100% N_2 kept isothermal at 450°C for 15 min, cooled to 120°C and finally heated to 750°C (10°C/min) in 10% O_2 and 90% N_2.
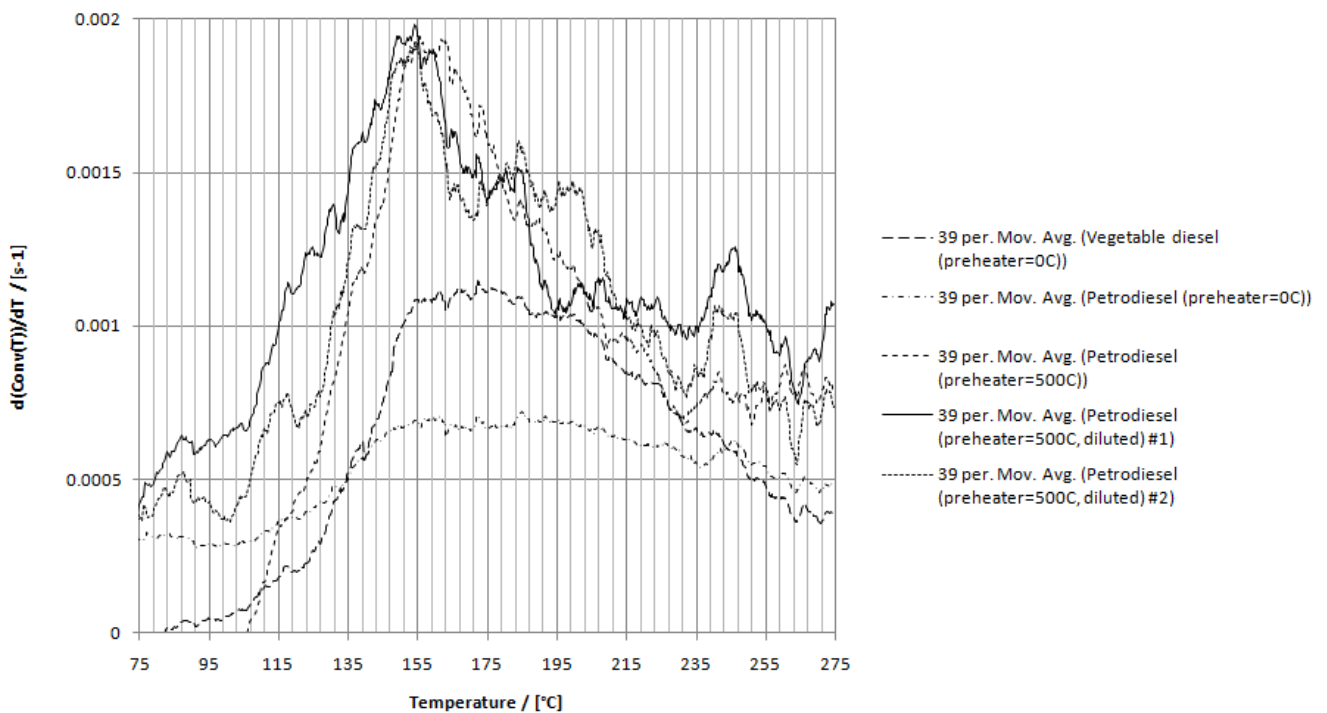
Point of Evaporation

Figure 48 The plot shows the curves obtained as a result of a moving average on differentiated mass loss data from TGA as a function of temperature for the initial part of the STA run where each soot sample is initially heated to 450°C (10°C/min) in 100% N_2. The obtained mass loss signal has been averaged for a full interval of 8 min evenly around each data point.
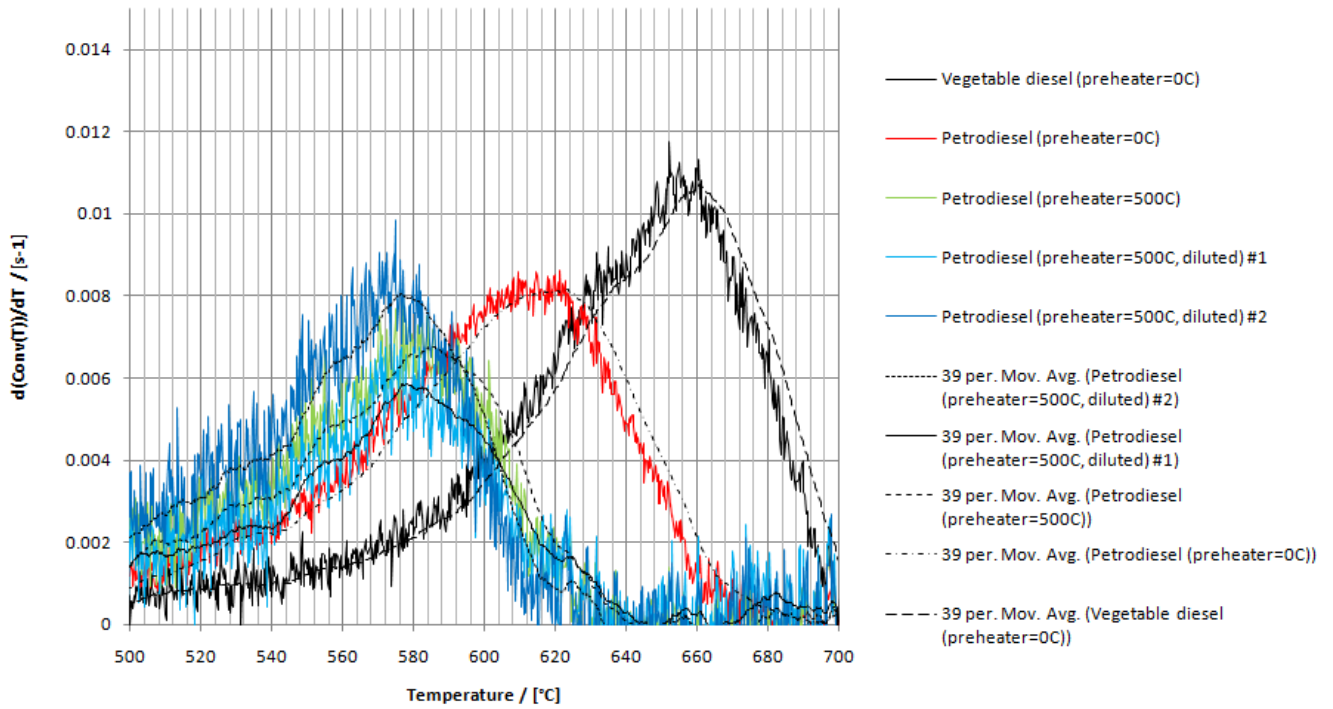
Reactivity

Figure 49 The plot shows both raw data and the curves obtained as a result of a moving average on differentiated mass loss data from TGA as a function of temperature for the final part of the STA run where each soot sample is heated to 750°C (10°C/min) in 10% O_2 and 90% N_2. The obtained mass loss signal has been averaged for a full interval of 4 min evenly around each data point.
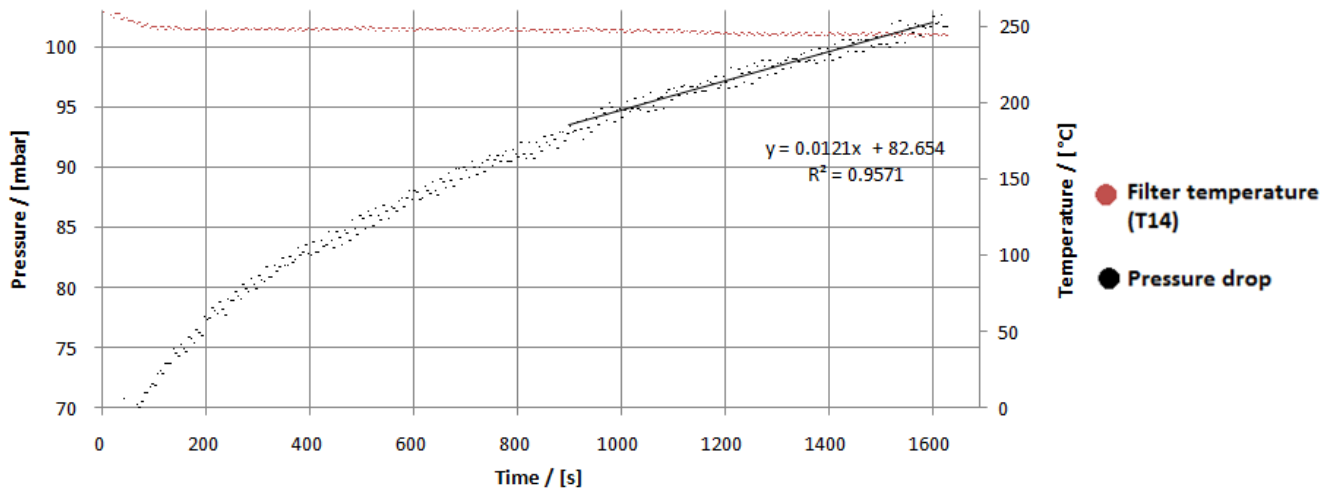
Appendix S – Vegetable Diesel DPF Loading

Figure 50 Deposition of soot in the DPF from the combustion of vegetable diesel at an engine load of 80%. Degree of dilution was 1-η=0.50. Both the pressure drop and the filter temperature are shown as a function of temperature. Linear regression on the pressure drop curve has been carried out for the time interval 900-1600s.

Appendix T - Procedure

Below is the standard operating procedure used for operating the experimental setup in this project. The SOP is written by Brian Brun Hansen (Hansen 2011)*:*

045-23 Standard operation procedure

Description

The diesel engine (backup generator) is located in a ventilated, noise-reducing casing.

Cooling air is withdrawn from outside the building and discharged to the atmosphere alongside the exhaust. 3 ventilators placed outside of building 228 are used to vary the engine load (0-6 kW). The fuel is stored in CHEC's fuel storage facility (up to 1000 L) and only minor amounts (up to 16 L) is transferred (in closed container) and poured into the fuel tank at the time. The generated exhaust can be heated (pre-heater HE1), diluted and NO_x can be added before it passes through a particulate filter (PF1), which is located in a three-stage oven (O1) to ensure a constant filter temperature. During start-up it is possible to bypass the filter (valves 2 & 15) until the desired exhaust temperature is obtained. The development in pressure and temperature across the filter (T14 and P2) is monitored in order to study the particle retention and possible onset of regeneration. The exhaust is subsequently cooled (HE2) and the flow rate measured by a venture nozzle (v1).

Sample withdrawal can be performed before and after the filter by a heated three-way valve (Valve 4). The sample stream is distributed to gas phase analysis (2 strings) or particulate analysis (3 combinations).

Start-up

- Check the oil and diesel levels and the "breaker" is on
  - Diesel indicator on top of generator (next to diesel tank)
  - Yellow oil-stick inside engine room of generator
  - "breaker" is located in the upper right corner of the engines front panel
- Check that the 2 handles on the venture flowmeter points towards the central pipe
- Start the pc and labview (data logging)
  - Double click "start page" icon on desktop
  - Click white arrow to start
  - Data collection:
    Choose location of file, name, sampling frequency and press start
  - In the screens menu choose "biodiesel"
  - Check that the maximum engine temperature is set to "45 ^{o}C" and max HE1 shell temperature is set to "0 ^{o}C"
- Turn on the electrical cabinet (right side of the cabinet)
  - Press "reset" on the front of the cabinet (blue button)
- Open the diesel supply
  - switch next to glass cylinder inside engine room (upper left side)
- Turn on the on/off switch on top of the engine
  - turn so it points left towards the wall
- Start the exhaust fan (F1)
  - Slowly increase the feed airflow to the ejector pump until a slight under-pressure (app 10 mbar) is obtained (see pressure indicator next to engine box)
- Start the engine box ventilation (green switch on the front of the electrical cabinet).
- Set V1-V3 and V15 to bypass (i.e. no flow through HE1 and oven)
- Check that the cooling water is running
  - Orange bar on flowswitch next to cooler - HE2
- Check that startup battery is connected and is not being charged
- Start the engine (ignition-switch on electrical cabinet)
  - Turn from off, to ignition, to on (for a few seconds)
  - If the engine doesn't start allow the switch to fall back into ignition and try again.
- Set the engine load
  - Turn on 1, 2 or 3 ventilators (front of electrical cabinet)

Use of pre-heater

- Check that the exhaust temperature does not exceed 425 C
- Ensure that exhaust passes through the preheater
- In labview – biodiesel screen – insert max HE1 temperature = 350 ^{o}C and click "ok"
- Approach the desired output temperature is small steps (labview - biodiesel screen – green box)

- be aware that the maximum is 675 ^{o}C (material specifications)
- Before shutting down the pre-heater, insert max HE1 temperature = 0 ^{o}C and click ok to "reset He1", change desired temperature to 0 ^{o}C and allow exhaust to continue to pass through in order to "cool"

Use of pre-heater + dilution
- Before starting the pre-heater measure the total exhaust by passing it all through (u1), slightly open the by-pass string (V26) until the flow passing though the filter is down to the desired level. And then start addition of dilution air (FC3) until the flow passing the filter is back to the original level.
- Only then turn on the pre-heater and do this in small increments of the desired output temperature.
- Check the dilution ratio obtained by measuring gas phase concentrations and comparing with an undiluted exhaust.
- When shutting down the experiment remember the procedure described under "shot-down" i.e. continue engine operation, but at the same time add dilution air, when this is done close V3 so only dilution air passes through the pre-heater and continue until it is cooled down."

Diesel particulate filter
- Turn on the 3 stage oven in which the filter is located
  - The oven panel is next to the cooler (HE2)
  - press "power"
  - Set the temperature of all 3 zones to the temperature of the exhaust
  - press "heat"
- Change the valve settings so the exhaust enters the particulate filter
- The pressure drop across the filter (dP) can now be seen in labview
  - Observe it increase over time as soot deposit
  - Be aware that the pressure drop is temperature dependent
- Filter regeneration can be obtained by bypassing the exhaust and heating the oven.
  - Follow T$_{filter}$ in labview and pass exhaust through the filter every now and then to check dP

Sampling
- Insert pre weighed filter in either PF2 or PF3
  - if particulate emissions is to be collected.
  - ensure that PF2 is heattraced
- Start the heat-tracing of the sampling lines
  - Choose the "eurotherm" screen in labview
  - Set T15 and T16 to desired temperature
    150 ^{o}C for FID, 50-150 for filters (check the actual filter temperature)
- Set the 3-way valve (V4) to either sampling site 1 or 2 (before or after filter)
- Ensure that the exhaust passes through the filter when sampling from site 1

Gaseous emissions
- Start the air flow to the permapure and open this analysis string
  - Open valve before permapure
  - Set the airflow to the permapure by the flowmeter
  - – Open valves in central gas analysis panel
  - Start pump leading to central gas analysis
  - Open flowmeter in central gas panel (aim for 1 l/min)
  - – Check that to condensation take place in the piping after the permapure.

Particulate emissions
- Insert pre weighed filter in either PF2 or PF3 before starting heat-tracing
- Check the filter temperature with a thermometer
- Note the time and airflow in the lab journal
- Open first valve in sample string
- Start the exhaust flow

- by starting the pump for PF2 – ensure that the gas flow pass through the gas clock
- or the dilution airflow for PF3 – ensure that the gas flow bypasses the gas clock.
- When sampling is complete note the time and airflow in the lab journal

FID

- Open the H_2 and FID calibration gas cylinders (gas central 27 and ??) as well valves next to the wall and on the rack. Ensure a calibration gas pressure of 2.5 bar, a H_2 pressure of 1 bar and a sample pressure of 1 bar.
- Start the FID and allow the auto calibration to take place

SMPS

- Bypass the gas clock (can't handle high flow rates)
- Start the CPC and SMPS located on a trolley and allow them to warm up while the sampling port is in contact with the atmosphere
- Set the correct flow rate on the CPC display and the DMA model, nozzle size and sheat flow rate on the SMPS (selected based on particle size to be determined)
- Set the SMPS display to "analog"
- Open software on PC and make a SMPS file and enter DMA, impactor, flow rates etc
- When the equipment is warmed up open the dilution string.
- Start the dilution by increasing the flow rate of air into the dilutor
- Connect a side stream from the dilutor to the SMPS and start the measurement by the software

Shut-down

- Ensure that the temperature guard of the preheater (HE1) is set to 0 C, click "ok" and the red light will appear. Set the HE1 target temperature to 0 C.
- Turn off any engine load (1-3 ventilators)
- Continue engine operation, but at the same time add dilution air, when this is done close V3 so only dilution air passes through the pre-heater
- Turn off engine
- Continue cooling air addition until the pre-heater is cooled down and only then stop it
- Stop labview
  - Press "stop all" on any screen
- Turn off the switch on top of the engine (points towards you)
- Close the diesel supply (switch next to glass cylinder inside engine)
- Open drain-valve underneath HE2 (careful may be hot) and in the bypass pipe string and allow condensation to drain. Then run dilution air through the system to dry.
- Stop dilution air addition and close drain-valves

4/4-2011
Brian Brun Hansen

Appendix IV

Performance of Diesel Particulate Filter Catalysts in the Presence of Biodiesel Ash Species

Brian B. Hansen, Anker D. Jensen[*] and Peter A. Jensen

[a] Department of Chemical and Biochemical Engineering, Technical University of Denmark, Building 229, DK-2800 Kgs. Lyngby, Denmark

[*] To whom correspondence should be addressed. Telephone +45 45252841, Fax +45 45882258, Email: aj@kt.dtu.dk.

Abstract

The utilization of bio-fuels, such as biodiesel, is expected to contribute significantly towards the planned increased percentage (10 %) of renewable energy within the EU transport sector by 2020. Increased biodiesel blend percentages may change engine exit flue gas ash composition and affect the long-term performance of cleaning technologies, such as oxidation catalysts and diesel particulate filters. In this work the performance of a commercial catalyst has been studied for conversion of diesel particulate matter (SRM 2975) at 10 % O_2, in the presence of salts simulating ash derived from engine oil and biodiesel. The simultaneous thermal analysis experiments showed that the particulate matter was dominated by soot with approximately 10 wt % condensed hydrocarbons. The presence of a commercial catalyst (5:1 wt. ratio of catalyst to soot), in tight contact with the diesel particulate matter, decreased the temperature at which the soot oxidation rate peaked from 662 ± 1^oC to 526 ± 19^oC. The introduction of biodiesel salts such as Na_2CO_3, K_2CO_3 or K_3PO_4 decreased the peak conversion temperature further $(422 \pm 12; 404 \pm 4$ and 423 ± 7^oC), with a limited dependence on salt concentration. A deterioration in

catalytic conversion, i.e. increased peak conversion temperatures, was seen for two simulated engine oil ashes and one mixed engine oil/biodiesel ash mixture – $CaSO_4$ (569 ± 6 ^{o}C), $Ca(H_2PO_4)_2$ (699 ± 13 ^{o}C) and K_2SO_4 (581 ± 16 ^{o}C).

Kinetic parameters (A and E_a), obtained from Arrhenius plots of the data, showed a lower activation energy in the presence of the commercial catalyst (E_a = 91 ± 5 kJ/mol) or CeO_2 (E_a = 62 ± 8 kJ/mol) compared to pure SRM 2975 (E_a = 220 ± 3 kJ/mol) The obtained kinetic data were able to describe the peak conversion temperature and the associated part of the mass loss curve, but an initial low-temperature gradual increase in conversion was not adequately described.

Keywords

DPF, catalytic filter, biodiesel, regeneration, catalyst activity, ash, soot

1. Introduction

Emissions from the transport sector and its contribution to global warming and detrimental effects on human health have become focus of growing concerns and awareness in recent years. This has caused the EU to aim for 10 % renewable energy in the transport sector and 20 % renewable energy overall by 2020 [1]. The introduction of biofuels (ethanol, biodiesel etc.) into the transport sector is expected to contribute significantly to these goals. The introduction of new fuels or changes in fuel properties may affect engine performance, emissions, ash composition and long-term interactions with cleaning technologies such as the oxidation catalyst (DOC), the diesel particulate filter (DPF) and selective catalytic reduction of NOx (SCR)[2]. Even a low concentration of catalyst poison in the exhaust/ash may severely affect the performance of cleaning technologies as seen for power plants burning biomass [3-5].

Previous engine emission improvements were obtained by stricter fuel specifications and in-cylinder modifications/engine optimization, while after treatment systems, such as DPF and SCR, will likely be necessary to comply with the latest U.S and European legislation [6]. In the case of particulate emissions, a flow through diesel oxidation catalyst is capable of oxidising CO and gaseous hydrocarbons, that otherwise could condense and contribute to particle formation. The highly efficient DPF traps 95-99 % PM by forcing the exhaust through a porous wall, thereby initially capturing PM in the pores followed by cake filtration on top of the channel walls [7-8]. To avoid excessive backpressure periodically DPF cleaning/regeneration by oxidation into CO_2 (reaction with O_2 or NO_2) is necessary. Two different regeneration strategies may be employed: Active regeneration at 500-800 ^{o}C (temperature increased by fuel conversion) or passive regeneration down to 250-300 ^{o}C by either a catalytic fuel additive, a catalytic DPF coating or an upstream conversion of NO to NO_2 [6,9]. A swift, cheap and energy efficient filter regeneration is desired, while maintaining filter integrity (no thermal run away or steep temperature gradients). Understanding the kinetics of filter regeneration is consequently of importance for filter optimization and regeneration strategies. The ash (incombustible residue) generated from engine oil, fuel, additives and engine/exhaust wear will accumulate in the DPF and eventually constitute the majority of trapped material. This influences catalytic DPF baseline pressure drop, pressure drop sensitivity and potentially affect regeneration frequency, heat release and performance [6,7,10]. The ash composition and properties will depend on fuel/oil origin, additives, DPF temperature history etc. and the introduction of new fuels, such as bio-fuels, may change these.

The introduction of biodiesel has been reported to cause an increased reactivity of particulate matter [11-12] and some changes in ash composition [6,13]. The increased reactivity has been attributed to a more open structure of the de-volatilized biodiesel PM, allowing swifter O_2 diffusion to reactive sites, which is supported by the extraction of overall ultra low sulphur diesel (ULSD)/pure biodiesel (B100)

kinetic data when normalising with the instantaneous surface area (E_a = 113 kJ/mol) [12]. Reported ash compositions from experiments with pure ULSD are dominated by species from the engine oil (~ 90 %: Ca, Mg, Zn, P, S, B, Mo) in the form of: calcium sulphate, zinc phosphate, magnesium phosphate, magnesium sulphate and calcium phosphate [6,8,10]. Minor amounts of engine/exhaust wear components (Al, Co, Cr, Cu, Fe, Mn, Ni, Pb, Si, Sn, Ti, V), primarily as Fe_3O_4, are also present [6]. The utilisation of a 20 % soybean methyl ester blend yielded ash similar in composition, except a somewhat higher content of engine/exhaust wear elements (~ 16 wt%) and fuel alkali (~ 6 wt. % Na & K) [6]. This is supported by the presence of biodiesel alkali elements (4.2 wt. % Na and 2.1 wt. % K) in a survey of the particulate matter (ash + soot) collected after pneumatic cleaning of DPF/DOC on US vehicles [13]. The introduction of biodiesel may generally contribute with the elements Na, K, Ca, Mg and P, but the concentration of these elements is limited by standards such as the European EN14214 standard (Na+K $\leq$ 5 mg/kg, Ca+Mg $\leq$ 5 mg/kg and P $\leq$ 4 mg/kg). The ash obtained from experiments with an off-spec 100 % canola methyl ester (Na+K & Ca+Mg exceeded specifications 10 times) yielded a significantly changed ash composition consisting of: calcium oxide, magnesium oxide, sodium phosphate, calcium phosphate and magnesium phosphate with 37 wt%. Na+K [6].

Several studies of carbon oxidation (carbon black as well as automotive PM containing both soot and adsorbed hydrocarbons) and screening studies of various catalyst for soot/hydrocarbon conversion have been published in the literature [9,14-16] as has a few studies on the interaction between ash and DPF/after treatment systems [7-8,10,17]. *Bardasz et. al.*[10] studied the influence of engine oil composition and ash content on continuously regenerating DPF, DOC and SCR performance on a 230 kW Euro IV prototype engine for simulated driving distance up to 115000 km. No significant changes in DPF or DOC catalytic activity were found. Doping high ash oil into the fuel, a practice used for disposal or accelerated tests, did however cause rapid increases in DPF backpressure, changes in ash distribution and an increased ash density within the DPF. *Sappok & Wong, [7]* studied the effect of ash on pressure drop and regeneration frequency by accelerated ash loading test with a 224 kW Cummins

ISB engine. Ash was observed to accumulate and form end plugs in the inflow channels, thereby decreasing the effective filter volume, increasing pressure drop and causing changes in local soot concentration.

The aim of this work is to extend the present knowledge on the interaction between automotive ash (especially from biodiesel) and catalytic DPF's by simulated filter regeneration experiments in lab-scale using simultaneous thermal analysis. This entails a detailed characterisation of non-catalytic and catalytic soot combustion in the presence of salts simulating different ash compositions.

2. Strategy of investigation

This investigation of soot reactivity, oxidation behaviour and the influence of catalytic materials and various salts (simulated ash) have been performed by ex situ studies in a Simultaneous Thermal Analyzer (Netzsch STA 449 F1 Jupiter) combining thermo gravimetric analysis (TGA) and differential scanning calorimetry (DSC). This apparatus offers a simple and versatile performance combined with well-controlled experimental conditions [11]. The experiments performed, shown in table 1, investigate the reactivity of mixtures of soot, catalysts and various salts/simulated ashes (carbonates, phosphates and sulphates). Chloride salts have furthermore been included due to their lower melting points and thereby potential for a higher mobility and tighter soot/catalyst contact. The effects of heating rates and O_2 concentration have furthermore been investigated for selected samples. The reactivity of the mixtures will be evaluated based on the temperature at which the maximal conversion rate takes place and kinetic data will be extracted based on Arrhenius plots.

3. Experimental setup and procedure

Procedure

The mixtures described in Table 1 were prepared by: Mixing the catalytic powder and the dissolved salt, drying at 50 $^{\circ}$C, PM/soot/carbon addition and grinding in a mortar for 5 minutes and finally

addition of a few drops of ethanol to further benefit soot-catalyst interaction as it evaporates. This procedure was used to obtain the close soot-catalyst interaction needed for studies of catalytic effects [15]. The generated mixture was then transferred to an alumina crucible and heated to 750 $^{\circ}$C in the STA (heating ramp 5-10 k/min) at a gas flow of 100 ml/min. The O_2 concentration (10 %) was chosen within the typical range of diesel exhausts (5-15 %) [15], but selected samples were also tested at 0 % and 20 % O_2. No pre-treatment of soot/carbon/PM in an inert atmosphere was carried out, as this would potentially remove the condensed hydrocarbons (a relevant part of automotive PM) and alter the available surface area [15].

Chemicals

A standard reference material from NIST (SRM 2975 – diesel particulate matter from fork lifts) was used as automotive particulate matter/diesel soot, but the carbon nanopowder (Sigma-Aldrich > 99,95 %) was also used for selected samples. The main part of this study is performed with a commercial catalyst supplied by Dinex A/S (~ 2 % Pt, ~ 20 % CeO_2 and ~ 78 % TiO_2), but experiments with CeO_2 (Sigma-Aldrich) and TiO_2 (Riede-de Haen 99 %) have also been performed to verify the active species and to test for a "dilution effect" by inert materials. The salts used were of analytical grade unless otherwise stated: $CaCl_2 \cdot 2H_2O$ (Brenntag Nordic), $CaSO_4 \cdot 2H_2O$ (Sigma), $Ca(H_2PO_4)_2$ (Aldrich - technical grade), $CaCO_3$ (J.T.Baker), KCl (Fluka), K_2SO_4 (Merck), K_3PO_4 (Sigma), K_2CO_3 (Merck), NaCl (Merck), Na_2SO_4 (Riedel-de Haen), $Na_2HPO_4 \cdot 7 H_2O$ (Merck), Na_2CO_3 (Merck) and $ZnC_4H_6O_4 \cdot 2H_2O$ (Fluka).

4. Estimation of characteristic oxidations temperatures and kinetic parameters

The development in sample mass as a function of temperature and time can be used for studies of characteristic oxidation temperatures as well as extraction of kinetic parameters [11]. A running average (up to 200 data points, corresponding to 15 $^{\circ}$C) was used to reduce signal noise and improve data interpretation, after it was verified that no data distortion occurred. Mixtures of soot, catalyst and salt

exhibit several different changes in mass during one run due to water evaporation, decomposition of the salt and soot combustion. In order to distinguish the different processes taking place in these experiments, runs with pure salts were performed and the DSC signal of the mixtures was furthermore used to identify the soot combustion segment. This work will mainly focus on the temperature at which the maximum mass loss rate takes place, but other additional characteristic temperatures (ignition/starting oxidation temperature, final oxidation temperature etc) have also been used in the literature [9,11,14].

An Arrhenius type equation, equation 1, has been used to extract the kinetic data used to simulate the soot oxidation in a 10 % O_2 atmosphere without water. A first order reaction with respect to soot and oxygen should be appropriate at the low temperature regime used in this study [11,14].

$$\frac{dm}{dt} = k \cdot m \cdot p_{O2} = k^* \cdot m \cdot = A \cdot \exp(-E_a / RT) \cdot m \tag{1}$$

$$\rightarrow \ln\left(-\frac{dm}{m \cdot dt}\right) = \ln(A) - \frac{E_a}{R \cdot T}$$

Where m is the actual soot mass, t is the time, k is the reaction rate constant, A is a pre-exponential factor (frequency factor), E_a is the activation energy and p_{O2} is the partial pressure of oxygen. For some purposes the reaction rate constant may furthermore be split into two terms: a total number of active sites and a temperature dependent reaction rate constant [15]. Rearranging equation 1 yields the well known form used for an Arrhenius plot, from which the pre-exponential factor (from y-axis intercept) and the activation energy (from slope) can be extracted. Experimentally estimated values of A are, however, affected by severe errors due to high sensitivity of the y-axis intercept on small variations of the slope [18]. Only the central linear part of mass vs. temperature TG curve was used to extract kinetic data in this study and this was only done for pure carbon samples and carbon/catalyst mixtures, because the carbon wt % of carbon-catalyst-salt mixtures became too low to obtain reasonable estimates for a linear Arrhenius plot. Extracted kinetic parameters may furthermore be dependent on flow rate, heating

ramp, sample mass or be partially controlled by diffusion [11,14,15]. Equations 2, 4 and 5 have been used to check whether the effects of film mass transfer, pore diffusion or oxygen diffusion into the crucible are significant [14,19].

$$k_{obs} \cdot V_p = k_{obs} \cdot \frac{\Pi \cdot d_p^3}{6} << k_g \cdot S_e = k_g \cdot \Pi \cdot d_p^2 \tag{2}$$

$$Sh = \frac{k_g \cdot 2 \cdot d_p / 2}{D} \approx 2 \tag{3}$$

$$L^2 \cdot k_{obs} / D = \left(\frac{d_p / 2}{3} \right)^2 \cdot k_{obs} / D < 0.15 \tag{4}$$

$$k_{obs} \cdot m \cdot \frac{M_{O2}}{M_C} < \frac{D_{O2}}{h} \cdot a \cdot C_{O_2,b} \tag{5}$$

Where k_{obs} is the observed rate constant (~ 0.01 s^{-1}), V_p the particle volume, d_p the particle size ($\sim 10^{-6}$ m), k_g the mass transfer coefficient (from eq 3), S_e the external particle surface area, D the diffusion coefficient ($\sim 10^{-4}$ m^2 s^{-1}), L a characteristic size ($d_p/6$ for spheres), m the carbon/soot mass ($\sim$ 1-2 10^{-6} kg), M the molar mass (0.012 g mol^{-1} (C) and 0.032 g mol^{-1} (O$_2$)), h the crucible height/depth ($\sim$ 3 10^{-3} m), a the cross sectional area ($\sim$ 3 10^{-5} m^2) and $C_{O2,b}$ the oxygen concentration outside the crucible (~ 0.03 kg m^{-3}). By inserting these approximate values it can be shown, that neither film mass transfer nor pore diffusion influence the results, and that molecular diffusion into the crucible approximately equals the maximal amount of oxygen needed (for the limited sample masses used (1-2 mg Carbon)).

5. Results and discussion

The experimental work includes experiments with pure particulate matter as well as mixtures of carbon, catalytic material and salts simulating biodiesel ash. Different mixture ratios, gas composition and heating rates have furthermore been investigated. Details of the experiments are given in Table 1.

Figure 1 shows the development in mass and conversion/mass loss rate for pure SRM 2975 particulate matter samples in both pure nitrogen and 10 % O_2, and at heating rates of 5 and 10 ^oC/min. Figure 2 compares the mass and conversion/mass loss rate for SRM 2975 and Sigma "carbon nanopowder". The pure SRM 2975 show a gradual decline in mass from app 200 ^oC in both 100 % N_2 and 10 % O_2. This is likely due to evaporation of condensed hydrocarbons or adsorbed sulphates [14], a hypothesis which is supported by the constant mass of the Sigma "carbon nanopowder" at these temperatures. At higher temperatures (~ 550-600 ^oC) combustion begins to take place in 10 % O_2, somewhat later for the Sigma "carbon nanopowder" than for the SRM 2975. Such differences in the oxidation behaviour of carbon and soot samples may originate from differences in size, structure or composition [15]. The obtained peak conversion temperature for SRM 2975 at 10 k/min (662 $\pm$ 1 ^oC) is similar to values reported for other soot STA experiments (655 ^oC) [9] but it is somewhat higher than what has been reported for devolatilised diesel PM (~550 ^oC) [11]. A decreased heating rate shifted the start of combustion and the peak in conversion rate towards lower temperatures, with reasonable repeatability for both heating rates - 5 k/min (3 experiments) and 10 k/min (2 experiments). Due to the faster processing time 10 k/min was chosen for the subsequent samples.

Figure 3 shows the mass and conversion/mass loss rate for 5:1 mixtures of catalytic material (Commercial catalyst, CeO_2 and TiO_2) and SRM 2975. The final mass obtained correspond to the wt % catalyst in the mixture. This property shows some variation, likely due to the elusive nature of carbon/soot during the grinding and transfer parts of the sample preparation procedure. The samples with higher residual mass and thereby a higher catalyst fraction also resulted in higher reactivities – i.e. peak in conversion rate at a lower temperature. The presence of a commercial catalyst decreased the peak conversion temperature (from 662 $\pm$ 1 to 526 $\pm$ 19^oC), a decrease similar to what have been reported elsewhere for other catalytic materials tested on soot [9,14]. The lower temperature reported for passive DPF regeneration (250-300 ^oC [6]) is likely due to the presence of NO_2 in exhaust – but this species could not be introduced to the STA. The samples with CeO_2 showed a higher reactivity than

samples with commercial catalyst. (~ 20 % CeO_2), while TiO_2 samples showed a reactivity similar to pure SRM 2975 and the presence of this compound in the commercial formulation are probably due to other factors such as providing a high surface area.

Figure 4 compares the temperature at which the conversion/mass loss rate peaks for different carbon-catalyst-salt mixtures. The mixtures with chloride salts added showed no significant changes in catalytic conversion behavior of SRM 2975. A significant beneficial effect of Na_2CO_3 and K_2CO_3 was seen, as it also has been reported for carbon black/model soot oxidation [15] and gasification of carbonaceous materials [16]. The beneficial effect of Na_2CO_3 was also present at an 80 % lower dosage and it did not change/decrease for two subsequent runs with reused Na_2CO_3/commercial catalyst mixtures. The beneficial effect of alkali carbonates are likely due to the formation of active alkali metal oxides and peroxides species [16]. However, $CaCO_3$ increased the peak conversion temperature slightly (from 526 $\pm$ 19°C to 554 $\pm$ 4°C). A deterioration was seen for mixtures with K_2SO_4 and $CaSO_4$ (581 $\pm$ 16 °C and 569 $\pm$ 6 °C), while no significant effect could be seen for Na_2SO_4 (537 $\pm$ 12 °C). Different phosphorous salts (K_3PO_4, Na_2HPO_4-$7H_2O$ and $Ca(H_2PO_4)_2$) were used causing different results. The K_3PO_4 caused a significant beneficial effect on catalytic conversion (423 $\pm$ 7 °C), while Na_2HPO_4-$7H_2O$ and $Ca(H_2PO_4)_2$ had a negligible (528 $\pm$ 20 °C) and a significantly deteriorating effect (699 $\pm$ 13 °C) respectively. Based on the behavior of sodium and potassium carbonate, sodium phosphate is expected have a beneficial effect on soot conversion similar to potassium phosphate. Zinc acetate also benefitted the catalytic conversion (467 $\pm$ 5 °C), but slightly less than sodium and potassium carbonate.

Table 2 shows the kinetic parameters (A and E_a) obtained from Arrhenius plots of the carbon and carbon/catalyst mixtures. As reported in the literature estimates of the pre-exponential factor (A) is not well determined due to the high sensitivity towards small variations in the slope of the Arrhenius plot [18]. This is most pronounced for mixtures of carbon and catalyst, because the mass loss only constituted a few percent of the initial sample mass. The obtained activation energy of pure particulate

matter (220 ± 3 kJ/mol) are just above what has been reported in the literature for carbon oxidation (102 – 210 kJ/mol) [14] which indicates that mass transport limitations were absent in this study. The lower values obtained for diesel PM (~ 110-115 kJ/mol [11-12]), may be the result of differences in carbon structure and the presence of catalytic metals/ash [14]. The presence of catalytic species decreased the activation energy to 62 ±8 kJ/mol (CeO_2) and 91 ±5 kJ/mol (commercial catalyst) which is similar to what has been reported in the literature for various catalysts [9,14].

Figure 5 compares the measured and simulated development in mass and conversion/mass loss rate for 5:1 catalyst/SRM 2975 mixtures. The simulation/kinetic data are able to describe the peak conversion temperature and the associated part of the conversion/mass loss curve, but the simulation does not describe the initial gradual increase in conversion. This behavior may originate from an initial oxidation of a more amorphous carbon layer which needs to be described by its own kinetic data [8].

6. Conclusions

A systematic lab-scale investigation of diesel particulate matter/soot conversion in the presence of catalytic materials and simulated biodiesel ashes (at 10 % O_2) has been performed. The presence of a commercial catalyst without biodiesel salts in tight contact with the particulate matter/carbon nanopowder (5:1 wt. ratio) caused a ~ 150 ^{o}C decrease in peak conversion temperature (to 526 ± 19 and 571 ± 16 ^{o}C. The lower temperature reported for catalytic DPF regeneration (250-300 ^{o}C) [2] is likely due to the presence of NO_2 – an aspect (NO_2/catalyst/soot/ash interactions) that is not covered by this work. Catalytic diesel PM conversion (5:1 wt. ratio) benefits from the presence of biodiesel salts such as Na_2CO_3, K_2CO_3 or K_3PO_4 – decreased peak conversion temperature from 526 ± 19°C to ~ 400-420 ^{o}C, with a limited dependence on salt concentration (+20 ^{o}C for a 80 % lower salt concentration). Other salts, which may form from engine oil ($CaSO_4$ and $Ca(H_2PO_4)$ or combinations of engine oil and fuel (K_2SO_4) can have a detrimental effect on catalytic PM conversion - i.e. peak conversion temperatures of 569 ± 6; 699 ± 13 and 581 ± 16 ^{o}C respectively.

Kinetic parameters (A and E_a) obtained from Arrhenius plots of the data showed a lower activation energy in the presence of the commercial catalyst ($E_a = 91 \pm 5$ kJ/mol) or CeO_2 ($E_a = 62 \pm 8$ kJ/mol) compared to pure SRM 2975 ($E_a = 220 \pm 3$ kJ/mol) The obtained kinetic data was able to simulate/describe the peak conversion temperature and the associated part of the conversion/mass loss curve, but an initial gradual increase in conversion was not adequately described.

With respect to the operation of diesel particulate filters while using biodiesel as fuel, the results obtained imply that the presence of sodium or potassium as carbonates or phosphates benefit the diesel particulate matter conversion and thereby DPF regeneration. However, as diesel particulate matter is converted the ash may accumulate locally in the filter, thereby removing the required tight PM/catalyst/ash contact. Build-up of excessive levels of ash in the filter may furthermore still be detrimental to DPF regeneration performance.

Nomenclature

A   pre-exponential factor (frequency factor) [s^{-1}]

a   Cross sectional area [m^2]

C   Concentration [kg m^{-3}]

d_p particle size [m]

D   diffusion coefficient [m^2 s^{-1}]

E_a activation energy [kJ mol^{-1}]

h   height [m]

k   reaction rate constant [s^{-1} Pa^{-1}]

k^* $k \cdot p_{O2}$ [s^{-1}]

k_g Mass transfer coefficient [m s^{-1}]

L   Characteristic size [m]

M   Molar mass [kg mol^{-1}]

m   soot mass [kg]

p   Partial pressure [Pa]

R   Universal gas constant [m^3 Pa K^{-1} mol^{-1}]

S_e External particle surface area [m^2]

t   time [s]

T   Temperature [^{o}C]

V_p particle volume [m^3]

Subscript

b   Bulk phase

obs   Observed

peak Peak in mass loss rate

Literature cited

[1] Directive 2009/28/EC of the European parliament and of the counsel of 23. April 2009 on the promotion of the use of energy from renewable sources and amending and subsequently repealing Directives 2001/77/EC and 2003/30/EC.

[2] Sappok, A.G.; Wong, V.W. Impact of Biodiesel on Ash Emissions and Lubricant Properties Affecting Fuel Economy and Engine Wear. *DEER* MI, August 2007.

[3] Castellino, F.; Jensen, A.D.; Johnsson, J.E.; Fehrmann, R. Influence of reaction products of K-getter fuel additives on commercial vanadia-bassed SCR catalysts – Part I Potassium phosphate. *Applied Catalysis B: Environmental.* **2009**, 86(3-4), 196-205

[4] Castellino, F.; Jensen, A.D.; Johnsson, J.E.; Fehrmann, R. Influence of reaction products of K-getter fuel additives on commercial vanadia-bassed SCR catalysts – Part II simultaneous addition of KCl, $Ca(OH)_2$,.H_3PO_4 and H_2SO_4 in a hot flue gas at a SCR pilot-scale setup. *Applied Catalysis B: Environmental.* **2009**, 86(3-4), 206-215

[5] Castellino, F.; Rasmussen, S.B.; Jensen, A.D.; Johnsson, J.E.; Fehrmann, R. Deactivation of vanadia-based commercial SCR catslysts by polyphosphoric acids. *Applied Catalysis B: Environmental.* **2008**, 83(1-2), 110-122

[6] Morcos, M.; Ayyappan, P.; Harris, T. Characterization of DPF Ash for Development of DPF Regeneration Control and Ash Cleaning Requirements. *SAE Technical papers* **2011**

[7] Sappok, A.; Wong, V. Ash Effects on Diesel Particulate Filter Pressure Drop Sensitivity to Soot and Implications for Regeneration Frequency and DPF Control. *SAE International.* **2010**, 3(1), 380-396

[8] Liati, A.; Eggenschwiler, P.D. Characterization of particulate matter deposited in diesel particulate filters: Visual and analytical approach in macro-, micro- and nano-scales. *Combustion and Flame* **2010**, 157 (9), 1658-1670

[9] Ciambelli, P.; Corbo, P.; Parrella, P.; Scialo, M.; Vaccaro, S. Catalytic oxidation of soot from diesel exhaust gases. 1. Screening of metal oxide catalysts by TG-DTG-DTA analysis. *Thermochimica Acta* **1990**, 162 (1), 83-89

[10] Bardasz, E.; Mackney, D.; Britton, N.; Kleinscheck, G.; Olofsson, K.; Murray, I.; Walker, A.P. Investigations of the Interactions between Lubricant-derived Species and Aftertreatment Systems on a State-of-the-Art Heavy Duty Diesel Engine. *SAE Transactions* **2003,** 112(4)*,* 1821-1839.

[11] Rodriguez-Fernandez, J.; Oliva, F.; Vazquez, R.A. Characterization of the Diesel Soot Oxidation Process through an Optimized Thermogravimetric Method. *Energy & Fuels* **2011,** 25(5)*,* 2039-2048.

[12] Strzelec, A.; Toops, T.; Daw, S.; Foster, D.; Rutland, C. Particulate Matter Oxidation Kinetics: surface Area Dependence. *CLEERS*, MI, April 2010.

[13] Composition of Diesel Particulate Filter Ash and Confirmation that FSX Pneumatic Cleaning Process does not Damage Washcoats, FSX Inc, http://www.fsxinc.com (accessed 25th May 2011), 2009

[14] Stanmore, B.R.; Brilhac, J.F.; Gilot, P. The oxidation of soot: a review of experiments, mechanisms and models. *Carbon* **2001,** 39(15)*,* 2247-2268.

[15] Neeft, J.P.A.; Makkee, M.; Moulijn, J.A. Catalytic oxidation of carbon black – I. Activity of catalyst and classification of oxidation profiles. *Fuel* **1998,** 77(3)*,* 111-119.

[16] McKee, D.W. Mechanisms of the alkali metal catalysed gasification of carbon. *Fuel* **1983,** 62(2)*,* 170-175.

[17] Beauboeuf, D.P. *Microscopy Investigations of Ash and Particulate Matter Accumulation in Diesel Particulate Filter Pores*, B.Sc. Thesis; Department of Mechanical Engineering, Massachusetts Institute of Technology: USA, 2010.

[18] Saracco, G.; Specchia, V. Catalytic filters for the abatement of volatile organic compounds. *Chemical Engineering Science* **2000,** 55(5)*,* 897-908.

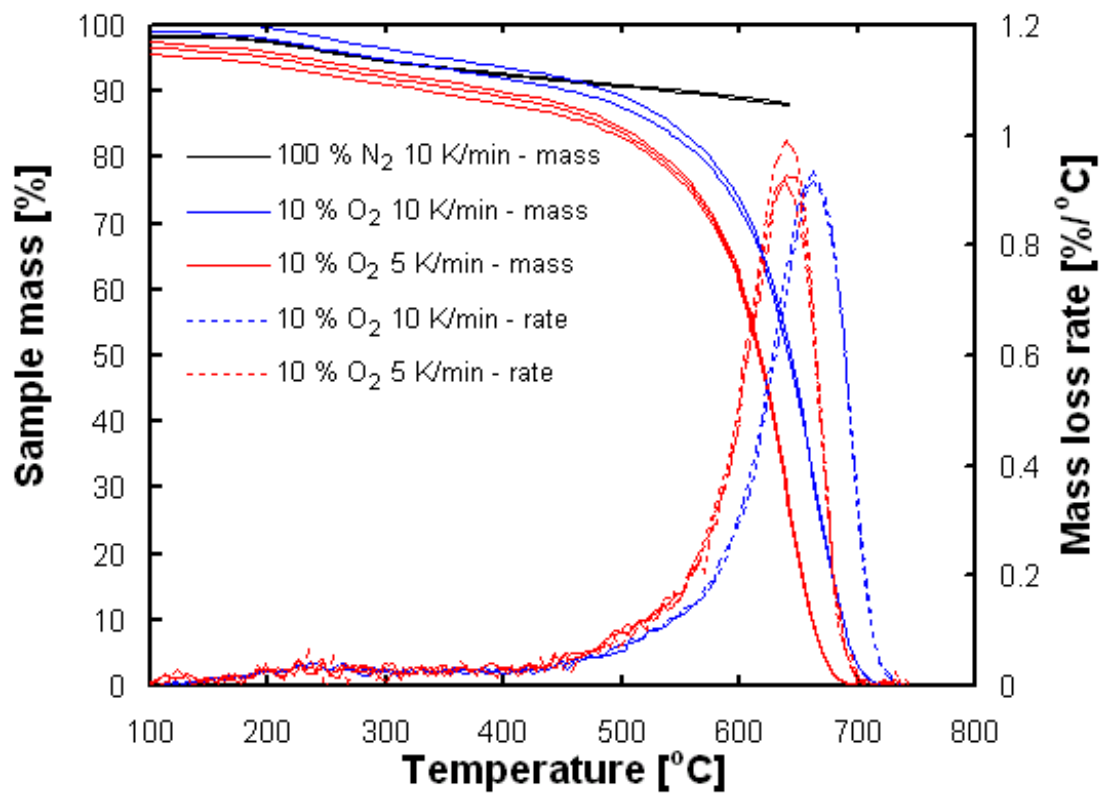[19] Levenspiel, O. Chemical Reaction Engineering, 3rd edition; John Wiley & Sons, 1999

Figure 1: Influence of heating rate and gas phase composition on the mass and conversion/mass loss rate of SRM 2975.
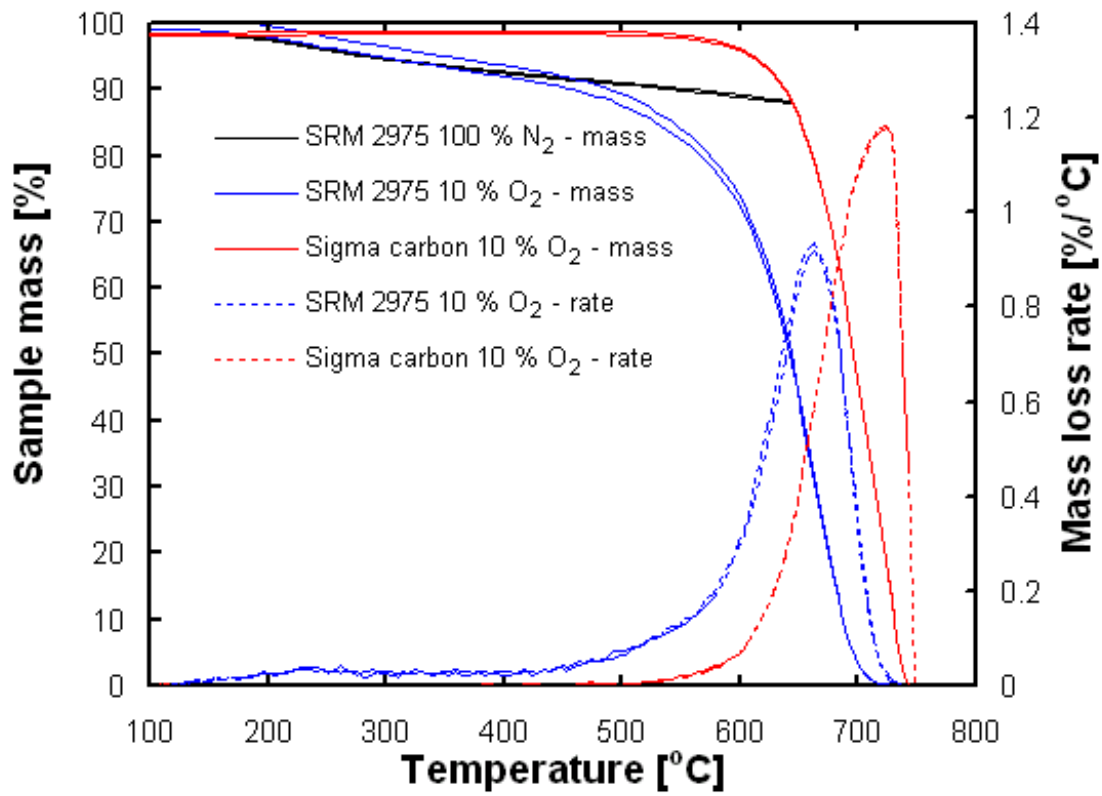
Figure 2: Mass and conversion/mass loss rate of different carbon samples.

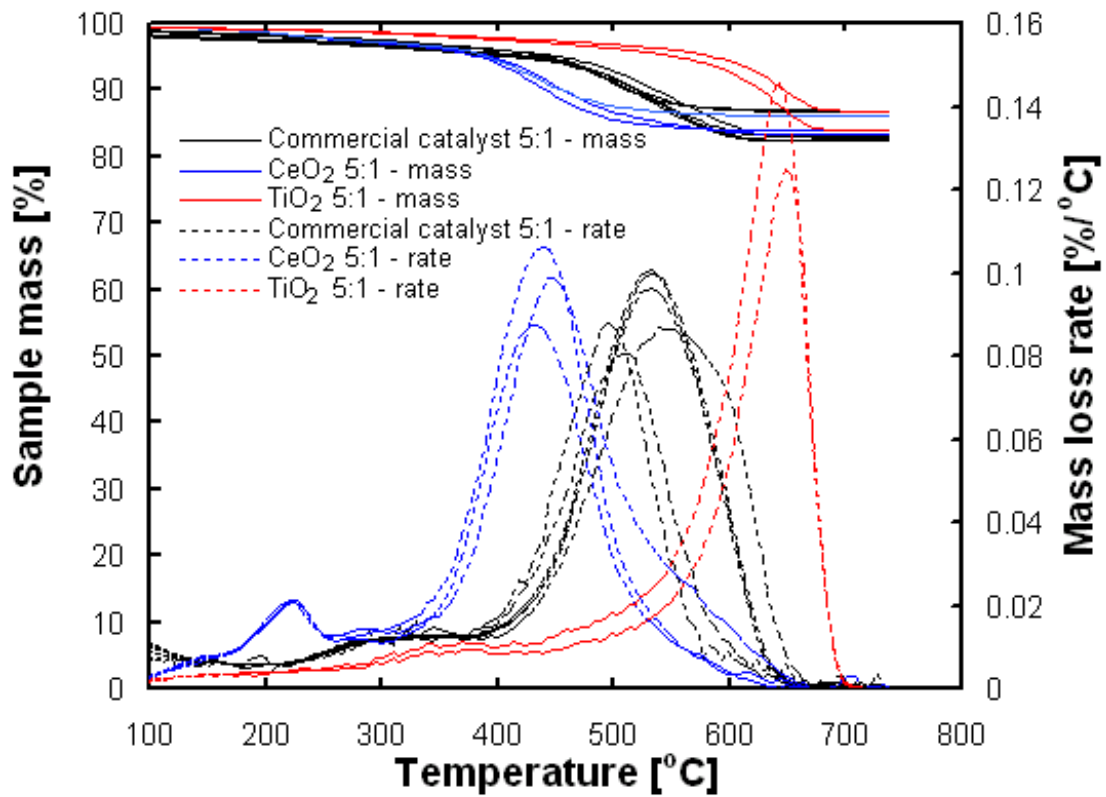**Figure 3:** Mass and conversion/mass loss rate of 5:1 catalyst/SRM 2975 mixtures (10 % O_2 at 10 k/min)

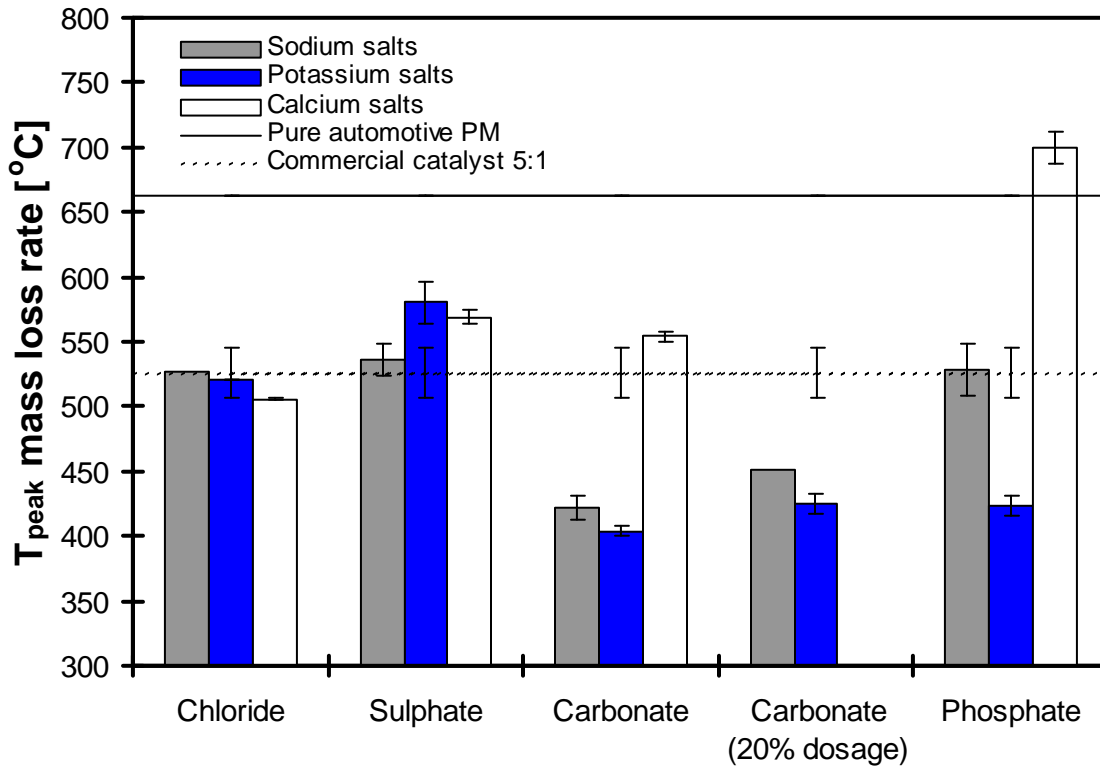**Figure 4:** Temperature of maximal mass loss rate for carbon/catalyst/salt mixtures (10 % O_2 at 10 K/min). Error bars indicate standard deviation. The solid and the dashed line illustrate the temperature at which mass loss rate peaked for pure SRM 2975 and a 5:1 mixture with the commercial catalyst respectively.
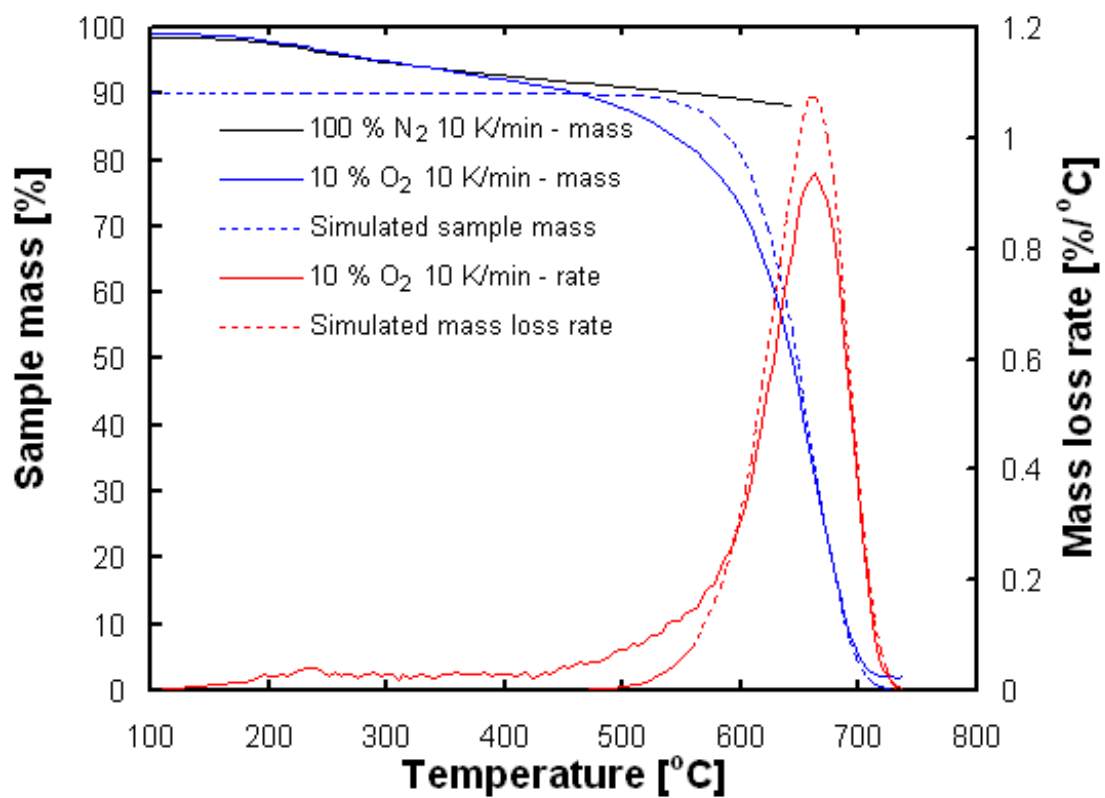
Figure 5: Measured and simulated sample mass and conversion/mass loss rate for 5:1 catalyst/SRM 2975 mixtures

Table 1: Overview of performed experiments.

Experiment	Heating rate	O$_2$	Carbon	Catalyst	Salt[a]	Wt. ratio[b]	T$_{peak}$e
	$^oC\ min^{-11}$	Vol %	Wt. %	Wt.%	Wt.%		^oC
1-2	10	10	SRM 2975	-	-	1:0:0	662 ±1
3-4	10	10	Sigma	-	-	1:0:0	723 ±1
5-10	10	10	SRM 2975	Commercial	-	1:5:0	526 ±19
11-12	10	10	Sigma	Commercial	-	1:5:0	571 ±16
13-15	10	10	SRM 2975	CeO$_2$	-	1:5:0	442 ±8
16-17	10	10	SRM 2975	TiO$_2$	-	1:5:0	648 ±6
18-19	10	10	SRM 2975	Commercial	-	1:10:0	480 ±10
20	10	10	SRM 2975	Commercial	-	1:20:0	497
21-22	10	10	SRM 2975	Commercial	CaCl$_2$	1:5:2.5	506 ±1
23-24	10	10	SRM 2975	Commercial	CaSO$_4$	1:5:2.5	569 ±6
25-29	10	10	SRM 2975	Commercial	Ca(H$_2$PO$_4$)$_2$	1:5:2.5	699 ±13
30-31	10	10	SRM 2975	Commercial	CaCO$_3$	1:5:2.5	554 ±4
32	10	10	SRM 2975	Commercial	KCl	1:5:2.5	520
33-34	10	10	SRM 2975	Commercial	K$_2$SO$_4$	1:5:2.5	581 ±16
35-37	10	10	SRM 2975	Commercial	K$_3$PO$_4$	1:5:2.5	423 ±7
38-39	10	10	SRM 2975	Commercial	K$_2$CO$_3$	1:5:0.5	425 ±8
40-41	10	10	SRM 2975	Commercial	K$_2$CO$_3$	1:5:1.5	413 ±4
42-43	10	10	SRM 2975	Commercial	K$_2$CO$_3$	1:5:2.5	404 ±4
44-45	10	10	SRM 2975	Commercial	NaCl	1:5:2.5	527 ±7
46-47	10	10	SRM 2975	Commercial	Na$_2$SO$_4$	1:5:2.5	537 ±12
48-49	10	10	SRM 2975	Commercial	Na$_2$HPO$_4$	1:5:2.5	528 ±20
50	10	10	SRM 2975	Commercial	Na$_2$CO$_3$	1:5:0.5	451
51	10	10	SRM 2975	Commercial	Na$_2$CO$_3$	1:5:1.5	434
52-53	10	10	SRM 2975	Commercial	Na$_2$CO$_3$	1:5:2.5	422 ±10
54-55	10	10	SRM 2975	Commercial	Zn(CH$_3$COO)$_2$	1:5:2.5	467 ±5
56-57	10	0	SRM 2975	-	-	1:0:0	-
58-60	5	10	SRM 2975	-	-	1:0:0	643 ±2
61-62	5	10	SRM 2975	Commercial	-	1:5:0	515 ±1
63	10	20	SRM 2975	Commercial	-	1:5:0	520

a weight percent of metal/cation only

b mass carbon/mass carbon: mass catalyst/mass carbon: mass salt (cation only)/ mass carbon.

Table 2: Estimated kinetic parameters (standard deviation indicated by ±).

Experiment	Composition *Carbon/catalyst/salt*	Wt. ratio[c]	Heating rate ^oC min^{-11}	O_2 Vol %	T_{peak} ^oC	A Min^{-1}	E_a Kj mol^{-1}
1-2	SRM 2975	1:0:0	10	10	662±1	5.8 (±2.0) 10^{11}	220 ±3
3-4	Sigma	1:0:0	10	10	723±1	5.5 (±1.2) 10^{12}	249 ±2
5-10	SRM 2975/Comercial	1:5:0	10	10	526±19	2.4 (±2.9) 10^5	91 ±5
11-12	Sigma/ Commercial	1:5:0	10	10	571±16	1.6 (±2.2) 10^5	91 ±19
13-15	SRM 2975/ CeO_2	1:5:0	10	10	442±8	8.6 (±10.6) 10^3	62 ±8
16-17	SRM 2975/ TiO_2	1:5:0	10	10	648±6	8.8 (±12.1) 10^{14}	258 ±25
18-19	SRM 2975/Comercial	1:10:0	10	10	480±10	1.0 (±1.4) 10^5	78 ±15
20	SRM 2975/Comercial	1:20:0	10	10	497	6.610^3	69
58-60	SRM 2975	1:0:0	5	10	643±2	1.6 (±1.3) 10^{12}	231 ±3
61-62	SRM 2975/Comercial	1:5:0	5	10	515±1	9.2 (±0.8) 10^4	90 ±1
63	SRM 2975/Comercial	1:5:0	10	20	520	5.610^5	98

c mass carbon/mass carbon: mass catalyst/mass carbon: mass salt (cation only)/ mass carbon.